NATIONAL CENTRE FOR NUCLEAR RESEARCH

Theoretical Physics Division

Department of Fundamental Research

DOCTORAL THESIS

Sebastian Trojanowski

Supersymmetric dark matter in light of recent searches for new physics

Supervisor
Prof. Leszek Roszkowski

Warsaw 2015

I dedicate this work to my beloved wife Mariola

Acknowledgments

I will always be immensely grateful to my advisor and the head of the BayesFITS group, Professor Leszek Roszkowski, for his constant encouragement and guidance, as well as invaluable help both during my studies and in the course of preparing the thesis.

I am very thankful to Dr Krzysztof Turzyński for his support and astonishing patience in answering all my questions. I am also indebted to the members of the BayesFITS group: Dr Nils-Erik Bomark, Dr Kamila Kowalska, Dr Shoaib Munir, Dr Enrico Maria Sessolo, Dr Yue-Lin Sming Tsai and Dr Andrew J. Williams for fruitful collaborations and many productive discussions.

Special thanks go to my wife for her unceasing encouragement, as well as everyday enthusiasm and heartening presence over the past several years. I am also very grateful to my parents for their continuous care and support that enabled me to obtain my education.

This work has been funded for the most part by the Welcome Program of the Foundation for Polish Science. In the last stage it was also partly supported by the National Science Center, Poland, under research grant DEC-2014/13/N/ST2/02555. The use of the CIŚ computer cluster at the National Centre for Nuclear Research is gratefully acknowledged.

Supersymmetric dark matter in light of recent searches for new physics

Abstract

Unraveling the nature of dark matter remains among the most important challenges of contemporary physics. Indisputably, the lightest supersymmetric particle is one of the most popular candidates for the dark matter particle.

In this thesis we first present an introduction to the topic of dark matter. It is followed by a discussion of the current status of supersymmetric dark matter in the framework of models constrained by some universality conditions at the scale of Grand Unified Theories. We discuss the most popular models of this class, in particular focusing on the dark matter relic density and direct detection, properties of the recently discovered Higgs boson and the fine-tuning problem. We employ methods of Bayesian statistics in order to incorporate into analysis many experimental constraints with their corresponding uncertainties.

Next we study supersymmetric dark matter in a more general framework of the Minimal Supersymmetric Standard Model with ten free parameters defined at low energy scale. First we investigate the lightest neutralino as a dark matter particle. Next we extend the framework to include other well-motivated supersymmetric dark matter candidates: the gravitino and the axino. A particular emphasis is put on a discussion of a non-standard cosmological scenario with low reheating temperature of the Universe after a period of cosmological inflation. We show that the consequences of this scenario for supersymmetric dark matter can be quite dramatic. In particular the relic abundance of dark matter can be reduced due to a modified expansion of the Universe, thus relaxing the impact of the usually strongest constraint coming from the requirement that the Universe does not overclose. On the other hand, effective dark matter production in decays of the inflaton field can cause an enhancement in the dark matter relic density in otherwise underabundant regions of the parameter space. In the case of extremely weakly interacting particles we derive interesting new limits on the reheating temperature and the mass of the dark matter particle.

Supersymetryczna ciemna materia w świetle obecnych poszukiwań nowej fizyki

Streszczenie

Poznanie natury ciemnej materii jest jednym z największych wyzwań, jakie stoją przed współczesną fizyką, zaś najlżejsza cząstka supersymetryczna pozostaje bez wątpienia jedną z najbardziej popularnych kandydatek na cząstkę ciemnej materii.

Niniejsza rozprawa rozpoczyna się wprowadzeniem do tematyki ciemnej materii. Następnie zaprezentowany jest obecny stan badań nad supersymetryczną ciemną materią w modelach z dodatkowymi ograniczeniami narzucanymi na skali Teorii Wielkiej Unifikacji. Rozważane są najpopularniejsze modele tego typu, ze szczególnym uwzględnieniem gęstości reliktowej i bezpośrednich poszukiwań ciemnej materii, własności niedawno odkrytego bozonu Higgsa oraz małego problemu hierarchi. Ograniczenia eksperymentalne w opisywanych analizach są nakładane przy użyciu metod statystyki bayesowskiej z uwzględnieniem niepewności wynikających z pomiarów oraz obliczeń teoretycznych.

W dalszej części pracy opisane jest zagadnienie supersymetrycznej ciemnej materii w bardziej ogólnym kontekście minimalnego supersymetrycznego rozszerzenia Modelu Standardowego z dziesięcioma swobodnymi parametrami zdefiniowanymi dla niskiej skali energii. Dyskutowane jest przy tym przypadek najlżejszego neutralina jako cząstki ciemnej materii. Następnie model ten jest rozszerzany poprzez dodanie dwóch innych supersymetrycznych kandydatek na cząstki ciemnej materii: grawitina i aksina. Ze szczególną uwagą rozważane są przypadki z niską temperaturą podgrzania Wszechświata po okresie inflacji kosmologicznej. Pokazany jest możliwy znaczny wpływ takich założeń na gęstość reliktową ciemnej materii. Jej wartość może zostać znacznie zredukowana w wyniku szybkiej ekspansji Wszechświata lub istotnie powiększona w wyniku rozpadów pola inflatonu, co pozwala na rozważanie przypadków typowo wykluczonych w standardowych scenariuszach kosmologicznych. Dla bardzo słabo oddziałujących cząstek wyprowadzone są nowe, interesujące ograniczenia na wartość temperatury podgrzania i masę cząstki ciemnej materii.

Contents

List of Figures

List of Tables

List of acronyms (used more than once in the text)

1TH (region)	1 TeV higgsino (region)
ATLAS	A Toroidal LHC ApparatuS
BAO	baryon acoustic oscillations
BBN	Big Bang Nucleosynthesis
BFP	best-fit point
BR	branching ratio
BSM (physics)	beyond Standard Model (physics)
CDM	cold dark matter
CL	confidence level
CM (frame)	center of mass (frame)
CMB (radiation)	Cosmic Microwave Background (radiation)
CMS	Compact Muon Solenoid
CMSSM	Constrained Minimal Supersymmetric Standard Model
CNMSSM	Constrained Next-to-Minimal Supersymmetric Standard Model
CNMSSM-NUHM	CNMSSM (with) non-universal Higgs masses
(dark matter) DD	(dark matter) direct detection
DM	dark matter
EWIMP	extremely weakly interacting massive particle
EWSB	electroweak symmetry breaking
FCNC	flavor changing neutral current
FRW	Friedmann-Robertson-Walker
GGM	generalized gauge mediation
GMSB	gauge mediated supersymmetry breaking
GUT	Grand Unified Theory
HB/FP (region)	Hyperbolic Branch / Focus Point (region)
HDM	hot dark matter
(dark matter) ID	(dark matter) indirect detection
LHC	Large Hadron Collider
LHS (of equation)	left hand side (of equation)
LOSP	lightest ordinary supersymmetric particle
LSP	lightest supersymmetric particle
LSS	large scale structures
LUX (experiment)	Large Underground Xenon (experiment)
MCMC (methods)	Markov Chain Monte Carlo (methods)

MSSM	Minimal Supersymmetric Standard Model
NLSP	next-to-the-lightest supersymmetric particle
NMSSM	Next-to-Minimal Supersymmetric Standard Model
NTP	non-thermal production
NUGM	non-universal gaugino masses
NUHM	non-universal Higgs masses
PMSB	Planck-scale mediated supersymmetry breaking
QCD	Quantum Chromodynamics
RD (epoch)	radiation dominated (epoch)
RGE	Renormalization Group Equation
RHS (of equation)	right hand side (of equation)
SC (region)	stau (slepton) coannihilation (region)
SE	Sommerfeld enhancement
SM	Standard Model
SSB	spontaneous supersymmetry breaking
SUSY	supersymmetry
TP	thermal production
VEV	vacuum expectation value
WDM	warm dark matter
WIMP	weakly interacting massive particle

Chapter 1

Introduction

Historically, one of the most important aims of philosophical and then scientific studies over the centuries has been the identification of the basic constituents of matter. This effort, which eventually led to the formulation of the Standard Model (SM) of particle physics, culminated in the recent discovery of the Higgs boson by the CMS [1] and the ATLAS [2] Collaborations at the Large Hadron Collider (LHC). In spite of its enormous success, however, the SM appears to be incomplete in light of the observed data. One such piece of evidence for beyond-the-SM physics is the existence of so-called dark matter (DM), making up about 27% of the total mass-energy density in the Universe [3], which is significantly more than the 5% attributed to ordinary (baryonic) matter. Understanding the nature of DM is one of the most important quests in contemporary physics.

This prompts one to consider extensions to the SM in the description of fundamental interactions. Among various extensions of the SM that have been proposed supersymmetric (SUSY) models remain arguably the most popular. They provide both an elegant theoretical description, as well as a possibility of simultaneously solving several other serious problems of the SM. They predict the existence of superpartners for the ordinary elementary particles. Remarkably, the lightest of these superpartners (the lightest supersymmetric particle, LSP) can play the role of the dark matter particle.

One example of such particle that can be found in the most popular supersymmetrized version of the Standard Model (Minimal Supersymmetric Standard Model, MSSM), is the lightest neutralino. It is electrically neutral and stable (assuming R-parity conservation), as well as it belongs to a group of massive weakly interacting particles that can be viable DM candidates with the correct value of the relic density. Importantly, in some of the most important scenarios neutralino DM can be potentially found in future dark matter direct or indirect detection experiments within the next few years. A requirement of reproducing the correct value of the relic abundance typically results in a strong reduction of the allowed parameter space of supersymmetric models. The neutralino DM scenario can be further restricted by imposing collider constraints. In particular, important constraints of this type are associated with the mass and signal rates of the recently discovered Higgs boson. Moreover, one typically considers additional experimental constraints that come from, *e.g.*, searches for supersymmetric particles at the LHC, B-physics and the anomalous magnetic moment of the muon.

The value of the Higgs boson mass measured at the LHC, as well as lower limits on the masses of SUSY particles suggest that the characteristic mass scale of supersymmetry should be at least of the order of 1 TeV. This mass scale is associated with quarks and gluinos, but in principle one could also consider scenarios with such heavy neutralinos. However, if one wants to discuss neutralino with mass noticeably heavier than about 1 TeV, one often finds it particularly difficult to satisfy the relic density constraint. One way to overcome this is to assume low value of the reheating temperature T_R after a period of cosmological inflation. In this scenario a modified expansion rate of the Universe in the reheating period, *i.e.*, before the radiation dominated epoch in the evolution of the Universe, results in an effective dilution of the dark matter particles. On the other hand, for low T_R additional production of DM in decays of the inflaton field is also possible. This improves a statistical validity of regions that are characterized by too low a relic abundance but can be favored, *e.g.*, from the point of view of naturalness.

Beside the lightest neutralino, supersymmetry also offers two other well-motivated DM candidates that can be the LSP: the gravitino and the axino. They interact extremely weakly but can populate the Universe typically originating from late-time decays of the next-to-LSP (NLSP) and from scatterings of SUSY particles in thermal equilibrium. The limitations of scenarios with gravitino or axino DM come from cosmological considerations. In particular, the aforementioned late-time decays of the NLSP can destroy light elements in the Universe and therefore violate constraints associated with the Big Bang Nucleosynthesis.

In this thesis we will discuss in detail all the subjects associated with supersymmetric dark matter outlined above. We begin with an introduction to the topic of dark matter. In Chapter 2 we introduce some basic concepts of cosmology that play a fundamental role in a further discussion. Next, in Chapter 3, we discuss the observational evidence for DM and the most popular DM candidates. Chapter 4 is devoted to a short description of essential features of the SM and a more extensive one for supersymmetry. It is followed by Chapter 5 in which we discuss the issue of the relic density of supersymmetric DM candidates. In Chapter 6 we present fundamental concepts of Bayesian statistics and the way it is applied to studying supersymmetric models.

The results presented in Chapter 7 concern supersymmetric models constrained by universality conditions at the scale of Grand Unified Theories. Beside the topic of neutralino DM, an emphasis is put on the implications stemming from the mass of the recently discovered Higgs boson. In particular, we discuss the possibilities that either the second lightest Higgs in the MSSM is responsible for the observed signal or that the signal comes from a combination of both the lightest scalar Higgs and another Higgs scalar or pseudoscalar. This chapter is based on research projects done by the author of the thesis in collaboration with other members of the BayesFITS group.

In Chapter 8 we discuss neutralino DM in a more general framework of the MSSM with ten free parameters defined at low energy scale, as well as for the NMSSM with three more parameters. In particular, we focus on a scenario in which the correct value of the DM relic density can be achieved after assuming low reheating temperature of the Universe. We consider cases both with and without effective direct and cascade decays of the inflaton field to DM.

Chapter 9 is devoted to gravitino and axino DM scenarios. We begin with a discussion of a case with sneutrino NLSP decaying into gravitino DM in a framework of SUSY models with some universality conditions at high energy scale. We then analyze the impact of taking low T_R on gravitino and axino DM scenarios in the MSSM. In these cases we find some interesting limits either on the reheating temperature or on the mass of DM particles.

We conclude in Chapter 10.

Chapter 2

Basics of cosmology

In this chapter we will briefly describe some of the basic concepts in cosmology that will be useful in the rest of the thesis (for a detailed discussion see [4, 5]).

2.1 Friedmann equation

We begin with the key observation by Hubble [6] that was interpreted as the evidence for the expansion of the Universe. Let us introduce the *scale factor* $a(t)$ that depends on a time t and is used to extract the expansion dependence of the physical distance $d(t)$ between any two objects in the Universe from their peculiar motion. It is related to $d(t)$ by

$$d(t) = a(t)\, d_0, \tag{2.1}$$

where d_0 is called the comoving distance. It corresponds only to the peculiar motion of the objects. Differentiating Eq. (2.1) with respect to time one obtains the *Hubble law*

$$\dot{d}(t) = \frac{\dot{a}(t)}{a(t)}\, d(t) = H(t)\, d(t), \tag{2.2}$$

where $H = \dot{a}/a$ is called the Hubble expansion parameter (rate). H is typically written in terms of its value h in units $100\,\mathrm{km/s/Mpc}$, $H_0 = 100\, h\,\mathrm{km\,s^{-1}\,Mpc^{-1}}$, where $h = 0.673(12)$ [7] and index 0 in the whole thesis denotes the value at present time.

The evolution of the Universe is well described in the framework of *Friedmann-Robertson-Walker* (FRW) *metric* that is the solution to Einstein's field equations of general relativity for a homogeneous, isotropic Universe. In particular this allows one to relate the Hubble expansion rate to the energy density ρ in the

Universe due to the *Friedmann equation*[1]. For the flat Universe it reads[2]

$$H^2 = \frac{8\pi\rho}{3M_P^2}, \tag{2.3}$$

where $M_P = 1.2 \times 10^{19}\,\mathrm{GeV} = \sqrt{8\pi}\,\overline{M}_P$ is the Planck mass ($\overline{M}_P = 2.435 \times 10^{18}\,\mathrm{GeV}$ is called the reduced Planck mass). The value of ρ that saturates Eq. (2.3) is called the *critical density* $\rho_c \simeq 10^{-5}\,h^2\,\mathrm{GeV/cm^3} \simeq 8 \times 10^{-47}\,h^2\,\mathrm{GeV}^4$ [7].

One of the contributions to ρ is related to the radiation energy density ρ_R, where by *radiation* we mean all the light (or massless) degrees of freedom (associated with the particles) that move with relativistic velocities at a given time t. As the Universe expands, the temperature T decreases and some of the light degrees of freedom become non-relativistic and they do not contribute to ρ_R any more. The radiation energy density can be written in terms of T as

$$\rho_R = \frac{\pi^2}{30} g_*(T)\,T^4, \tag{2.4}$$

where $g_*(T)$ is the number of relativistic degrees of freedom at temperature T.

The energy density of the matter content of the Universe ρ_{M} can be decomposed into two parts associated with ordinary baryonic matter ρ_b and with DM ρ_{DM}

$$\rho_{\mathrm{M}} = \rho_b + \rho_{\mathrm{DM}}. \tag{2.5}$$

The relative contribution of a given species (*e.g.*, DM, b or Λ) to the critical density is often called the abundance

$$\Omega_i\,h^2 = \frac{\rho_i}{\rho_c}\,h^2, \tag{2.6}$$

where, *e.g.*, $i = \mathrm{DM}, b, \Lambda$.

2.2 Reheating and the radiation dominated epoch

It is usually assumed that the early Universe underwent a period of *cosmological inflation* during which an accelerated expansion of the Universe was driven by the vacuum energy density of a scalar field – an *inflaton*. After inflation the large potential energy of the inflaton field was transformed into the kinetic energy of produced particles. As a result of this process, dubbed *reheating*, the Universe entered a *radiation-dominated* (RD) epoch.

A careful analysis shows that the maximum temperature T_{max} in the evolution of the Universe after inflation was reached during reheating. At that time the energy

[1]We present here the first Freedman equation. The second equation involves $\ddot{a}$ and will play less important role in the thesis.

[2]We use the convention where $c = 1$. The cosmological constant term proportional to Λ can be formally absorbed in ρ by a redefinition of the energy density $\rho_{\mathrm{new}} = \rho_{\mathrm{old}} + (\Lambda\,M_P^2)/8\pi$.

density ρ of the Universe was dominated by the contribution ρ_ϕ associated with coherent oscillations of the inflaton field around the minimum of the potential. As ρ_ϕ decreased with time producing light degrees of freedom, *i.e.*, radiation, at some moment condition $\rho_R \geqslant \rho_\phi$ was achieved that marked the onset of the RD epoch. The temperature at which this happened, *i.e.*, the initial temperature of the RD epoch, will be later denoted by $T_{\rm RD}$.

For simplicity it is often assumed that reheating was an instantaneous process that happened when the decay rate of the inflaton field Γ_ϕ was equal to the Universe's expansion rate $H(t)$. In the *instantaneous reheating approximation* we further assume that the whole ρ_ϕ was transformed simply to ρ_R. Using Eq. (2.3) and (2.4) one then obtains

$$\Gamma_\phi = \sqrt{\frac{4\pi^3 g_*(T_R)}{45}}\,\frac{T_R^2}{M_{Pl}} \qquad \text{definition of } T_R, \tag{2.7}$$

where we introduced a so-called *reheating temperature* T_R. In the simplified approach of instantaneous reheating one interprets this quantity as the largest temperature $T_{\max}$ after a period of cosmological inflation

$$T_R = T_{\rm RD}^{\rm inst.\ reh.} = T_{\max}^{\rm inst.\ reh.}. \tag{2.8}$$

However, when the dynamics of reheating is taken into account, Eq. (2.8) does not hold exactly and one typically obtains [8]

$$T_{\max}^{\rm non\text{-}inst.\ reh.} \gg T_R \gtrsim T_{\rm RD}^{\rm non\text{-}inst.\ reh.}. \tag{2.9}$$

In this case T_R still serves as an useful parameter in a discussion of the transition from the period of cosmological inflation to the RD epoch since $T_R \approx T_{\rm RD}$, although there is no exact equality.

During the RD epoch, with no additional production of the light degrees of freedom, radiation energy density scales as $\rho_R \sim a^{-4}$ with expansion. Applying this to Eq. (2.4) one obtains $T \sim a^{-1}$. In this case the entropy density associated with dominant light degrees of freedom is given by

$$s = \frac{2\pi^2}{45}\,g_{*s}\,T^3, \tag{2.10}$$

where g_{*s} is the effective number of relativistic degrees of freedom for entropy. In absence of additional entropy production one obtains constant total entropy $S = sa^3 = const$ and therefore $s \sim a^{-3}$.

2.3 Thermal equilibrium and freeze-out

Let us now assume that the matter content is dominated by a non-relativistic particle χ with mass m_χ which we will later identify with a DM candidate. Its energy density is approximately equal to $\rho_\chi \simeq m_\chi n_\chi$, where n_χ is the number density. Taking into account only expansion one obtains $n_\chi \sim a^{-3}$.[3] However, *e.g.*, in the presence of $\chi\chi$ annihilations or χ decays the evolution of n_χ can be much more complicated.

In particular, let us assume that χ interacts efficiently enough so that at some moment its annihilation rate[4] exceeds the expansion rate of the Universe, $\Gamma_{\rm ann} = n_\chi \sigma_{\rm ann} v > H$, where $\sigma_{\rm ann}$ is the annihilation cross section and v is the relative velocity of two annihilating particles. In this case they remain in *thermal equilibrium*. The equilibrium number density is determined by the temperature and m_χ. In the (non-)relativistic limit one obtains

$$n_{{\rm eq},\chi} \simeq \begin{cases} \frac{g_\chi T^3}{\pi^2}, & \text{when } T \gg m_\chi, \quad \text{relativistic limit,} \\ g_\chi \left(\frac{m_\chi T}{2\pi}\right)^{3/2} e^{-m_\chi/T}, & \text{when } T \ll m_\chi, \quad \text{non-relativistic limit,} \end{cases} \tag{2.11}$$

where g_χ is the number of degrees of freedom of the particle χ.

When T becomes sufficiently low so that $\Gamma_{\rm ann} < H$, the χ particles *freeze-out* from the thermal equilibrium state. Using Eq. (2.3) in the RD epoch, when $\rho_R \simeq \rho$, and Eq. (2.4) one obtains the condition for freeze-out

$$n_\chi(T_f)\,(\sigma_{\rm ann} v) = \Gamma_{\rm ann} \simeq H \sim \frac{T_f^2}{M_P}, \tag{2.12}$$

where T_f is the freeze-out temperature. After freeze-out in the RD epoch the comoving number density of χ particles remained fixed, $n_\chi\, a^3 \simeq const$. One typically presents this in terms of a yield that is defined as

$$Y_\chi = \frac{n_\chi}{s} \sim \frac{n_\chi}{T^3}, \tag{2.13}$$

and $Y\chi = const$ after freeze-out.

[3]This means that $n_\chi a^3 = const$, where the comoving number density $n_\chi a^3$ is defined as the average number of particles in a cube with size a^3 that is growing with the expansion of the Universe.

[4]The quantity $(\sigma_{\rm ann} v)$ represents an effective volume per unit time in which some probe χ particle moving with the velocity v can annihilate if it meets another particle χ. Hence the number of such annihilation events that can occur per unit time is equal to $(\sigma_{\rm ann} v)$ multiplied by the average number density n_χ that can be met inside this volume, *i.e.*, $\Gamma_{\rm ann} = n_\chi\,(\sigma_{\rm ann} v)$. We assume here that $n_\chi = const$ within the volume $(\sigma_{\rm ann} v)$ which is, *e.g.*, well satisfied if $(\sigma_{\rm ann} v)$ is tiny.

2.4 Boltzmann equations

An accurate calculation of Y_χ requires solving the Boltzmann equation that describes the out-of-equilibrium behavior of a thermodynamic system. In a general form it reads

$$\hat{L}[f] = \hat{C}[f], \tag{2.14}$$

where $f(\mathbf{x}, \mathbf{p}, t)$ is the phase space density, the Liouville operator $\hat{L}$ describes the time evolution of the system due to diffusion and "external forces",[5] while $\hat{C}[f]$ is the so-called "collision term" that is associated with collisions between particles.

In the homogeneous, isotropic FRW Universe in the presence of annihilations $\chi\chi \to$ *any final state* one can rewrite Eq. (2.14) as (see, *e.g.*, [4, 9])

$$\frac{dn_\chi}{dt} = -3Hn_\chi - \langle \sigma v_{\mathrm{Møl}} \rangle \big(n_\chi^2 - n_{\mathrm{eq},\chi}^2 \big), \tag{2.15}$$

where $\sigma = \sum_{\mathrm{final}} \sigma_{\chi\chi \to \mathrm{final}}$ and the quantities $\sigma_{\chi\chi \to \mathrm{final}}$ denote the corresponding annihilation cross sections. The first term on the right hand side (RHS) of Eq. (2.15) corresponds to the expansion of the Universe, while the second to the annihilation processes. Similarly, one can derive the Boltzmann equation for the radiation

$$\frac{d\rho_R}{dt} = -4H\rho_R + 2\langle \sigma v_{\mathrm{Møl}} \rangle \langle E \rangle \big(n_\chi^2 - n_{\mathrm{eq},\chi}^2 \big), \tag{2.16}$$

where $\langle E \rangle$ is the average energy of the annihilating particles. The pair of coupled Boltzmann equations (2.15) and (2.16) can be solved to find Y_χ at freeze-out. The role of Eq. (2.16) is to determine ρ_R and therefore the temperature of the Universe via Eq. (2.4) and the equilibrium number density of χ.

The *Møller velocity* $v_{\mathrm{Møl}}$ in the rest frame of any of the incident particles or in the center of mass (CM) frame is equal to $v_{\mathrm{Møl}} = |\mathbf{v}_1 - \mathbf{v}_2| = v$, where v denotes the relative velocity of both annihilating particles. A thermal average $\langle \sigma_{\mathrm{ann}}\, v_{\mathrm{Møl}} \rangle$ for the $\chi\chi$ annihilations reads

$$\langle \sigma_{\mathrm{ann}}\, v_{\mathrm{Møl}} \rangle_{m_1 = m_2 = m_\chi} = \frac{2\pi^2\, T \int_{4m_\chi^2}^{\infty} ds\, \sigma\, (s - 4m_\chi^2)\, \sqrt{s}\, K_1\!\left(\frac{\sqrt{s}}{T}\right)}{\left(4\pi\, m_\chi^2\, T\, K_2\!\left(\frac{m_\chi}{T}\right)\right)^2}, \tag{2.17}$$

where K_i is the i-th order modified Bessel function of the second kind.

[5] In general this means an "external influence" on particles, *i.e.*, not from particles themselves.

2.5 Large Scale Structure and cold/warm/hot dark matter

Although the χ particles do not annihilate efficiently after freeze-out, they can typically still effectively scatter on light particles of the SM (radiation). The light species have usually masses significantly lower than the mass of the particle χ, $m_{\rm SM} \ll m_\chi$. Thus their number densities are not Boltzmann suppressed. Thanks to these scatterings, momentum transfer between the SM and the χ sector is efficient and χ remains in *kinetic equilibrium*. The time of decoupling from kinetic equilibrium (*kinetic decoupling*) t_{kd} of the DM particles plays a crucial role in the dynamics of the Large Scale Structures (LSS) formation in the Universe (for a review see, *e.g.*, [10]). The LSS denotes an observable pattern of structures at scales of hundreds of millions of light years that consists of galactic filaments, great walls and cosmic voids. They arose from initial small fluctuations in the DM density distribution that had grown due to the gravitational attraction, but could have been effectively smoothed by radiation pressure or *free streaming* of DM particles before the matter-radiation equality.

The lower limit on the characteristic length scale of fluctuations in DM density can be translated into a lower limit for the mass of initial clusters of matter (so-called protohalo mass $M_{\rm proto}$). For the non-relativistic (cold) DM (CDM) particles such protohalos could eventually grow to the size of galaxies. On the other hand if the DM particles were moving with relativistic velocities, as it is in the case of so-called hot DM (HDM), the smoothing effect would be large leading to relatively high $M_{\rm proto}$. In this scenario we would expect that galaxies were formed later in the evolution of the Universe due to some other mechanism that caused fragmentation of large protohalos. However, this prediction is in contrast with deep field astronomical observations.

The warm dark matter (WDM) case corresponds to a somewhat intermediate situation between CDM and HDM. N-body simulations suggest that galaxies with WDM halos may be surrounded by a smaller number of dwarf galaxies than in the case of CDM. This could potentially resolve the so-called missing satellite problem, *i.e.*, low number of such surrounding galaxies in the observational data of the Local Group [11]. On the other hand the best theoretically motivated candidates for the DM particles seem to follow the CDM scenario.

Chapter 3

Dark matter

In this chapter we will first discuss the observational evidence of the existence of DM (for a review see, *e.g.*, [12]). In particular, we will focus on selected observations that are most often mentioned in this context. Then we will present several possible candidates for the DM particles with particular emphasis on the ones that are important from the point of view of this thesis.

3.1 Observational evidence

The first speculation about the existence of DM is usually attributed to Zwicky's original paper [13] published more than eighty years ago in which he studied the Coma Cluster. The cluster consists of about $1,000$ galaxies moving along complicated orbits that are determined by gravitational force. Careful analysis of this movement led to the conclusion that there should be a large amount of non-luminous matter contained in the cluster. Zwicky referred to it as *dunkle Materie* (dark matter).

One of the most widely recognized arguments for the existence of DM nowadays is based on galaxy rotation curves, *i.e.*, the relation between orbital velocities v of visible stars or gas and their radial distance r from the center of galaxy. It was first noted in the late 30s [14] and then confirmed more than thirty years later [15, 16] that the outer parts of the M31 disc were moving with unexpectedly high velocities. According to these observations velocities of distant stars in M31 remain constant over the wide range of r. Similar results were later obtained [17] for various other spiral galaxies. This is in contradiction to the standard calculation based on the distribution of visible matter in the galaxy. The balance between gravitational and centrifugal forces

$$GmM/r^2 = mv^2/r, \tag{3.1}$$

outside the region where majority of galaxy mass is enclosed should lead to so-called Keplerian fall

$$v \propto 1/\sqrt{r}, \tag{3.2}$$

i.e., descending (not flat) rotation curve. The flat behavior suggests that the core of the mass distribution in M31 spans much larger distances than it could be inferred from the visible matter. Similar results were also obtained for different galaxies.

The next extremely important argument is associated with gravitational lensing, *i.e.*, the bending of light in a strong gravitational field (for a review see, *e.g.*, [18]). The effect is most easily observed when light passes through a very massive and/or dense object like a galaxy cluster or the central region of a galaxy. Light rays can bend around such an object (lens) which leads to a multiplication of the image of the light source for the observer, as can be seen in Fig. 3.1 (left panel). In this case we call this effect *strong lensing*. In an ideal situation, when the source lies directly behind the circular lens, one can obtain the so-called "Einstein ring". The size and shape of the image can be used to determine the distribution of mass in the lens which can then be compared with the visible mass.

If the lens is not as massive as in the case of strong lensing, or light moves far from the core of the galaxy or cluster, the effect becomes much weaker. However, it can still be analyzed even in the case of individual stars. In particular it was proposed [19, 20] to use such *microlensing* effect to look for DM in the Milky Way in form of Massive Compact Halo Objects (MACHOs) which should cause occasional brightening of stars from nearby galaxies. This strategy led to an exclusion of MACHOs with masses $0.6 \times 10^{-7} < M < 15 M_\odot$ as a dominant form of DM in the Galaxy [21].

Weak lensing corresponds to a somewhat intermediate situation to both cases described above. The most spectacular example of this effect can be seen in the Bullet Cluster which consist of two clusters of galaxies after a recent collision. The hot-gas clouds (observed thanks to the X-ray emission) that contain the majority of the baryonic mass in both clusters, have been decelerated in the collision, while the movement of the galaxies in clusters remained almost intact. The analysis of the gravitational lensing shows that the center of mass for both clusters is clearly separated from the gas clouds as can be seen in Fig. 3.1 (right panel). As a result we conclude that there is large amount of additional mass in both clusters usually identified with DM. It was the first, and so far only, case when one observed a dynamical system with the total center of mass displaced from that of the baryonic visible part of the cluster.

An important role in determining the DM abundance is played by the Cosmic Microwave Background (CMB) radiation that originates from the recombination

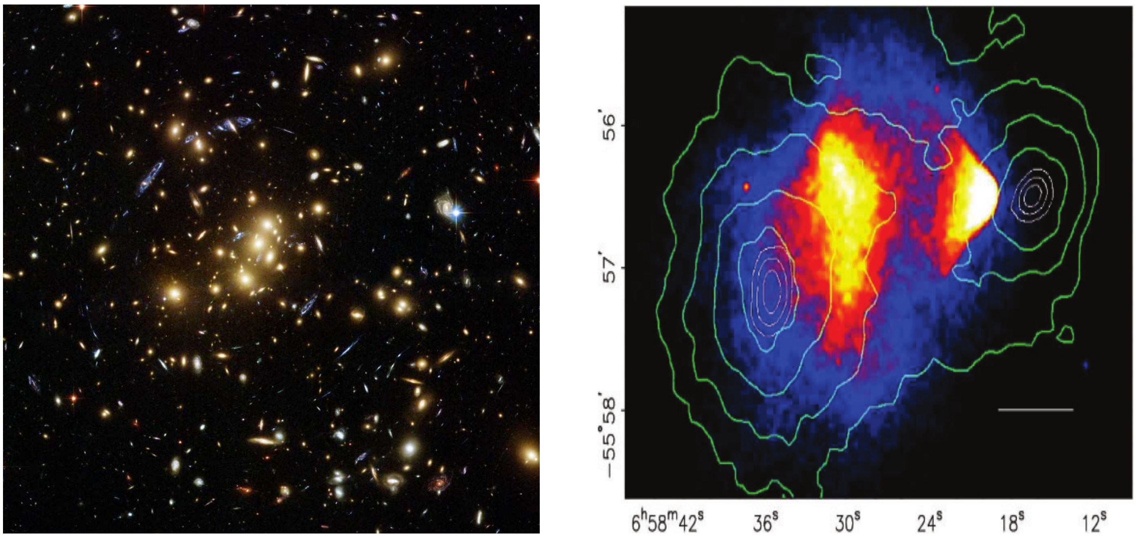

Figure 3.1: *Left panel*: Strong gravitational lensing around galaxy cluster CL0024+17. Taken from Ref. [18]. *Right panel*: Bullet Cluster mass density contours (green) and the distribution of baryonic matter. Taken from Ref. [12].

epoch. It is characterized by the thermal black body spectrum with the temperature $T = 2.7255(6)\,\mathrm{K}$ [7]. Small non-uniformity of the distribution of this temperature corresponds to the tiny fluctuations of the matter density in the early Universe that subsequently gave rise to all the structures in the Universe. The temperature anisotropies are usually expanded in terms of spherical harmonics and then cosmological parameters (*e.g.*, $\Omega_M = \Omega_b + \Omega_{\mathrm{DM}}$ or Ω_b for ordinary baryonic matter) can be obtained by fitting to such spectrum with underlying assumption of some cosmological model, *e.g.*, the ΛCDM model. The currently measured values [3] of Ω_M and Ω_b obtained by fitting the six-parameter ΛCDM model suggest that the matter component of the Universe is dominated by non-baryonic DM,

$$\Omega_b\, h^2 = 0.02207(27), \tag{3.3}$$

$$\Omega_{\mathrm{DM}}\, h^2 = 0.1198(26), \tag{3.4}$$

The remaining dominant contribution $\Omega_\Lambda \simeq 0.685$ account for the so-called *dark energy*. A schematic cartoon showing different contributions to the mass-energy content of the Universe, as well as an all-sky CMB map released by the Planck Collaboration [3] is shown in Fig. 3.2.

Further data about the amount of matter and dark energy components of the Universe can be derived from analyses of baryon acoustic oscillations (BAO)[1], supernovae type Ia or from *Lyman-α forest*. In the case of elliptical galaxies and

[1] They are periodic fluctuations in the density of baryonic matter that originated from opposing effects of gravitational attraction and radiation pressure.

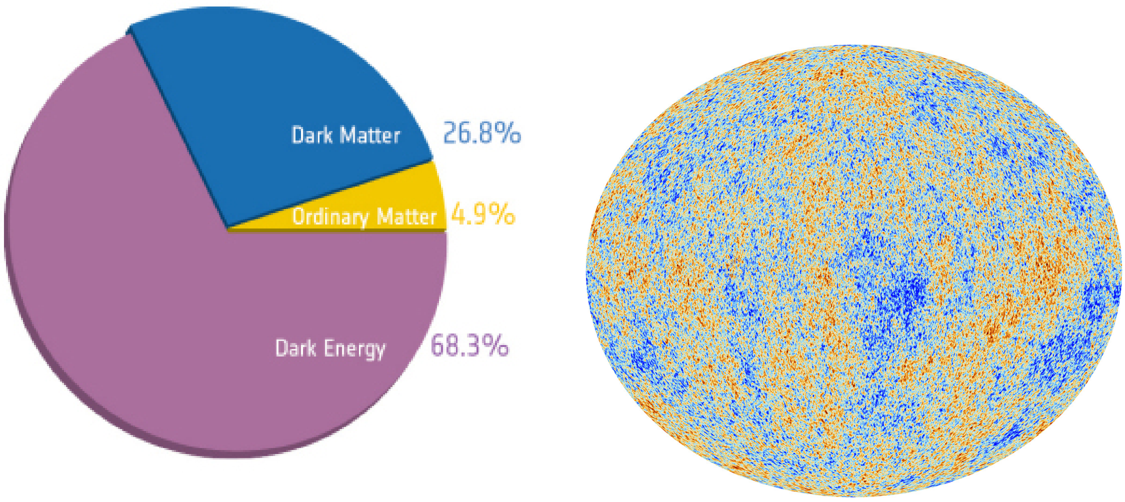

Figure 3.2: *Left panel*: The total mass-energy distribution in the Universe and *Right panel*: the temperature anisotropy of CMB after the first results released by the Planck Collaboration [3].

galaxy clusters another important piece of evidence for the existence of DM comes from the X-ray emission from hot gas (for further discussion see, *e.g.*, [12]).

3.2 Dark matter candidates

We will now discuss some of the most popular candidates for the DM particles (for a recent review see [22]). We will begin with a brief summary of what we can learn from the experimental observations discussed in Section 3.1. We then move on to a more detailed discussion of specific DM candidates.

3.2.1 Properties of dark matter candidates

The first important conclusion derived from observations is that DM particles should carry no electric charge and interact preferably only weakly (or subweakly) with ordinary matter.[2] Moreover, from the CMB data we have already seen in Eqs (3.3) and (3.4) that the baryonic component constitutes only about 20% of all matter in the Universe. Hence a majority of DM should have non-baryonic nature.

We have pointed out that the LSS data accompanied by deep-field observations constrain from above the allowed average velocity of the DM particles. As a result one can conclude that relativistic HDM particles, in particular neutrinos, cannot constitute the majority of DM. It should be dominated by non-relativistic species as in the CDM scenario.

[2]Compare, *e.g.*, the Bullet Cluster where DM clouds passed the gas clouds and each other almost intact.

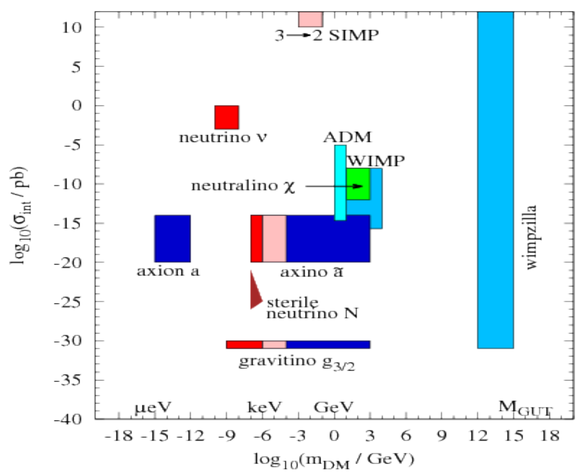

Figure 3.3: Characteristic cross section of DM interactions with ordinary matter as a function of DM mass is shown for some of well-motivated DM candidates. The red, pink and blue colors represent HDM, WDM and CDM, respectively. Taken from Ref. [22].

Last, but not least, the lifetime of the DM particles should be long enough so as to make sure that they can survive until now.

To summarize a good DM candidate should be:

- either stable or long-lived with the lifetime exceeding the age of the Universe (for a recent discussion about lower bounds on the decaying DM lifetime see [23]),
- non-baryonic, *i.e.* with no electric and (preferably) color charges,
- non-relativistic and massive.

In Fig. 3.3 we summarize the features of some of the most popular DM candidates that are motivated by particle theory. The candidate that will be of particular interest to us, namely the *neutralino*, which is a *weakly interacting massive particle* (WIMP) appearing in the MSSM, is characterized by masses from about 1 GeV to 10^4 GeV. It interacts with the electroweak strength. Another possible supersymmetric DM candidates, *i.e.*, the *gravitino* and the *axino* have typically masses lower than in the case of neutralino DM.[3] They also interact significantly more weakly. Some of the candidates presented in Fig. 3.3 can compose either CDM or WDM or even HDM depending on the mass.

[3]The gravitino is the supersymmetric partner of the graviton, the particle that mediates gravitational interactions. The axino is the superpartner of the axion (see Section 3.2.4).

3.2.2 Weakly Interacting Massive Particles

As we have already discussed, neutrinos, the only weakly interacting particles in the SM, remain relativistic and therefore can only constitute HDM. However, in a minimal approach this can be circumvented by taking the DM candidate to be a kind of "heavy neutrino". A simplest such possibility with massive left-handed neutrinos was proposed in [24], but subsequently excluded in light of direct DM searches. However, the main idea survived and is often referred to as a WIMP DM scenario.

Today's value of the DM relic abundance is given by

$$\Omega_\chi h^2 \simeq \frac{m_\chi\, n_\chi(T_0)}{\rho_c}\, h^2 = \frac{m_\chi\, T_0^3}{\rho_c}\, \frac{n_\chi(T_0)}{T_0^3}\, h^2, \tag{3.5}$$

where $T_0 \simeq 2.35 \times 10^{-13}\,\mathrm{GeV}$ [7] is the temperature of the Universe at present and $\rho_\chi(T_0) \simeq m_\chi\, n_\chi(T_0)$ is the corresponding WIMP's energy density. The yield Eq. (2.13) remains constant after freeze-out $Y_f = Y_0$. Using this and applying the condition for freeze-out Eq. (2.12) one can rewrite Eq. (3.5) as

$$\Omega_\chi\, h^2 \simeq \frac{T_0^3}{\rho_c}\, \frac{x_f}{\overline{M}_P}\, \frac{1}{\langle \sigma_{\mathrm{ann}} v_{\mathrm{M\o l}} \rangle_f}\, h^2, \tag{3.6}$$

where T_f is the WIMP freeze-out temperature and

$$x = \frac{m_\chi}{T}. \tag{3.7}$$

The value of x_f can be roughly estimated as follows. Let us assume for simplicity that around freeze-out $n_\chi \approx n_\chi^{\mathrm{eq}}$ with the non-relativistic equilibrium number density from Eq. (2.11). From Eqs (2.12) and (3.6) one then obtains

$$x_f^{3/2} e^{-x_f} \sim \frac{x_f}{m_\chi\, \overline{M}_P\, \langle \sigma_{\mathrm{ann}} v_{\mathrm{M\o l}} \rangle_f} \simeq \Omega_\chi\, \frac{\rho_c}{T_0^3}\, \frac{1}{m_\chi} \simeq \frac{10^{-8}\,\mathrm{GeV}}{m_\chi}, \tag{3.8}$$

where we also assumed $\Omega_\chi\, h^2 \simeq 0.12$ in the last step. Such a rough estimate leads to $x_f \sim 30$ for $m_\chi \sim 100\,\mathrm{GeV} - 10\,\mathrm{TeV}$. More careful checking shows that the appropriate value is closer to $x_f \sim 25$.

Finally we put the estimated value of x_f back into Eq. (3.6) and find

$$\langle \sigma_{\mathrm{ann}} v \rangle_f \simeq 3 \times 10^{-26}\,\mathrm{cm}^3/\mathrm{s}, \tag{3.9}$$

for which the correct value of the WIMP DM relic density is obtained. For typical velocities $v \sim 0.1\,c$ one obtains $\sigma \sim 10^{-36}\,\mathrm{cm}^2$, which corresponds to a cross section of weak strength for WIMP with mass around the electroweak scale. On the other hand, as we will see in Section 4.2.1, some new physics around this energy scale should be expected in order to avoid possible large loop corrections to the Higgs boson mass. This remarkable coincidence is widely known as the *WIMP miracle*. However, it is important to note that one does not have to be strictly confined to the electroweak scale in order for WIMP DM scenario to work. If g is the coupling constant connected with the WIMP annihilation process, then one expects

$$\sigma_{\rm ann} \propto \frac{g^4}{m_\chi^2}. \tag{3.10}$$

Eq. (3.9) can be satisfied for a wide range of masses (from 10 MeV to 10 TeV) and coupling constants (from gravitational to strong) as long as their ratio is kept fixed [25].

In a very precise treatment, which takes into account the dynamics of freeze-out, one needs to solve the set of Boltzmann equations (2.15) and (2.16) to find Y_f. One can identify major steps of this procedure. The first one is to determine the temperature at which freeze-out begins $T_{f,\rm beg}$ which lies close to T_f defined by Eq. (2.12).[4] In the second step one needs to calculate $\langle \sigma_{\rm ann}\, v_{\rm Møl}\rangle$ for T around $T_{f,\rm beg} \approx T_f$. Finally, in the third step, the DM relic density can be effectively calculated by a proper integration of the Boltzmann equation starting from $T_{f,\rm beg}$.[5]

A prototypical example of WIMP, the neutralino, appears in the context of supersymmetric extensions of the SM in which it often plays the role of the LSP. This serves as an important argument (though not the only one) for SUSY as a theory of physics beyond the SM as we will discuss in Section 4.2.3.

3.2.3 Extremely Weakly Interacting Massive Particles

In addition to the neutralino, supersymmetric extensions of the SM provide us also with the other DM candidates, namely the gravitino and the axino (for a recent review see [26]). They belong to a group of so-called *extremely weakly interacting massive particles* (EWIMPs)[6] since they interact much more weakly than ordinary WIMPs. Nevertheless, in general they can still constitute CDM and give the right value of $\Omega_{\rm CDM}h^2$. EWIMPs remain for the most part elusive from the point of

[4] The temperature when the WIMP yield begins to differ from its equilibrium value is also referred to as the decoupling temperature $T_{\rm dec}$. In the following we will denote it by $T_{f,\rm beg}$. Similarly, the freeze-out temperature is often in the literature defined as the temperature at which the yield becomes constant. We will denote this temperature by $T_{f,end}$.

[5] One could in principle omit the first step and then in the third one integrate the Boltzmann equation from $T \approx 0$ (this would also require knowing $\langle \sigma_{\rm ann}\, v_{\rm Møl}\rangle$ for a vast range of T.). Nevertheless, this turns out to be extremely ineffective from the point of view of numerical integration since for $T > T_{f,\rm beg}$ the WIMP number density is determined by its equilibrium value $n_\chi \approx n_\chi^{\rm eq}$ which depends only on m_χ and T. $T_{f,\rm beg}$ has to somehow be estimated. However, such estimates can be accurate enough so that $\Omega_\chi h^2$ can be calculated with high accuracy.

[6] They are sometimes referred to as *super-weakly interacting massive particles* (super-WIMPs) [27] or, particularly in the specific context of "freeze-in" thermal production [28], *feebly interacting massive particles* (FIMPs).

view of current DM searches, but in some specific cases it could be possible in such scenarios to get some interesting hints about the early Universe from collider physics (see, *e.g.*, [29]). On the other hand models with gravitino or axino DM can be tightly constrained by cosmological considerations.

In EWIMP DM scenarios we typically assume that after a period of cosmological inflation, the temperature in the Universe was never high enough for EWIMPs to remain in thermal equilibrium. However, they could still be produced in scatterings and decays of other particles that were themselves in equilibrium. This mechanism will be called *thermal production* (TP). The Boltzmann equation for TP of supersymmetric EWIMP DM reads

$$\frac{dn_{\rm EWIMP}}{dt} + 3Hn_{\rm EWIMP} = \Sigma_{\rm scat} + \Sigma_{\rm dec}, \tag{3.11}$$

where $\Sigma_{\rm scat} = \sum_{i,j} \langle \sigma(i + j \to \tilde{a} + \ldots) v_{\rm Møl} \rangle n_i\, n_j$ and $\Sigma_{\rm dec} = \sum_i \langle \Gamma(i \to \tilde{a} + \ldots) \rangle n_i$ and n_i are the number densities of heavier supersymmetric species. In the RD epoch, when $T \sim a^{-1}$, Eq. (3.11) can be rewritten in terms of the yield and integrated from $T_R = T_{\rm RD}$ to T_0. This leads to

$$Y_{\rm EWIMP,0} = \int_{T_0}^{T_{\rm RD}} dT\, \frac{\Sigma_{\rm scat} + \Sigma_{\rm dec}}{s\, H\, T}. \tag{3.12}$$

We will discuss TP with more details in a more general case of non-instantaneous reheating in Appendix E.

Another possible source of relic EWIMPs is late-time decays of some heavier particle after it froze-out from thermal plasma. In particular for gravitino or axino LSP such a heavier species can be the next-to-LSP [30, 31].[7] This is typically referred to as the *non-thermal production* (NTP) and resulting contribution to the EWIMP DM relic density is given by

$$\Omega_{\rm EWIMP}\, h^2 = \frac{m_{\rm EWIMP}}{m_{\rm NLSP}}\, \Omega_{\rm NLSP} h^2, \tag{3.13}$$

where $\Omega_{\rm NLSP}\, h^2$ is calculated as if the NLSP was actually the DM particle.

EWIMPs can also in principle be produced in direct inflaton field decays at the end of inflation. However, such a mechanism is highly model-dependent and we will not treat this in the rest of the thesis.

3.2.4 Axion

Axion basics An interesting viable DM candidate emerges from the solution to the strong CP problem (for reviews see [32, 33, 34]). Probably the only still viable

[7]It is important to distinguish this from the production in decays of the NLSPs being in thermal equilibrium that by definition is included in TP.

and certainly the most popular solution to this problem was proposed in [35, 36]. It introduces a spontaneously broken (at some energy scale f_a) global chiral $U(1)_{\rm PQ}$ symmetry known as the Peccei-Quinn symmetry. The associated pseudo-Goldstone boson, which is the CP-conserving axion field a, carries PQ charge. To make sure that $U(1)_{\rm PQ}$ possesses gluon anomaly one adds an additional term to the Lagrangian density[8] of Quantum Chromodynamics (QCD) $\mathcal{L}_{\rm QCD}$. It reads

$$\mathcal{L}_a \ni \frac{\alpha_s}{8\pi}\,\frac{a}{f_a}\,G_{a\mu\nu}\widetilde{G}_a^{\mu\nu}. \tag{3.14}$$

It contributes to an effective axion potential and the minimization condition reads $\langle a\rangle = -f_a\bar{\theta}$. The parameter $\bar{\theta}$ is *a priori* required to be tiny[9] $\bar{\theta} \lesssim 10^{-11}$ and it corresponds to the following term in $\mathcal{L}_{\rm QCD}$

$$\mathcal{L}_{\rm QCD} \ni \bar{\theta}\,\frac{\alpha_s}{8\pi}\,G_{a\mu\nu}\widetilde{G}_a^{\mu\nu}. \tag{3.15}$$

This term is shifted away to $\bar{\theta}_{\rm eff} = 0$ after a spontaneous $U(1)_{\rm PQ}$-breaking, $a \to a_{\rm phys} + \langle a\rangle$, as can be seen from Eqs (3.14) and (3.15).

The simplest possibility of $f_a \approx v$ has been ruled-out long ago [37] and we will instead assume $f_a \gg v$. This leads to a light and extremely weakly interacting *invisible axion*. In order to justify the separation between f_a and the EWSB scale one assumes that a resides in an $SU(2)_L\times U(1)_Y$ singlet complex scalar field carrying non-zero PQ charge. However, a still needs to couple to the $SU(3)_c$ sector in order to introduce the gluon anomaly. There are two popular approaches to address this issue. One is the Kim-Shifman-Vainstein-Zakharov (KSVZ) model [38, 39] in which we assign non-zero PQ charges to some new heavy quark(s). The other possibility is the Dine-Fischler-Srednicki-Zhitnitskii (DFSZ) approach [40, 41] where one assigns non-zero PQ charges to two Higgs doublets that couple to both a and the SM quarks (that also carry PQ charges).[10] The gluon anomaly term is then generated by SM quark loops.

The effective axion interaction Lagrangian after integrating out all heavy PQ charged fields can be written up to the lowest order terms in $1/f_a$ as

$$\begin{aligned}\mathcal{L}_{a,\rm int}^{\rm eff} &= c_1\,\frac{(\partial_\mu a)}{f_a}\,\Sigma_q\bar{q}\,\gamma^\mu\,\gamma_5\,q - \Sigma_q(\bar{q}_L\,m\,q_R\,e^{i\,c_2\,a/f_a} + h.c.)\\ &\quad + \frac{c_3}{32\pi^2\,f_a}\,a\,G\,\tilde{G} + \frac{C_{aWW}}{32\pi^2\,f_a}\,a\,W\,\tilde{W} + \frac{C_{aYY}}{32\pi^2\,f_a}\,a\,B\,\tilde{B} + \mathcal{L}_{\rm leptons},\end{aligned} \tag{3.16}$$

[8]In the following, we will simply call $\mathcal{L}$ as the "Lagrangian".

[9]It is where the strong CP problem manifests itself. The smallness of $\bar{\theta}$ is required since the CP-violating term in $\mathcal{L}_{\rm QCD}$ contributes to the neutron electric dipole moment d_n which is tightly constrained by experimental data.

[10]Direct axion-SM quarks couplings are absent since the axion is a gauge singlet.

where (by a partial integration over on-shell quark fields) the c_1 term can be reabsorbed into the c_2 term. The KSVZ case can be identified with $c_1 = 0$, $c_2 = 0$, $c_3 \neq 0$, while the DFSZ one with $c_1 = 0$, $c_3 = 0$, $c_2 \neq 0$. In general, axion models can have both $c_2 \neq 0$ and $c_3 \neq 0$, but their sum turns out to be constant.[11] It is called the domain wall number $N_{\rm DW} = |c_2 + c_3|$.

The axion mass [42] can be estimated to be [32]

$$m_a \simeq 0.6 \times 10^7 \, \text{eV} \left(\frac{\text{GeV}}{f_a} \right), \tag{3.17}$$

where f_a is constrained by astrophysical and cosmological data to $10^9 \, \text{GeV} \lesssim f_a \lesssim 10^{12} \, \text{GeV}$ [34]. However, the upper limit depends on the initial value of the axion misalignment angle and can be relaxed if $\theta_{\rm ini} < \mathcal{O}(1)$ [43].

Axion DM energy density As can be seen from Eq. (3.17) and limits on f_a, axions are typically very light and very weakly interacting. After being produced they could thermalize and fill up the Universe by forming a Bose-Einstein condensate [44] that could closely resemble CDM. Their energy density would then be determined by the mechanism of *bosonic coherent motions* (BCM) [45, 46, 47].

The equation of motion for the scalar field in the expanding Universe is given by

$$\ddot{\phi} + 3 \, H(T) \, \dot{\phi} + \frac{\partial V}{\partial \phi} = 0, \tag{3.18}$$

with the potential energy $V \approx \frac{1}{2} \, m^2(T) \, \phi^2$ for small values of ϕ. Initially the field ϕ moves very slowly so that one can assume $\ddot{\phi} \approx 0$. Thus $3H\dot{\phi} \approx -m^2\phi$. For sufficiently high temperatures of the Universe, one can take additionally $m(T) \approx 0$ and the solution of Eq. (3.18) is given by an approximately constant field $\phi \sim const.$ However, once T decreases and the condition $3H(T) \simeq m(T)$ is achieved the scalar field starts to oscillate giving rise to BCM.

From Eq. (3.18) one can derive the evolution of the average (over one oscillation cycle) energy density of the scalar field $\rho = \langle \dot{\phi}^2 \rangle = 2\langle V \rangle$ that reads

$$\frac{d}{dt} \left(\frac{\rho a^3}{m} \right) = 0, \tag{3.19}$$

Hence, to some approximation $\langle \rho \rangle \sim a^{-3}$ and the oscillating axion field behaves like non-relativistic matter. The same is true for the oscillating inflaton field during the reheating period in the evolution of the Universe.

The list of DM candidates could be supplemented by many other possibilities. For a more extensive discussion see [22] and references therein.

[11]It is preserved by an unbroken finite subgroup of $U(1)_{\rm PQ}$.

Chapter 4

Standard Model and supersymmetry

As we have seen supersymmetry provides a natural class of candidates for DM, the LSP. In this chapter we will first discuss some basic features of the SM and of supersymmetry and then introduce the most popular SUSY extensions of the SM, namely the Minimal Supersymmetric Standard Model and the Next-to-Minimal Supersymmetric Standard Model (NMSSM).

4.1 Standard Model

Before we move to a discussion of supersymmetry it is useful to briefly remind some basic features of the SM.

4.1.1 Structure of the Standard Model

Currently our understanding of fundamental interactions is encoded in the SM of particle physics. After its final formulation in the 60s and the 70s of the last century, remarkable effort was put into the experimental verification of its predictions. In particular, several new elementary particles were discovered, among them the c, b and t quarks, heavy gauge bosons $W^{\pm}$ and Z, the tau lepton τ and its neutrino ν_τ. Last, but not least, the remaining missing particle species from the SM, namely the Higgs boson, has recently been found by the CMS [1] and ATLAS [2] Collaborations at the LHC.

The SM provides us with an elegant description of interactions among quarks and leptons, *i.e.*, all basic constituents of matter that we have already discovered. The electroweak theory succeeded in unifying the electromagnetic and the weak forces, while the strong interactions between quarks are described by the quantum chromodynamics. Importantly, one needs to notice that each fundamental force is in the framework of the SM accompanied by an appropriate symmetry. Requiring that the Lagrangian of the theory $\mathcal{L}$ is invariant under a specified local gauge group of transformations leads unavoidably to the introduction of additional terms in $\mathcal{L}$ that are associated with so-called gauge fields. They couple to the matter content of $\mathcal{L}_{\text{SM}}$. Such a symmetry group is often referred to as a *gauge group* or *gauge symmetry group*. In particular, the gauge groups for the electroweak and strong interactions are $SU(2)_L \times U(1)_Y$ and $SU(3)_c$, respectively.[1]

In the theoretical description of the SM one decomposes quark and lepton spinors into chiral components thanks to the appropriate projection operators $P_L = (1-\gamma_5)/2$ and $P_R = (1+\gamma_5)/2$. The "weak" $SU(2)_L$ group transformations act differently on left and right chiral fields. The former are grouped into doublets under $SU(2)_L$, while the latter remain singlets, *i.e.*, effectively they are not sensitive to the weak interactions. The conserved quantum number associated with the $SU(2)_L$ group is called the weak isospin T. Its third component is equal to $T^3 = \pm 1/2$ for the components of the left-chiral doublets and $T^3 = 0$ for the right-chiral singlets.

In the framework of the unified electroweak theory we introduce another conserved quantum number, the weak hypercharge Y. It is associated with the $U(1)_Y$ subgroup[2] of $SU(2)_L \times U(1)_Y$ and can be written in terms of the electric charge Q and the third component of the weak isospin as $Y = 2(Q - T^3)$. The matter component of the SM consists of quarks and leptons characterized by various values of Y and Q. The set of elementary particles is further enlarged when one takes into account representations of the $SU(3)_c$ group. In particular quarks turn out to be color triplets, while leptons are color singlets.

In addition to the matter fields, the SM contains vector fields of the intermediate spin-one gauge bosons. In the electroweak sector B_μ and $W_\mu^{1,2,3}$ fields correspond to the generators of the $U(1)_Y$ and $SU(2)_L$ groups, respectively. The eight generators of the $SU(3)_c$ group lead to a so-called *color octet* of the gluon fields $G_\mu^{1,2,\ldots,8}$.

Importantly, in the Lagrangian of the SM the mass terms for the fermions $m\,\bar{\psi}\,\psi$ are allowed by the $SU(3)_c$ gauge transformations, but are forbidden by the $SU(2)_L$ group since

$$m\,\bar{\psi}\,\psi = m\,\bar{\psi}\left(P_L + P_R\right)\psi = m\,\bar{\psi}\left(P_L^2 + P_R^2\right)\psi = m\,\bar{\psi}_R\,\psi_L + m\,\bar{\psi}_L\,\psi_R, \tag{4.1}$$

and terms that consist of one left-chiral and one right-chiral field cannot be invariant as both fields transform under different representations of the $SU(2)_L$ group. A careful examination of the transformation of the gauge fields ensures that the mass terms for them are also forbidden by the $SU(2)_L \times U(1)_Y$ symmetry. In the next section we will proceed with the discussion of how to incorporate masses for the matter and gauge fields of the SM.

[1]The lower index c in $SU(3)_c$ stands for *color*. The lower indices Y and L denote *hypercharge* and *left chiral*, respectively (see a discussion below).

[2]$U(1)_Y$ is different from $U(1)_{\text{em}}$ corresponding to the electromagnetic interactions.

4.1.2 Spontaneous symmetry breaking and the Higgs mechanism

Let us start here with some general remark. The fact that a Lagrangian $\mathcal{L}$ of a theory preserves some symmetry does not necessarily mean that this is also true for the ground state of a quantum system described by $\mathcal{L}$. This is in analogy to the well-known behavior of the solutions to the classical equation of motion for a particle in the Newtonian description of gravity. The equation itself is rotationally invariant, but each given solution describes motion along an elliptical orbit that is moreover limited to a plane. However, one can obtain other solutions by rotating a specific one, *i.e.*, by applying symmetry transformations that preserve the equation of motion. In other words one could simply state that the whole set of solutions is invariant under the symmetry group. The symmetry is “hidden” when one takes into account only a single solution.

Similarly, when the symmetry transformation of a Lagrangian of a quantum system can be described by a set of continuous parameters and the ground state is not invariant under this symmetry, we expect to have a continuous set of degenerate ground states. Once we choose one of these ground states, the underlying symmetry becomes “hidden”. In other words it does not manifest itself explicitly in the expansion of the Lagrangian around the chosen ground state. We call such a behavior as *spontaneous breaking of the symmetry*.

The Lagrangian $\mathcal{L}$ can still be invariant under some residual symmetry group which contains a smaller number of generators. According to *Goldstone's theorem* [48, 49, 50, 51] for every spontaneously broken continuous symmetry there has to appear in a theory a set of massless *Goldstone bosons*. The number of such bosons is determined by the number of generators that vanished during spontaneous symmetry breaking. However, after applying such a procedure one may obtain the Lagrangian containing fields with the total number of degrees of freedom greater than in the initial $\mathcal{L}$. That means that some of the fields present in $\mathcal{L}$ are unphysical and can be removed by an appropriate choice of the gauge. Thanks to this, some of the massless Goldstone bosons can be absorbed by the gauge bosons that then become massive. This is the general principle of the celebrated Higgs mechanism [52, 53, 54, 55, 56].

In order to perform a spontaneous symmetry breaking of the $SU(2)_L \times U(1)_Y$ group in the SM (for a more extensive discussion see, e.g., [57]) one introduces additionally an $SU(2)_L$ doublet of complex scalar fields $\Phi^\dagger = (\psi^+, \psi^0)^*$ that contains four degrees of freedom. As a result it is possible to obtain three massive gauge bosons since this requires three massless degrees of freedom to be absorbed. The remaining degree of freedom from the Φ field will not produce the massless Goldstone boson, since $U(1)_{\mathrm{em}}$ for Quantum Electrodynamics (QED) remains a physical symmetry of the Lagrangian.[3] The Lagrangian associated with this new field is given by

$$\mathcal{L}_{\text{Higgs}} = (D^\mu \Phi)^\dagger (D_\mu \Phi) - \mu^2 \Phi^\dagger \Phi - \lambda (\Phi^\dagger \Phi)^2. \tag{4.2}$$

It is expanded around the minimum in the direction of the neutral component of Φ which develops a vacuum expectation value (vev) v for $\mu^2 < 0$

$$\Phi \to \frac{1}{\sqrt{2}} \begin{pmatrix} 0 \\ v + h \end{pmatrix}, \tag{4.3}$$

where $v = (-\mu^2/\lambda)^{1/2}$ and h is called the Higgs field. After a transformation to the unitary gauge one obtains three massive gauge bosons, namely the $W^\pm$ and Z bosons, and one massless photon field A_μ. They can be rewritten in terms of the initial fields B_μ and W_μ^a as

$$A_\mu = \frac{g_2 W_\mu^3 + g_1 B_\mu}{\sqrt{g_2^2 + g_1^2}}, \qquad Z_\mu = \frac{g_2 W_\mu^3 - g_1 B_\mu}{\sqrt{g_2^2 + g_1^2}}, \qquad W_\mu^\pm = \frac{1}{\sqrt{2}} (W_\mu^1 \mp i W_\mu^2). \tag{4.4}$$

When one puts these new fields into the $(D^\mu \Phi)^\dagger (D_\mu \Phi)$ term in $\mathcal{L}_{\text{Higgs}}$, one obtains the mass terms for W and Z bosons with masses

$$m_W = \frac{1}{2} v\, g_2, \qquad m_Z = \frac{1}{2} v \sqrt{g_1^2 + g_2^2}. \tag{4.5}$$

From these one can also calculate the actual value of the vev $v \simeq 246\,\text{GeV}$.

The same doublet of complex scalar fields with hypercharge $Y = 1$ and isodoublet $\widetilde{\Phi} = i\,\tau_2\,\Phi^*$ with $Y = -1$ can be used to generate fermion masses by introducing additional $SU(2)_L \times U(1)_Y$ invariant terms in the Lagrangian

$$\mathcal{L}_{\text{Yukawa}} = -\lambda_e^{ij}\, \bar{L}_i \cdot \Phi\, e_{R,j} - \lambda_d^{ij}\, \bar{Q}_i \cdot \Phi\, d_{R,j} - \lambda_u^{ij}\, \bar{Q}_i \cdot \widetilde{\Phi}\, u_{R,j} + h.c., \tag{4.6}$$

where λ_e, λ_d and λ_u are Yukawa matrices. Expanding around the ground state and applying unitary gauge we obtain the fermion mass matrices

$$m_e = \frac{\lambda_e\, v}{\sqrt{2}}, \qquad m_d = \frac{\lambda_d\, v}{\sqrt{2}}, \qquad m_u = \frac{\lambda_u\, v}{\sqrt{2}}. \tag{4.7}$$

Last, but not least, one can derive also the interaction terms for the Higgs boson from $(D^\mu \Phi)^\dagger (D_\mu \Phi)$ and its mass from the scalar potential $V(\Phi) = \mu^2 \Phi^\dagger \Phi + \lambda (\Phi^\dagger \Phi)^2$,

$$m_h^2 = 2\,\lambda\, v^2 = -2\mu^2. \tag{4.8}$$

The Higgs boson mass remained a free parameter of the SM with only mild theoretical constraints (see, e.g., discussion in [57]).

[3]Hence only three generators of the $SU(2)_L \times U(1)_Y$ group were absorbed.

4.2 Challenges to the Standard Model

The SM of particle physics that we described in the previous section, is indisputably an extremely successful theory. It predicted many experimental results that provided stringent tests of this model and allowed one to measure its undetermined parameters. However, despite such an enormous achievement, there still remain several unresolved puzzles at the theoretical side that are often interpreted as hints for "new physics" beyond the SM (BSM). In this section we will discuss several such issues with a particular emphasis on the ones that can find a successful resolution within the framework of supersymmetry.

4.2.1 Hierarchy problem

One such open question is called the *hierarchy problem*. It is sometimes referred to as *big hierarchy problem* in order to distinguish from the *little hierarchy problem* (see a discussion in Section 4.7). It originates from the fact that the scalar mass in the SM, *i.e.*, the Higgs boson mass, is not protected from receiving large quantum corrections by either the chiral or the gauge symmetry, in contrast to the case of the fermion or gauge boson masses. As we now know from the actual measurements [1, 2], but even before could expect from simple estimations using Eq. (4.8) and the value of v, the Higgs boson mass is of the order of about 100 GeV. However, the couplings of the Higgs field to the fermions, which are of the form $\lambda\, h\, \bar{f}\, f$, give rise to loop corrections to m_h such that [58]

$$\Delta_f(m_h^2) \simeq \frac{N_f\,\lambda_f^2}{8\pi^2}\Big[-\Lambda_{\rm UV}^2 + 6\,m_f^2\,\log\frac{\Lambda_{\rm UV}}{m_f} - 2m_f^2\Big] + \mathcal{O}\Big(\frac{1}{\lambda_{\rm UV}^2}\Big), \tag{4.9}$$

where N_f is the number of fermions with given m_f and λ_f. The Feynman diagram can be found in Fig. 4.1a. The cut-off scale Λ_{UV} is introduced to regulate the otherwise divergent loop integral and is usually interpreted as the energy scale at which effects from BSM physics enter. If there was no such new physics up to the Planck scale, $\Lambda_{\rm UV} \sim \overline{M}_{\rm Pl}$, or the GUT scale, $\Lambda_{\rm UV} \sim M_{\rm GUT}$, then in principle the quantum corrections to m_h^2 in the SM would be as large as $\Lambda_{\rm UV}^2 > 10^{30}$ GeV. This could be technically canceled with the appropriate counterterm, but would require fine-tuning with a precision at least of the order of 10^{-30} .

One way to solve this issue [60, 61, 62, 63, 64] is to introduce to a theory additional scalar fields. For a single such field S we assume the coupling to the Higgs field of the form $\lambda_S\,|h|^2\,|S|^2$ with[4] $\lambda_S = -\lambda_f^2 = -2m_f^2/v^2$ and $N_S = 2\,N_f$. The Feynman diagrams for the loop corrections are shown in Fig. 4.1b. The resulting

[4]Compare eq. (4.7) for diagonal fermion mass matrices,

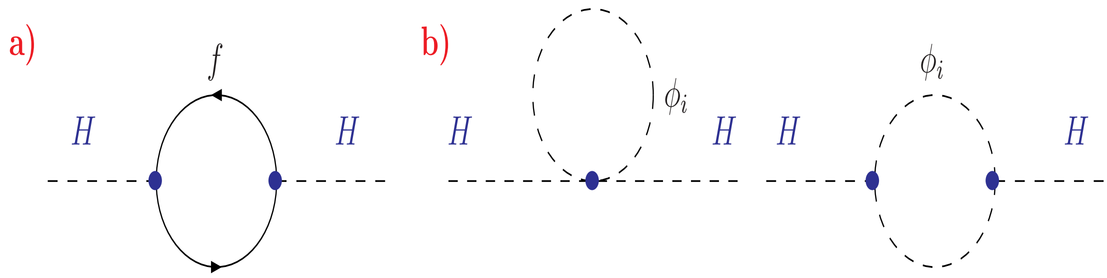

Figure 4.1: Feynman diagrams for the loop corrections of the Higgs boson mass. Contribution from fermions (a) and scalars (b) are shown. Taken from Ref. [59].

contribution to m_h^2 from the scalar field is given by

$$\Delta_S(m_h^2) \simeq \frac{N_S\,\lambda_s}{16\pi^2}\left[-\Lambda_{\rm UV}^2 + 2\,m_S^2\,\log\frac{\Lambda_{\rm UV}}{m_S}\right] - \frac{\lambda_S^2\,v^2}{16\pi^2}\left[-1 + 2\,\log\left(\frac{\Lambda_{\rm UV}}{m_S}\right)\right] + \mathcal{O}\Big(\frac{1}{\lambda_{\rm UV}^2}\Big). \tag{4.10}$$

The quadratic divergences between Eq. (4.9) and Eq. (4.10) cancel and as a consequence one obtains

$$\Delta m_h^2 \simeq \frac{N_f\,\lambda_f^2}{4\pi^2}\left[\left(m_f^2 - m_S^2\right)\,\log\left(\frac{\Lambda_{\rm UV}}{m_S}\right) + 3\,m_f^2\,\log\left(\frac{m_f}{m_S}\right)\right] + \mathcal{O}\Big(\frac{1}{\Lambda_{\rm UV}^2}\Big). \tag{4.11}$$

However, the cancellation obtained in this way is valid only for the 1-loop corrections and in principle the quadratic divergence could reappear in some higher order diagrams. In order to forbid this, one needs to introduce stricter assumption about the extension of the SM. An elegant and efficient way of doing this is to assume a proper symmetry relating the fermionic and the bosonic sectors of the model, so that in each order of the loop calculations a quadratically divergent contribution from fermionic loops will be necessarily canceled by an appropriate scalar contribution. This is achieved within the framework of *supersymmetry* which we will introduce in Section 4.3.

4.2.2 Gauge couplings unification

Another usually mentioned complication within the SM is related to the *gauge coupling unification* around the GUT scale. One of the most remarkable successes in constructing the SM was associated with the unification of the electromagnetic and weak interactions. Needless to say that the concept of the electromagnetic theory itself arose from initially disconnected electric and magnetic phenomena. Following this line of reasoning it could be assumed that there exists an energy scale at which strong and electroweak forces should manifest themselves as a single interaction, *i.e.*, corresponding gauge couplings should unify into a single coupling.

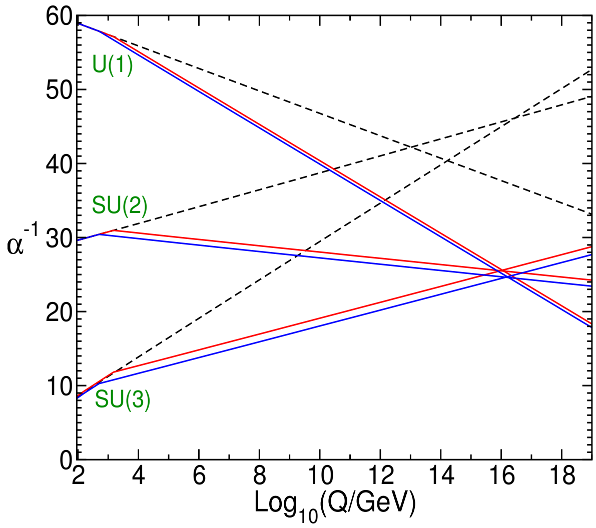

Figure 4.2: Two-loop renormalization group evolution of the gauge couplings ($\alpha_a = g_a^2/4\pi$) of the SM (dashed lines) and the Minimal Supersymmetric Standard Model (solid lines). Taken from Ref. [67].

Consequently the product of the gauge groups $SU(3)_c \times SU(2)_L \times U(1)_Y$ should be embedded in some larger group of symmetry of the GUT theory, *e.g.*, $SU(5)$ [65] or $SO(10)$ (for a review see, *e.g.*, [66]).

The energy scale of grand unification can be estimated due to running of the gauge couplings from an infrared measured value to the high energy scale using Renormalization Group Equations (RGEs). Applying this to the SM one finds that the unification of the gauge couplings is not achieved. Early estimates in the 80s showed $M_{\text{GUT}} \sim 10^{15}$ GeV for the SM. However, after obtaining results from the Large Electron-Positron Collider (LEP), where the gauge couplings were precisely measured, it turned out that the lines describing the RGE evolution intersect in pairs around the energy scale $M_{\text{GUT}} \sim 10^{13} - 10^{17}$ GeV (see Fig. 4.2 where $\alpha_a = g_a^2/4\pi$). In principle, this still allows one to estimate the value of the GUT scale, though with quite a big uncertainty. On the other hand in the case of minimal supersymmetric extension of the SM the unification is strongly improved as can be seen in Fig. 4.2 leading to $M_{\text{GUT}} \sim 10^{16}$ GeV.

4.2.3 Dark matter

According to experimental evidence that was discussed in Section 3.1, baryonic matter makes up only about 5% of the total mass-energy of the Universe. A significant part of the rest (about 27%) is attributed to dark matter. The SM does not provide us with any satisfactory candidate for the DM particle (see a discussion in Section 3.2). This can be circumvented in the framework of SUSY as it is discussed in Section 4.3.4.

Yet another issue is connected with the *vacuum stability*. As has been recently discussed in [68], the measured values of the Higgs boson mass [1, 2] $m_h \simeq 126\,\mathrm{GeV}$ and the top quark mass [69] $m_t \simeq 173.3\,\mathrm{GeV}$ point towards the metastable vacuum state of the SM. In the case of the MSSM one finds a stable vacuum for a wide range of parameters [70].

4.3 Basics of supersymmetry

Having justified the motivation for considering the BSM physics, in particular the supersymmetric extension of the SM, we will now describe the fundamental features of supersymmetry (for reviews see, *e.g.*, [67, 71] or textbooks, *e.g.*, [72, 73]).

4.3.1 Algebra of supersymmetry

As we have already mentioned in Section 4.2.1, in order to avoid large quantum corrections to the mass of the Higgs boson to all orders in perturbation theory it is sufficient to assume that a special symmetry holds between fermions and bosons. However, symmetries of the S-matrix of a quantum field theory cannot be chosen arbitrarily. In particular due to the Coleman-Mandula no-go theorem [74] if such a symmetry was generated by bosonic operators B, *i.e.*, obeying commutation relations, it would have to be connected with the Poincare group in a trivial way as a direct product. Then, according to Witten's [75] interpretation of this result, non-zero scattering amplitudes can be obtained only for discrete scattering angles and they wouldn't be analytic functions of the Mandelstam variables. Moreover, a direct product of the symmetry group and the Poincare group would manifest itself in vanishing commutators between their generators. As a result B would commute with the mass-square operator P^2 and the square of the Pauli-Lubanski vector W^2.[5] Therefore multiplets of such a symmetry could only contain particles with the same mass and (more importantly for us) the same spin.

These difficulties can be circumvented if one assumes that the internal symmetry is generated by anti-commuting (fermionic, spinorial) operators Q, $Q^\dagger$.[6] Such operators are still a subject of important constraints from the Coleman-Mandula theorem. A careful analysis of this issue led to the formulation of the well-known Haag-Łopuszański-Sohnius theorem [76], which can be summarized in a set of (anti-)

[5] $W^2 = W_\mu W^\mu$ is a Lorentz invariant operator that commutes with P^μ. Thus it is a Casimir operator of the Lorentz group (its eigenvalues can label the irreducible representations of the group) and is used to label the spin s via

$$W^2 = -m^2\, s\,(s+1),$$

where m is the mass of a particle.

[6] Here we assume for simplicity that there is only one pair of such generators Q, $Q^\dagger$, *i.e.*, we limit ourselves to so-called $\mathcal{N} = 1$ supersymmetry.

commutation relations for the Qs and the generators of the Poincare group. Such an algebra is often referred to as supersymmetry algebra or super-Poincare algebra.

4.3.2 Supermultiplets and particle content of supersymmetry

One important consequence that can be derived from the (anti-)commutation relations mentioned in the previous section is that W^2 is not the Casimir operator of the super-Poincare algebra. As a result *supermultiplets*, *i.e.*, irreducible representations of the supersymmetry algebra, can now contain both bosons and fermions.

On the other hand, the mass-square operator P^2, as well as the generators of the gauge transformations still commute with Qs. Hence supermultiplets should contain only the particles with the same mass, electric charge, weak isospin and color. However, in this case superpartners of the fermions of the SM should have already been discovered. The lack of such experimental observations points towards the necessity of introducing a mechanism of supersymmetry breaking (see Section 4.4).

Each supermultiplet must contain an equal number of bosonic n_B and fermionic n_F degrees of freedom.[7] This serves as an useful guiding principle. In particular, a single Weyl spinor for a fermion of the SM has two helicity degrees of freedom n_F.[8] The corresponding bosonic superpartner can then be described as a complex scalar field with $n_B = 2$. They both form a so-called *chiral (matter, scalar) supermultiplet*. The scalar superpartners are usually called *squarks* or *sleptons* and are denoted with tilde over the particle symbol, *e.g.*, tau sneutrino $\tilde{\nu}_\tau$. The superpartners of left-handed or right-handed fermions are often marked with corresponding “handedness”, *e.g.*, “right” stop $\tilde{t}_R$, although this does not refer to a specific helicity state, since they are scalars.

On the other hand for a vector gauge boson of the SM (with $n_B = 2$ degrees of freedom before spontaneous symmetry breaking) the corresponding superpartner can be a single massless spin-1/2 Weyl fermion ($n_F = 2$) within a so-called *gauge (vector) supermultiplet*. The rule to create a name of a superpartner of the SM gauge boson is to add suffix *-ino*, *i.e.*, we obtain bino $\tilde{B}$, wino $\tilde{W}$ and gluino $\tilde{g}$. Gauginos must transform as the adjoint representation of the gauge groups (just as the gauge bosons) which is its own conjugate. As a result the gauginos are identical to their anti-particles and they are examples of so-called *Majorana fermions*.

In the case of the $SU(2)_L$ doublet of complex scalar Higgs fields, introduced in the mechanism of EWSB in the SM, one could simply obtain proper supermultiplets

[7] This can be verified by evaluating $0 = \sum_i \langle i|(-1)^{2s} P^\mu|i\rangle = p^\mu (n_B - n_F)$ for a subset of states $|i\rangle$ that correspond to a fixed eigenvalue p^μ of the operator P^μ (see, *e.g.*, [67]).

[8] One has to remember that particles within each supermultiplet should not differ by weak isospin. Hence it is natural to use two-component Weyl spinors to describe fermionic fields within a supersymmetry.

Name	Symbol	spin-0	spin-1/2	Y
"left" squarks (spin-0), left quarks (spin-1/2)	Q_1	$(\tilde{u}_L\ \tilde{d}_L)$	$(u_L\ d_L)$	$\frac{1}{3}$
	Q_2	$(\tilde{c}_L\ \tilde{s}_L)$	$(c_L\ s_L)$	
	Q_3	$(\tilde{t}_L\ \tilde{b}_L)$	$(t_L\ b_L)$	
"right" up-type squarks, right up-type quarks	$\bar{u}^1 = \bar{u}$	$\tilde{u}^*_R$	$u^\dagger_R$	$-\frac{4}{3}$
	$\bar{u}^2 = \bar{c}$	$\tilde{c}^*_R$	$c^\dagger_R$	
	$\bar{u}^3 = \bar{t}$	$\tilde{t}^*_R$	$t^\dagger_R$	
"right" down-type squarks, right down-type quarks	$\bar{d}^1 = \bar{d}$	$\tilde{d}^*_R$	$d^\dagger_R$	$\frac{2}{3}$
	$\bar{d}^2 = \bar{s}$	$\tilde{s}^*_R$	$s^\dagger_R$	
	$\bar{d}^3 = \bar{b}$	$\tilde{b}^*_R$	$b^\dagger_R$	
"left" sleptons, left leptons	L_1	$(\tilde{\nu}_e\ \tilde{e}_L)$	$(\nu_e\ e_L)$	-1
	L_2	$(\tilde{\nu}_\mu\ \tilde{\mu}_L)$	$(\nu_\mu\ \mu_L)$	
	L_3	$(\tilde{\nu}_\tau\ \tilde{\tau}_L)$	$(\nu_\tau\ \tau_L)$	
"right" sleptons, right leptons	$\bar{e}^1 = \bar{e}$	$\tilde{e}^*_R$	$e^\dagger_R$	2
	$\bar{e}^2 = \bar{\mu}$	$\tilde{\mu}^*_R$	$\mu^\dagger_R$	
	$\bar{e}^3 = \bar{\tau}$	$\tilde{\tau}^*_R$	$\tau^\dagger_R$	
Higgs, higgsinos	H_u	$(H_u^+\ H_u^0)$	$(\tilde{H}_u^+\ \tilde{H}_u^0)$	$+1$
	H_d	$(H_d^0\ H_d^-)$	$(\tilde{H}_d^0\ \tilde{H}_d^-)$	-1

Table 4.1: Chiral supermultiplets in the MSSM with corresponding hypercharges. Weak isodoublets are shown in brackets. For each row the upper label in the first column refers to spin-0 scalar particles, while the lower to spin-1/2 fermions.

by adding appropriate Weyl spinors, namely higgsinos. However, it turns out that one such doublet is not enough when constructing the MSSM. This is due to the cancellation of the gauge anomalies, as well as a mechanism that gives masses to up- and down-type quarks. As a result in the MSSM we need to add the second weak isodoublet of the Higgs superfields that is characterized by the opposite value of the weak hypercharge. We denote positive and negative hypercharge isodoublets of the complex scalar fields by H_u and H_d, respectively.

The list of all matter particle content and Higgs boson supermultiplets in the MSSM can be found in Table 4.1. We apply a standard convention for constructing "right-handed" supermultiplets in terms of their conjugates, *i.e.*, using left-handed Weyl spinors. As a result we put bar over respective symbols which should be treated as a part of their name.

4.3.3 Supersymmetric Lagrangian density

Having discussed the particle content of the MSSM we will now describe how to construct a Lagrangian for a supersymmetric model. Before we present a particular example of the MSSM we first make some more general remarks.

Lagrangian for chiral supermultiplets We begin with a Lagrangian $\mathcal{L}$ containing a set of n chiral supermultiplets with complex scalar fields ϕ_i and Weyl spinors ψ_i, where $i = 1, \ldots, n$. A particular example of such a Lagrangian for $n = 1$ is the massless, non-interacting *Wess-Zumino model* [77]. We additionally include in $\mathcal{L}$ a term describing a set of auxiliary complex scalar fields F_i that vanish on-shell due to their equations of motion

$$F_i = F_i^* = 0. \tag{4.12}$$

This turns out to be needed in order to make sure that supersymmetric transformations acting on fields off-shell generate a closed algebra. The F_i fields with two degrees of freedom are also needed off-shell to account for two additional real degrees of freedom in the fermionic component.

The Lagrangian for the n interacting chiral fields is given by

$$\mathcal{L}_{\text{chiral}} = \mathcal{L}_{\text{chiral,free}} + \mathcal{L}_{\text{chiral,int}}, \tag{4.13}$$

where

$$\mathcal{L}_{\text{chiral,free}} = -\partial^\mu \phi^{i*}\, \partial_\mu \phi_i + i\psi^{i\dagger}\, \bar{\sigma}^\mu\, \partial_\mu \psi_i + F^{i*} F_i, \tag{4.14}$$

and the interaction Lagrangian can be written as

$$\mathcal{L}_{\text{chiral,int}} = \Big(-\frac{1}{2} W^{ij} \psi_i \psi_j + W^i F_i \Big) + c.c, \tag{4.15}$$

with W^{ij} and W^i being polynomials in the scalar fields ϕ_i, ϕ^{i*} with degrees 1 and 2, respectively. Moreover, they can be written as functional derivatives of a so-called *superpotential* calculated with respect to the complex scalar fields

$$W^i = \frac{\delta W}{\delta \phi_i} \qquad W^{ij} = \frac{\delta^2 W}{\delta \phi_i\, \delta \phi_j}. \tag{4.16}$$

The superpotential W provides a unique description of interactions in the considered model. It is a holomorphic polynomial of the complex scalar fields that can be written as

$$W = L^i \phi_i + \frac{1}{2} M^{ij} \phi_i \phi_j + \frac{1}{6} y^{ijk} \phi_i \phi_j \phi_k, \tag{4.17}$$

where, as we will see below, M^{ij} corresponds to the (symmetric) mass matrix for the mass-degenerate ϕ_i and ψ_i fields and y^{ijk} are Yukawa couplings between ϕ_k and the two fermionic fields $\psi_i \psi_j$. From Eq. (4.17) we see that y^{ijk} must be totally symmetric. Moreover, in the MSSM we take *a priori* $L^i = 0$, since non-zero L^i would only be allowed for a gauge singlet chiral supermultiplet. However, such linear terms in the superpotential do play an important role in supersymmetry breaking.

The equations of motion (4.12) for the auxiliary fields F_i are now modified

$$F_i = -W_i^*, \qquad F^{i*} = -W^i. \tag{4.18}$$

Because of this one can remove the F_is from $\mathcal{L}$.

Lagrangian for gauge supermultiplets In the case of a gauge supermultiplet we have to consider massless gauge boson fields A_μ^a and fermionic fields λ^a. Both of them have two degrees of freedom on-shell, but off-shell we obtain $n_B = 3$ and $n_F = 4$. Similarly to the chiral supermultiplets, we add a set of auxiliary real (not complex) scalar fields D^a.

The supersymmetry invariant Lagrangian for a gauge supermultiplet is given by

$$\mathcal{L}_{\text{gauge}} = -\frac{1}{4} F_{\mu\nu}^a F^{\mu\nu a} + i\lambda^{a\dagger}\bar{\sigma}^\mu D_\mu \lambda^a + \frac{1}{2} D^a D^a. \tag{4.19}$$

The auxiliary fields D^a can be removed from $\mathcal{L}$ using their equations of motion

$$D^a = -g(\phi^* T^a \phi). \tag{4.20}$$

Total $\mathcal{L}$ The Lagrangian for the supersymmetric model contains now both $\mathcal{L}_{\text{chiral}}$ and $\mathcal{L}_{\text{gauge}}$. There are also some additional interaction terms that are allowed and that incorporate fields from both types of supermultiplets

$$\mathcal{L} = \mathcal{L}_{\text{chiral}}^{\partial_\mu \to D_\mu} + \mathcal{L}_{\text{gauge}} - \sqrt{2} g \big(\phi^* T^a \psi\big)\lambda^a - \sqrt{2} g \lambda^{a\dagger}\big(\psi^\dagger T^a \phi\big) + g\big(\phi^* T^a \phi\big) D^a. \tag{4.21}$$

In order to make sure that $\mathcal{L}_{\text{chiral}}$ is gauge invariant one needs to replace ordinary derivatives with covariant ones.

Scalar potential From the Lagrangian Eq. (4.21) we can derive the *scalar potential* of a supersymmetric model. It is given by

$$\begin{aligned} V(\phi, \phi^*) &= F^{i*} F_i + \frac{1}{2} D^a D^a && (4.22) \\ &= M_{ik}^* M^{kj} \phi^{i*} \phi_j + \frac{1}{2} M^{in} y_{jkn}^* \phi_i \phi^{j*} \phi^{k*} + \frac{1}{2} M_{in}^* y^{jkn} \phi^{i*} \phi_j \phi_k \\ &\quad + \frac{1}{4} y^{ijn} y_{kln}^* \phi_i \phi_j \phi^{k*} \phi^{l*} + \frac{1}{2} g_a^2 (\phi^* T^a \phi)^2, && (4.23) \end{aligned}$$

where in Eq. (4.23) we used Eqs (4.16), (4.17), (4.18) and (4.20). We identify a so-called F-term and a D-term in Eq. (4.22), respectively. The scalar potential is always greater than zero as a sum of squares.

As one can see, the mass matrix for the bosonic component of a chiral supermultiplet is given by $(M^2)_{ij} = M_{ik}^* M^{kj}$. The same mass matrix is obtained for the fermionic component, as can be verified using appropriate identities for two-component Weyl spinor fields (see, e.g., [67]). One could also argue that this must be the case based on general arguments for supermultiplets from Section 4.3.2. In other words the bosonic and fermionic components have the same mass.

Another important issue is that the scalar potential is fully determined by the mass terms, as well as by the Yukawa and the gauge couplings. As a result, in particular for the Higgs fields in the MSSM the quartic couplings are no longer free parameters, in contrast to the SM.

4.3.4 R-parity

The lightest of superparticles, the LSP, can be stable due to a conservation of so-called *R-parity* that originates from the *matter parity*. The latter symmetry is introduced to the supersymmetric models in order to suppress baryon B and lepton L number violating terms in the Lagrangian. The conserved quantum number for the R-parity is given by

$$P_R = (-1)^{3(B-L)+2s}, \tag{4.24}$$

where s stands for the spin of a particle. As can be easily verified for all the SM particles $P_R = +1$, while the superpartners are characterized by $P_R = -1$. As a consequence the LSP can be a viable DM candidate.

However, even in the absence of R-parity conservation the LSP can still be a DM particle as its lifetime can exceed the age of the Universe. This can be in particular realized for gravitino LSP [78] or axino LSP (see, e.g., [79]).

4.4 Supersymmetry breaking

As we have already seen, unbroken supersymmetry would unavoidably lead to phenomenologically inviable predictions since the masses of the superpartners must then be equal to these of the particles from the SM. Therefore they should have been already discovered. Hence, if supersymmetry is indeed a true symmetry of nature, it must be broken.

In the following section we will focus on this issue. We will start with an effective description at the level of explicit supersymmetry breaking by additional terms added to $\mathcal{L}$. Then we will mention some of the possible underlying mechanism of *spontaneous supersymmetry breaking* (SSB) that are usually considered.

4.4.1 Soft supersymmetry breaking

The simplest phenomenologically acceptable approach to supersymmetry breaking is to parametrize our ignorance about the actual mechanism by introducing additional terms into a supersymmetric Lagrangian. In principle this could result in a lack of cancellation of quadratically divergent parts of Eqs (4.9) and (4.10) and the (big) hierarchy problem would then reappear. In order to prevent this we assume that the additional terms in $\mathcal{L}$ contain only mass terms and couplings with positive mass dimension. We denote the largest mass scale associated with such terms by m_{soft}. Respective corrections to m_h^2 should then vanish in the limit of $m_{\text{soft}}^2 \to 0$ and even by a simple dimensional analysis one can expect them to be only logarithmically divergent with Λ_{UV}. Such a procedure is often referred to as *soft supersymmetry breaking* [80].

The possible form of the additional terms in the Lagrangian that will be applicable to the MSSM is given by[9]

$$\mathcal{L}_{\text{soft}} = -\Big(\frac{1}{2} M_a\, \lambda^a \lambda^a + \frac{1}{6} a^{ijk}\, \phi_i \phi_j \phi_k + \frac{1}{2} b^{ij}\, \phi_i \phi_j\Big) + c.c. - (m^2)^i_j\, \phi^{j*} \phi_i, \qquad (4.25)$$

with M_a being gaugino masses, where $a = 1, 2, 3$, $(m^2)^j_i$ and b^{ij} scalar mass terms and a^{ijk} scalar trilinear couplings, where $i, j, k = 1, 2, 3$. Gaugino mass terms are not forbidden by gauge symmetries but this does not have to be true for the other terms. In particular, $b^{ij} \neq 0$ and $a^{ijk} \neq 0$ are allowed if the corresponding M^{ij} and y^{ijk} terms in the superpotential can be non-zero.

4.4.2 Mechanisms of supersymmetry breaking

In a more fundamental framework the soft SUSY-breaking terms in the Lagrangian should emerge from some underlying mechanism. We expect this to work in a similar fashion to the EWSB, *i.e.*, that supersymmetry would be preserved at the level of $\mathcal{L}$, but not by the ground state of a theory. Such a mechanism is usually referred to as the spontaneous supersymmetry breaking. The analogue of Goldstone's theorem for the fermionic generators of the supersymmetry algebra Q states that the SSB should result in the appearance of a massless, fermionic particle in a model that is called a *goldstino*.

The SSB mechanism is driven by the non-zero vev of the scalar potential which, according to Eq. (4.22), results from a non-zero vev of some F or D fields in a model. We will focus on scenarios with $\langle F \rangle \neq 0$ that are realized in so-called *O'Raifeartaigh* models of SSB [81].[10] The main idea is to introduce additional chiral supermultiplets into a theory and to construct their superpotential in such a way that some of the auxiliary F fields will necessarily acquire a non-zero vev. In order to do so, one needs to add a linear term in the superpotential which therefore must be a gauge singlet.

[9]There are also other terms that can be in principle considered, though they play a less important role or are excluded in the context of the MSSM (for a discussion see, e.g., [67]).

[10]In the case of $\langle D \rangle \neq 0$ the SSB is associated with an additional, so-called *Fayet-Iliopoulos*, term in $\mathcal{L}$ that is linear in D [82, 83].However, it turns out that, even for the specific case of $U(1)_Y$ in the MSSM, the Fayet-Ilipoulos mechanism would rather result in an unwanted breaking of the color and/or electroweak symmetry, instead of the SSB (see a discussion in [67]).

This, in particular, requires going beyond the MSSM. As a result we expect the SSB to be governed by the fields that belong to the *hidden sector* of a model which is only very weakly coupled to the *visible sector*. We further distinguish different mechanisms of the SSB due to the way it is mediated between both sectors. We will mention here two such scenarios that are especially important for the rest of the thesis.

One such mechanism is called *gravity mediated* or *Planck-scale mediated* supersymmetry breaking (PMSB)(see, e.g., [84, 85, 86, 87]). We first introduce to $\mathcal{L}$ a set of non-renormalizable terms containing F that are suppressed by the Planck mass M_P. Then we obtain $\mathcal{L}_{\mathrm{soft}}$ after employing $\langle F\rangle \neq 0$. In particular, one often assumes that a universality condition holds for various coupling constants in the non-renormalizable $\mathcal{L}$ in the so-called minimal supergravity (mSUGRA) description. As a result, at a high energy scale (typically chosen to be the GUT scale) one obtains a common gaugino mass $m_{1/2}$, common scalar mass m_0 and common trilinear coupling A_0. This may serve as the underlying SSB mechanism that gives rise to the Constrained MSSM (see Section 7.1). The characteristic mass scale for supersymmetric particles in the PMSB can be estimated by $m_{\mathrm{soft}} \sim \langle F\rangle/M_P$. For $m_{\mathrm{soft}} \sim 1\,\mathrm{TeV}$ this implies the SSB scale of the order of $\sqrt{\langle F\rangle} \sim 10^{10} - 10^{11}\,\mathrm{GeV}$.

Another mechanism for mediating SSB from the hidden sector to the visible sector is called *gauge-mediated* supersymmetry breaking (GMSB) [88, 89, 90, 91, 92, 93]. We add to a model a gauge singlet chiral supermultiplet S and a set of chiral supermultiplets q, $\bar{q}$, l, $\bar{l}$ (so-called *messenger fields*) that have non-trivial $SU(3)_c \times SU(2)_L \times U(1)_Y$ interactions. The scalar part of S (usually also denoted by S) and the auxiliary field F_S acquire non-zero vevs that give rise to a mass splitting between the scalar and the fermionic components of the messenger fields. It is then mediated to the visible sector by loop corrections to the mass parameters. Such loop corrections to the A terms are typically small and therefore in the GMSB scenario one often assumes that $A_t = A_b = A_\tau = 0$ at a high energy scale. In the GMSB one expects $m_{\mathrm{soft}} \sim \langle F\rangle/M_{\mathrm{mess}}$, where M_{mess} is the mass scale of the messenger fields. The $\sqrt{\langle F\rangle}$ can then vary depending on the assumed value of M_{mess}, but in principle it can be as low as $10^4\,\mathrm{GeV}$.

The gaugino masses at the SSB scale in the GMSB scenario are given by $M_a = (\alpha_a/4\pi)\,\Lambda$, where $\Lambda = \langle S\rangle/\langle F_S\rangle$. One can allow more freedom in choosing M_a in the framework of *generalized gauge-mediated* supersymmetry breaking (GGM) [94, 95, 96, 97] by replacing q, $\bar{q}$, l, $\bar{l}$ fields by a more general set of chiral supermultiplets Φ_I, $\bar{\Phi}_I$. The mass parameters of the GGM models at high energy scale expressed in terms of more fundamental parameters can be found in Appendix C.

4.5 Minimal Supersymmetric Standard Model (MSSM)

In Section 4.3.2 we described the particle content of the MSSM. We will now discuss the MSSM in more details with an emphasis on the features the will be important from the point of view of the rest of the thesis.

4.5.1 Superpotential and soft supersymmetry-breaking terms

The Lagrangian for renormalizable, gauge-invariant supersymmetric models is determined by the superpotential W and by gauge transformation properties of the fields that can further constrain $\mathcal{L}$. Taking this into account, one finds that the general structure of the superpotential given by Eq. (4.17) in the framework of the MSSM reads

$$W_{\mathrm{MSSM}} = \tilde{\bar{u}}_i \, (\mathbf{y}_u)_{ij} \, \widetilde{Q}_j \, H_u - \tilde{\bar{d}}_i \, (\mathbf{y}_d)_{ij} \, \widetilde{Q}_j \, H_d - \tilde{\bar{e}}_i \, (\mathbf{y}_e)_{ij} \, \widetilde{L}_j \, H_d + \mu \, H_u \, H_d, \tag{4.26}$$

where we used the notation from Table 4.1 with $i, j = 1, 2, 3$ being family indices.[11] The contraction of spinor indices involves a totally antisymmetric matrix $\epsilon_{\alpha\beta}$, with $\alpha, \beta = 1, 2$, *e.g.*, $H_u \, H_d = H_u^{\beta} \, H_{d\,\beta} = H_{u\,\alpha} \, H_{d\,\beta} \, \epsilon^{\alpha\beta}$. Most of the elements of the 3×3 Yukawa matrices are often assumed to be negligible except for the ones that correspond to the top and the bottom quarks, as well as the tau lepton

$$(\mathbf{y}_u)_{ij} \approx y_t \, \delta_{i3} \, \delta_{j3}, \qquad (\mathbf{y}_b)_{ij} \approx y_b \, \delta_{i3} \, \delta_{j3}, \qquad (\mathbf{y}_e)_{ij} \approx y_\tau \, \delta_{i3} \, \delta_{j3}. \tag{4.27}$$

The μ-term in W_{MSSM} gives raise to the higgsino mass. We now see the necessity of having two distinct supermultiplets H_u and H_d with different hypercharge to account for the masses of the up- and the down-type quarks, respectively. One could not use in $\mathcal{L}$, *e.g.*, H_d^* since it would violate the holomorphicity of the superpotential.

[11] The symbols in Eq. (4.26) correspond to the scalar components of supermultiplets. This is explicitly marked by adding tildes above the squark fields. Alternatively, one use the symbols of the whole supermultiplets in the *superspace* formalism (see, *e.g.*, [67]).

The soft supersymmetry-breaking terms in the Lagrangian of the MSSM that are allowed by gauge symmetries, are given by

$$\begin{aligned}\mathcal{L}_{\text{MSSM,soft}} &= -\frac{1}{2}\Big(M_1\,\tilde{B}\,\tilde{B} + M_2\,\tilde{W}\,\tilde{W} + M_3\,\tilde{g}\,\tilde{g} + c.c.\Big) \\ &\quad -\Big[\tilde{\bar{u}}_i\,(\mathbf{a}_u)_{ij}\,\widetilde{Q}_j\,H_u - \tilde{\bar{d}}_i\,(\mathbf{a}_d)_{ij}\,\widetilde{Q}_j\,H_d - \tilde{\bar{e}}_i\,(\mathbf{a}_e)_{ij}\,\widetilde{L}_j\,H_d + c.c.\Big] \\ &\quad -\widetilde{Q}_i^\dagger\,(\mathbf{m_Q^2})_{ij}\,\widetilde{Q}_j - \tilde{\bar{u}}_i^\dagger\,(\mathbf{m_u^2})_{ij}\,\tilde{\bar{u}}_j - \tilde{\bar{d}}_i^\dagger\,(\mathbf{m_d^2})_{ij}\,\tilde{\bar{d}}_j \\ &\quad -\widetilde{L}_i^\dagger\,(\mathbf{m_L^2})_{ij}\,\widetilde{L}_j - \tilde{\bar{e}}_i^\dagger\,(\mathbf{m_e^2})_{ij}\,\tilde{\bar{e}}_j \\ &\quad -m_{H_u}^2\,H_u^*\,H_u - m_{H_d}^2\,H_d^*\,H_d - (b\,H_u\,H_d + c.c.). \end{aligned} \tag{4.28}$$

M_1, M_2 and M_3 are the bino $\tilde{B}$, wino $\tilde{W}$ and gluino $\tilde{g}$ masses, respectively. One usually assumes that the soft supersymmetry-breaking parameters in Eq. (4.28) are real and all the mass parameter matrices are diagonal.[12] The matrices $\mathbf{a}_u$, $\mathbf{a}_d$ and $\mathbf{a}_e$ are also assumed to be diagonal. They are often expressed as $(\mathbf{a})_{ii} = A_{ik}\,(\mathbf{y})_{ki}$ which, combined with Eq. (4.27), leads to

$$(\mathbf{a}_u)_{ij} \approx A_t\,y_t\,\delta_{i3}\,\delta_{j3}, \qquad (\mathbf{a}_d)_{ij} \approx A_b\,y_b\,\delta_{i3}\,\delta_{j3}, \qquad (\mathbf{a}_e)_{ij} \approx A_\tau\,y_\tau\,\delta_{i3}\,\delta_{j3}, \tag{4.29}$$

with real parameters A_t, A_b and A_τ called the top, the bottom and the tau trilinear coupling, respectively. A complete list of Feynman rules for the MSSM can be found in [98].

4.5.2 Renormalization Group Equations (RGEs)

The physical quantities evaluated within the framework of the MSSM that can be compared with experimental results relate to the values of the parameters in $\mathcal{L}_{\text{MSSM}}$ that are given at the EWSB scale. However, from a theoretical perspective we expect that these parameters should rather initially appear in some more fundamental theory at a high-energy scale, *e.g.*, the GUT scale. One then needs to run them down according to the respective RGEs.

The RGEs for the MSSM up to the second loop can be found, *e.g.*, in [99]. Here we will emphasize several features of their solutions (at 1-loop) that are important from the point of view of the rest of the thesis. The RGEs for the gauge couplings and the gaugino masses are given by

$$\frac{dg_a}{dt} = g_a^3\,b_a, \qquad \frac{dM_a}{dt} = 2b_a\,g_a^2\,M_a, \tag{4.30}$$

where $t = \ln[Q/M]\,/\,(16\pi^2)$ with M being some reference scale and Q – the renormalization scale, while $b_{1,2,3} = (33/5, 1, -3)$ for $U(1)$, $SU(2)$ and $SU(3)$,

[12] The off-diagonal terms in matrices in $\mathcal{L}_{\text{MSSM}}$ and non-zero complex phases may potentially induce large flavor- or CP-violating effects.

respectively. One can easily verify that

$$\frac{d}{dt}\frac{M_a}{g_a^2} = \frac{1}{g_a^2}\frac{dM_a}{dt} + M_a \frac{d}{dt}\frac{1}{g_a^2} = 0 \quad \Rightarrow \quad \frac{M_1}{g_1^2} = \frac{M_2}{g_2^2} = \frac{M_3}{g_3^2} = \frac{m_{1/2}}{g_U^2}, \tag{4.31}$$

where in the last equality we assumed gauge coupling unification at the GUT scale which implies unification of the gaugino masses to the *common gaugino mass* $m_{1/2}$ (up to some 2-loop corrections).

Approximate solutions to the one-loop RGEs are given in Appendix A. To obtain them we used the method that follows [100]. In order to treat the running more precisely one should in principle go to the two-loop RGEs. A simplified analysis of this kind for the slepton mass parameters is given in Appendix B.

4.5.3 Electroweak symmetry breaking

So far we have described soft SUSY-breaking terms in the MSSM that generate different masses of the superpartners. We now want to embed the EWSB mechanism into the MSSM to generate masses of the SM fermions. In the MSSM there are two complex Higgs $SU(2)_L$ doublets and both in principle can acquire non-zero vev. One can rotate the fields in order to have $\langle H_u^+ \rangle = \langle H_d^- \rangle = 0$. The scalar potential for the Higgs fields can then be written in a simplified form as

$$V = \left(|\mu|^2 + m_{H_u}^2\right)|H_u^0|^2 + \left(|\mu|^2 + m_{H_d}^2\right)|H_d^0|^2 - (b\, H_u^0\, H_d^0 + c.c.) + \frac{1}{8}\left(g_1^2 + g_2^2\right)\left(|H_u^0|^2 + |H_d^0|^2\right). \tag{4.32}$$

As was pointed out above, the Higgs quartic couplings are fully determined by the gauge couplings. The non-zero vevs are denoted by $\langle H_u^0 \rangle = v_u/\sqrt{2}$ and $\langle H_d^0 \rangle = v_d/\sqrt{2}$, with $v_u^2 + v_d^2 = v^2 \simeq 246\,\mathrm{GeV}$ as in the SM. The ratio of the two vevs is typically denoted by

$$\tan\beta = \frac{v_u}{v_d}, \tag{4.33}$$

and plays an important role as an additional parameter in phenomenological considerations. One can absorb any complex phase in b by an appropriate redefinition of the phases in the Higgs fields. Thus we assume that b is real and positive.

It turns out that in order to achieve the EWSB one needs either $\mu^2 + m_{H_u}^2$ or $\mu^2 + m_{H_d}^2$ to become sufficiently small, or negative. As $m_{H_u}^2$ typically receives larger negative corrections when running from high energy to the electroweak scale one can assume that the necessary condition for the EWSB to occur is to have $\mu^2 + m_{H_u}^2 \lesssim 0$ at low energy scale.

In order to derive the mass spectrum for the MSSM, we minimize the scalar potential with respect to H_u^0 and H_d^0. In particular one of the minimization conditions reads

$$M_Z^2 = \frac{|m_{H_d}^2 - m_{H_u}^2|}{1-\sin^2 2\beta} - m_{H_u}^2 - m_{H_d}^2 - 2|\mu|^2 \approx -2(m_{H_u}^2 + |\mu|^2) + \frac{2}{\tan^2\beta - 1}(m_{H_d}^2 - m_{H_u}^2), \tag{4.34}$$

where the approximation holds for sufficiently large $\tan\beta$.

Eq. (4.34) was obtained from the tree level expression for the scalar potential. This may not be accurate enough, in particular if there is a significant mass splitting between the lighter and heavier stops. The loop correction to the scalar potential $V \to V + \Delta V$ [101, 102] modify the minimization conditions that can be effectively rewritten in terms of (check, *e.g.*, discussion in [67])

$$m_{H_u}^2 \to m_{H_u}^2 + \frac{1}{\sqrt{2}\,v_u}\frac{\partial \Delta V}{\partial v_u} = m_{H_u}^2 + \Sigma_u^u, \qquad m_{H_u}^2 \to m_{H_d}^2 + \frac{1}{\sqrt{2}\,v_d}\frac{\partial \Delta V}{\partial v_d} = m_{H_d}^2 + \Sigma_d^d. \tag{4.35}$$

The term in Eq. (4.34) proportional to Σ_d^d is suppressed by $\tan^2\beta$, but Σ_u^u can play more important role (compare [103]).

4.5.4 Mass spectrum

Higgs sector After the EWSB, three of the eight real degrees of freedom in the Higgs fields become Goldstone bosons that are then eaten up by the $W^\pm$ and Z bosons because of the Higgs mechanism. The remaining degrees of freedom form the lighter h and the heavier H scalar Higgs bosons, the pseudoscalar A and two charged scalars $H^\pm$. Expanding the scalar potential around the ground state one finds the physical masses. In particular at the tree level

$$m_{h,\text{tree}}^2 = \frac{1}{2}\Big(m_{A^0}^2 + m_Z^2 - \sqrt{(m_{A_0}^2 - m_Z^2)^2 + 4m_Z^2 m_{A^0}^2 \sin^2 2\beta}\Big) < m_Z^2|\cos 2\beta|. \tag{4.36}$$

The upper limit on m_h can be saturated at the tree level for $m_A \gg m_Z$. The lighter Higgs boson mass is increased by one-loop corrections. This leads to the following approximation at one-loop level [104, 105, 106, 107, 108]

$$m_h^2 \approx m_Z^2\cos^2 2\beta + \frac{3}{4\pi^2}\frac{m_t^4}{v^2/\sqrt{2}}\left[\log\frac{M_{\text{SUSY}}^2}{m_t^2} + \frac{X_t^2}{M_{\text{SUSY}}^2}\Big(1 - \frac{X_t^2}{12\,M_{\text{SUSY}}^2}\Big)\right], \tag{4.37}$$

where m_t is the top quark mass, $M_{\text{SUSY}} = \sqrt{m_{\tilde t_1} m_{\tilde t_2}}$ and $X_t = A_t - \mu/\tan\beta$. One can simply verify that X_t term is maximized for $X_t = \pm\sqrt{6}\,M_{\text{SUSY}}$. The radiative corrections tend to ameliorate the upper bound on the lighter Higgs boson mass to $m_h \lesssim 135\,\text{GeV}$, or even 150 GeV in non-minimal scenario (see, e.g., discussion in [67]). Needless to mention that the recently measured value of the Higgs boson mass satisfies these improved limits.

Gauginos The two neutral higgsinos mix with the bino and $\widetilde{W}^0$ to form four mass eigenstates called neutralinos $\chi^0_{1,\ldots,4}$. Similarly the two charged higgsinos mix with $\widetilde{W}^{\pm}$ to form two charginos (with positive and negative electric charge) $\chi^{\pm}_{1,2}$.

The soft SUSY-breaking parameters M_1 and M_2 can be chosen real and positive by a redefinition of phases of $\widetilde{B}$ and $\widetilde{W}$. On the other hand, μ can have *a priori* an arbitrary complex phase. However, in order to suppress significant contributions to the electron and neutron dipole moments, one usually assumes that μ is real. The sign of μ remains a free parameter.

If a neutralino is dominated by a single gaugino or higgsino contribution, a corresponding eigenvalue of the mass matrix is well approximated by the value of the soft SUSY-breaking parameter or μ

$$m_{\chi_i} \approx \begin{cases} M_1 & \text{for bino-like } \chi_i, \\ M_2 & \text{for wino-like } \chi_i, \\ \mu & \text{for higgsino-like } \chi_i. \end{cases} \tag{4.38}$$

Similarly most often in the case of charginos we obtain $m_{\chi_i^{\pm}} \approx M_2$ or μ. The gluino mass is to a good approximation determined by M_3. However, as it was shown in [109], loop corrections can be as high as $\sim 25\%$.

Sleptons and squarks Mixing within the 1st and the 2nd generation of sleptons and squarks is typically negligible and their masses are simply given by the respective soft SUSY-breaking parameters. However, this is not the case of the 3rd generation. In particular, for the stau masses at the tree level we obtain

$$m^2_{\tilde{\tau}_{1,2}} \approx \frac{1}{2}\,(m^2_{\tilde{\tau}_L} + m^2_{\tilde{\tau}_R}) \mp \sqrt{\frac{1}{4}\,(m^2_{\tilde{\tau}_L} - m^2_{\tilde{\tau}_R})^2 + m^2_{\tau}\, X^2_{\tau}}, \tag{4.39}$$

where $m_{\tilde{\tau}_L} = m_{L,3}$, $m_{\tilde{\tau}_R} = m_{\bar{e},3}$ and $X_\tau = A_\tau - \mu/\tan\beta$. The left-right mixing in the stau sector can be large if $m_{\tilde{\tau}_L} \approx m_{\tilde{\tau}_R}$ and/or $X_\tau \sim A_\tau$ is large. The tau sneutrino mass is given by

$$m^2_{\tilde{\nu}_\tau} = m^2_{\tilde{t}_L} + \frac{1}{2}\, m^2_Z \cos 2\beta. \tag{4.40}$$

The sbottom and the stop masses are given by similar formulas with $m_{\tilde{\tau}_{L,R}}$, m_τ and A_τ exchanged with the appropriate quantities.

4.6 Next-to-Minimal Supersymmetric Standard Model (NMSSM)

As we have already seen in Section 4.5, in the MSSM the EWSB mechanism is tightly related to the appropriate value of the μ parameter. It cannot be arbitrarily high in order to allow $\mu^2 + m^2_{H_u}$ to become negative. On the other hand LEP limits on the chargino masses introduce a lower bound $|\mu| \gtrsim 100\,\mathrm{GeV}$. Moreover, the minimization condition Eq. (4.34) suggests that $|\mu|$ should not exceed significantly (by many orders of magnitude) the mass of the Z boson m_Z.

Within the framework of the MSSM μ is simply put by hand into the superpotential and therefore it is not *a priori* a subject of any constraints that could confine its value as desired. This can be circumvented if one goes beyond the MSSM. In particular, the simplest such extension is to add a gauge singlet chiral supermultiplet in the so-called Next-to-MSSM. We will limit ourselves to a discussion the $\mathbb{Z}_3$-invariant version of the NMSSM (for a review see [110]) with the superpotential given by

$$W_{\mathrm{NMSSM}} = W_{\mathrm{MSSM}} + \lambda\, S\, H_u\, H_d + \frac{1}{3}\,\kappa\, S^3. \tag{4.41}$$

The soft SUSY-breaking terms in the corresponding Lagrangian can be written as

$$\mathcal{L}_{\mathrm{NMSSM}} = \mathcal{L}_{\mathrm{NMSSM}} - (\lambda A_\lambda\, H_u H_d\, S + \frac{1}{3}\kappa\, A_\kappa\, S^3 + c.c.) - m_S^2\,|S^2|, \tag{4.42}$$

where S stands for scalar component of the additional chiral supermultiplet. As one can see, the Higgs sector of the NMSSM is supplemented with several new parameters in comparison to the MSSM. After the EWSB one typically chooses the following set of such parameters to deal with

$$\lambda, \kappa, A_\lambda, A_\kappa, \tan\beta, \mu_{\mathrm{eff}} = \lambda\, s, \tag{4.43}$$

where the effective μ term is generated by the vev of scalar component of the additional supermultiplet $\langle S\rangle = s$ and is therefore naturally expected to be of the order of M_{SUSY}. Adding the S field introduces into the NMSSM two more (scalar and pseudoscalar) Higgs fields in comparison with the MSSM.

The scalar potential also receives several new terms and, importantly, in the description of the EWSB one needs to take into account one more minimization condition than in the MSSM. It is of course due to a non-zero s and it introduces additional term $\lambda^2\, v^2\, \sin^2 2\beta$ in the m_h value calculated at the tree level. The lightest Higgs boson mass in the limit of heavy singlet scalar now reads (up to one-loop level) [110]

$$\begin{aligned} m_h^2 \;\approx\; & m_Z^2 \cos^2 2\beta + \lambda^2 v^2 \sin^2 2\beta - \frac{\lambda^2}{\kappa^2}\, v^2\, (\lambda - \kappa \sin 2\beta)^2 \\ & + \frac{3}{4\pi^2}\, \frac{m_t^4}{v^2/\sqrt{2}} \Big[\log \frac{M_{\mathrm{SUSY}}^2}{m_t^2} + \frac{X_t^2}{M_{\mathrm{SUSY}}^2} \Big(1 - \frac{X_t^2}{12\, M_{\mathrm{SUSY}}^2} \Big) \Big]. \end{aligned} \tag{4.44}$$

In the neutralino sector the bino and the wino $\widetilde{W}^0$ mix with the two higgsinos and a fermionic partner of S that is called the *singlino* $\widetilde{S}$. As a result the neutralino mass matrix has now rank 5×5 with an eigenvalue corresponding to a singlino-dominated state equal to

$$m_{\chi_i} \approx 2\,\kappa\, s = 2\,\kappa\,\frac{\mu_{\rm eff}}{\lambda} \qquad \text{for singlino like } \chi_i. \tag{4.45}$$

4.7 Little hierarchy problem and fine-tuning

Current LHC limits on squark and gluino masses suggest that the characteristic mass scale for supersymmetry $M_{\rm SUSY}$ lies above 1 TeV. This gives rise to the *little hierarchy problem* (known also as the *fine-tuning problem*). As one can see from Eq. (4.34), if μ becomes too large an uncomfortable amount of the fine-tuning between μ and m_{H_u} is needed in order to obtain the proper value of M_Z. However, μ appears in the superpotential, while m_{H_u} is the soft SUSY-breaking parameter. Hence *a priori* one does not expect them to be correlated.[13]

For a more quantitative treatment of the fine-tuning problem we will use the so-called Barbieri-Giudice measure [111, 112], $\Delta = \max\{\Delta_{p_i}\}$, where

$$\Delta_{p_i} = \left|\frac{\partial \ln M_Z^2}{\partial \ln p_i^2}\right| = \frac{1}{2}\left|\frac{\partial \ln M_Z^2}{\partial \ln p_i}\right|, \tag{4.46}$$

and p_i are the parameters of the model. For the GUT constrained models they are defined at the scale $M_{\rm GUT}$ and they are renormalized through the RGEs to $M_{\rm SUSY}$. According to Eq. (4.34) with loop corrections to the scalar potential (Σ_u^u) taken into account one can write

$$\frac{\partial \ln M_Z^2}{\partial \ln p_i^2} \approx 2\frac{p_i^2}{M_Z^2}\left[-\frac{\partial \mu^2}{\partial p_i^2} - \frac{\partial m_{H_u}^2(M_{\rm SUSY})}{\partial p_i^2} - \frac{\partial \Sigma_u^u(M_{\rm SUSY})}{\partial p_i^2}\right]. \tag{4.47}$$

If the input parameters are independent from one another, Δ_{p_i} must be calculated for each of them separately. On the other hand, if some soft parameters p_i depend on one "fundamental" parameter p_0 because of new physics beyond the GUT scale, $p_i = a_i p_0$, the fine tuning due to p_0 is just the sum with signs of the individual contributions

$$\frac{\partial \ln M_Z^2}{\partial \ln p_0^2} = \frac{p_0^2}{M_Z^2}\sum_i \left(a_i^2 \frac{\partial M_Z^2}{\partial p_i^2}\right). \tag{4.48}$$

One needs to remember that the amount of fine-tuning associated with the little hierarchy problem is by no means comparable to the one characteristic for the (big) hierarchy problem. Beside that, it turns out that the actual measured value of the Higgs boson mass $m_h \simeq 126$ GeV that is somewhat larger than expected in the past, is consistent with $M_{\rm SUSY} \gtrsim 1$ TeV (see, *e.g.*, discussion for prototypical Constrained MSSM in [113, 114, 115]).

[13] Moreover, we prefer values of μ close to the EWSB scale. The issue of how to guarantee such low value of μ is known as the *μ problem*.

Chapter 5

Supersymmetric dark matter candidates

In the previous chapters we presented several arguments for the existence of DM. We also introduced some SUSY frameworks that provide viable DM candidates. We will now connect these two subjects and discuss supersymmetric DM in more details (for a review see [116, 117, 118]).

5.1 The lightest neutralino as a dark matter candidate

We begin our considerations with by far the most popular SUSY DM candidate. It is the lightest neutralino. We first need to generalize the Boltzmann equation from Section 3.2.2 to the case of many SUSY particles in the thermal plasma. Then we describe possible mechanisms that can lead to the correct value of the neutralino relic density.

5.1.1 Solving the Boltzmann equations

We have already discussed a simplified analytical approach to calculating the WIMP DM relic density in Section 3.2.2. In the context of supersymmetric theories with the LSP being a DM candidate this description should, in principle, be generalized to considering a separate Boltzmann equation for each supersymmetric particle species that is heavier than the LSP. This is particularly important when some of the heavier SUSY species have masses close to the LSP mass m_{LSP} in which case their thermal abundance is not Boltzmann suppressed at the time of the LSP freeze-out.

Fortunately, it was shown in [119, 120] that in SUSY the evolution of the Universe can still be effectively described by Eqs (2.15)-(2.16), if one replaces the number density of a single particle species by $n = \sum_i n_i$, where the index i runs over all the particle species, each with a number density n_i, and with $\langle \sigma v \rangle$ replaced by

$$\langle \sigma v \rangle_{\mathrm{eff}} = \sum_{i=1}^{N} \sum_{j=1}^{N} \langle \sigma_{ij} v_{ij} \rangle \frac{n_i^{\mathrm{eq}}}{n^{\mathrm{eq}}} \frac{n_j^{\mathrm{eq}}}{n^{\mathrm{eq}}}, \tag{5.1}$$

where $\langle \sigma_{ij} v_{ij} \rangle$ stands for a thermally averaged (co)annihilation rate for ith and jth particle species (for a detailed discussion see, *e.g.*, [9]). Similarly, $n_{\mathrm{eq}} = \sum n_{\mathrm{eq},i}$. In Eq. (2.16) the effective average energy released in the (co)annihilations of relic species is given by

$$\langle \sigma v \rangle_{\mathrm{eff}} \langle E \rangle_{\mathrm{eff}} = \sum_{i=1} \sum_{j=1} \big(\langle E_i \rangle + \langle E_j \rangle \big) \langle \sigma_{ij} v_{ij} \rangle \frac{n_{\mathrm{eq},i}}{n_{\mathrm{eq}}} \frac{n_{\mathrm{eq},j}}{n_{\mathrm{eq}}}, \tag{5.2}$$

where we approximate $\langle E_i \rangle \simeq \sqrt{m_i^2 + 9T^2}$.

Due to decays of the heavy SUSY species to the LSP (in presence of R-parity), n becomes the number density of the single stable species, the LSP. However, one needs to mention here another hidden assumption that lies behind this approximation. When replacing $\langle \sigma v \rangle$ by the effective quantity it is assumed that the relevant (lightest) SUSY particles remain in kinetic equilibrium around the time of freeze-out.[1] As a result one can assume $n_i/n \approx n_{\mathrm{eq},i}/n_{\mathrm{eq}}$.

5.1.2 Coannihilations

As we will see below, in the case of neutralino DM in phenomenologically interesting scenarios often the LSP (denoted here by χ) is mass-degenerate with some heavier supersymmetric species. Thus, in particular, coannihilations χ + NLSP $\to$ SM play a major role in determining the DM relic density. This mass degeneracy can lead to either decrease or increase of the final relic abundance $\Omega_\chi h^2$.

If the NLSP annihilates and coannihilates with χ with larger rates than $\langle \sigma_{\mathrm{ann}} v \rangle_{\chi\chi}$, the resulting $\Omega_\chi h^2$ is lower than in the case without mass degeneracy (see Fig. 5.1 (left panel)). It is because even after the condition $n_\chi \langle \sigma_{\mathrm{ann}} v \rangle_{\chi\chi} < H$ is met, *i.e.*, when the LSP would decouple from thermal plasma, its yield can be further reduced due to coannihilations with the NLSPs that remain in thermal equilibrium.[2]

One the other hand, if the NLSP annihilates less efficiently than the LSP, it decouples from thermal equilibrium before χ. This would lead to the NLSP yield at freeze-out that is larger than Y_χ. Y_{NLSP} is to some extent further reduced due to coannihilations with χ, but its final value can possibly remain large (see Fig. 5.1

[1] An accurate treatment shows that the kinetic decoupling temperature T_{kd} for neutralino is typically in a range from several MeV to several GeV [121, 122].

[2] In this scenario the NLSP will annihilate more efficiently than the LSP, but also the inverse processes will more easily produce the NLSP-NLSP pairs. As a result, the NLSP will stay longer in thermal equilibrium than the LSP.

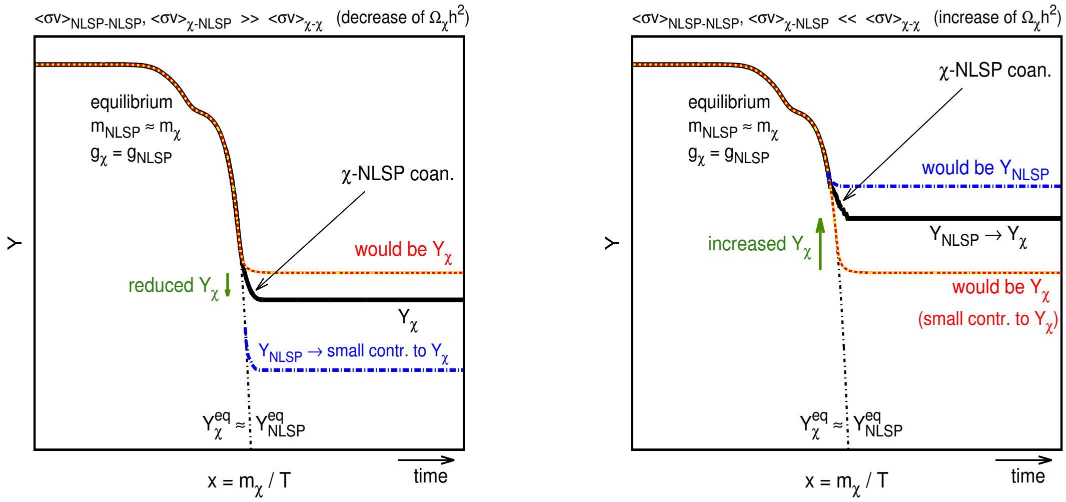

Figure 5.1: Schematic plots showing evolution of the LSP (Y_χ) and the NLSP ($Y_{\rm NLSP}$) yields in the case of mass degeneracy $m_{\rm NLSP} \approx m_\chi$. For simplicity we assume the same number of degrees of freedom for χ and the NLSP, $g_\chi = g_{\rm NLSP}$. The case with decreased (increased) final LSP abundance is shown in the left (right) panel. The scale in the pictures is not maintained.

(right panel)). However, the NLSPs will finally decay into the LSPs and $Y_{\rm NLSP}$ will provide a dominant contribution to the final DM relic abundance.[3]

In the following we will see examples of both a decrease and an increase of $\Omega_\chi h^2$ due to the LSP-NLSP mass degeneracy.

5.1.3 Neutralino relic density

The lightest neutralino χ_1^0 (later denoted simply by χ) can be a viable DM candidate if it is the LSP. It does not carry either electric or color charges, has mass m_χ and remains stable due to R-parity.[4] Depending on its dominant composition we distinguish bino-, higgsino-, wino-, or singlino-like χ (the last one for the NMSSM), or a mixed state with non-negligible admixture of two or more gauge eigenstates.

Bino-like LSP In the case of the bino-like neutralino $\widetilde{B}$ the relic density can vary by several orders of magnitude for a given m_χ, since it is very sensitive to the details of the MSSM spectrum. Generically, the bino annihilation rate is dominated by

[3] The mass degeneracy $m_{\rm NLSP} \approx m_\chi$ is required in this case to guarantee that the NLSPs can decouple before they decay into the LSPs.

[4] The case with light sneutrino LSP, constituting even a small portion of DM, is very strongly constrained in the framework of the MSSM by direct detection experiments [123]. In fact, the current experimental limits [124] require this contribution to be $\ll 10^{-3}$ of a relic sneutrino abundance.

t-channel slepton exchange $\chi\chi \to l\bar{l}$ and the relic density reads [125]

$$\Omega_{\tilde{B}} h^2 \approx \frac{1}{(460\,\mathrm{GeV})^2 \sqrt{g^*_{\mathrm{fo}}}} \frac{(m^2_{\tilde{l}} + m^2_{\tilde{B}})^4}{m^2_{\tilde{B}}\,(m^4_{\tilde{l}} + m^4_{\tilde{B}})}, \tag{5.3}$$

where $g_{*,f}$ stands for the number of relativistic degrees of freedom at χ decoupling. By varying the bino and the slepton $\tilde{l}$ masses, one can obtain $\Omega_{\tilde{B}} h^2$ spanning a few orders of magnitude. Typically, for $m_{\tilde{l}} > 200\,\mathrm{GeV}$, Eq. (5.3) gives the bino relic density that is too large and one faces the problem of its reduction. This can be done due to proper (co)annihilations or resonances, as discussed below. Nevertheless, one can obtain $\Omega_{\tilde{B}} h^2 \simeq 0.12$ even from Eq. (5.3) alone, if $m_{\tilde{B}} < m_{\tilde{l}} \lesssim 150\,\mathrm{GeV}$, in the so-called *bulk region* [119, 125]. Although such a scenario requires light sleptons, it is not fully excluded by the current LHC searches [126, 127].

For somewhat larger, though degenerate, masses $m_{\tilde{B}} \approx m_{\tilde{l}} \lesssim (400 \div 500)\,\mathrm{GeV}$ one can still reduce the neutralino relic density to the desired valuein the *stau coannihilation region* (SC) [128].[5] In the case of even heavier bino the correct relic density can be obtained due to coannihilations with squarks, if $m_{\tilde{B}} \approx m_{\tilde{q}}$, or gluinos, when $m_{\tilde{B}} \approx m_{\tilde{g}}$. In these cases it is possible to achieve $\Omega_{\tilde{B}}\, h^2 \simeq 0.12$ for $m_{\tilde{B}} \lesssim 3 - 3.5\,\mathrm{TeV}$ [129, 130].

Other mechanisms that can lead to a reduction of $\Omega_\chi\, h^2$ for the bino-like neutralino with some subdominant admixture of the higgsino is associated with the resonant annihilation $\chi\chi$ via the s-channel exchange of boson Z, the lighter scalar Higgs particle h [131] (*h-resonance region*) or heavy (pseudo)scalar Higgs bosons H/A (*A-funnel region* (AF), sometimes called the A-resonance) [125]. If the exchanged particle has mass m, the condition for the resonant annihilation reads $\langle s\rangle \simeq m^2$, where $i = 1, 2$ and $p_{\chi,i}$ is the four-momentum of the ith annihilating neutralino.[6] In the CM frame this can be recast as $m^2 \simeq \langle s\rangle \simeq 4m_\chi^2 + 6T_f m_\chi \sim \left[(2. \div 2.1)\, m_\chi\right]^2$. Hence both the Z-resonance and the h-resonance require a light neutralino with mass $m_\chi < 100\,\mathrm{GeV}$ as $m_Z \simeq 91\,\mathrm{GeV}$ and $m_h \simeq 126\,\mathrm{GeV}$, respectively. On the other hand, in the A-funnel region the neutralino can be much heavier.

For $m_{\tilde{B}} \gtrsim 3.5\,\mathrm{TeV}$ the correct relic density can still be obtained for a combination of the aforementioned scenarios. In particular this can be achieved if the

[5] We apply here the name for such a scenario that is well justified if some common slepton mass is assumed at the high energy scale. Then, due to τ Yukawa impact on the RGE running, stau remains the lightest slepton. However, in the context of general MSSM one can, in principle, consider smuon or selectron with mass lower than stau. Thus in general we should rather write about *slepton coannihilation region*. For the purpose of our discussion all such possibilities are simply encoded in the name "SC region". In [128] $m_{\tilde{B}} \lesssim 600\,\mathrm{GeV}$ is presented as an upper limit on the mass in the SC region. It originates from relatively large value of the cosmological upper limit on the relic density $\Omega_\chi h^2 < 0.3$ that should be now reduced.

[6] The thermal average value of s is associated with a typical (average) energy in the CM frame of two annihilating χs.

squark/gluino coannihilation mechanism is accompanied by the A-resonance in the bino sector.

Higgsino-like LSP The lightest higgsino-like neutralino $\widetilde{H}_1$ with mass $m_\chi \simeq \mu$ annihilates predominantly into W^+W^- and ZZ pairs if it is heavy enough. The corresponding cross sections for these processes were first calculated in [132, 133, 134] (see also [125]). However, taking into account only $\chi\chi \to$ SM channels turns out to be insufficient to properly calculate $\Omega_{\tilde{H}_1} h^2$ since the $\widetilde{H}_1$ is always mass-degenerate with the second to the lightest neutralino and the lighter chargino. Thus coannihilations play an important role in determining the relic density of the higgsino-like LSP [135]. One can approximately write [136]

$$\langle \sigma v \rangle_{\mathrm{eff},\tilde{H}} \simeq \frac{g^4}{512\pi\,\mu^2}\left(21 + 3\tan^2\theta_W + 11\tan^4\theta_W\right), \tag{5.4}$$

and therefore

$$\Omega_{\tilde{H}_1} h^2 \simeq 0.1 \left(\frac{\mu}{1\,\mathrm{TeV}}\right)^2. \tag{5.5}$$

The correct value of the DM relic density can be obtained for $\mu \simeq 1\,\mathrm{TeV}$ in a so-called **1** *TeV higgsino region* (1TH). Although such a heavy neutralino was initially thought not to be appealing [137], it now becomes consistent with the current LHC limits for SUSY searches that suggest $M_{\mathrm{SUSY}} \gtrsim 1\,\mathrm{TeV}$. Moreover, such a scenario remains allowed by DM direct and indirect detection limits. In fact, to a large extent it will be testable in the upcoming experiments (see, *e.g.*, a discussion in [138]).

Coannihilations with sleptons (the SC mechanism) in the context of higgsino-like χ lead to an increase of the relic density [139] similarly to the mechanism illustrated in Fig. 5.1 (right panel).[7] As a result, one can obtain $\Omega_{\tilde{H}_1} h^2 \simeq 0.12$ for the higgsino mass even as low as $m_{\tilde{H}} \sim 600\,\mathrm{GeV}$ [138]. For heavier higgsinos the correct relic density can be achieved by employing squark or gluino coannihilations.

Wino-like LSP In the case of the wino-like LSP $\widetilde{W}$, similarly to the higgsino, in calculating $\Omega_{\widetilde{W}} h^2$ one needs to take into account coannihilations with the lighter chargino [140]. The wino relic density is then approximately given by [136]

$$\Omega_{\widetilde{W}} h^2 \simeq 0.13 \left(\frac{M_2}{2.5\,\mathrm{TeV}}\right)^2. \tag{5.6}$$

This would suggest that the correct value of the relic density for the wino DM can be obtained for $M_2 \sim 2.5\,\mathrm{TeV}$ or lower. However, in the case of wino LSP a perturbative

[7] An accurate description of this scenario is somewhat more complicated since it corresponds to a quadruple mass degeneracy between the two lightest neutralinos, the lighter chargino and the lighter stau. It is the lighter stau that plays the role of the "NLSP" in Fig. 5.1 (right panel), although in this case it is often not true NLSP since $m_{\tilde{\tau}_1} \gtrsim m_\chi \simeq m_{\chi_2^0} \simeq m_{\chi_1^\pm}$.

calculation turns out to be not sufficient. The wino relic density is quite sensitive to a so-called Sommerfeld enhancement (SE) of the annihilation cross-section due to attractive Yukawa potentials induced by the electroweak gauge bosons [141] (see also [142, 143] for a recent discussion). Incidentally, the SE is particularly important in the wino mass range for which one obtains $\Omega_{\widetilde{W}}\, h^2 \simeq 0.12$. This results in a visible broadening of a cosmologically acceptable wino mass range to $M_2 \sim (2-3)\,\mathrm{TeV}$.

Similarly to the higgsino case, the SC mechanism leads to an increase of the relic density for the wino lighter than about 3 TeV, while squark/gluino coannihilations reduce it for heavier $\widetilde{W}$. Taking this into account additionally extends the mass range for which $\Omega_{\widetilde{W}}\, h^2 \simeq 0.12$ is obtained to $1.6\,\mathrm{TeV} \lesssim m_{\widetilde{W}} \lesssim 4\,\mathrm{TeV}$ [138].

Singlino-like LSP In the framework of the NMSSM the lightest neutralino can become singlino-dominated (see Section 4.6). The largest values of the singlino relic density can be significantly larger than the largest values obtained for the bino LSP with the same mass. This can be explained by the fact that a nearly pure singlino interacts very weakly. It annihilates mainly into scalar-pseudoscalar pairs (mainly $H_2 A_1$) with the associated couplings proportional to κ or λ that are suppressed for singlino-like LSP. Intermediate values of the relic density can be obtained due to coannihilations with the bino ($10^3 < \Omega_{\widetilde{S}} h^2 < 10^5$) or the higgsino ($\Omega_{\widetilde{S}} h^2 \sim 10^2$). Obtaining even smaller values requires coannihilations with the higgsino, wino, stau/sneutrino, stop or gluino, as well as Z- or Higgs- resonant annihilations. For an extensive discussion about the issue of DM relic density in the NMSSM see [144].

Mixed neutralino LSP A general neutralino state in the MSSM (or the NMSSM) is the mixed state between the bino, wino, higgsino (and the singlino). Among various possible mixed states of the lightest neutralino the most important one is the bino-higgsino LSP. In the mass range $100\,\mathrm{GeV} \lesssim m_\chi \lesssim 1\,\mathrm{TeV}$ typically pure bino LSP has too large, while pure higgsino too small, relic density. This can be circumvented for an appropriate admixture of $\widetilde{B}$ and $\widetilde{H}_{u,d}$. In the context of GUT-constrained SUSY models this is called the *hyperbolic branch/focus point region* (HB/FP) [145, 146]. In the following we will apply this name also to the corresponding region in the MSSM with parameters defined at low energy scale. The correct value of the relic density can be achieved in the HB/FP region due to $\chi\chi$ annihilations into gauge bosons, as well as through t-channel exchange of a higgsino-like lighter chargino and/or the second lightest neutralino.

Among other mixed scenarios discussed in the literature one can distinguish bino-wino (see, *e.g.*, [147, 148, 136], singlino-higgsino (in the context of the NMSSM) [144] or even bino-higgsino-wino (see, *e.g.*, [149, 150]) admixtures.

5.2 Gravitino dark matter

We will now briefly discuss the gravitino DM scenario. We begin with short introduction of the theoretical background and then describe gravitino TP.

5.2.1 Basics

So far we have assumed that supersymmetry is a global symmetry. However, if one wants to take into account gravity, SUSY must be promoted to a local symmetry. This leads to so-called *supergravity* [151, 152, 153, 154].

In the context of supergravity we introduce an additional supermultiplet that contains spin-2 graviton and its fermionic superpartner spin-3/2 gravitino. For unbroken SUSY both the graviton and the gravitino are massless particles with two degrees of freedom. After spontaneous supersymmetry breaking the gravitino acquires mass by absorbing two goldstino degrees of freedom in the super-Higgs mechanism [155, 156, 157, 158] analogously to the weak gauge bosons in the SM.[8] The gravitino plays a role of a gauge field for local supersymmetry.

The mixing between the gravitino ψ_G^μ and the fermionic components of the chiral and gauge supermultiplets (χ and λ, respectively) is described by the following terms in the Lagrangian of supergravity

$$\mathcal{L} \supset \frac{1}{2}\, g\, D^a\, (\psi_G)_\mu\, \sigma^\mu\, \bar{\lambda}^a - e^{G/2}\, \frac{i}{\sqrt{2}}\, G_i\, \chi^i\, \sigma^\mu\, (\bar{\psi}_G)_\mu + h.c. \tag{5.7}$$

They can be eliminated by an appropriate shift of the gravitino field

$$\psi_G^\mu \to \psi_G^\mu + \frac{1}{3}\, \bar{\eta}\bar{\sigma}^\mu = \psi_G^\mu + \frac{1}{3}\left(\frac{i}{\sqrt{2}}\, G_i\, \bar{\chi}^i + \frac{1}{2}\, e^{-G/2}\, g\, D^a\, \bar{\lambda}^a\right)\bar{\sigma}^\mu, \tag{5.8}$$

where the fermionic field $\bar{\eta}$ corresponds to the massless goldstino. One can then obtain the gravitino mass,

$$m_{\widetilde{G}}^2 \equiv m_{3/2}^2 = e^{\langle G \rangle/2}\, M_P = \frac{\langle K_j^i\, F_i\, F^{j*} \rangle}{3\, M_P^2}, \tag{5.9}$$

where $K_j^i = (\delta^2 K/\delta\phi_i \delta\phi^{j*})$, $G = K/M_P^2 + \ln WW^*/M_P^6$ and the function $K = K(\phi, \phi^*)$, which contributes to the Lagrangian, is called the *Kähler potential*. In the PMSB scenario, where $\sqrt{\langle F \rangle} \sim 10^{10} - 10^{11}\,\mathrm{GeV}$, the gravitino mass $m_{\widetilde{G}}$ is typically at least of the order of $100\,\mathrm{GeV}$. On the other hand in the GMSB, $m_{\widetilde{G}}$ can be much lower depending on the M_{mess}.

[8] In the case of fermionic operators that generate supersymmetry, Goldstone bosons from the ordinary Higgs mechanism are replaced by fermionic goldstinos.

The Lagrangian term that is relevant for gravitino thermal production is given by

$$\mathcal{L} \ni \frac{m_{\tilde{g}}}{m_{\widetilde{G}}} \frac{1}{6\sqrt{2}\, M_P} \bar{\phi}_G \left[\gamma^\mu, \gamma^\nu\right] \tilde{g}^a\, G^a_{\mu\nu}, \tag{5.10}$$

where ϕ_G is the goldstino component of gravitino. Note the characteristic ratio between the gluino and the gravitino masses $m_{\tilde{g}}/m_{\widetilde{G}}$. The other interaction terms for the gravitino that are relevant for the thesis can be found, *e.g.*, in [159].

5.2.2 Gravitino thermal production

Due to their extremely weak interactions, primordial gravitinos decouple from thermal plasma at very high temperatures. For the gravitino with mass $m_{\widetilde{G}} \gtrsim 1\,\mathrm{GeV}$ ($10\,\mathrm{GeV}$) its decoupling temperature is of the order of $T^{\mathrm{dec}}_{\widetilde{G}} \gtrsim 10^{14}\,\mathrm{GeV}$ ($10^{16}\,\mathrm{GeV}$) [160]. Thus it is typically assumed that, after a period of cosmological inflation, the maximum temperature $T_{\max}$ of the Universe was never high enough for the gravitino to be in thermal equilibrium. Any population of primordial (equilibrium) gravitinos can then be effectively diluted during inflation [161]. Otherwise the gravitinos would be easily overproduced and would dominate the energy density of the Universe unless they were very light with $m_{\widetilde{G}} \lesssim 1\,\mathrm{keV}$ [162].

In the following we will assume that $T^{\mathrm{dec}}_{\widetilde{G}} > T_{\max}$. Within this approach the gravitinos can still be produced in the early Universe in TP and NTP processes, as discussed in Section 3.2.3. NTP is determined by the NLSP's (typically neutralino or slepton) yield at freeze-out and by the $m_{\widetilde{G}}/m_{\mathrm{NLSP}}$ ratio as shown in Eq. (3.13). On the other hand TP depends more on the $SU(3)_c$ sector of the MSSM and is dominated by the production in scatterings of gluinos, gluons and (s)quarks.

The present yield of TP gravitinos [163, 164, 165] can be estimated by

$$Y^{\mathrm{TP}}_{\widetilde{G}} \simeq \left(\frac{T_R}{10^{10}\,\mathrm{GeV}}\right) \sum_{r=1}^{3} y_r\, g_r^2(T_R) \left(1 + \frac{M_r(T_R)}{3\, m_{\widetilde{G}}}\right)^2 \ln\left(\frac{k_r}{g_r(T_R)}\right), \tag{5.11}$$

where $y_{1,2,3} = (0.653, 1.604, 4.276)$, $k_{1,2,3} = (1.266, 1.312, 1.271)$, while $M_r(T_R)$ and $g_r(T_R)$ denote gaugino mass parameters and gauge couplings evaluated at $Q = T_R$, respectively. They can be replaced by values M_r and g_r at low energy scale after imposing on Eq. (5.11) additional numerical factors obtained from running of RGEs.

If the gluino is the heaviest gaugino with mass significantly exceeding $m_{\widetilde{G}}$, Eq. (5.11) can be recast as

$$\Omega^{\mathrm{TP}}_{\widetilde{G}} \propto m_{\widetilde{G}}\, Y^{\mathrm{TP}}_{\widetilde{G}} \propto \frac{T_R}{m_{\widetilde{G}}}\, m_{\tilde{g}}^2. \tag{5.12}$$

Assuming that $\Omega_{\widetilde{G}}^{\rm TP} \lesssim 0.12$, Eq. (5.12) can be rewritten as an upper limit on the reheating temperature

$$T_{R,\max} \propto \frac{m_{\widetilde{G}}}{m_{\tilde{g}}^2}. \tag{5.13}$$

Clearly larger $m_{\widetilde{G}}$ leads to larger T_R. However, the gravitino mass cannot be arbitrarily high since we want it to remain the LSP. Moreover, for too small a mass difference ($m_{\rm NLSP} - m_{\widetilde{G}}$) the NLSP lifetime becomes often too long and Big Bang Nucleosynthesis (BBN) constraints become violated as will be discussed in Section 6.6.1. As a result one typically obtains $T_{R,\max} < 2 \times 10^9\,{\rm GeV}$, *i.e.*, below the minimum value required by simple models of thermal leptogenesis with zero initial abundance of the lightest right-handed neutrinos and sneutrinos [166]. The gravitino LSP scenario either suffers from thermal overproduction of $\widetilde{G}$ or the reheating temperature has to suppressed. Nevertheless, even in the case of thermal leptogenesis one can obtain lower $T_R \sim 2 \times 10^8\,{\rm GeV}$ if thermal initial abundance of ν_R and $\tilde{\nu}$ is assumed [167]. Beside that, baryogenesis is still a subject of an ongoing discussion and in particular many models were proposed with low values of T_R (see, *e.g.*, [168] or recent review [169]).

Eq. (5.11) should be modified for sufficiently low $T_{\rm R}$ in order not to overestimate the abundance of TP gravitinos. This is due to a possible decoupling of heavy SUSY species before the RD epoch, *i.e.*, in the reheating period when $T > T_{\rm RD}$. Nevertheless, in this limit even the yield calculated using Eq. (5.11) typically leads to very low $\Omega_{\widetilde{G}}^{\rm TP} h^2$ and the DM relic density has to be dominated by the NTP component in order to keep $\Omega_{\widetilde{G}}^{\rm TP} h^2 \simeq 0.12$. Hence such a modification plays a negligible role in the case of gravitino DM. The exception could be a very light gravitino (see, *e.g.*, [170]) which we will not address in this thesis.

Another possible modification of Eq. (5.11) appears in the GMSB-type models of SUSY breaking. If the reheating temperature exceeds the messenger scale $T_R > M_{\rm mess}$, the gravitino production rate becomes suppressed by about $M_{\rm mess}^2/T^2$ with respect to supergravity calculations. As a result $Y_{\widetilde{G}}^{\rm TP}$ becomes effectively insensitive to T_R [171, 172]. In the following, when discussing GGM models with gravitino DM in Section 9.1, we will assume that the messenger scale is always high enough so that this effect plays a negligible role.

One needs to mention here that there are also other possible production mechanisms for the gravitinos in the early Universe, *e.g.*, from inflaton decay [173, 174]. They are very model-dependent and not necessarily important [175]. Hence we will ignore them in the rest of the thesis.

5.3 Axino dark matter

The case of axino CDM [176, 177] is, at least at the phenomenological level, similar to the gravitino DM scenario. Axino is a neutral Majorana particle. Likewise the gravitino, it is an EWIMP, though with the interaction rates suppressed by the energy scale f_a that is typically significantly lower than M_P.[9] Other than that, the main difference between axino and gravitino DM arises from the dominant terms in the corresponding effective interaction Lagrangians.

5.3.1 Basics

In a supersymmetrized version of an axion model [178, 179, 180] the real scalar axion field a resides in a chiral supermultiplet since it is a gauge singlet. The other members of the axion supermultiplet are the fermionic superpartner axino $\tilde{a}$ and the real scalar field *saxion* s that provides a remaining bosonic degree of freedom on-shell.[10]

The interaction Lagrangian for the axion supermultiplet can be obtained by supersymmetrizing Eq. (3.16). In particular, the axino-gaugino-gauge boson and the axino-gaugino-sfermion-sfermion interaction terms are given by [177, 181]

$$\begin{aligned}
\mathcal{L}^{\rm eff}_{\tilde{a}} &= i\frac{\alpha_s}{16\pi\, f_a}\,\bar{\tilde{a}}\,\gamma_5\,[\gamma^\mu,\gamma^\nu]\,\tilde{g}^b\,G^b_{\mu\nu} + \frac{\alpha_s}{4\pi\, f_a}\,\bar{\tilde{a}}\,\tilde{g}^a\,\Sigma_{\tilde{q}} g_s\,\tilde{q}^*\,T^a\,\tilde{q} \\
&\quad + i\frac{\alpha_2\, C_{aWW}}{16\pi\, f_a}\,\bar{\tilde{a}}\,\gamma_5\,[\gamma^\mu,\gamma^\nu]\,\widetilde{W}^b\,W^b_{\mu\nu} + \frac{\alpha_2}{4\pi\, f_a}\,\bar{\tilde{a}}\,\widetilde{W}^a\,\Sigma_{\tilde{f}_D} g_2\,\tilde{f}^*_D\,T^a\,\tilde{f}_D \\
&\quad + i\frac{\alpha_Y\, C_{aYY}}{16\pi\, f_a}\,\bar{\tilde{a}}\,\gamma_5\,[\gamma^\mu,\gamma^\nu]\,\widetilde{B}\,B_{\mu\nu} + \frac{\alpha_Y}{4\pi\, f_a}\,\bar{\tilde{a}}\,\widetilde{B}^a\,\Sigma_{\tilde{f}} g_Y\,\tilde{f}^*\,Q_Y\,\tilde{f}, \qquad (5.14)
\end{aligned}$$

where $\tilde{f}_D$ and $\tilde{f}$ denote sfermions carrying non-zero T^3 and Y, respectively. C_{aWW} and C_{aYY} are model-dependent parameters that correspond to axino-gaugino-gauge boson anomaly interactions for the $U(1)_Y$ and the $SU(2)_L$ groups, respectively. The $SU(2)_L$ coefficient can be always set to zero $C_{aWW} = 0$ by a proper rotation of the axion field.

A generic form of interaction between the axion and matter supermultiplets was considered in [182]. In particular, it was pointed out that, for $v_{\rm PQ} > T \gtrsim M_\Phi$, where M_Φ is the mass of the heaviest PQ-charged and gauge-charged supermultiplet Φ, the axino-gaugino-gauge boson interaction term is suppressed by M_Φ^2/T^2. This is particularly important for the DFSZ axino, where Φ corresponds to the Higgs supermultiplets and therefore $M_\Phi = \mu$ (the higgsino mass). The dominant contribution to axino TP is then associated with a higgsino decay to the axino and the

[9] f_a is constrained by astrophysical and cosmological data to $10^9\,\text{GeV} \lesssim f_a \lesssim 10^{12}\,\text{GeV}$ [34].
[10] Off-shell the additional two bosonic degrees of freedom are provided by an auxiliary field F_A.

Higgs boson that is described by [182, 183, 184]

$$\mathcal{L}^{\rm eff}_{\tilde{a},{\rm DFSZ}} \ni c_H \frac{\mu}{f_a} \tilde{a} \, [\widetilde{H}_d \, H_u + \widetilde{H}_u \, H_d] + h.c. \tag{5.15}$$

The axino mass $m_{\tilde{a}}$ (for a recent review see [185]) is generated as a result of supersymmetry breaking and in the spontaneously broken global SUSY is expected to be at the tree level at least of the order of $\sim \mathcal{O}(M^2_{\rm SUSY}/f_a)$ [179]. In various models considered in the literature $m_{\tilde{a}}$ can be either much lower than $M_{\rm SUSY}$ [180, 186, 187, 188, 189] or much higher [190]. In the following we will not limit ourselves to any particular scenario of the SSB and will treat the axino mass as a free parameter.

5.3.2 Axino thermal production

The axino decoupling temperature from thermal plasma is given by [191]

$$T^{\rm dec}_{\tilde{a}} = 10^{11}\,{\rm GeV} \left(\frac{f_a}{10^{12}\,{\rm GeV}}\right)^2 \left(\frac{0.1}{\alpha_s}\right)^3 . \tag{5.16}$$

If the temperature in the RD epoch following inflation were high enough, regenerated axinos would remain in thermal equilibrium and the corresponding relic density would be given by $\Omega^{\rm ther}_{\tilde{a}} \simeq m_{\tilde{a}}/2\,{\rm keV}$ [191]. In this case in order to obtain the correct value of $\Omega_{\rm DM}$ one requires $m_{\tilde{a}} \simeq 0.2\,{\rm keV}$ which leads to axino WDM scenario. In the following we will focus on sufficiently low $T_{\rm max} < T^{\rm dec}_{\tilde{a}}$ and heavier axino which can constitute CDM.

For high reheating temperature the most important contribution to the TP of KSVZ axino is associated with the first term in $\mathcal{L}$ given by Eq. (5.14). One can notice the absence of a term analogous to the $m_{\tilde{g}}/m_{\widetilde{G}}$ term in Eq. (5.10). This results in a different $\Omega^{\rm TP}_{\tilde{a}}\,h^2$ dependence on $m_{\tilde{a}}$ [177] that in the gravitino case. The approximate formula for the yield of the KSVZ axinos for high T_R (see the left panel of Fig. 5.2) reads [192]

$$Y^{\rm TP}_{\tilde{a}} \simeq 2\times 10^{-7}\, g_s^6 \, \ln\left(\frac{1.108}{g_s}\right) \frac{T_R}{10^4\,{\rm GeV}} \left(\frac{10^{11}\,{\rm GeV}}{f_a}\right)^2, \qquad \text{KSVZ, high } T_R. \tag{5.17}$$

As a result, for the TP relic density one obtains

$$\Omega^{\rm TP}_{\tilde{a}} \sim m_{\tilde{a}}\, Y^{\rm TP}_{\tilde{a}} \sim m_{\tilde{a}} \frac{T_R}{f_a} \qquad \text{KSVZ, high } T_R. \tag{5.18}$$

In addition, as can be seen from Eq. (5.17), the KSVZ axino TP yield in the high T_R regime is to a good approximation independent of a SUSY spectrum. Similarly to the gravitino DM scenario, Eq. (5.18) can be used to derive an upper limit on the reheating temperature $T^{\rm max}_R \sim \frac{f_a}{m_{\tilde{a}}}$. As can be seen from Fig. 5.2 (right panel), KSVZ axino CDM with $m_{\tilde{a}} \gtrsim 0.1\,{\rm GeV}$ naturally points towards rather low values of the

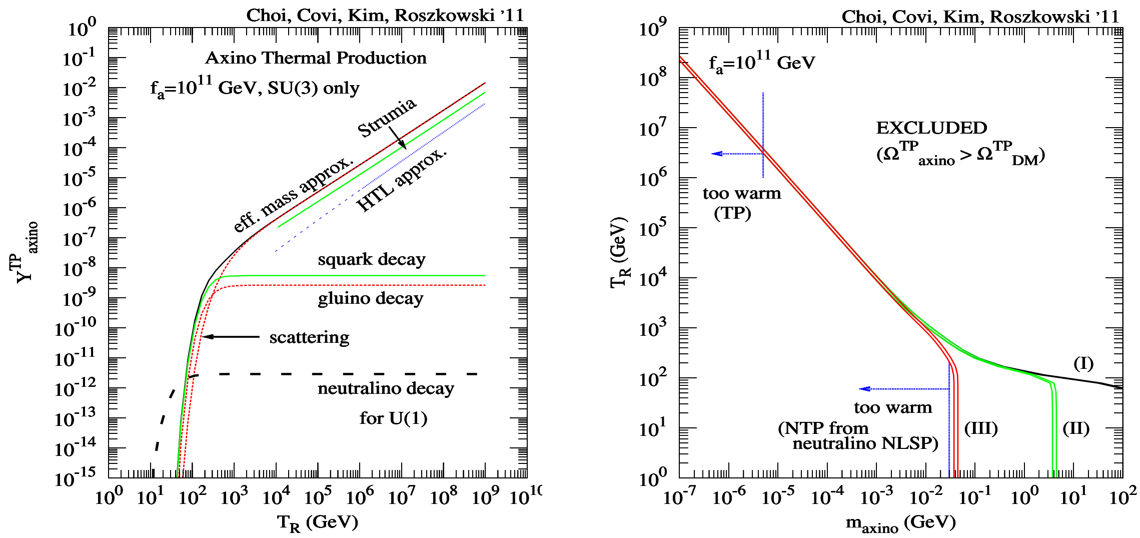

Figure 5.2: *Left panel*: Axino TP yield $Y_{\tilde{a}}^{\rm TP}$ for the KSVZ model as a function of the reheating temperature T_R. Gluino and squark masses are assumed to be $m_{\tilde{g}} = m_{\tilde{q}} = 1\,$TeV, while $f_a = 10^{11}\,$GeV. Solid black line corresponds to the effective thermal mass approximation, while solid/dotted blue (solid green) describes HTL (Strumia's) approach (see a discussion in text). Horizontal red (green) line shows yield from gluino (squark) decays that add to the dominant (for $T_R \gtrsim 10^3\,$GeV) contribution from $SU(3)_c$ scatterings. Taken from Ref. [181]. *Right panel*: $T_R^{\rm max}$ vs $m_{\tilde{a}}$ in the KSVZ model for $m_{\tilde{g}} = m_{\tilde{q}} = 1\,$TeV and $f_a = 10^{11}\,$GeV. Regions excluded from the Large Scale Structure formation are marked with vertical blue lines for $m_{\tilde{a}} \lesssim 5\,$keV (TP axino) and $m_{\tilde{a}} \lesssim 30\,$MeV (NTP axino with a neutralino NLSP). Solid black (I) (green (II),red (III)) line corresponds to non-thermal yield $Y^{\rm NTP} = 0$ (10^{-10} for (II), 10^{-8} for (III)). Taken from Ref. [181].

reheating temperature $T_R \lesssim 1\,$TeV. One should note that in the case of axino such low T_R can still lead to a non-negligible TP contribution to the DM relic density in contrast to the gravitino DM scenario.[11] We will examine axino TP in low T_R regime with more details in Section 9.3 and Appendix E.

In the case of the DFSZ framework TP is dominated by higgsino decays into axinos (see Eq. (5.15)) and (less importantly) by scatterings involving $SU(2)_L$ interactions. Because of this the DFSZ axino yield for vast range of T_R, but not too low, becomes independent of the reheating temperature [182, 184, 193]

$$Y_{\tilde{a}}^{\rm TP} \simeq 10^{-5}\,\zeta\left(\frac{\mu}{\rm TeV}\right)\left(\frac{10^{11}\,{\rm GeV}}{f_a}\right)^2, \qquad \text{DFSZ}, \tag{5.19}$$

where $\zeta \sim \mathcal{O}(1)$. If T_R becomes very high, depending on the value of the higgsino mass μ, axino production from $SU(2)_L$ scatterings start to dominate and the T_R dependence is recovered even for DFSZ axino.

[11]This is because, as discussed above, axino interaction rates are suppressed by $f_a \sim 10^{11}\,$GeV, which is large, but still significantly lower than M_P.

Dependence on a SUSY spectrum In the KSVZ model, in the limit of high T_R, scatterings associated with the $SU(3)_c$ group dominate in $Y^{\rm TP}$. The additional $U(1)$ scatterings (for non-zero C_{aYY}) contribute typically by no more than a few percent. In this regime of high T_R, the yield from scatterings is practically independent of a SUSY spectrum, as mentioned above. This is because the thermal kinetic energy of the incident particles can be high enough so that the suppression of phase space for heavier SUSY particles (incident or produced) is negligible. In particular, in the case of the scatterings of the SM particles leading to the production of the axino and a heavy SUSY particle (*e.g.*, gluino) $\sigma(s)$ does not depend on a supersymmetric particle mass, *e.g.* [194],

$$\sigma(s)_{qq} \simeq \frac{\alpha_s^3}{72\pi^2 f_a^2}\left[1 - 3\left(\frac{m_{\tilde{g}}^2}{s}\right)^2 + 2\left(\frac{m_{\tilde{g}}^2}{s}\right)^3\right] \xrightarrow{s\to\infty} \frac{\alpha_s^3}{72\pi^2 f_a^2}, \tag{5.20}$$

for the dominant quark-quark scattering.[12]

One should mention here a technical issue that arises when dealing with infrared divergences in the scattering cross sections. One way to solve this problem is to use a Hard Thermal Loop (HTL) resummation technique [195] that is, however, valid only for $g_s \ll 1$, *i.e.*, $T_R \gg 10^6\,$GeV [192]. Another method, used by Strumia [196], is to apply fully resumed finite-temperature propagators for gluons and gluinos. This results in an increase of $Y_{\tilde{a}}^{\rm TP}$ compared to the HTL method (see the left panel of Fig. 5.2) due to an addition of the axino production via gluon decays.[13] However, this technique is applicable only to $T_R \gtrsim 10^4\,$GeV, which still remains far too high for the purpose of our discussion. Hence we will follow [177] and use the effective thermal mass (ETM) approximation, *i.e.*, employ a thermal gluon mass.[14] It gives somewhat larger $Y_{\tilde{a}}^{\rm TP}$ in the high T_R regime than Strumia's result, as shown in Fig. 5.2 (left panel). The difference (up to a factor of three) can be treated as an estimate of the theoretical uncertainty of using ETM for the high reheating temperature [181].

The important advantage of using the ETM approach is the possibility of considering axino TP in a low T_R regime. When the reheating temperature drops below about $10^5\,$GeV, the axino yield from TP may acquire non-negligible contribution from squark and gluino decays to the axino. As a result $Y_{\tilde{a}}^{\rm TP}$ starts to depend on the gluino and squark masses.[15] For heavy squarks, phase space suppression reduces

[12] In general other scattering channels producing axinos can also be important in the high T_R regime and one can find similar arguments for them (compare [194]).

[13] For a similar discussion in the case of gravitino DM see [165].

[14] Low-energy gluons (more strictly – plasmons, that are gluon-like collective excitations of a quark-gluon plasma) cannot propagate as free fields in the high-temperature plasma. This effect is taken into account in the framework of the thermal field theory by introducing an effective thermal mass $m_{\rm eff} \sim gT$ that corresponds to the plasma frequency.

[15] For even lower $T_R \lesssim 100\,$GeV TP can get important impact from $U(1)_Y$ scatterings and decays. However, for such low reheating temperature one has to additionally take into account the impact of non-instantaneous reheating. Thus we will postpone the discussion of this regime until Section 9.3 and Appendix E.

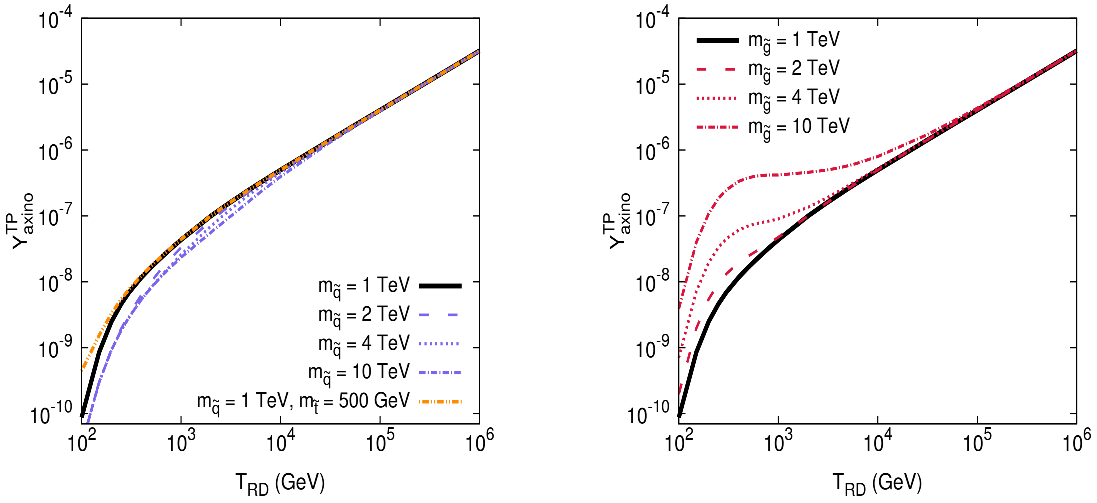

Figure 5.3: $Y_{\tilde{a}}^{\rm TP}$ vs $T_R \approx T_{\rm RD}$ in the KSVZ model intermediate with $10^6\,{\rm GeV} \geqslant T_R \leqslant 10^2\,{\rm GeV}$. Solid black line the same as in Fig. 5.2. *Left panel*: Yield for the common squark mass $m_{\tilde{q}} = 2\,{\rm TeV}$ ($4\,{\rm TeV}$, $10\,{\rm TeV}$) (at the low energy scale) is shown with dashed (dotted,dash-dotted) blue line. Dash-dotted yellow line was obtained for $m_{\tilde{q}} = 1\,{\rm TeV}$ except from the lighter stop mass $m_{\tilde{t},1} = 500\,{\rm GeV}$. *Right panel*: Yield for the gluino mass $m_{\tilde{g}} = 2\,{\rm TeV}$ ($4\,{\rm TeV}$, $10\,{\rm TeV}$) is shown with dashed (dotted,dash-dotted) red line.

the scattering contributions by a factor no more than a few, as can be seen in Fig. 5.3 (left panel), where $m_{\tilde{q}}$ denotes common squark mass at $M_{\rm SUSY}$ scale. The opposite effect is obtained for smaller mass of the lighter stop. On the other hand, for heavy gluinos the corresponding scattering contributions are also suppressed due to phase space effect. However, enhanced squark decays lead to an increase in $Y_{\tilde{a}}^{\rm TP}$ possibly by more than an order of magnitude (see the right panel of Fig. 5.3). The correct thermal axino yield from squark decays is to some approximation proportional to $m_{\tilde{g}}^2$ for $T_R > m_{\tilde{q}}$ [194]

$$\begin{aligned}
\left(Y_{\tilde{a}}^{\rm TP}\right)_{\tilde{q},{\rm dec}} &\simeq \frac{6\,\zeta(5)\,\alpha_s^4}{(2\pi)^6}\,\bar{g}\left(\frac{M_P}{m_{\tilde{q}}}\right)\left[\frac{m_{\tilde{g}}}{f_a}\log\left(\frac{f_a}{m_{\tilde{g}}}\right)\right]^2 && (5.21)\\
&\simeq 3\left(\frac{m_{\tilde{g}}}{m_{\tilde{q}}}\right)\left(Y_{\tilde{a}}^{\rm TP}\right)_{\tilde{g},{\rm dec}} \qquad \text{for}\quad f_a = 10^{11}\,{\rm GeV}, && (5.22)
\end{aligned}$$

where $\zeta(5) \simeq 1$, $\bar{g} = 135\sqrt{10}/(2\pi^3\,g_*^{3/2})$ and in the second line $\left(Y_{\tilde{a}}^{\rm TP}\right)_{\tilde{g},{\rm dec}}$ denotes the contribution from gluino decays. As can be seen from Eq. (5.22) the relative impact of squark and gluino decays depends on their mass ratio, but typically squark decays dominate.

In the case of the DFZS model $Y_{\tilde{a}}^{\rm TP}$ depends on the higgsino mass μ as shown in Eq. (5.19). For sufficiently low T_R both DFSZ and KSVZ yields become Boltzmann suppressed.

Chapter 6

Bayesian approach and constraints

In this chapter we introduce fundamental concepts that lie behind a Bayesian statistical approach to analyzing SUSY models. We begin with a description of the Bayes theorem and of its application in the context of SUSY. We further discuss relevant constraints imposed in such analyses that come from current high- and low-energy particle physics experiments, as well as these related to dark matter.

6.1 Bayesian statistics

In this section we briefly describe some basic concepts behind Bayesian statistics. We first discuss fundamental notions of a probability theory and then apply them to the specific case of a SUSY model analysis.

6.1.1 Probability theory and Bayes theorem

Axiomatic probability theory The classical Kolmogorov's definition of probability refers to the concept of measuring sets. We first define a set Ω of all possible outcomes of some experiment, *i.e.*, a so-called sample space. A subset of Ω is called an *event* and all possible events compose a set that is usually denoted by $\mathcal{F}$. Next we introduce a function (measure on Ω) $P : \mathcal{F} \to [0, 1]$ such that $P(\Omega) = 1$. It is referred to as a *probability measure* or simply *probability*. The whole triple $(\Omega, \mathcal{F}, P)$ is formally called a *probability space*.[1] Last, but not least, we define a *random variable* X that is a function $X : \Omega \to \mathbb{R}^n$ which transforms subsets from $\mathcal{F}$ into Lebesgue measurable subsets of $\mathbb{R}^n$.[2]

[1] In general, in order to construct a reliable probability theory, one needs to restrain an issue of event so that not any possible subset of Ω can belong to $\mathcal{F}$. Strictly writing, $\mathcal{F}$ must comply with the definition of so-called σ-field. In practice, when considering results of physical experiments, we typically limit ourselves either to a discrete set Ω with $\mathcal{F} = 2^\Omega$ being set of all subsets of Ω or to $\Omega \subset \mathbb{R}$ and $\mathcal{F}$ composed of Borel sets that remain measurable in a sense of the Lebesgue measure.

[2] Note that $P : \mathcal{F} \to \mathbb{R}_+$, while X takes arguments from the sample space Ω.

Suppose we have two events $A, B \subset \Omega$ with corresponding probabilities $P(A)$ and $P(B)$. By definition a conditional probability of A under the assumption that B happened is given by

$$P(A|B) = \frac{P(A \cap B)}{P(B)}, \tag{6.1}$$

where $\cap$ denotes the intersection of sets A and B. From Eq. (6.1) it immediately follows that

$$P(A|B) = \frac{P(B|A)\,P(A)}{P(B)}. \tag{6.2}$$

Eq. (6.2), which relates the conditional and the unconditional probabilities of A and B, is called the *Bayes theorem*.

When Ω is a subset of $\mathbb{R}^n$, it is convenient to identify Ω with a random variable X being an identity function, *i.e.*, for each $\omega \in \Omega$ one obtains $X(\omega) = \omega$. From now on, we will continue to discuss selected aspects of a probability theory in terms of random variables or sample space interchangeably. If additionally Ω is a continuous set, as it is often the case with results of physical experiments, we introduce a *probability density* function p such that the probability of $X \in A$, *i.e.*, that $X(\omega) \in A$ for some $\omega \in \Omega$, is given by

$$P(X \in A) = \int_A p(\omega)\,d\omega, \tag{6.3}$$

where an ordinary Lebesgue integration is used.

Let us now consider a 2-dimensional random variable (X, Y) with a joint probability density $p_{(X,Y)}$, where both X and Y take arguments from $\mathbb{R}$. We obtain a marginal probability density of X by integrating $p_{(X,Y)}$ over Y

$$p_X(x) = \int_{\mathbb{R}} p_{(X,Y)}(x, y)\;dy. \tag{6.4}$$

Now, analogously to Eq. (6.1), we define a conditional probability density of X given $Y = y$

$$p_{X|Y}(x|y) = \begin{cases} \frac{P_{(X,Y)}(x,y)}{p_Y(y)}, & \text{if } \; p_Y(y) \neq 0, \\ 0, & \text{otherwise.} \end{cases} \tag{6.5}$$

Eq. (6.2) can then be rewritten in terms of conditional probability densities (for $p_Y(y) \neq 0$)

$$p_{X|Y}(x|y) = \frac{p_{Y|X}(y|x)\;p_X(x)}{p_Y(y)} \tag{6.6}$$

A generalization of Eq. (6.6) to more than two dimensions is straightforward.

Frequentist and Bayesian approaches to probability theory From a practical point of view we often need to employ more operational definitions of probability than the one associated with measuring sets. One can then interpret them in a way that guarantees a fulfillment of the Kolmogorov axioms (see, *e.g.*, [197]).

One such (so-called *frequentist*) approach defines a probability based on a series of repeatable experiments. The probability that event A can happen is associated with the number of n trials of the experiment in which it actually happened out of the total number of repetitions N. In order to make this definition exact one employs a limit $N \to \infty$ and obtains

$$P_{\text{fr}}(A) = \lim_{N\to\infty} \frac{n}{N}. \tag{6.7}$$

In practice it is enough to assume that one can always perform one more experiment to obtain $P_{\text{fr}}(A)$ with any desired accuracy.

Another, namely *Bayesian*, approach to probability theory is based on a *degree of belief* of an observer. The main advantage here over the frequentist probability is such that Bayesian probability can be applied to non-repeatable experiments. It also allows one to take into account a prior expectations before experimental data are employed. Some methods to construct Bayesian probability consistent with the Kolmogorov axioms can be proposed (see, *e.g.*, *coherent bet* introduced by Finetti [198]).[3] However, one can in principle employ the Bayes theorem and the Bayesian interpretation of probability without referring to a specified probability space and the Kolmogorov axioms (*e.g.*, based on the Cox theorem).

In the following we will employ the Bayes theorem to statistical analyses of SUSY models.

Bayesian analysis of SUSY models In the context of a Bayesian analysis of supersymmetric models (for a discussion see, *e.g.*, [199]) we introduce a multidimensional random variable

$$\eta = (\theta, \psi), \tag{6.8}$$

where θ corresponds to SUSY model parameters and ψ contains so-called *nuisance* parameters that encode the uncertainty in determination of relevant parameters of the SM. Moreover, we define a set of *derived variables*

$$\xi = (\xi_1, \ldots, \xi_m). \tag{6.9}$$

They describe the observable quantities calculated for a given model point η that can be compared with the experimental data

$$d = (d_1, \ldots, d_m). \tag{6.10}$$

Let Θ be a set of allowed values of η and $\mathcal{D}$ describe all the possible experimental results. The sample space is defined then as $\Omega = \Theta \times \mathcal{D}$ with a joint probability

[3] This is a so-called *subjective* Bayesian approach. Alternatively, in an *objective* approach, one can try to construct more opinion-independent priors (see, *e.g.*, the Jeffreys prior).

density $p_{(\eta,d)}$. Integrating $p_{(\eta,d)}$ over $\mathcal{D}$ or Θ we can obtain marginal probability densities $\pi(\eta)$, a so-called *prior*, and $\mathcal{Z}(d)$, a so-called *evidence*, respectively. Eq. (6.6) can then be rewritten as

$$p(\eta|d) = \frac{p(d|\xi)\ \pi(\eta)}{\mathcal{Z}(d)}, \tag{6.11}$$

where the probability density $p(\eta|d)$ is called the *posterior*, while $p(d|\xi) = \mathcal{L}$ is the *likelihood* function.[4]

It is easy to see that the prior, the likelihood and the posterior depend on a SUSY model that is considered since they explicitly depend on the choice of η. This may not be so evident in the case of $\mathcal{Z}(d)$, but one has to remember that, in order for Eq. (6.11) to hold, the evidence must be understood as a marginalized probability

$$\mathcal{Z}(d) = \int p_{(\eta,d)}(\eta, d)\ d\eta = \int \mathcal{L}\, \pi(\eta)\, d\eta, \tag{6.12}$$

where in the second step we used Eq. (6.5). In other words, $\mathcal{Z}(d)$ depends on details of a chosen SUSY model by a choice of a specific probability space. This is sometimes marked explicitly by a formal addition of yet another condition M that encodes the type of a considered SUSY model. We may treat then all the probability densities in Eq. (6.11) as conditional probability densities under a model hypothesis M. This may serve as a method of comparing validity of two different models via so-called *Bayes factors* (see, *e.g.* a discussion in [200]) within the Bayesian approach to probability theory. In the following, the evidence will serve only as a constant (not η dependent) normalization factor in the definition of the posterior.

The prior $\pi(\eta)$ describes our initial belief about the probability distribution of η parameters. The requirement of choosing π may lead to a possible prior-dependence of results that is often considered as a drawback of a Bayesian approach. One way to ameliorate this is to choose a simple *flat prior* $\pi(\theta_i) = const$ for SUSY model parameters, which effectively leads to $p(\theta|d) \propto \mathcal{L}$ in Eq. (6.11). However, one may argue that the flat prior is by no means more natural than some other choices of π, although it just seems to be due to a special choice of parametrization θ. In particular, let us focus on a mass parameter m with the allowed range $m \in [0.1\,\mathrm{TeV}, 10\,\mathrm{TeV}]$. In this case flat prior assigns much larger probability to the region $m \in [1\,\mathrm{TeV}, 10\,\mathrm{TeV}]$ than to the region of low mass $m \in [0.1\,\mathrm{TeV}, 1\,\mathrm{TeV}]$. This so-called *volume effect* may not be desirable both from the point of view of the sampling efficiency (therefore also favored regions in the parameter space) and naturalness (in a sense of the little hierarchy problem). In order to overcome this one could, *e.g.*, use a so-called *log prior* that is flat in $\log m$. Therefore freedom of choosing π may be considered as an advantage of the Bayesian approach. In the case

[4]One should formally write $p(d|\eta)$ rather than $p(d|\xi)$, but this change in notation is well justified by the fact that the parameters η determine the values of ξ, which are then explicitly compared with data d. See also a discussion of theoretical uncertainties in Section 6.1.2.

of the nuisance parameters ψ we typically construct priors as Gaussian probability densities with mean and variance dictated by experimental data.

When presenting results of a Bayesian scan as 1D or 2D plots, one needs to integrate posterior probability densities over all remaining parameters, *i.e.*, use *marginalize posteriors*, *e.g.*,

$$p(\theta_1, \theta_2|d) = \int p(\eta|d)\ d\theta_{i\geqslant 3}\, d\psi. \tag{6.13}$$

6.1.2 Likelihood function and χ^2

The likelihood function $\mathcal{L}$ is the probability density of obtaining some experimental data d given the values of derived variables ξ that are themselves determined by the parameters η. However, one should mention an important caveat here. For a given η the calculated values of derived variables ξ are not necessarily equal to "true" derived variables $\hat{\xi}$. The latter ones would be obtained if the calculation was exact. The former suffers from various theoretical uncertainties and approximations. Unfortunately, we do not know the "true" $\hat{\xi}$ and rather have to compare ξ with the data d, which introduces an additional error. We take this into account by integrating over $\hat{\xi}$ with a proper probability density,

$$\mathcal{L} = p(d|\xi) = \int p(d|\hat{\xi})\, p(\hat{\xi}|\xi)\, d\hat{\xi}. \tag{6.14}$$

We will further assume that all the derived variables $\hat{\xi}_i$ are pairwise independent and that most often a single probability densities $p(\hat{\xi}_i|\xi_i)$ are of Gaussian type with mean values ξ_i and theoretical errors τ_i. Similarly for the experimental data we will take average values d_i and an experimental errors σ_i. Thus Eq. (6.14) leads to

$$\mathcal{L}_i = p(d_i|\xi_i) = \frac{1}{\sqrt{2\pi\,(\sigma_i^2 + \tau_i^2)}}\ \exp\left(-\frac{(d_i - \xi_i)^2}{2(\sigma_i^2 + \tau_i^2)}\right). \tag{6.15}$$

In this case, the total likelihood is a product of single-variable likelihoods

$$\mathcal{L} = \Pi_i \mathcal{L}_i. \tag{6.16}$$

In a construction of the total $\mathcal{L}$ we initially assume that the variables ξ_i have marginal likelihood of Gaussian type, Eq. (6.15). We further assume that Eq. (6.16) holds, which means that the ξ_is are independent random variables.[5] In our statistical

[5]If we only assume that the ξ_is are pairwise uncorrelated, then this will not guarantee that a joint probability distribution of $\xi = (\xi_1, \ldots, \xi_n)$ is a multi-dimensional Gaussian function. To see this let us, *e.g.*, consider two random variables X and $Y = XW$ such that X has a normal distribution $\mathcal{N}(0,1)$ and W has a *Rademacher distribution*. Then X and Y both have the same normal distribution and are uncorrelated but their joint distribution is not a two-dimensional Gaussian function. X and Y are also not independent.

approach the assumption of independent random variables is strictly fulfilled for the parameters η_i and this results in a possible decomposition of prior,

$$\pi(\eta) = \Pi_i \pi(\eta_i). \tag{6.17}$$

Because of this, we can set a prior for each model parameter independently. In principle, the derived variables ξ_i do not have to be independent.[6] However, we will assume for simplicity that Eq. (6.16) holds, which is expected to be a valid approximation as long as we do not over-constrain our model, *i.e.*, do not use too many ξ_is.

Importantly, for some of the experimental limits imposed in our analysis, *e.g.*, SUSY searches at the LHC, we will not use the Gaussian approximation. However, we will still use Eq. (6.16) for the total likelihood which is valid (by definition) for any set of independent random variables with not necessarily Gaussian likelihood. These specific cases will be described in Section 6.3 separately for each relevant constraint.

In order to quantify the difference between the observables ξ_i and the data d_i for a given point in a SUSY model we will follow an approach of the χ^2-test, *i.e.*, we will calculate

$$\chi^2 = \sum_i \left(\frac{d_i - \xi_i}{\sqrt{\sigma_i^2 + \tau_i^2}} \right)^2. \tag{6.18}$$

If random variables ξ_i have Gaussian distributions $\mathcal{N}(d_i, \sqrt{\sigma_i^2 + \tau_i^2})$, χ^2 in Eq. (6.18) has a χ^2-distribution. For simplicity we normalize the likelihood functions in Eq. (6.15) to unity, *i.e.*, we neglect a factor $1/\sqrt{2\pi(\sigma_i^2 + \tau_i^2)}$ in front, and obtain

$$\chi^2 = -2 \sum_i \ln \mathcal{L}_i. \tag{6.19}$$

In the following, for simplicity we will use Eq. (6.19) to calculate χ^2 even in some rare cases when the likelihood function $\mathcal{L}_i$ will not be of Gaussian type. We will always normalize $\mathcal{L}_i$ to unity in order to make sure that for a perfect fit χ^2 vanishes.

[6] A simple pedagogical example goes as follows. Suppose X, Y are independent random variables uniformly distributed over a range $[0, 1]$ and we construct new random variables $W = X + Y$ and $Z = X - Y$. They are not independent since, *e.g.*,

$$0 = P(W > 1.9, Z > 0.9) \neq P(W > 1.9)\, P(Z > 0.9).$$

6.1.3 Confidence and credible intervals

Using χ^2 we will construct the *confidence intervals*. By definition a $(1-\alpha)$ confidence interval contains the true value of a parameter with a probability equal to $1-\alpha$.[7] They can be constructed in terms of the difference between actual values of χ^2 and its minimum value $\chi^2_{\rm min}$ obtained for the best fit point in the whole model[8]

$$\Delta\chi^2 = \chi^2 - \chi^2_{\rm min}. \tag{6.20}$$

Points in the parameter space lie inside the $(1-\alpha)$ confidence interval if $\Delta\chi^2 \leqslant \Delta\chi^2_{{\rm crit},1-\alpha,N}$, where N denotes the number of degrees of freedom that corresponds to the dimension of the confidence interval. For example $\Delta\chi^2_{{\rm crit},95\%,2} = 5.99$ for the two-dimensional interval with 95% confidence level (CL).

Within the Bayesian approach we construct $(1-\alpha)$ *credible regions* that contain $1-\alpha$ portion of the posterior. In a two-dimensional case we choose the smallest of all such possible intervals. In one-dimensional plots we define $(1-\alpha)$ credible region by assuming that both above and below this region the remaining posterior corresponds to $\alpha/2$ probability (so-called equal-tail-probabilities ordering rule). The credible regions in general depend on parametrization. This means that an actual set of points in a $(1-\alpha)$ credible region can change when one marginalizes the posterior with respect to different parameters. They also do not have to contain the best fit point in contrast to the confidence intervals.

6.2 Scanning technique

So far we have described the statistical treatment of various points in the parameter space of a SUSY model that allows us to assess the validity of a given point in the parameter space, $\eta \in \Theta$, as well as the credibility of the whole model. Ideally one would like to find $\mathcal{L}$ for each η, rewrite it in terms of the posterior and present results by a proper marginalization. However, this procedure meets obvious difficulties. For instance, in numerical scans of the parameter space Θ only a small fraction of points can be evaluated within a reasonable computing time. The issue arises of how to efficiently sample Θ and find the best fitted regions. A naive grid scan is in most cases not manageable, *e.g.*, for a rectangular grid in $\eta = (\eta_1, \ldots, \eta_n)$ parameters space, with n being the number of parameters (model's and nuisance), performing m steps in each dimension requires m^n point evaluations in total. This can easily become an unreasonably large number, unless one limits m to be a very small integer.

[7] In order to make this definition unique one often assumes additionally that the $(1-\alpha)$ confidence interval is the most compact of all the intervals satisfying the aforementioned condition. In our approach the confidence intervals are defined uniquely and independently of reparametrization by a construction described in the text.

[8] We approximate $\chi^2_{\rm min}$ with the lowest value of χ^2 obtained in the scan.

However, in this case the scan resolution will typically be not satisfactory enough to find interesting regions in Θ.

One way to solve the sampling efficiency problem is provided by a wide family of numerical methods based on random scans that are commonly referred to as Markov Chain Monte Carlo (MCMC) methods [201]. MCMC methods allow one to dramatically improve the sampling efficiency in comparison with grid scans. However, in general they still require a major computing effort to derive reliable results.

One further step in increasing the sampling efficiency that we employ in our numerical analyses can be performed thanks to the Nested Sampling algorithm [202] implemented in the `MultiNest` computer package [203, 204]. The method was initially proposed for computing the evidence but the posterior can be inferred from the scan. We introduce a so-called *prior volume*

$$X(\lambda) = \int_{\mathcal{L}\geqslant\lambda} \pi(\eta)\, d\eta. \tag{6.21}$$

As can be easily seen, $0 \leqslant X(\lambda) \leqslant 1$. One can then formally rewrite Eq. (6.12) using a volume element dX

$$\mathcal{Z} = \int_0^1 \mathcal{L}\, dX, \tag{6.22}$$

which allows one to replace a multidimensional integral by a one-dimensional one that is evaluated in the algorithm. In order to calculate $\mathcal{Z}$ one needs to identify the regions with the highest $\mathcal{L}$ that contributes the most to the integral in Eq. (6.22). We first randomly (according to the prior) find a set of N initial, so-called *live*, points and order them by the likelihood $\mathcal{L}_1 < \ldots < \mathcal{L}_N$. We then discard point with the lowest likelihood $\mathcal{L}_1$ and replace it with a new point that has larger likelihood $\mathcal{L}_{\text{new}}$. This means that we effectively look for a new point within an iso-likelihood contour $\mathcal{L} > \mathcal{L}_1$. Next, the procedure is repeated with $\min\left[\mathcal{L}_{\text{new}}, \mathcal{L}_2\right]$ *etc.* A schematic plot presenting the main idea of the Nested Sampling algorithm is shown in Fig. 6.1.

The real power of the Nested Sampling algorithm manifests itself in the way how X_i at each step can be estimated without performing a multi-dimensional integral in Eq. (6.21) (for details see [202])

$$X_i \approx \exp\left(-\frac{i}{N}\right). \tag{6.23}$$

The evidence can then be evaluated from Eq. (6.22), *e.g.*, by applying the trapezoidal rule

$$\mathcal{Z} = \sum_{i=1}^{M} \mathcal{L}_i\, w_i, \tag{6.24}$$

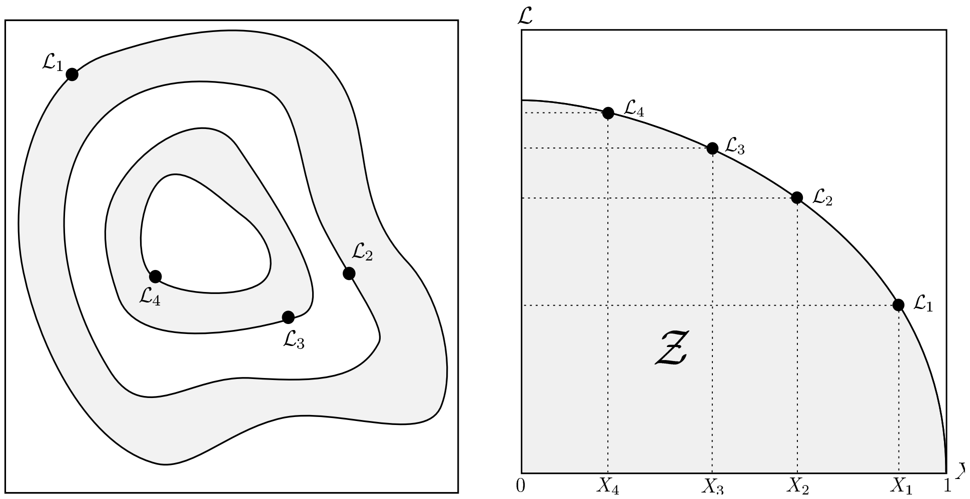

Figure 6.1: Cartoon illustration of *Left panel*: iso-likelihood contours in the case of two-dimensional scan and *Right panel*: likelihood function values $\mathcal{L}_i$ with corresponding prior volumes X_i. Taken from Ref. [205].

where $\mathcal{L}_i$ is the likelihood for the point replaced in the ith step, M is the total number of replacements (steps) and "weights" are equal to $w_i = (X_{i-1} - X_{i+1})/2$. The posterior for the "replaced" points can be derived from[9]

$$p_i = \frac{\mathcal{L}_i \, w_i}{\mathcal{Z}}. \tag{6.25}$$

BayesFITS package Having discussed the basic features of the sampling algorithm we will now move to a brief description of a numerical tool used by us when performing scans over the parameter space of a SUSY model, namely the `BayesFITS` package (see [206, 207]). `BayesFITS` is an interface between several external, publicly available numerical packages. In particular, the aforementioned `Multinest` [203, 204] constitutes the core of the package as the sampling tool. The SUSY mass spectrum is computed with `SOFTSUSY` [208] for the MSSM and with `NMSSMTools` [209, 210, 211] for the NMSSM. This is then taken as input to compute various observables. We use `SuperIso Relic` [212] to calculate B-physics related branching ratios (see Section 6.3.4) and $(g-2)_\mu$ (see Section 6.3.5). The DM observables, such as the relic density and direct detection cross sections, are calculated with `MicrOMEGAs` [144, 213, 214, 215]. The electroweak observables m_W, $\sin^2\theta_{\mathrm{eff}}$ and ΔM_{B_s} (see Section 6.3.6) are calculated using `FeynHiggs` [216].

The `BayesFITS` package is sometimes used by us just as a very efficient sampling tool that allows us to simply identify physically interesting regions of a given SUSY

[9]In the case of the live points that remain at the end of a scan (not having been replaced before) we also apply Eq. (6.25) with the weights $w_i = X_M/N$, *i.e.*, we assume for simplicity that they have almost equal values of the likelihood and we divide corresponding prior volume into equal parts. This is justified since (close to the convergence) the remaining live points have $\mathcal{L} \approx 1$.

model. We then typically present results in terms of two-dimensional 95% confidence intervals instead of 2σ credible regions characteristic for the Bayesian approach.

6.3 Constraints included in the likelihood function

In this section we will describe the constraints imposed on SUSY models in our Bayesian scans via the likelihood function. As mentioned in Section 6.1.2, most of them are implemented assuming Gaussian distribution given by Eq. (6.15). The other cases will be described separately for each contribution to the likelihood. The relevant parameters for the probability distributions are given in Table 6.1.

6.3.1 Dark matter relic density and (in)direct detection limits

DM relic density By far the most significant influence on the parameter space of SUSY models is provided by the relic density constraint. It is implemented via the Gaussian likelihood. When dealing with the Sommerfeld enhancement in the wino DM case, we use enhancement factors from [142].

DM direct detection The other important constraint associated with neutralino DM comes from direct searches through elastic scatterings of DM particles off nuclei. As the neutralinos are WIMPs with non-relativistic velocities, one typically applies the $v \to 0$ limit when calculating cross section. The corresponding cross section can then be decomposed into two contributions: the spin-independent (SI) and the spin-dependent (SD), $\sigma \simeq \sigma^{\rm SI} + \sigma^{\rm SD}$. In general for heavy nuclei targets the SI contribution dominates. It reads

$$\sigma^{\rm SI} = \frac{4\mu_A^2}{\pi}\big[Z\, f_p + (A-Z) f_n\big]^2, \tag{6.26}$$

where Z and A are the nuclei electric charge and atomic number, respectively. $\mu_A = (m\chi\, M_A)/(m_\chi + M_A)$ is the WIMP-nucleus reduced mass with M_A being nucleus atomic mass, while f_p and f_n are the amplitudes for DM scattering on proton and neutron, respectively. Typically $f_p \approx f_n$ and one can rewrite Eq. (6.26) as

$$\sigma^{\rm SI} \approx \frac{4\mu_A^2}{\pi} A^2\, f_p^2 = \sigma_p^{\rm SI}\, \frac{\mu_A^2}{\mu_p^2}\, A^2, \tag{6.27}$$

where $\mu_p = (m\chi\, m_p)/(m_\chi + m_p)$, m_p is the proton mass and we defined

$$\sigma_p^{\rm SI} = \frac{4\mu_p^2}{\pi}\, f_p^2. \tag{6.28}$$

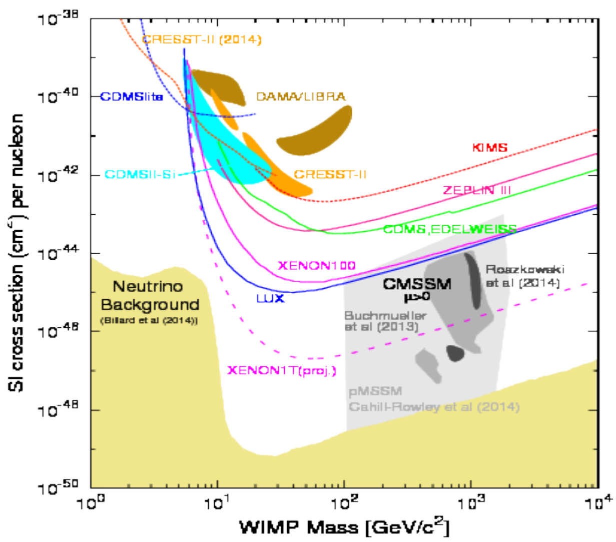

Figure 6.2: Upper limits on σ_p^{SI} as a function of the WIMP mass from various DM direct detection experiments. Solid blue (purple) line corresponds to LUX (Xenon100). Dashed purple line is a projected limit for future Xenon1T experiment. The yellow region on the bottom is the neutrino background. Taken from Ref. [22].

It is this last quantity that we will be comparing with experimental upper limits. Similarly one can obtain the cross section for neutron σ_n^{SI} by replacing $\mu_p \to \mu_n$ and $f_p \to f_n$, but it is basically the same.

Neutralino DM can scatter off of quark via s-channel squark exchange, t-channel CP-even Higgs or Z boson exchange. It is also possible for χ to scatter off of gluons via one-loop diagrams. In the case of EWIMP DM, the cross sections are by far too small to be observed. Hence we do not impose DD constraints on the gravitino or the axino LSP scenarios.

The advantage of using heavy nuclei in detectors can be clearly see from Eq. (6.27) where $\sigma^{\mathrm{SI}} \sim \mu_A^2 A^2$. In particular, in the two DD experiments that we will use to constrain SUSY models, *i.e.*, the Xenon experiment with about 100 kg target material (Xenon100) and the Large Underground Xenon (LUX) experiment, the target is made of liquid xenon.[10] Current upper bounds on σ_p^{SI} are shown in Fig. 6.2. In our Bayesian scans we will treat these limits as a sharp cut-off, *i.e.*, we will assign $\mathcal{L} = 1$ for all the points lying below the exclusion lines, while $\mathcal{L} = 0$ for the remaining ones. Such an approach is often acceptable, since most of phenomenologically interesting regions reach σ_p^{SI} well below the current limits. For the points lying close to the exclusion lines, exhibit the whole FP region for $\mu > 0$, a more proper and elaborate treatment taking into account uncertainties was used in [217].[11]

[10]The other advantages of using xenon are, *e.g.*, high density and scintillation yield.

[11]As can be seen from Fig. 6.2, for sufficiently low σ_p^{SI}, direct searches of DM will meet another difficulty that comes from nuclear recoils due to the elastic scatterings of solar, atmospheric and diffuse supernovae neutrinos. Although this is not a strict lower limit ("neutrino floor") for

One should mention here that a DM signal with mass of the order of several GeV has been claimed by some DD experiments. However, it has not been confirmed by several other experiments including Xenon100 [218, 219] and LUX [124].

DM indirect detection Neutralinos as DM particles freeze-out from thermal plasma in the early Universe. After that point, their subsequent annihilations play a negligible role in determining the DM relic density. Nevertheless, some annihilation events indeed still take place and can give rise to interesting signals in astrophysical observations. In order to increase expected signal rates one typically looks for such signatures from nearby regions of the Universe with potentially large DM density, *i.e.*, from the center of our Galaxy or from nearby galaxy clusters.

The list of possible signals consist mainly of (anti-)protons, (anti-)electrons, γ-rays and energetic neutrinos. However, in DM indirect detection (ID) experiments one needs to take into account various sources of astrophysical background. Because of such background it turns out that it is particularly difficult to use cosmic protons or electrons to observe signals from DM annihilations. Several possible signals of DM in ID experiments have already been claimed, but the nature of these results is still a matter of discussion and its possible astrophysical origin is taken into account.

In the numerical analyses presented in this thesis we do not impose ID limits on bino and higgsino DM due to their relative weakness. However, the situation is entirely different in a scenario with wino DM as will be discussed in Section 8.1.

Gravitino or axino DM candidates do not lead to observable effects in DM ID due to annihilations, but could potentially generate an interesting signal from decays in R-parity violating scenarios. An example of such an analysis with a possible explanation of 3.5 keV line that incorporates decaying gravitino DM with mass $m_{\tilde{G}} \simeq 7\,\text{keV}$ was given in [170]. For a similar study in the case of axino DM see [220, 221].

6.3.2 Higgs boson mass and signal rates

Higgs boson mass The recent discovery of the Higgs boson has introduced another important constraint on SUSY models. It is implemented as a Gaussian likelihood. The theoretical error of m_h that we incorporate is due to residual difference between calculations using different approaches and renormalization schemes. It is estimated in the literature to be of the order of $2-3\,\text{GeV}$ [59].

When discussing the CNMSSM in Section 7.2 we take into account the possibility that the lightest Higgs scalar h_1 has mass below 126 GeV and remains invisible in the current searches, while the observed signal corresponds to the second-to-lightest scalar h_2. In this case we replace m_{h_1} with m_{h_2} in the likelihood function. In another

experimentally accessible values of σ_p^{SI}, without a proper treatment of this background one would not be able to successfully look for WIMP DM giving such a low scattering cross section.

scenario we consider a mass degeneracy $m_{h_1} \simeq m_{h_2} \simeq 126\,\mathrm{GeV}$. According to the discussion in Section 6.1.2, we assume that in our statistical approach the random variables $m_{h_1}^{\mathrm{calc}}$ and $m_{h_2}^{\mathrm{calc}}$ (calculated) are independent. Thus we employ a product likelihood $\mathcal{L}_{m_h} = \mathcal{L}_{m_{h,1}} \mathcal{L}_{m_{h,2}}$ with the $\mathcal{L}_{m_{h,i}}$ being an appropriate Gaussian function. A similar approach is used in Section 7.3 in the context of the partially non-universal version of the CNMSSM where we consider a possible mass degeneracy between h_1 and lighter pseudoscalar a_1 with $m_{h_1} \simeq m_{a_1} \simeq 126\,\mathrm{GeV}$.

Higgs boson signal rates In the initial announcement of the Higgs boson discovery in the year 2012 an enhancement in the $h \to \gamma\gamma$ decay channel was reported by ATLAS, with $\mu(\gamma\gamma) = 1.9 \pm 0.5$, as well as by CMS, with $\mu(\gamma\gamma) = 1.6 \pm 0.4$, where $\mu(X)$ is the ratio of the observed Higgs production cross section to the one predicted by the SM in a Higgs decay channel $h \to X$. On the other hand, the updated values of $\mu(ZZ)$ by CMS [222] and ATLAS [223] were, within 1σ error, SM-like. We took this into account when performing scans at that time.[12]

We calculated for both Higgs bosons $h_{1,2}$ the reduced cross sections

$$R_{h_i}(X) = \frac{\sigma(pp \to h_i)}{\sigma(pp \to h_{\mathrm{SM}})} \times \frac{BR(h_i \to X)}{BR(h_{\mathrm{SM}} \to X)}\,, \tag{6.29}$$

for a given Higgs decay channel X. Equation (6.29) can be approximated by

$$R_{h_i}(X) = \sum_{Y \in \text{ prod}} R_{h_i}^{Y}(X) \mathcal{R}_{\mathrm{SM}}(Y)\,, \tag{6.30}$$

where the sum runs over the Higgs production channels Y (with $Y = gg$ for gluon-fusion, VV for vector boson-fusion and Higgs-strahlung off a Z boson, $t\bar{t}$ and $b\bar{b}$ for associated Higgs production with top and bottom quarks, respectively). The ratios $\mathcal{R}_{\mathrm{SM}}(Y) \equiv \sigma(pp \to Y \to h_{\mathrm{SM}})/\sigma(pp \to h_{\mathrm{SM}})$ were obtained from public tables provided by the LHC Higgs Cross Section Working Group [224, 225] for $\sqrt{s} = 8\,\mathrm{TeV}$.

The reduced cross sections $R_{h_i}^{Y}(X)$ for the individual production channels were calculated as

$$\begin{aligned} R_{h_i}^{Y}(X) &\equiv \frac{\sigma(Y \to h_i)}{\sigma(Y \to h_{\mathrm{SM}})} \times \frac{\mathrm{BR}(h_i \to X)}{\mathrm{BR}(h_{\mathrm{SM}} \to X)} \\ &= C^2(Y) \times \frac{\Gamma(h_i \to X)/\Gamma_{\mathrm{tot}}}{\Gamma(h_{\mathrm{SM}} \to X)/\Gamma_{\mathrm{tot}}^{\mathrm{SM}}} \\ &= C^2(Y) C^2(X) \sum_{F \in \text{ SM decay}} \frac{\mathrm{BR}(h_i \to F)}{C^2(F)}\,, \end{aligned} \tag{6.31}$$

[12]We only used the dominant decay channels where an about 5σ excess had already been observed.

where the sum runs over the decay channels F open to the SM Higgs boson and quantities $C(X)$ are called the Higgs reduced couplings (the ratio of the couplings of the Higgs boson with a given mass to a pair of X particles within SUSY, to the ones calculated in the SM).

In the case of mass-degenerate h_1 and h_2 only the combined production rate for h_1 and h_2 needed to be equal to $R_{\rm obs}(X)$. Hence the observation likelihood was defined as

$$\mathcal{L}_{\rm obs}(X) = \exp\left\{-\left[R_{\rm obs}(X) - (R_{h_1}(X) + R_{h_2}(X))\right]^2/2(\sigma_X^2 + \tau_X^2)\right\}. \tag{6.32}$$

In addition to constraining $h_{\rm sig}$, we also required that the second of the two lightest CP-even Higgs bosons remained "hidden", *i.e.*, it must had escaped detection at the LHC (or at LEP if light enough). In the following we refer to this as $h_{\rm hid}$. We constructed an "exclusion" likelihood. Following the procedure outlined in [199] for the exclusion bounds we first defined a step function,

$$\mathcal{L}_{\rm excl}^{\rm (step)}\left(m_{h_{\rm hid}}, R_{h_{\rm hid}}(X), \mu_{95}(X)\right) = \begin{cases} 1 & \text{for } R_{h_{\rm hid}}(X) \leqslant \mu_{95}(X) \\ 0 & \text{for } R_{h_{\rm hid}}(X) > \mu_{95}(X), \end{cases} \tag{6.33}$$

where $\mu_{95}(X)$ is the value of the *signal strength modifier* $\mu(X) \equiv \sigma_{h_{\rm hid}}(X)/\sigma_{h_{\rm SM}}(X)$ that was excluded at 95% C.L. by the LHC searches for a Higgs with a given mass $m_{h_{\rm hid}}$, obtained from the exclusion plots published by the CMS Collaboration[226]. The LEP exclusion limits were also taken into account.

In order to include the theoretical error on the true values of the reduced cross section and the Higgs mass, $\mathcal{L}_{\rm excl}^{\rm (step)}$ became then smeared out further by convolving it with Gaussian functions centered around their true theoretical values $\hat{R}_{h_{\rm hid}}(X)$ and $\hat{m}_{h_{\rm hid}}$, respectively

$$\begin{aligned}\mathcal{L}_{\rm excl}^{\rm (smear)}\left(m_{h_{\rm hid}}, R_{h_{\rm hid}}, \mu\right) = &\int d\hat{m}_{h_{\rm hid}} \int d\hat{R}_{h_{\rm hid}}\, \mathcal{L}_{\rm excl}^{\rm (step)}\left(\hat{m}_{h_{\rm hid}}, \hat{R}_{h_{\rm hid}}, \mu\right) \\ &\times \exp\left[-\frac{(\hat{m}_{h_{\rm hid}} - m_{h_{\rm hid}})^2}{2\tau^2}\right] \exp\left[-\frac{(\hat{R}_{h_{\rm hid}} - R_{h_{\rm hid}})^2}{2\tilde{\tau}^2}\right],\end{aligned} \tag{6.34}$$

where the theoretical errors were taken to be $\tau = 3\,\text{GeV}$ and $\tilde{\tau} = 15\% \cdot R_{h_{\rm hid}}$[227], respectively. The exclusion likelihood was calculated for $X = \gamma\gamma$, ZZ, WW and $\tau\tau$. Finally, in order for our exclusion criterion to be consistent with our criterion for signal observation at $125.8 \pm 3.1\,\text{GeV}$ (with theory and experimental errors added in quadrature), we further imposed the condition

$$\mathcal{L}_{\rm excl}(X) = \begin{cases} 0 & \text{for } 122.7\,\text{GeV} \leqslant m_{h_{\rm hid}} \leqslant 128.9\,\text{GeV}, \\ \mathcal{L}_{\rm excl}^{\rm (smear)}(X) & \text{elsewhere.} \end{cases} \tag{6.35}$$

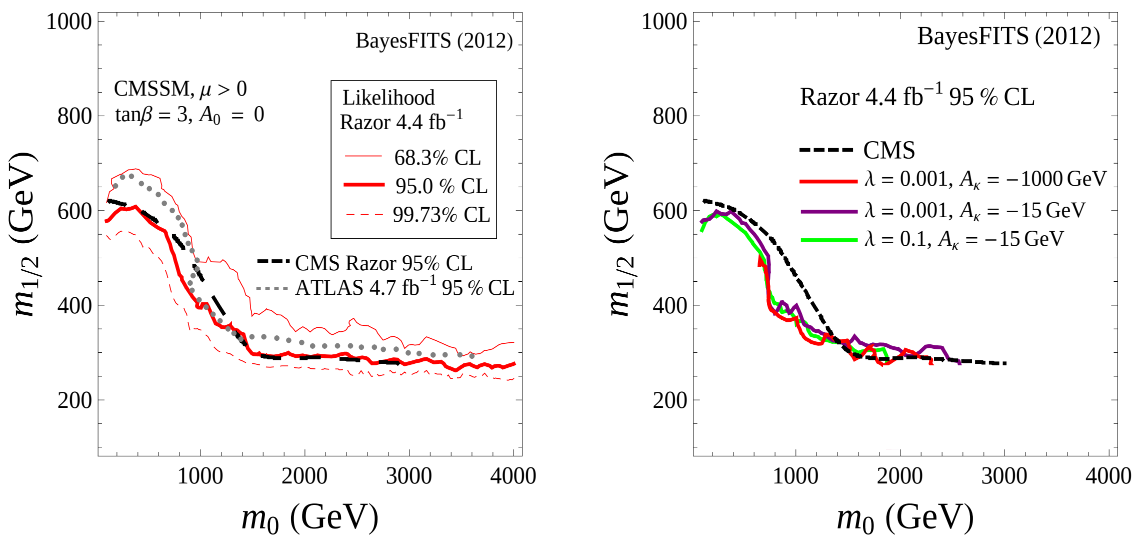

Figure 6.3: *Left panel*: Our approximation of the CMS razor $4.4\,\mathrm{fb}^{-1}$ likelihood map for the CMSSM. $\tan\beta = 3$ and $A_0 = 0$ are fixed. The thick solid line shows the 95.0% CL (2σ) bound. It approximates the CMS 95% CL exclusion contour, shown by the dashed black line. The thin solid line and the thin dashed line show our calculations of the 68.3% CL (1σ) the 99.73% CL (3σ) exclusion bound, respectively. The dotted gray line shows the ATLAS 95% CL exclusion bound. Taken from Ref. [206]. *Right panel*: The 95% C.L. lower bounds from our razor likelihood for the CNMSSM, for different values of λ and A_κ, compared with the experimental line (in dashed black). Taken from Ref. [207].

6.3.3 Direct searches for supersymmetric particles

In our Bayesian analyses we need also to take into account the LHC lower limits on the SUSY mass particles that come from lack of SUSY signal in data so far. We focus on the $SU(3)_c$ sector of the MSSM, where bounds are the strongest.

When performing CMSSM and CNMSSM (see Sections 7.1 and 7.2) analysis we derived our LHC likelihood for the CMS search [228] following the so-called razor method [229]. We generated a two-dimensional grid of points in the $(m_0,\ m_{1/2})$ plane, namely the *likelihood map*. The other parameters can be shown to play a much less important role [230, 231], because they have little effect on the squark and gluino masses. For each point in a grid we assigned a value of the likelihood function describing exclusion limits, *i.e.*, we put $\mathcal{L} \approx 1$ for allowed points and $\mathcal{L} \approx 0$ for points corresponding to SUSY particle masses that were well below the exclusion limits. The values of $\mathcal{L}$ for points close to the exclusion limits were obtained by approximate razor analysis that followed closely the full one of the CMS Collaboration [229]. A similar approach was applied when discussing a ten-parameter version of the MSSM (p10MSSM) in Chapter 8. However, in this case we constructed a likelihood map in the gluino and squark mass plane $(m_{\tilde{g}}, m_{\tilde{q}})$.

We present our results for the CMSSM in Fig. 6.3 (left panel) as the 68.3% (1σ), 95.0% (2σ) and 99.73% CL (3σ) limits obtained from our likelihood. The reproduced 95% CL razor contour for the CNMSSM is shown in Fig. 6.3 (right panel). We also show that the dependence of the limit on λ and A_κ is negligible.

6.3.4 B-physics

Rare leptonic decays of neutral B mesons in the SM are absent at tree-level and appear dominantly at one-loop level in W-box and Z-penguin diagrams. Moreover, the corresponding branching ratios (BRs) of these flavor changing neutral current (FCNC) decays are helicity suppressed (for a review see, *e.g.*, [232, 233]). Because of this, it is possible for a loop-level supersymmetric contributions to become comparable with the SM values. Thus one expects that SUSY could manifest itself in a precise determination of such BRs. Conversely, this can also serve as an useful constraint on SUSY models when comparing with experimental data.

Similarly the effect of SUSY can be seen in radiative inclusive decays of B meson that is driven by the process $b \to s\gamma$ (for a review see, *e.g.*, [232, 234]) or in the $B_s - \bar{B}_s$ mixing (for a pedagogical introduction see [235]).

$\boldsymbol{B_s \to \mu^+\mu^-}$ One such example of a rare process is the decay of strange meson B_s, composed of $\bar{b}s$ pair of quark and anti-quark, to a pair of muons. The corresponding BR is proportional to [236, 237, 238, 239]

$$\mathrm{BR}(B_s \to \mu^+\mu^-) \propto \left\{ \left(1 - \frac{4\, m_\mu^2}{M_{B_s}}\right) |F_S^2| + |F_P + F_A|^2 \right\}, \tag{6.36}$$

where m_μ and M_{B_s} denotes the muon and the B_s meson mass, respectively. F_A, F_S, and F_P are the axial-vector, pseudo-scalar and scalar form factor, respectively.

In the SM the dominant contribution to $\mathrm{BR}(B_s \to \mu^+\mu^-)$ is associated with $F_A = -i\, m_\mu\, f_{B_s}\, C_{10}$, where f_{B_s} is the B_S decay constant and C_{10} is the corresponding Wilson coefficient. Other terms are suppressed by m_μ/M_W, where M_W is the W-boson mass. Since B_s is a flavor eigenstate, rather than a mass eigenstate, when comparing with experimental data, one uses a value of $\overline{\mathrm{BR}}(B_s \to \mu^+\mu^-)$ that is flavor-averaged and time-integrated over $B_s - \bar{B}_s$ oscillations [240]. According to recent calculations [241], its SM value is equal to

$$\overline{\mathrm{BR}}(B_s \to \mu^+\mu^-) = (3.65 \pm 0.23) \times 10^{-9}. \tag{6.37}$$

In the case of SUSY the F_S and F_P terms can become comparable to the F_A one. Their dominant dependence on the SUSY parameters [242, 243] can be recast as [115]

$$F_{S,P} \propto \frac{\tan^3\beta}{m_A^2}\mathcal{F}_{\rm LO}, \tag{6.38}$$

where for the phenomenologically interesting regions of SUSY models that we will consider,

$$\mathcal{F}_{\rm LO} \simeq -\mu\, A_t\, \mathcal{D}_3\, \frac{m_t^2}{m_{\tilde{t}_1}^2 - m_{\tilde{t}_2}^2}, \tag{6.39}$$

where $\mathcal{D}_3 \sim 0.1 - 0.3$, m_t is the top mass, while $m_{\tilde{t}_1}$ and $m_{\tilde{t}_1}$ denote the mass of the lighter and heavier stop, respectively. As can be seen $\overline{\rm BR}(B_s \to \mu^+\mu^-)$ in SUSY is enhanced for large $\tan\beta$, μ and $|A_t/M_{\rm SUSY}|$ and relatively small m_A.

The choice of the theoretical error $\tau_{B_s\mu\mu}$ in the corresponding Gaussian likelihood follows [244]. We subtract the uncertainty, about 1%, due to the top pole mass since it is included by adding a corresponding nuisance parameter to our scans (see Section 6.4). The recent calculation suggests a reduction of $\tau_{B_s\mu\mu}$ in the SM, as can be seen in Eq. (6.37).

$\boldsymbol{B_u \to \tau\nu}$ In our analysis we also take into account the B_u meson $(u\bar{b})$ leptonic decay to tau and anti-neutrino. Because of the helicity suppression, the decay into τ is dominant, in comparison with the decays into muon or electron, due to lepton mass hierarchy $m_\tau > m_\mu, m_e$. In the SM the decay occurs via W-boson exchange. In the MSSM there appears an additional decay channel via charged Higgs boson that can interfere both constructively and destructively with the SM contribution. The ratio between the SM and the MSSM branching ratios is given by [245]

$$\frac{{\rm BR}(B_u \to \tau\nu)^{\rm MSSM}}{{\rm BR}(B_u \to \tau\nu)^{\rm SM}} \approx \left[1 - \tan^2\beta\left(\frac{m_{B_u}}{m_{H^\pm}}\right)^2\right]. \tag{6.40}$$

Current average [7] of the experimental results obtained by Bell [246, 247] and BaBar [248, 249] Collaborations reads ${\rm BR}(B_u \to \tau\nu)^{\text{exp, aver.}} = (1.14 \pm 0.23) \times 10^{-4}$. However, only the recent Belle analysis [247] has been updated using the hadronic B decay sample. We use the results of this analysis to determine the parameters of the Gaussian likelihood in our recent scans. The theoretical uncertainty results from uncertainties in the CKM matrix elements, as well as from the B_u meson lifetime and its decay constant [205].

As can be derived from Eq. (6.40), an enhancement in ${\rm BR}(B_u \to \tau\nu)^{\rm MSSM}$ in comparison with the SM can be obtained for $\tan\beta/m_{H^\pm} > (0.25 - 0.3)\,{\rm GeV}^{-1}$. When $\tan\beta/m_{H^\pm} \approx 0.19\,{\rm GeV}^{-1}$ both W-boson and $H^\pm$ contributions cancel each other. However, the ratio $\tan\beta/m_{H^\pm}$ is often significantly lower leading to ${\rm BR}(B_u \to \tau\nu)^{\rm MSSM} \approx {\rm BR}(B_u \to \tau\nu)^{\rm SM}$.

$\bar{\boldsymbol{B}} \to \boldsymbol{X_s\gamma}$ Another constraint associated with B-physics comes from the $\bar{B}$ meson ($\bar{d}b$) decay into a hadron X_s with a strange flavor. It is mediated by the FCNC process $b \to s\gamma$, which is loop-suppressed in the SM [13] and therefore can obtain important contributions from SUSY particles. The corresponding branching ratio in the SM was calculated in [251, 252] and the result reads

$$\mathrm{BR}(b \to s\gamma)^{\mathrm{SM}} = (3.15 \pm 0.23) \times 10^{-4}. \tag{6.41}$$

In the context of SUSY penguin loop diagrams involving W-boson are accompanied by charged Higgs, chargino, neutralino and gluino loops (see, *e.g.* [253, 254]). Depending on which diagrams dominate the SUSY contribution can be proportional to $1/\tan\beta$ or A_t.

$\boldsymbol{\Delta M_{B_s}}$ B_s and $\bar{B}_s$ are flavor eigenstates rather than mass eigenstates. They mix non-trivially to form two mass eigenstates: $B_{s,l}$ (lighter) and $B_{s,h}$ (heavier). A transition between B_s and $\bar{B}_s$ may occur via box diagrams involving quarks and the W-boson in the SM, as well as, *e.g.*, squarks, gluinos, charginos, Higgs bosons in SUSY. As a result one can observe oscillations between pure flavor states with a frequency determined by the mass difference between $B_{s,l}$ and $B_{s,h}$. The SM prediction of this quantity is currently equal to [235]

$$\Delta M_{B_s}^{\mathrm{SM}} = (17.3 \pm 1.5)\,\mathrm{ps}^{-1}. \tag{6.42}$$

When calculating SUSY contributions we follow [254, 255].

6.3.5 Anomalous magnetic moment of muon

For a particle with mass m, electric charge e and spin $\vec{S}$ the magnetic moment $\vec{\mu}$ can be written as

$$\vec{\mu} = g\left(\frac{e}{2m}\right)\vec{S}, \tag{6.43}$$

where g is the gyromagnetic ratio that is equal to $g = 2$ at tree level in QED for elementary spin-1/2 particles. Involving loop diagrams, strong and weak interactions, as well as (potentially) new physics like SUSY leads to the so-called *anomalous magnetic moment*

$$a = \frac{1}{2}(g-2), \tag{6.44}$$

that describes the difference $g \neq 2$. This quantity for muon was measured with great precision at the Brookhaven national Laboratory [256]

$$a_\mu^{\mathrm{exp}} = 11\,659\,208.0(6.3) \times 10^{-10}. \tag{6.45}$$

[13] In can be also CKM suppressed, see [250].

The SM prediction of a_μ can be decomposed to QED, weak and hadronic contributions. The QED one is dominant and well theoretically controlled. The weak contribution is the smallest, although within the precision of the experimental result. In general it has similar magnitude to the corrections expected from new physics [257]. The most problematic part is associated with hadronic processes. It can be further decomposed into vacuum polarization and light-by-light scatterings contributions. The former can be derived from experimental data in electron-positron collisions or hadronic decays of tau [258]. However, these methods lead to the results that are not entirely consistent with each other [257]. The light-by-light contribution cannot be inferred from experiment. A discrepancy between its various theoretical evaluations is one of the important sources of the theoretical uncertainty in a_μ.

An enhancement in a_μ in the context of SUSY is mainly due to an increase of the Yukawa coupling of muon by a factor of $1/\cos\beta \approx \tan\beta$ for large $\tan\beta$. This, *e.g.*, enters into the coupling of muon to Higgs bosons and higgsinos in corresponding loop diagrams. Another contributions are associated with loop diagrams involving, *e.g.*, bino, wino or squarks. To summary the SUSY contribution to the muon anomalous magnetic moment is approximately given by (see, *e.g.*, [257])

$$\delta a_\mu = a_\mu^{\mathrm{MSSM}} - a_\mu^{\mathrm{SM}} \approx 13 \times 10^{-10}\, \mathrm{sgn}(\mu)\ \tan\beta \left(\frac{100\,\mathrm{GeV}}{m_{\tilde{\mu}}}\right)^2, \tag{6.46}$$

where $m_{\tilde{\mu}}$ is the smuon mass.

6.3.6 Electroweak precision observables

Another pair of constraints is associated with two of the fundamental parameters used in a description of the EWSB, namely the W-boson mass M_W and the effective weak mixing angle $\sin\theta_{\mathrm{eff}}$. They both can acquire SUSY loop corrections that could be seen after comparing the SM calculations with experimental values.

***W*-boson mass** The dominant SUSY contributions to M_W at one loop level stem from stops and sbottoms via gauge-boson self energies [259, 260]. They are typically written in terms of $\Delta\rho$ that is equal to

$$\Delta\rho = \frac{\Sigma^Z(0)}{M_Z^2} - \frac{\Sigma^W(0)}{M_W^2}, \tag{6.47}$$

where $\Sigma^W(0)$ and $\Sigma^Z(0)$ are transverse parts of the unrenormalized W- and Z-boson self energies at zero momentum transfer, respectively (for more details see [261]). The correction to the W-boson mass can be approximated by [261]

$$\delta M_W \approx \frac{M_W}{2} \frac{c_W^2}{c_W^2 - s_W^2}\, \Delta\rho, \tag{6.48}$$

where $c_W = \cos\theta_W$ and $s_W = \sin\theta_W$ are cosine and sine of the weak mixing angle (see below), respectively.

Effective weak mixing angle At tree level after EWSB the weak mixing angle satisfies

$$\sin^2\theta_W = 1 - \frac{M_W^2}{M_Z^2}. \tag{6.49}$$

However, *e.g.*, in the context of the MSSM, this quantity[14] receives corrections that predominantly arise from loops involving squarks [262], and can be recast as

$$\delta\sin^2\theta_{\text{eff}} \approx \frac{c_W^2\, s_W^2}{c_W^2 - s_W^2}\,\Delta\rho. \tag{6.50}$$

6.4 Nuisance parameters

When performing our Bayesian analyses we also take into account uncertainties in experimental determination of selected SM quantities ψ_i that themselves can have a non-negligible influence on calculated values of the observables described in Section 6.3. To implement this effect we allow these nuisance parameters to vary from their experimental mean values d_{ψ_i} according to a Gaussian prior distribution with the corresponding experimental standard deviations σ_{ψ_i}. We treat as the nuisance parameters: the top mass M_t, the bottom mass m_b, the strong coupling constant α_s and the fine-structure constant α_{em}.

Top mass M_t One nuisance parameter that we employ is the top pole mass defined in the perturbative regime as the pole in top quark propagator. We follow a PDG approach [7] that identifies the top pole mass with a top mass parameter in Monte Carlo event generators. The latter is obtained by fitting the reconstructed kinematic distributions to experimental data [263, 264]. We add in quadrature statistical and systematic uncertainties (1σ).

Bottom mass $m_b(m_b)^{\overline{\text{MS}}}$ The running mass of the bottom quark in the $\overline{\text{MS}}$ renormalization scheme is related to the pole mass M_b by (see [7] and references therein)

$$M_b = m_b(m_b)^{\overline{\text{MS}}}\left\{1 + 0.09 + 0.05 + 0.03\right\}, \tag{6.51}$$

which is valid up to a three-loop level. The choice of the renormalization scale, $\mu = m_b^{\overline{\text{MS}}}$, is a convention. The bottom mass M_b can be inferred from measured

[14]Strictly, the quantity in Eq. (6.50) is the so-called leptonic mixing angle that differs no more [261] than about 1% from $\sin^2\theta_W$ defined in the on-shell renormalization scheme that was used in Eq. (6.49),

energy spectra of the products of B-meson decays [265, 266, 267, 268]. Using Eq. (6.51) one can then obtain $m_b(m_b)^{\overline{\rm MS}}$ with the corresponding uncertainty.

Strong coupling $\boldsymbol{\alpha_s(M_Z)^{\overline{\rm MS}}}$ The energy-scale dependence of the strong coupling strength, defined as $\alpha_s = g_s^2/4\pi$, is described by the corresponding renormalization group equation. We conventionally use as a nuisance parameter the $\overline{\rm MS}$ scheme value of α_s evaluated at the renormalization scale $\mu = M_Z$.

The current world average of $\alpha_s(M_Z)^{\overline{\rm MS}}$ has been obtained [269] by combining many experimental results and theoretical predictions including, *e.g.*, tau-lepton decays, radiative Υ ($b\bar{b}$) decays, lattice QCD calculations, deep inelastic lepton-nucleon scatterings, hadronic events in e^+e^- annihilations, electroweak precision data like the hadronic decay width of the Z-boson *etc.*

In the case of the CMSSM analyses we additionally used as a nuisance parameter an inverse of the **fine-structure constant $\boldsymbol{1/\alpha_{\rm em}(M_Z)^{\overline{\rm MS}}}$** calculated in the $\overline{\rm MS}$ scheme at the renormalization scale $\mu = M_Z$. Its error introduces uncertainty in determining the GUT scale and therefore can change the soft supersymmetric masses at the EWSB scale (after RGE running).

6.5 Parameters of probability distributions

In Table 6.1 we list the parameters of the likelihood function for various constraints taken into account in our analyses. A treatment of direct SUSY searches and DM direct detection is described in Sections 6.3.1 and 6.3.3, respectively.

6.6 Additional cosmological constraints

So far we have discussed various collider and dark matter constraints which were taken into account when performing Bayesian scans of the parameter space of SUSY models. In this section we will focus on additional cosmological constraints that were not included in the likelihood but were imposed later on the results of the scan. They are particularly important when considering EWIMP DM scenarios.

6.6.1 Big Bang Nucleosynthesis

The first such constraint is associated with the Big Bang Nucleosynthesis epoch in the evolution of the Universe (for a review see, *e.g.*, [274]), known also as *primordial nucleosynthesis* epoch. In this process light nuclei (heavier than the proton) were formed. Nuclear fusions led mainly to a production of ^{4}He with smaller abundances of ^{3}He and deuterium ^{2}H, as well as trace amounts of the lithium, beryllium and boron isotopes or nuclei with higher atomic number. In general, the comparison

Measurement	Mean	Error: exp., theor.	Ref.
$\Omega_\chi h^2$	0.1199	0.0027, 10%	[3]
m_h	125.7 GeV	0.4 GeV, 3 GeV	[59, 270]
$R(h \to \gamma\gamma)$	1.6	0.4, 15%	[1, 227]
$R(h \to ZZ)$	0.8	(+0.35, −0.28), 15%	[222, 227]
$\mathrm{BR}(b \to s\gamma) \times 10^4$	3.43	0.22, 0.21	[251, 252, 271]
$\mathrm{BR}(B_u \to \tau\nu) \times 10^4$	0.72	0.27, 0.38	[247]
$\mathrm{BR}(B_s \to \mu^+\mu^-) \times 10^9$	2.9	0.7, 10%	[244, 272, 273]
ΔM_{B_s}	17.719 ps^{-1}	0.043 ps^{-1}, 2.400 ps^{-1}	[7, 205]
$\delta a_\mu \times 10^{10}$	28	8, 1	[7, 258]
$\sin^2\theta_{\mathrm{eff}}$	0.23116	0.00013, 0.00015	[7]
M_W	80.385 GeV	0.015 GeV, 0.015 GeV	[7]
Nuisance parameters			
M_t	173.5 GeV	1 GeV	[7]
$m_b(m_b)^{\overline{\mathrm{MS}}}$	4.18 GeV	0.03 GeV	[7]
$\alpha_s(M_Z)^{\overline{\mathrm{MS}}}$	0.1184	0.0007	[269]
$1/\alpha_{\mathrm{em}}(M_Z)^{\overline{\mathrm{MS}}}$	127.916	0.015	[7]

Table 6.1: The parameters of the likelihood function and Gaussian prior probability distributions for the nuisance parameters.

leads to an excellent agreement between the BBN predictions and the abundances inferred from observations. This serves as one of the major pillars of the Big Bang theory. Some discrepancy in the ^{7}Li abundance can be either associated with its primordial enhanced production[15] or with the post-BBN evolution.

Successful predictions of the BBN may be violated by an inclusion of hadronic or electromagnetic cascades in the early Universe. They could potentially destroy some nuclei X changing the X/H ratios. From now on we will focus on a scenario in which such cascades were initiated by decays of some heavy particle. In particular, we will treat them as generated by the decays of the NLSPs to gravitino or axino DM (for such analyses in the framework of the CMSSM see [275, 276, 277, 278, 279]). We take into account a wide range of the NLSP lifetimes τ_{NLSP} from about 10^{-1} sec to 10^{12} sec. For lower lifetimes the decay products of the NLSPs would thermalize before the proton-neutron decoupling. Thus they would not influence the BBN.

When discussing the BBN constraints below, we will employ limits on the light nuclei abundances used in [280]

$$Y_p < 0.258, \tag{6.52}$$

$$1.2 \times 10^{-5} \lesssim {}^2\,\mathrm{H/H} \lesssim 5.3 \times 10^{-5}, \tag{6.53}$$

$$^3\mathrm{He}/^2\mathrm{H} < 1.52, \tag{6.54}$$

[15]Therefore it can be used to constrain models with a heavy particle decaying during the BBN.

$$^7\text{Li/H} > 0.85 \times 10^{-10}, \tag{6.55}$$

$$^6\text{Li}/^7\text{Li} \lesssim \begin{cases} 0.1 & \text{less conservative,} \\ 0.66 & \text{conservative.} \end{cases} \tag{6.56}$$

Uncertainties in treatment of the lithium-6 and lithium-7 production in stars lead to a possible weakening of the less conservative upper limit on $^6\text{Li}/^7\text{Li} \lesssim 0.1$. Because of this, we will also use the other, more conservative, limit as can be seen in Eq. (6.56).

We distinguish between electromagnetic and hadronic cascades taking into account primary particles produced in such decays. Such a distinction appears to be useful due to a difference in thermalization processes. However, one needs to note that, *e.g.*, an NLSP decay into a pair of quark and anti-quark $q\bar{q}$ does not necessarily lead to a hadronic cascade. In particular, if $q\bar{q}$ form primary π^0, its dominant decay into two photons will induce an electromagnetic cascade. Each such cascade typically contains tens or hundreds of secondary particles.

Depending on the NLSP lifetime such cascades can cause violation of various limits Eq. (6.52)-(6.56) (for an extensive discussion see, *e.g.*, [280]). A schematic plots valid for decays of a 1 TeV electrically neutral NLSP to EWIMP DM which show the regions excluded by BBN constraints in the $(\tau_{\text{NLSP}}, \Omega_{\text{NLSP}} h^2)$ plane where $\Omega_{\text{NLSP}} h^2$ is calculated as if the WIMP was DM can be seen in Fig. 6.4.

If the decaying NLSP is electrically charged, one can obtain stronger BBN bounds for lifetimes $\tau_{\text{NLSP}} \gtrsim 300\,\text{sec}$. This is due to a catalysis of an overproduction of nuclei X with the atomic mass number $A > 4$. It results from the possibility of forming meta-stable bounds states between nuclei and the charged NLSP [281]. This has particular importance for ^{6}Li production rate. An example of this scenario is a stau NLSP decaying into either gravitino or axino DM. In the following we will incorporate this constraint following exclusion plots from [282].

In a simplified approach to the BBN constraints we use the exclusion plots from [280]. The lifetime of the NLSP depends on its mass and the mass of the DM particles. In the case of a neutralino NLSP decaying into gravitino DM the corresponding lifetime for $m_\chi \gg m_{\tilde{G}}$ can be estimated as (see, *e.g.*, [283])

$$\tau_{\chi \to \tilde{G}} \simeq \begin{cases} 57\,\text{sec} \left(\frac{m_{\tilde{B}}}{1\,\text{TeV}}\right)^{-5} \left(\frac{m_{\tilde{G}}}{10\,\text{GeV}}\right)^2, & \text{for bino-like } \chi, \\ 250\,\text{sec} \left(\frac{m_{\tilde{W}}}{1\,\text{TeV}}\right)^{-5} \left(\frac{m_{\tilde{G}}}{10\,\text{GeV}}\right)^2, & \text{for wino-like } \chi, \\ 114\,\text{sec} \left(\frac{m_{\tilde{H}}}{1\,\text{TeV}}\right)^{-5} \left(\frac{m_{\tilde{G}}}{10\,\text{GeV}}\right)^2, & \text{for higgsino-like } \chi. \end{cases} \tag{6.57}$$

If the neutralino mass is closer to the gravitino mass, the lifetime becomes larger due to a phase space suppression. In the case of neutralino decay into axino the lifetime depends on the bino fraction N_{11} of χ, as well as on the values of C_{aYY} and

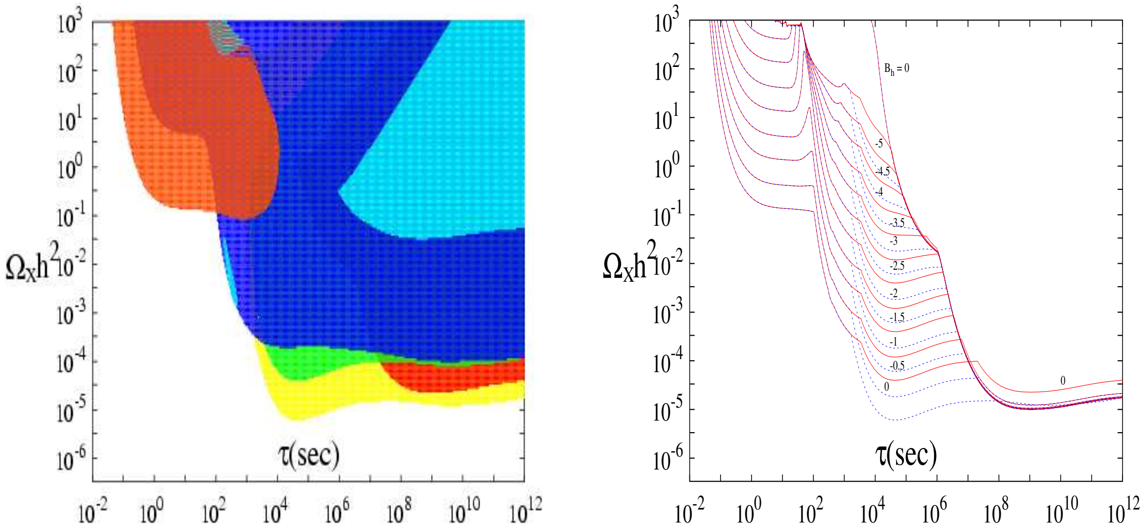

Figure 6.4: *Left panel*: BBN bounds on the abundance of a relic decaying electrically neutral particle (*e.g.*, the NLSP) with mass equal to 1 TeV and hadronic branching ratio $B_h = 1$ as a function of its lifetime τ. The colored regions are excluded due to ^{4}He overabundance (orange, low τ regime), ^{2}H overabundance (dark blue), violation of the upper limit on ^{3}He/^{2}H (red, high τ regime) or the lower limit on ^{7}Li/H (light blue). Conservative (less conservative) upper limit on ^{6}Li/^{7}Li is violated in green (yellow) excluded region. Taken from Ref. [280]. *Right panel*: The same excluded region as in the left panel, but for various hadronic branching ratios: $B_h = 0$ or $\log_{10} B_h$ ranging from 0 to -5. The solid red (dotted blue) lines correspond to the most stringent BBN constraint for a given τ taking into account the conservative (less conservative) upper limit on ^{6}Li/^{7}Li. Taken from Ref. [280].

f_a [177],

$$\tau_{\chi\to\tilde{a}\gamma} \simeq 0.33\,\mathrm{sec}\,\frac{1}{C_{aYY}^2\,|N_{11}|^2}\left(\frac{f_a}{10^{11}\,\mathrm{GeV}}\right)^2\left(\frac{m_\chi}{100\,\mathrm{GeV}}\right)^{-3}\left(1-\frac{m_{\tilde{a}}^2}{m_\chi^2}\right)^{-3}. \tag{6.58}$$

One can verify that, in comparison to decays into gravitinos, axino DM scenario with neutralino NLSP is only mildly constrained by the BBN since often $\tau_{\chi\to\tilde{a}\gamma} < 0.1\,\mathrm{sec}$. Strong constraints can be obtained only either for light neutralinos or for $m_\chi \simeq m_{\tilde{a}}$. Slepton NLSP decays into gravitino DM are described by

$$\tau_{\tilde{l}\to\tilde{G}l} = 59\,\mathrm{sec}\left(\frac{m_{\tilde{l}}}{1\,\mathrm{TeV}}\right)^{-5}\left(\frac{m_{\tilde{G}}}{10\,\mathrm{GeV}}\right)^2\left(1-\frac{m_{\tilde{G}}^2}{m_\chi^2}\right)^{-4}. \tag{6.59}$$

We use existing results for hadronic branching ratios of neutralinos [283], sneutrinos [284] and charged sleptons [285] decaying into gravitino DM. In the case of a bino decaying into axino DM with $m_{\tilde{a}} \ll m_\chi$ the hadronic branching fraction is typically of the order of $0.03 - 0.04$ if $m_\chi < m_Z$ and can grow up to about 0.06 for

$m_\chi \simeq 150\,\mathrm{GeV}$ [177]. For heavier neutralino its lifetime is usually too small to affect the BBN.

In the case of analysis described in Section 9.1 with a sneutrino decaying into gravitino DM we perform a much more detailed study. This approach allows us not to overestimate the impact of BBN constraints and therefore treat an upper limit on T_R with higher accuracy.

A sneutrino NLSP decays into gravitino DM dominantly via two-body decay channel $\tilde{\nu} \to \tilde{G}\nu$. High energetic neutrinos produced in such decays may annihilate with cosmic background neutrinos to an electron-positron pair $\nu\nu_{\mathrm{BG}} \to e^+e^-$, and therefore initiate an electromagnetic cascade. However, the rate of this process is suppressed by the weak interaction strength. As a result, the BBN constraints are typically determined by hadronic cascades associated with subdominant four-body decays $\tilde{\nu} \to \nu\tilde{G}q\bar{q}$ via real or virtual gauge bosons.

One possible way to treat them (see, *e.g.*, [159]) is to estimate the hadronic energy release

$$\xi_h \equiv \epsilon_h\, B_h\, Y_{\tilde{\nu}}, \tag{6.60}$$

where $Y_{\tilde{\nu}}$ is the sneutrino yield at freeze-out, by assuming that the energy released into hadronic particles per a single decay $\tilde{\nu} \to \nu\tilde{G}q\bar{q}$ is approximately equal to

$$\epsilon_h \simeq \frac{m_{\tilde{\nu}} - m_{\tilde{G}}}{3}. \tag{6.61}$$

Instead, we will calculate ϵ_h more accurately using [285]

$$\epsilon_h(\tilde{\nu} \to \nu\tilde{G}q\bar{q}) \equiv \frac{1}{\Gamma(\tilde{\nu} \to \nu\tilde{G})} \int_{m_{q\bar{q}}^{\mathrm{cut}}}^{m_{\tilde{\nu}}-m_{\tilde{G}}} dm_{q\bar{q}}\, m_{q\bar{q}}\, \frac{d\Gamma(\tilde{\nu} \to \nu\tilde{G}q\bar{q})}{dm_{q\bar{q}}}, \tag{6.62}$$

where we introduce low energy cut-off on the invariant mass of the $q\bar{q}$ pair $m_{q\bar{q}} > m_{q\bar{q}}^{\mathrm{cut}} = 2\,\mathrm{GeV}$. This is well justified by the fact that only quarks with high enough initial energy could initiate hadronic cascades of relevance for BBN. This assumption also helps to overcome some problems with infrared divergences when dealing with an intermediate off-shell photon γ^* since $m_{q\bar{q}} = \sqrt{p_{\gamma^*}^2}$. When we calculate the hadronic branching fraction $B_h = \Gamma(\tilde{\nu} \to \nu\tilde{G}q\bar{q})\,/\,\Gamma(\tilde{\nu} \to \nu\tilde{G})$, we take into account the masses and the decay constants of the intermediate W and Z bosons in Breit-Wigner propagators. Finally, we calculate abundances of light elements obtained during the BBN with a state-of-the-art numerical code [280].

6.6.2 Large Scale Structure formation

Non-thermal gravitinos or axinos produced in NLSP decays can have velocities much larger than those characteristic for thermal distribution. Such fast moving DM particles tend to erase small scales of large scale structures, especially when they constitute a sizable fraction of the dark matter density. The impact of the injection of high energetic DM particles on LSS can vary depending on the time when the process took place, *i.e.*, on the NLSP lifetime. We typically take this into account by imposing constraints on the present day velocity of DM particles $v^0_{\rm DM}$. Following [286], we impose the LSS constraints by requiring that the present root mean square velocity of non-thermally produced EWIMP DM particles is smaller than $v^0_{\rm DM} \lesssim 1\,\mathrm{km/s}$.[16]

As an example, let us focus on a dominant channel of a sneutrino decay to gravitino DM, *i.e.*, the process $\tilde{\nu} \to \nu \tilde{G}$. Treating neutrino as a massless particle we obtain the velocity at the time of decay for non-relativistic gravitinos

$$v_{\tilde{G}} \simeq \frac{m^2_{\tilde{\nu}} - m^2_{\tilde{G}}}{2\, m_{\tilde{\nu}}\, m_{\tilde{G}}}. \tag{6.63}$$

The present day velocity can be obtained from $v_{\tilde{G}}$ by applying an appropriate redshift

$$v^0_{\tilde{G}} \simeq \frac{m^2_{\tilde{\nu}} - m^2_{\tilde{G}}}{2m_{\tilde{\nu}} m_{\tilde{G}}} \frac{T_0}{T_d} \left(\frac{g_0}{g_d}\right)^{\frac{1}{3}} \simeq 4.57 \times 10^{-5}\, \frac{\mathrm{km}}{\mathrm{s}}\, g_d^{-1/12} \left(\frac{m^2_{\tilde{\nu}} - m^2_{\tilde{G}}}{2m_{\tilde{\nu}} m_{\tilde{G}}}\right) \left(\frac{\tau_{\tilde{\nu}}}{1\,\mathrm{s}}\right)^{1/2}, \tag{6.64}$$

where T_0 and T_d are the present day and the decay epoch's temperature, respectively, while g_0 and g_d are the corresponding effective number of degrees of freedom.

6.6.3 Cosmic Microwave Background Radiation

Another possible constraint is associated with the CMB radiation [288, 289]. An injection of energetic photons γ_{HE} from the late-time decays of the NLSP could distort the blackbody shape of the CMB spectrum.

For the NLSP lifetimes $\tau_{\rm NLSP} \lesssim 10^{10}$ sec that we are typically dealing with, high energetic photons could lose their energy via elastic Compton scatterings. In these processes the number of photons was kept constant.[17] Thus the CMB spectrum follows the Bose-Einstein distribution with the chemical potential μ. Following the procedure outlined in [276] we apply an upper limit $|\mu| < 9 \times 10^{-5}$ [290]. This can be translated into a limit on electromagnetic energy release[18] [288, 289]

In the following, we typically obtain lifetimes $\tau_{\rm NLSP}$ that are too low to violate the CMB constraint. Rare points that could have been excluded by this are usually already ruled out by the BBN constraints.

[16]In the analysis [287] discussed in Section 9.1, where present day gravitino DM velocities are typically larger than in other cases discussed in this thesis, we additionally applied a stringent approach in which we required that non-thermal component makes less than 20% of the total dark matter abundance.

[17]Moreover, *e.g.*, double Compton scattering or bremsstrahlung processes were inefficient.

[18]It is defined analogously to the hadronic energy release mentioned above.

Chapter 7

Constrained supersymmetric models

In this chapter we discuss phenomenological properties of some basic GUT constrained SUSY models. A particular emphasis is put on DM and Higgs boson properties. In Section 7.4 we analyze the issue of fine-tuning. The chapter is based on the results published in [206, 207, 291, 292] and partly in [293].

7.1 Constrained MSSM

The results presented in this section are based mostly on [206] (earlier study) and partly on [293] (recent study).

The CMSSM The Constrained Minimal Supersymmetric Standard Model (CMSSM) is a phenomenological realization of the mSUGRA unification conditions mentioned in Section 4.4.2. Three of the parameters of the model are given at the GUT scale: the common scalar mass m_0, the common gaugino mass $m_{1/2}$ and the common trilinear coupling A_0. Remaining parameters are $\tan\beta$ and $\mathrm{sgn}(\mu) = \pm 1$ which is not determined by the EWSB conditions. In our approach the sign of μ will be fixed for a given scan. The ranges of the parameters are given in Table 7.1. As can be seen, they were significantly extended in the recent study [293] in comparison with the older study [206]. As it will be discussed, this is justified by the measured value of the Higgs boson mass that favors $M_{\mathrm{SUSY}} = \sqrt{m_{\tilde{t}_1} m_{\tilde{t}_2}} \gtrsim 1\,\mathrm{TeV}$.

The CMSSM is a prototypical example of the GUT constrained SUSY model. Despite having very limited number of free parameters, it allows to discuss several most interesting scenarios for which the correct neutralino DM relic density can be obtained in the framework of the MSSM.

Constraints The earlier study [206] was performed shortly before the first announcement of the Higgs boson discovery [1, 2]. However, when performing scan we

Parameter	Range [206] (earlier study)	Range [293] (recent study)	Prior
m_0	0.1 TeV, 4 TeV	0.1 TeV, 10 TeV	Log
$m_{1/2}$	0.1 TeV, 2 TeV	0.1 TeV, 10 TeV	Log
A_0	−7 TeV, +7 TeV	−15 TeV, +15 TeV	Flat
$\tan\beta$	3, 62	2, 62	Flat
$\mathrm{sgn}(\mu)$	± 1	$+1$	Fixed

Table 7.1: Prior ranges of the parameters in the CMSSM analyses. The sign of μ is fixed for a given scan.

Measurement	Mean	Error: exp., theor.	Ref.
$\Omega_\chi h^2$	0.1120	0.0056, 10%	[294]
m_h	125 GeV	2 GeV, 2 GeV	(assumed)
$\mathrm{BR}(b \to s\gamma) \times 10^4$	3.60	0.23, 0.21	[295]
$\mathrm{BR}(B_u \to \tau\nu) \times 10^4$	1.66	0.66, 0.38	[296]
$\mathrm{BR}(B_s \to \mu^+\mu^-) \times 10^9$	< 4.5	0, 14%	[297]

Table 7.2: Important differences between the experimental constrains used in [206] (earlier study) and values shown in Table 6.1.

had assumed a Higgs signal with $m_h = 125\,\mathrm{GeV}$ which turned out to be close to the actual measured value. This analysis took place also before the measurement of $\mathrm{BR}(B_s \to \mu^+\mu^-)$ [272, 273]. Thus we used an upper limit on this branching ratio implemented via half-Gaussian likelihood. Appropriate parameters are provided in Table 7.2.[1] The parameters of the likelihood for the recent study [293] follow Table 6.1, but without a_μ taken into account. We will comment on this below.

Results (earlier study) In Fig. 7.1 (left panel) we present the 1σ and 2σ marginalized posterior plots for the CMSSM in the $(m_0, m_{1/2})$ plane obtained in [206] for $\mu > 0$. One can identify two main 1σ credible regions: the SC region (lower left corner) and the AF region (upper half of the plot). In addition a 2σ posterior corresponds also to the HB/FP region (lower right corner).

The SC region lies close to the exclusion line from direct SUSY searches. Low values of m_0 are needed to keep the mass of the lighter stau close to the bino mass $m_{\tilde{\tau}_1} \simeq M_1$. Therefore the requirement of having the bino LSP introduces also an upper limit on $m_{1/2}$. Light smuons in the SC region also help to enhance a_μ to become closer to the experimental value according to Eq. (6.46). However, in general a_μ remains poorly satisfied. The SC region also corresponds to relatively low values of $\tan\beta \lesssim 30$ and $A_0 \sim 0$ as can be seen in Fig. (7.1) (right panel). This allows one to suppress the mixing in the stau sector and therefore to keep the mass

[1] The experimental value of $\mathrm{BR}(B_u \to \tau\nu)$ also differ significantly in comparison with Table 6.1. However, since calculated $\mathrm{BR}(B_u \to \tau\nu)$ is typically very close to the SM value, as discussed in Section 6.3.4, this difference has negligible impact on the parameter space of the CMSSM (it corresponds to an almost constant shift in χ^2).

of the lighter stau slightly above the bino mass. Low values of m_0 and $m_{1/2}$ in the SC region lead to low $M_{\rm SUSY}$. This suppresses the one-loop correction to m_h that is proportional to $\log M^2_{\rm SUSY}$, as can be seen in Eq. (4.37). However, the correct value of the Higgs boson mass can be obtained thanks to a saturation of the mixing term for $X_t \sim \sqrt{6}\, M_{\rm SUSY}$. This is shown in Fig. 7.2. In the right panel of this figure the SC region corresponds to $M_{\rm SUSY}$ close to 1 TeV.

On the other hand, the AF region can be obtained for larger $m_{1/2}$ and wide range of m_0. It also favors larger values of $\tan\beta$ due to the a_μ constraint (compare Eq. (6.46) in absence of light smuons). Larger $m_{1/2}$ in this region leads to increased $M_{\rm SUSY}$ due to RGE running of the third generation soft squark masses. This helps to obtain $m_h \simeq 125\,\mathrm{GeV}$ as can be seen in Fig. 7.2. The mixing term is no more saturated. However, one can increase it by allowing large $X_t \simeq A_t$. This results in a possible increase of $|A_0|$ in Fig. 7.1 (right panel) in the AF region in comparison with the other two regions.

The HB/FP region corresponds to low $m_{1/2}$, large m_0, intermediate values of $\tan\beta$ (between the SC and AF regions) and small $|A_0|$. The condition $m_0 \gg m_{1/2}$ with $A_0 \sim 0$ guarantees that μ is kept small according to [292]

$$-\mu^2 \simeq m^2_{H_u}(\mathrm{SUSY}) \simeq 0.074\, m_0^2 - 1.008\, m^2_{1/2} - 0.080\, A_0^2 + 0.406\, m_{1/2}\, A_0, \quad (7.1)$$

where we employed the EWSB minimization condition Eq. (4.34) and the the solution of the one-loop RGE for m_{H_u}. The value of μ is close to M_1 resulting in the lightest neutralino being the mixed bino-higgsino state (dominantly bino). Low values of $|A_0|$ result in $X_t \ll \sqrt{6} M_{\rm SUSY}$ and typically too low radiative corrections to m_h. Moreover, the a_μ constraint is even more poorly satisfied than in the other two regions because of relatively low $\tan\beta$ and lack of light smuons. Therefore the HB/FP region is statistically less important than the SC and the AF regions.

The a_μ constraint is by far the worst satisfied in all the regions described above. However, as shown in Table 6.1, it is characterized by quite substantial errors (especially the experimental one). It is therefore useful to additionally study the allowed parameter space in the CMSSM without this constraint taken into account. It also allows one to consider negative value of μ, which is highly disfavored in presence of the a_μ constraint according to Eq. (6.46). Once one abandons a_μ, the relative impact of other constraints increases. As a result, the SC region becomes slightly less favored in contrast to both the AF and the HB/FP regions as can be seen in Fig. 7.3 (left panel). Interestingly, the change in the posterior is in general small. In other words, given the large value of the χ^2 contribution associated with a_μ, this constraint is to some approximation equally poorly fitted in all the considered regions. We will utilize this feature of the allowed parameter space in the more recent study described below, in which we neglect the a_μ constraint (see further comments below).

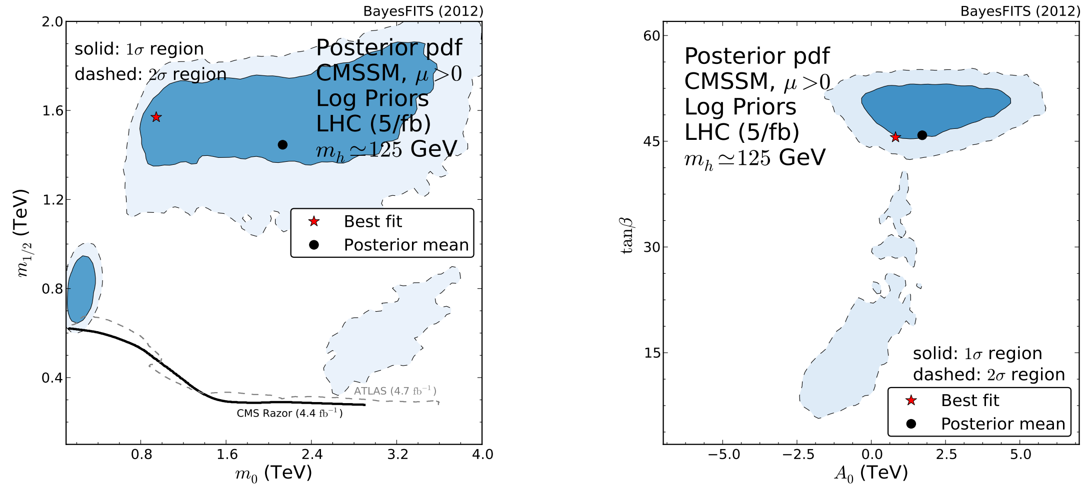

Figure 7.1: Marginalized posterior for the CMSSM (earlier study) in the $(m_0, m_{1/2})$ plane (left panel) and the $(A_0, \tan\beta)$ plane (right panel). The positive sign of μ is assumed. Taken from Ref. [206].

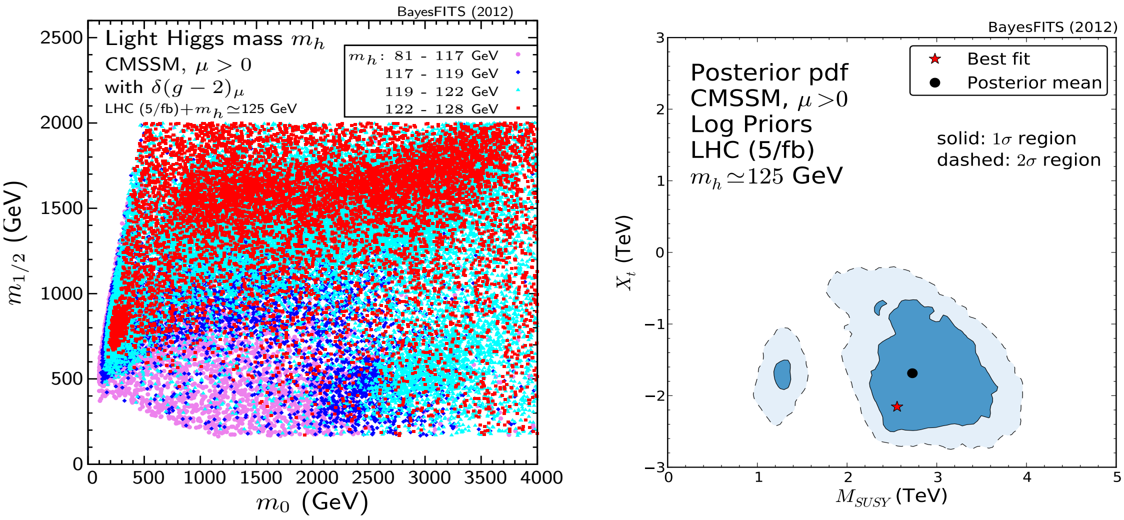

Figure 7.2: *Left panel*: Scatter plot showing the value of m_h in the $(m_0, m_{1/2})$ plane of the CMSSM. *Right panel*: Marginalized posterior in the parameters X_t vs $M_{\rm SUSY}$, relevant for the loop corrections to the Higgs mass. Positive μ is assumed. Taken from Ref. [206].

One can then additionally assume negative μ which helps to reduce the BR$(B_s \to \mu^+\mu^-)$ below the upper limit from Table 7.2. In particular, this allows to extend the AF region to lower values of m_0 and $m_{1/2}$.[2] As a result a relative statistical

[2] Lower $m_{1/2}$ leads to the lower neutralino mass which is given by $m_\chi \sim m_A/2$ in the AF region. Thus one obtains lighter pseudoscalar which could enhance BR$(B_s \to \mu^+\mu^-)$ too much according to a discussion in Section 6.3.4. This can be circumvented for $\mu < 0$.

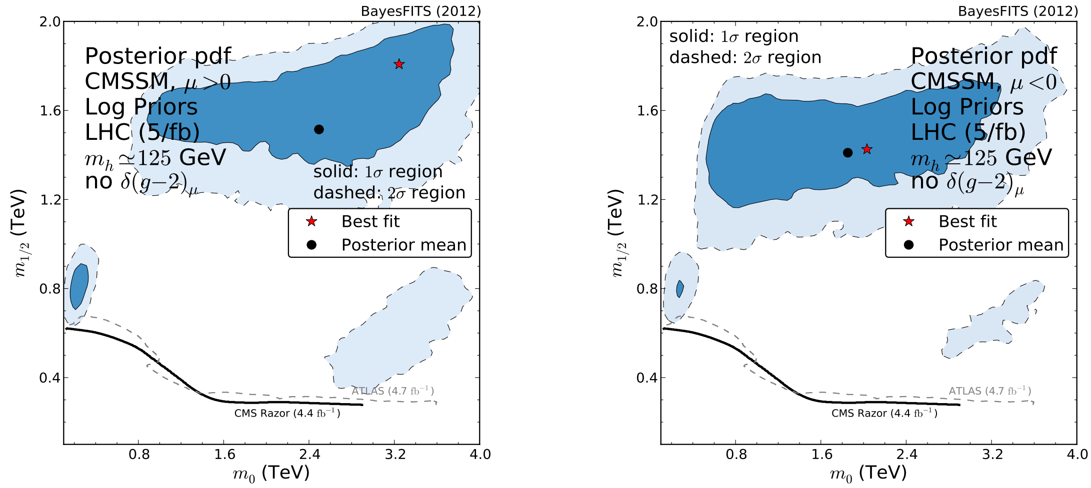

Figure 7.3: Marginalized posterior for the CMSSM (earlier study) in the $(m_0, m_{1/2})$ plane without the a_μ constraint. The positive (negative) sign of μ is assumed in the left (right) panel. Taken from Ref. [206].

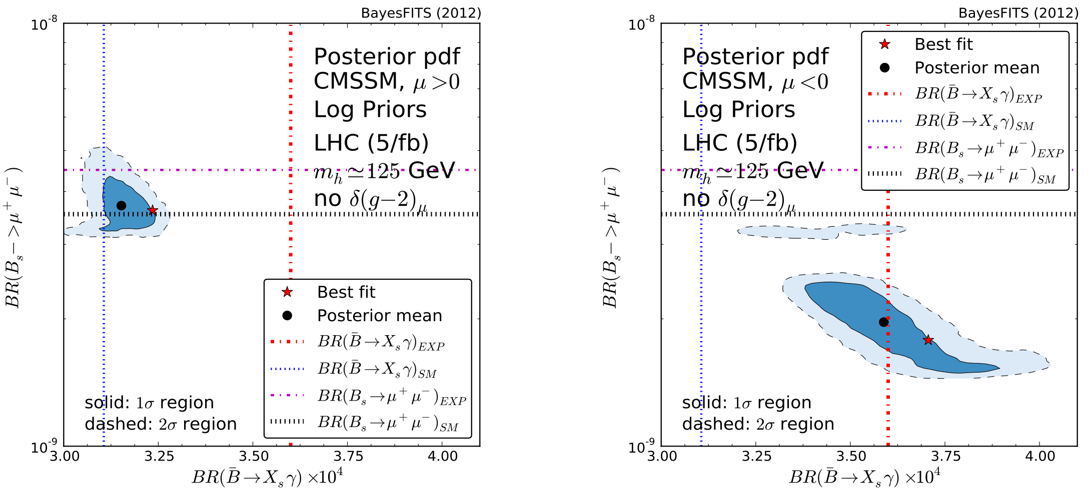

Figure 7.4: Marginalized posterior for the CMSSM (earlier study) in the BR$(b \to s\gamma) \times 10^4$ vs. BR$(B_s \to \mu^+\mu^-)$ plane. Results for positive (negative) μ are shown in the left (right) panel. Taken from Ref. [206].

importance of the SC and HB/FP regions is reduced as shown in Fig. (7.3 (right panel)).

The reduction of BR$(B_s \to \mu^+\mu^-)$ in the case of negative μ can be better seen in Fig. 7.4. The branching ratio can be reduced to values even below the SM one. This may be consistent with currently measured branching ratio given in Table 6.1. It is also important to note that negative μ helps to increase BR$(b \to s\gamma)$ closer to the experimental value. It is due to a change of sign of the chargino-stop loop contribution.

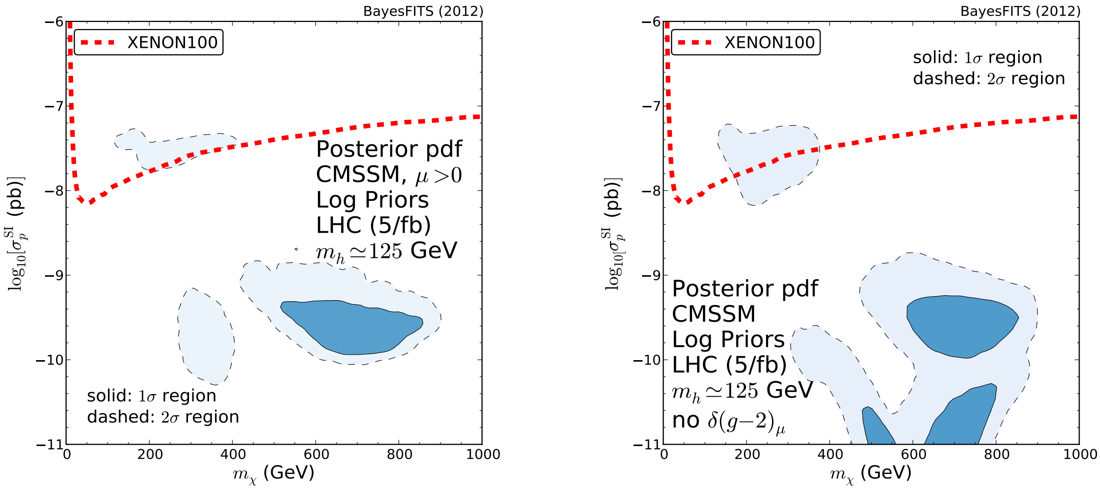

Figure 7.5: Marginalized posterior for the CMSSM (earlier study) in the $(m_\chi, \sigma_p^{\rm SI})$ plane. *Left panel*: Results for positive μ with the a_μ constraint taken into account. *Right panel*: Combined results for $\mu > 0$ and $\mu < 0$ with no a_μ. Taken from Ref. [206].

Last, but not least, one needs to take into account the exclusion limits from dark matter DD searches. In the older study [206] we employed the Xenon100 data. As can be seen in Fig. 7.5, majority of the parameter space of the CMSSM remained then well below the lower limit on $\sigma_p^{\rm SI}$. The situation is different for the HB/FP region. The lightest neutralino can elastically scatter off of quarks via the t-channel CP-even Higgs exchange or the s-channel squark exchange. In each of these cases the corresponding cross section is proportional to $\sigma_{\chi N} \sim |N_{11}|^2 |N_{1i}|^2$ where $i = 3, 4$ and N_{ij} is the respective entry of the neutralino mixing matrix (see, *e.g.*, [298]). N_{11} term corresponds to the bino composition, while N_{13} and N_{14} to the higgsino ones. As a result, $\sigma_p^{\rm SI}$ is typically reduced for the pure bino or the pure higgsino neutralino, while it is enhanced for a mixed state in the HB/FP region. The enhancement can be to some extent ameliorated for negative μ as can be seen in Fig. 7.5 (right panel). In this scenario a cancellation between diagrams involving the heavy and the light Higgs can reduce $\sigma_p^{\rm SI}$ below the experimental limits (see, *e.g.*, [138] and references therein).

To summarize our discussion we show in Fig. 7.6 the χ^2 contributions to the best-fit points (BFPs) obtained in the scans for both positive and negative μ, as well as with or without the a_μ constraint taken into account. As it was mentioned above, a_μ provides by far the largest χ^2 contribution if it included in the likelihood. Another important contribution comes from BR$(b \to s\gamma)$, but it can be reduced for negative μ as discussed above. Interestingly, the relic density constraint contributes

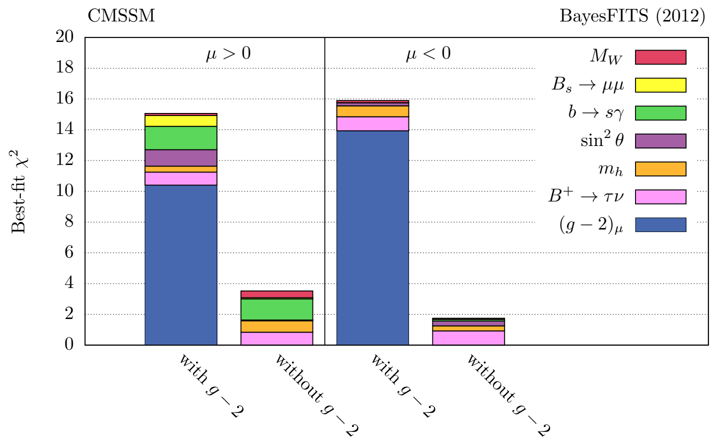

Figure 7.6: A bar chart showing the main contributions to the χ^2 of the best-fit points of different scans in the CMSSM. Taken from Ref. [206].

negligibly to χ^2 of the BFP. It is because the relative importance of $\Omega_\chi h^2$, which guarantees that it has to be satisfied for the phenomenologically acceptable regions.[3]

In some sense the a_μ and $\Omega_\chi h^2$ constraints lie on the opposite side on the scale of effectiveness. The former is very poorly fitted, gives large contribution to χ^2 of the BFP and its abandonment leaves posterior plots almost intact. The latter is very well satisfied for phenomenologically acceptable regions, contributes negligibly to χ^2 of the BFP and to a large extent determines the shape of the posterior plots. Thus, as long as we do not compare different models, but are interested in the preferred parameter space of a given SUSY model, we may often safely omit the a_μ constraint in a discussion. Hence we will give much more attention to $\Omega_\chi h^2$.

On the other hand, a_μ, after further reduction of the experimental error, can potentially play a very important role in excluding SUSY models. It is because of the tension within the framework of SUSY that appears when one tries to simultaneously explain a large discrepancy of the measured value of a_μ with respect to the SM value and the lack of signal from new physics in various other experiments, *e.g.*, direct SUSY searches at the LHC.

Results (recent study) The results for the more recent analysis [293] are shown in Fig. 7.7. They are presented as the 95%CL regions instead of posterior plots, but this has minor impact on the physics discussed below.

A major difference in comparison with Fig. 7.1 is the appearance of the 1TH region (shown in red) for large values of m_0 and $m_{1/2}$ that go beyond the allowed ranges in the previous study [206].[4] This allows one to obtain the correct DM relic

[3]This importance results from a combination of the relatively small errors in the corresponding likelihood function and a limited number of specific scenarios in which the correct neutralino DM relic density can be obtained.

[4]For the first time it was shown that the 1TH region appears in the CMSSM in [115].

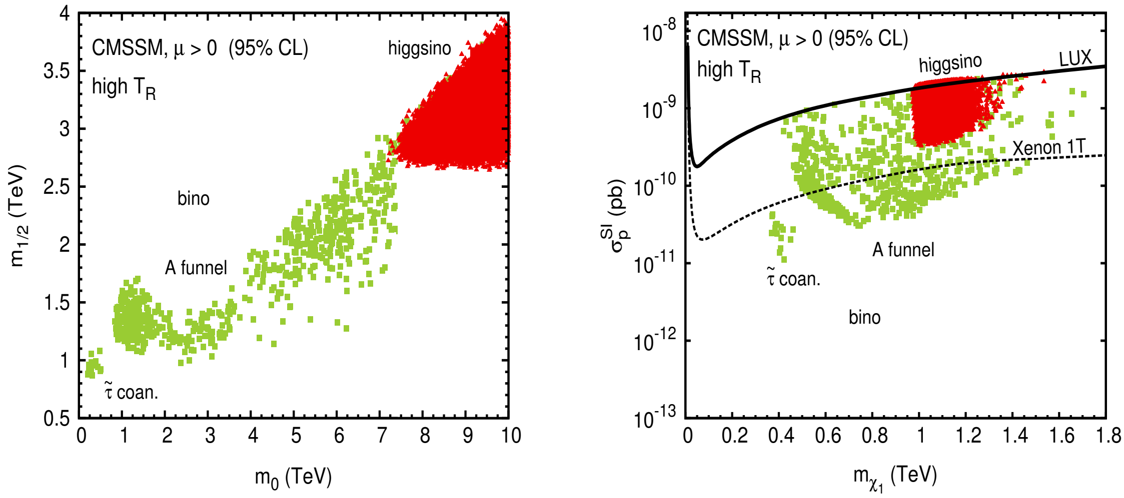

Figure 7.7: 95%CL regions in the CMSSM (recent study) in the $(m_0, m_{1/2})$ plane (left panel) and the $(m_\chi, \sigma_p^{\rm SI})$ plane (right panel). The positive sign of μ is assumed. Taken from Ref. [293].

density for higgsino-like LSP with $m_\chi = \mu \simeq 1\,\text{TeV} < M_1$. According to another recent analysis of the CMSSM [299] with three-loop corrections to m_h taken into account a 2σ marginalized posterior in the 1TH region reaches up to $m_0 \lesssim 12.5\,\text{TeV}$ and $m_{1/2} \lesssim 4.5\,\text{TeV}$. For larger of values of both the common scalar and the common gaugino masses one typically obtains too large m_h. For a given value of m_0 in the 1TH region one can obtain neither too low nor too large $m_{1/2}$ because of the condition $\mu \simeq 1\,\text{TeV}$. The lower limit corresponds to the bino that becomes lighter than the higgsino, while the upper one can be derived from Eq. (7.1). As can be seen there, $m_{1/2}$ cannot be too large for a given m_0 in order to keep $\mu \simeq 1\,\text{TeV}$.[5]

The 1TH region in the CMSSM remains currently not excluded by the DD searches, but can be probed by the future Xenon1T experiment as shown in Fig. 7.7 (right panel). It also true for some part of the AF region. The HB/FP region is entirely absent in the recent study due to updated DM direct detection limits.[6]

On the other hand, in Fig. (7.7) the SC region lies outside the range of the Xenon1T experiment. However, to a large extent it can be tested by the upcoming second run of the LHC. Note that in the recent study this region is statistically less important than in the previous one. It is both due to the absence of the a_μ constraint and more stringent exclusion limits from direct SUSY searches.

[5] The freedom of choosing A_0 is often limited by other constraints, *e.g.*, m_h.

[6] In the case of the unconstrained MSSM some points within the HB/FP scenario can survive even the LUX exclusions [138], if $\mu < 0$, due to the cancellation mentioned above.

7.2 Constrained NMSSM

The results presented in this section are based on [207].

In this section we will present a Bayesian study of the Constrained NMSSM (CNMSSM). In particular, due to an extended Higgs sector present in the framework of the NMSSM (in comparison with the MSSM) we will be able to consider scenarios in which the recently discovered Higgs boson is not the lightest CP-even Higgs particle in the model.

CNMSSM and constraints We define the CNMSSM in analogy to the CMSSM. In particular, we use the common scalar m_0 and the common gaugino $m_{1/2}$ mass parameters, as well as the common trilinear coupling A_0. All of them are defined at the GUT scale. The mass of the singlet m_S (see Eq. (4.42)) is not unified to m_0. From the theoretical point of view, it has been argued [300] that the mechanism for SUSY breaking might treat the singlet field differently from the other superfields. From the phenomenological point of view, the freedom in m_S allows for easier convergence when the renormalization group equations are evolved from the GUT scale down to $M_{\rm SUSY}$. It also yields, in the limit $\lambda \to 0$, and with λs fixed, effectively the CMSSM plus a singlet and singlino fields that both decouple from the rest of the spectrum. Through the minimization equations of the Higgs potential, m_S^2 can then be traded for $\tan\beta$ and either $\mathrm{sgn}(\mu_{\rm eff})$ or κ. We choose $\mathrm{sgn}(\mu_{\rm eff})$ for conventional analogy with the CMSSM. Both λ and $\tan\beta$ are defined at $M_{\rm SUSY}$. A_λ and A_κ are unified with A_0 at the GUT scale.

The ranges of parameters that we use are given in Table 7.3. The perturbativity condition leads to an upper limit $\lambda \lesssim 0.7$. On the other hand we have checked that allowing $\lambda < 0.001$ hardly increases the number of points allowed by the physicality conditions. Beside that, it would have most likely driven the scan towards a purely CMSSM-like scenario.

The experimental constraints that we employed in the scan are given in Table 6.1 with modifications shown in Table 7.4 similarly to the CMSSM case (earlier study) described in the previous section. The differences are associated with the first measurements of the Higgs boson mass and $\mathrm{BR}(B_s \to \mu^+\mu^-)$.

Results Marginalized posterior plots for the CNMSSM in the $(m_0, m_{1/2})$ plane are shown in Fig. 7.8. The left panel of the plot corresponds to the CMSSM-like scenario in which the lightest Higgs scalar h_1 plays a role of the discovered Higgs boson. We identify the SC and AF regions similarly to the CMSSM. In the CNMSSM the SC region appears to be more extended relative to the CMSSM (earlier study) [206]. It is due to somewhat larger m_{h_1} that is closer to the experimental value. However, this is not a specific feature of the CNMSSM, but is rather connected with an increase

Parameter	Range	Prior
m_0	$0.1\,\mathrm{TeV},\ 4\,\mathrm{TeV}$	Log
$m_{1/2}$	$0.1\,\mathrm{TeV},\ 2\,\mathrm{TeV}$	Log
A_0	$-7\,\mathrm{TeV},\ +7\,\mathrm{TeV}$	Flat
$\tan\beta$	1, 62	Flat
$\mathrm{sgn}(\mu)$	± 1	Fixed
λ	0.001, 0.7	Flat

Table 7.3: Prior ranges of the parameters in the CNMSSM analysis. The sign of μ is fixed for a given scan.

Measurement	Mean	Error: exp., theor.	Ref.
m_h	125.8 GeV	$0.6\,\mathrm{GeV},\ 3\,\mathrm{GeV}$	[301]
$\mathrm{BR}(B_s \to \mu^+\mu^-) \times 10^9$	3.2	(+1.5,−1.2), 10%	[302]

Table 7.4: Important differences between the experimental constrains used in [207] and values shown in Tables 6.1 and 7.2.

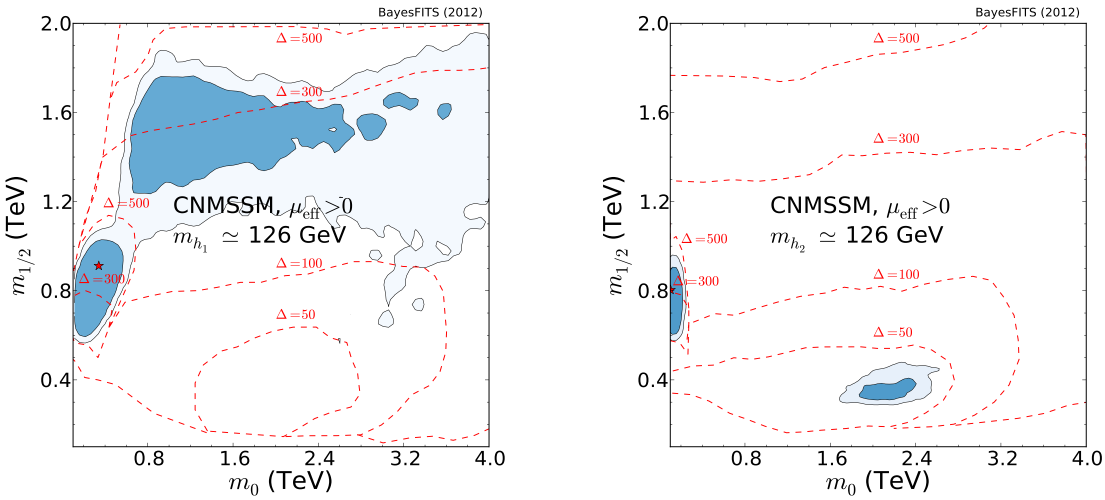

Figure 7.8: Marginalized posterior for the CNMSSM in the $(m_0, m_{1/2})$ plane for the case with $m_{h_1} \simeq 126\,\mathrm{GeV}$ (left panel) and $m_{h_2} \simeq 126\,\mathrm{GeV}$ (right panel). Positive μ is assumed. Isocontours of the fine-tuning measure Δ are also shown. Taken from Ref. [207].

of the top mass used in the scan (compare Eq. (4.44)).[7] The increase of a statistical relevance of the SC region leads also to a reduction of the marginalized probability in the HB/FP region. 2σ credible region encompasses only small fraction of the HB/FP region which lies in the $m_0 \gg m_{1/2}$ sector and merges with the AF region in Fig. 7.8 (left panel).

[7] In the study of the CNMSSM we used an updated central value of the top pole mass $M_t = 173.5\,\mathrm{GeV}$ (see Table 6.1), while in the earlier study of the CMSSM [206] we employed $M_t = 172.9\,\mathrm{GeV}$.

In the right panel of Fig. 7.8 we present the results for a scenario in which the second lightest h_2 has a mass $m_{h_2} \simeq 126\,\text{GeV}$, while h_1 is lighter. The case with both the lightest CP-even Higgs particles being mass-degenerate leads to very similar posterior plot. In this scenario h_1 and h_2 combine to generate an observed signal in detectors.

In Fig. 7.8 (right panel) the 2σ credible region in the $(m_0, m_{1/2})$ plane is dramatically reduced in comparison with the $m_{h_1} \simeq 126\,\text{GeV}$ case described above. We found the SC and the HB/FP regions, while the AF region could not satisfy $m_{h_2} \simeq 126\,\text{GeV}$ condition. A careful analysis of the allowed parameter space ensures that the requirement of having low mass of h_2 typically suppresses also κs. As a result, the lightest neutralino for the values of $m_{1/2}$ characteristic for the would-be AF region or for the SC region is singlino-like. Therefore its relic density cannot be effectively reduced due to A-resonance mechanism, but such reduction is still possible thanks to coannihilations with the lighter stau. The statistical relevance of the HB/FP region increases simply due to a suppression of the AF region.

In Fig. 7.8 we additionally present the fine-tuning measure (see Section 4.7) calculated for the CNMSSM. One typically obtains $\Delta \sim 300-500$ for a vast majority of points in the $m_{h_1} \simeq 126\,\text{GeV}$ scenario.[8] Smaller fine-tuning can be achieved only in the HB/FP region due to the relatively low values of μ_{eff}. For the same reason Δ is in general slightly larger in the SC region than in the AF one which is characterized by smaller μ_{eff}. On the other hand, in the light h_2 case one can obtain $\Delta < 50$ in the HB/FP region.

In Fig. 7.9 we show the Higgs signal rates for both $m_{h_1} \simeq 126\,\text{GeV}$ and $m_{h_2} \simeq 126\,\text{GeV}$. As can be seen, the first case corresponds to the SM-like Higgs boson similarly to the CMSSM. On the other hand, light h_2 can have a non-negligible singlet component. This allowed to simultaneously reduce both of the corresponding signal rates. Therefore it was not possible to explain the discrepancy between $R_{h_2}(\gamma\gamma)$ and $R_{h_2}(ZZ)$ shown in Table 6.1.[9] Moreover, in both scenarios $R_{h_2}(\gamma\gamma)$ could hardly exceed 1 over the 2σ credible region.

Interestingly, a combination of $\text{BR}(B_s \to \mu^+\mu^-)$ and dark matter DD constraints could have been used to disfavor the light h_2 scenario already at the time of the analysis. This is shown in Fig. 7.10. For comparison, in the left panel we present results for the $m_{h_1} \simeq 126\,\text{GeV}$ case. They closely resemble the CMSSM with the HB/FP region lying above the Xenon100 exclusion line. The majority of the preferred parameter space lies within a reach of the future Xenon1T experiment. In the case of light h_2 the HB/FP remains disfavored by dark matter DD, while the SC region with singlino-like χ is characterized by very low σ_p^{SI}. On the other hand,

[8] It is also the case of the CMSSM as we will see below in Section 7.4.

[9] Current experimental data [303, 304] points towards the SM-like nature of the discovered Higgs boson.

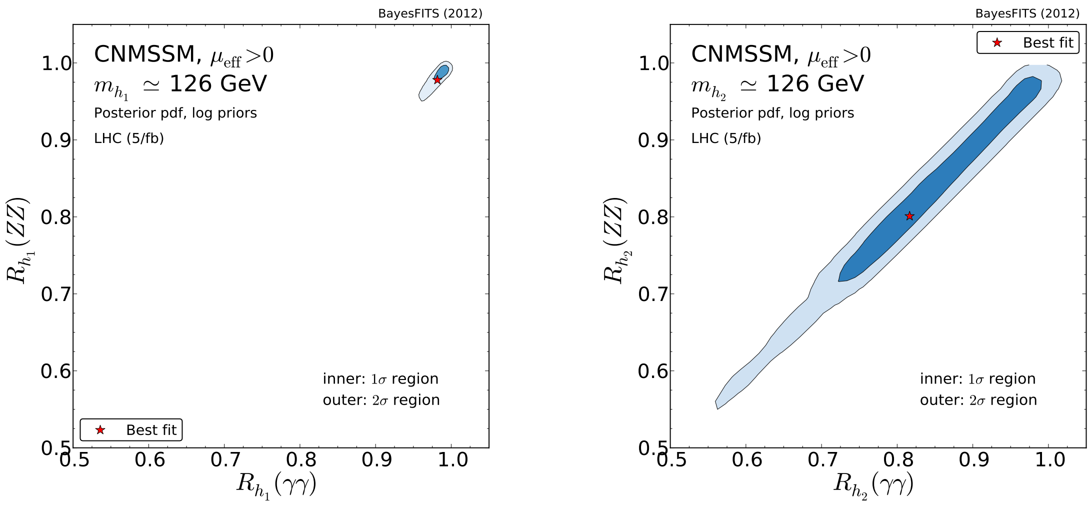

Figure 7.9: Marginalized posterior for the CNMSSM in the $R_{h_{\rm sig}}(\gamma\gamma)$ vs. $R_{h_{\rm sig}}(ZZ)$ plane for the case with $m_{h_1} \simeq 126\,\text{GeV}$ (left panel) and $m_{h_2} \simeq 126\,\text{GeV}$ (right panel). Positive μ is assumed. Taken from Ref. [207].

it leads to too large value of the BR$(B_s \to \mu^+\mu^-)$ branching ratio. This is due to larger $\tan\beta$ than in the SC region in $m_{h_1} \simeq 126\,\text{GeV}$ case.[10]

Last, but not least, we could abandon the a_μ constraint and employ negative μ. As a result (not shown in the plots), the SC region appears to be slightly less favored, while the HB/FP region becomes clearly separated from the AF one. Similarly to the CMSSM, negative μ helps to reduce both BR$(B_s \to \mu^+\mu^-)$ and $\sigma_p^{\rm SI}$.

The χ^2 contributions for the BFPs of all the scans of the CNMSSM are shown in Fig. 7.11. Not surprisingly, in the $m_{h_1} \simeq 126\,\text{GeV}$ case χ^2 is dominated by the a_μ contribution if it is included. BR$(b \to s\gamma)$ can be improved for negative μ similarly to the CMSSM. In all the scans one obtains significant contribution from $R_{h_1}(\gamma\gamma)$ since it cannot exceed one as discussed above. Interestingly, in the scenarios with light h_2, the a_μ contribution can be reduced. This is due to a larger $\tan\beta$ in the SC region than in the $m_{h_1} \simeq 126\,\text{GeV}$ case. However, the total χ^2 is increased back by poorly fitted BR$(B_s \to \mu^+\mu^-)$.

It is important to mention that due to a limited ranges of m_0 and $m_{1/2}$ we did not find 1TH region in [207]. However, one expects to obtain this region in the parameter space for an extended scan, as in the CMSSM case.

[10]Requirement of having light h_2 can be translated into an approximate upper limit $|A_\kappa| \lesssim \kappa s$. This can be obtained from a physicality condition $m_{h_1} \geqslant 0$ at the tree level for tiny λ and $\kappa s < M_Z$ that are characteristic for singlino-like χ with mass below 200 GeV in the SC region in the light h_2 scenario (see a discussion in [207]). This suppression of A_κ leads to a reduction of A_0 and therefore also A_τ. In order to obtain satisfactory mixing in the stau sector (to reduce the lighter stau mass to the level of the singlino mass), *i.e.*, to keep $|X_\tau| = |A_\tau - \mu/\tan\beta|$ greater than zero, one then needs to increase $\tan\beta$ (for positive μ). The other possibility of allowing small $\tan\beta$ and therefore $|X_t| \sim |\mu|$ is disfavored by the a_μ constraint.

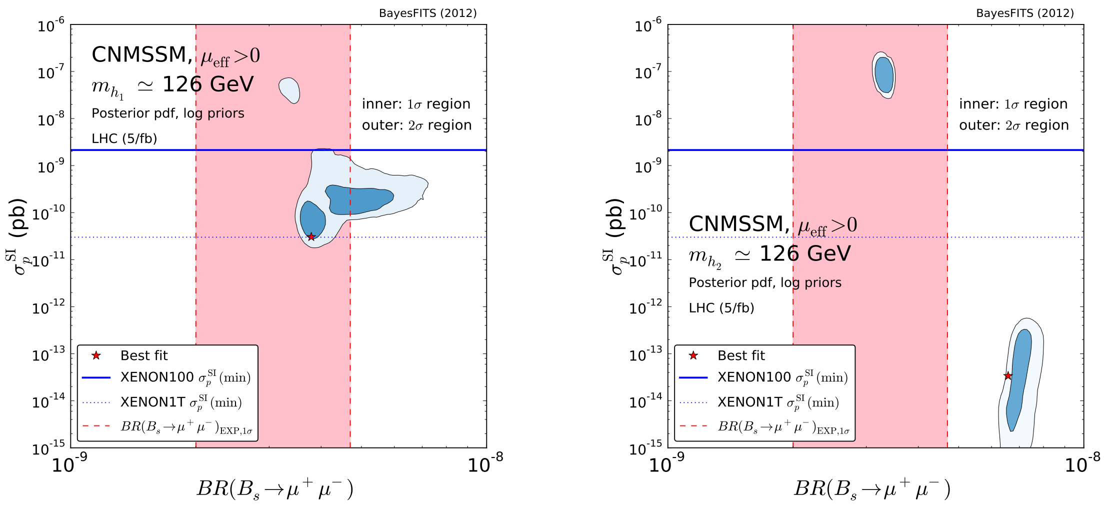

Figure 7.10: Marginalized posterior for the CNMSSM in the BR$(B_s \to \mu^+\mu^-)$ vs. $\sigma_p^{\rm SI}$ plane for the case with $m_{h_1} \simeq 126\,$GeV (left panel) and $m_{h_2} \simeq 126\,$GeV (right panel). Positive μ is assumed. The solid (dotted) blue horizontal line corresponds to Xenon100 (Xenon1T) dark matter DD exclusion limit. The pink vertical band shows the 1σ experimental uncertainty on the measurement of BR$(B_s \to \mu^+\mu^-)$ from Table 7.4. Taken from Ref. [207].

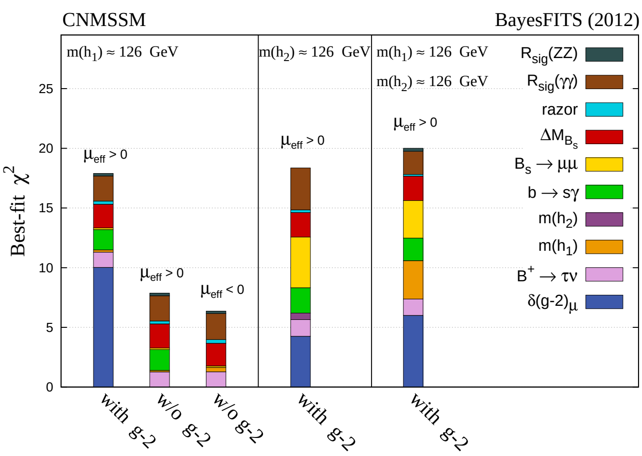

Figure 7.11: A bar chart showing the main contributions to the χ^2 of the best-fit points of different scans in the CNMSSM. Taken from Ref. [207].

7.3 Constrained NMSSM with non-universal soft Higgs masses

The results presented in this section are based on [291].

We have so far discussed two GUT constrained SUSY models in which either the lightest or the second lightest Higgs scalar has mass about 126 GeV (or both). In this section we will study yet another possibility of having pseudoscalar Higgs particle mass-degenerate with h_1 (h_1 plays o role of the discovered Higgs boson).[11] This scenario is excluded in the MSSM, as noted in [306, 307], since in this framework in order to obtain h_1 with mass around 126 GeV, m_A is required to be at least about 300 GeV (decoupling regime).[12] However, it appears to be possible in the framework of the NMSSM where we can obtain $m_{h_1} \simeq m_{a_1} \simeq 126\,\text{GeV}$ with doublet-dominated h_1 and singlet-like a_1.

Observed signal rates The lighter pseudoscalar in this scenario can have sizable one-loop effective coupling to $\gamma\gamma$ in the presence of a light higgsino-like chargino in the loop. The corresponding contribution to the Higgs signal rate at the LHC can be calculated by replacing h_i with a_1 in Eqs (6.29)-(6.31). However, despite the potentially non-negligible size of $\text{BR}(a_1 \to \gamma\gamma)/\text{BR}(h_{\text{SM}} \to \gamma\gamma)$, no net enhancement in the $\gamma\gamma$ rate of a_1 with decreasing chargino mass would be visible in the ggh (gluon fusion) production mode. The reason is that the first term in the product always has a very small magnitude due to a highly reduced effective coupling of a_1 to two gluons compared to that of a SM Higgs boson, which is dominated by the top quark loop.

However, the overall enhancement in $R_X^Y(a_1)$ due to a light chargino should be visible in the associated $b\bar{b}h$ production mode, which we will focus on, since the conditions necessary to obtain a light chargino also result in an enhanced coupling of a_1 to $b\bar{b}/\tau^+\tau^-$. The $b\bar{b}h$ Higgs production mode is very subdominant for a SM Higgs boson and is therefore generally considered to be of less interest. In contrast, in SUSY it is enhanced by $\tan^2\beta$ (see, *e.g.*, [59]). This allows one to obtain a clear signature of our scenario that is a simultaneous "triple enhancement" in the signal rates of the three Higgs decay channels, $\gamma\gamma$, $b\bar{b}$ and $\tau^+\tau^-$ (collectively referred to as X henceforth).[13]

The lighter pseudoscalar mass The approximate expression for the lighter pseudoscalar mass in the NMSSM can be written as

$$m_{a_1}^2 \simeq -3\kappa s A_\kappa^{\text{SUSY}} - \frac{M_{P,12}^4}{M_{P,11}^2}. \tag{7.2}$$

In the above equation $M_{P,12}^2 \simeq \lambda(A_\lambda^{\text{SUSY}} - 2\kappa s)\sqrt{2}\,v$ is the off-diagonal entry of the pseudoscalar mass matrix (see [110]), where $A_{\lambda/\kappa}^{\text{SUSY}}$ denote $A_{\lambda/\kappa}$ at M_{SUSY}.

[11] Another recent study of the issue of light pseudoscalar in the framework of the NMSSM can be found in [305].

[12] In addition, while it is also possible to have a 126 GeV h_2, this can only be achieved for 95 GeV $< m_A <$ 110 GeV, in a tiny portion of the "non-decoupling regime".

[13] On the other hand, a_1, being a pseudoscalar, would not contribute to the WW and ZZ decay channels. The absence of signal here would also be a part of the signature.

$M^2_{P,11} \simeq \mu_{\rm eff} B_{\rm eff} \tan\beta$, with $B_{\rm eff} \equiv A^{\rm SUSY}_\lambda + \kappa s$, is the diagonal term corresponding to the mass-squared of the doublet-like heavy pseudoscalar, a_2. The leading term in eq. (7.2) implies that, for positive κ, which we will assume here, the condition of the positivity of $m^2_{a_1}$ depends predominantly on the relative signs of $\mu_{\rm eff}$ and $A^{\rm SUSY}_\kappa$. Assuming the leading term to be positive, the negative contribution from the second one should be kept close to zero. This would require $M^2_{P,11} \gtrsim M^4_{P,12}$.

A careful analysis [291] shows that for negative $\mu_{\rm eff}$ the values of A_0 at the GUT scale are bounded from below by the condition of the physicality of a_1. This causes a slight tension between m_{h_1} and m_{a_1}, since in order to obtain h_1 which is SM-like with mass about 125 GeV large negative values of A_0 are preferred. For positive $\mu_{\rm eff}$ there is no such tension because A_0 is relatively free, as long as the correct a_1 mass can be achieved by adjusting other free parameters. However, in practice according to Eq. (7.2) this requires a non-unification of A_0 with A_κ at the GUT scale, as well as keeping κ as a free parameter. This can be realized in the GUT constrained extension of the CNMSSM with non-universal Higgs masses (NUHM) m_{H_u} and m_{H_d}. We will call this model CNMSSM-NUHM. Through the minimization conditions of the Higgs potential m_{H_u} and m_{H_d} at the electroweak scale can be traded for the parameters κ and $\tan\beta$. Thus we will use the following set of free parameters

$$m_0, m_{1/2}, A_0, \tan\beta, {\rm sgn}(\mu_{\rm eff}), \lambda, \kappa, A_\kappa = A_\lambda. \tag{7.3}$$

Pseudoscalar signal rates The effective coupling of the lighter pseudoscalar a_1 to two photons (see, e.g.,[59]), is dominated by a light chargino in the loops and can be approximated by

$$C^{\rm eff}_{a_1}(\gamma\gamma) \simeq \frac{g_{a_1\chi_1^\pm\chi_1^\pm}}{\sqrt{\sqrt{2}G_F}\, m_{\chi_1^\pm}} A^{a_1}_{1/2}(\tau_1), \tag{7.4}$$

where $\tau_1 = m^2_{a_1}/4m^2_{\chi_1^\pm}$. For $\tau_1 \leqslant 1$, which is applicable here,[14] the form-factor $A^{a_1}_{1/2}(\tau_1)$ lies in the range $1 < A^{a_i}_{1/2}(\tau_i) \lesssim 1.2$ [57]. Assuming singlet-like a_1 and higgsino-like $\chi_1^\pm$ one can derive the upper limit

$$C^{\rm eff}_{a_1}(\gamma\gamma) \lesssim \lambda \times \frac{130\ {\rm GeV}}{\mu_{\rm eff}}, \tag{7.5}$$

for $m_{a_1} \simeq 126$ GeV and $m_{\chi_1^\pm} \simeq \mu_{\rm eff}$.

The signal rates can be calculated with Eq. (6.31). For the $b\bar{b}h$ associated production mode one obtains

$$R^{bb}_{\gamma\gamma}(a_1) \simeq |P'_{11}|^2 \lambda^2 \tan^2\beta \left(\frac{130\ {\rm GeV}}{\mu_{\rm eff}}\right)^2 \left(\frac{1}{\Gamma^{\rm total}_{a_1}/\Gamma^{\rm total}_{h_{\rm SM}}}\right), \tag{7.6}$$

[14] We assume $m_{a_1} \simeq 126$ GeV, while the light chargino obeys the lower limit, $m_{\chi_1^\pm} > 94$ GeV [7]

$$R^{bb}_{b\bar{b}/\tau^+\tau^-}(a_1) \simeq \frac{|P'_{11}|^4}{\Gamma^{\rm total}_{a_1}/\Gamma^{\rm total}_{h_{\rm SM}}}, \tag{7.7}$$

where

$$P'_{11} \simeq \frac{\lambda(A_\lambda^{\rm SUSY} - 2\kappa s)v}{\mu_{\rm eff}(A_\lambda^{\rm SUSY} - \kappa s)\tan\beta}. \tag{7.8}$$

As can be seen, all the three signal rates are enhanced for large λ and small $\mu_{\rm eff}$. The dependence of the above expressions on $\tan\beta$ is not straightforward, since it only enters indirectly through $\Gamma^{\rm total}_{h_{\rm SM}}/\Gamma^{\rm total}_{a_1}$.

Both the $b\bar{b}$ and the $\tau^+\tau^-$ decay channels show exactly the same behavior as far as their signal rates are concerned, despite the fact that $\mathrm{BR}(a_1 \to \tau^+\tau^-)$ is considerably smaller than $\mathrm{BR}(a_1 \to b\bar{b})$. From an experimental point of view, the $b\bar{b}$ decay mode will result in four b-jets which may be quite challenging to tag owing to the large hadronic background, although this mode has been visited in the past [3]. The $\tau^+\tau^-$ decay mode, on the other hand, is subject to a much smaller leptonic background.

Results We perform a scan over the CNMSSM-NUHM parameter space using the same set of experimental constraints as in the CNMSSM study described in the previous section, but we neglect the a_μ constraint. We additionally require that $122\,\mathrm{GeV} < m_{a_1} < 130\,\mathrm{GeV}$ similarly to the h_1 mass. After applying all the constraints we find that the preferred parameter space of the CNMSSM-NUHM giving an enhancement in the aforementioned signal rates due to the lighter pseudoscalar with mass about $126\,\mathrm{GeV}$ can be divided into three main regions depending on the composition of the lightest neutralino χ: the singlino-higgsino region, the pure higgsino region, and the HB/FP region.

In the **singlino-higgsino region** χ is a mixture of a large higgsino component and a smaller $(20\% - 30\%)$ but important singlino one. Owing to the significant singlino component the neutralino will interact very weakly with matter and will thus typically have too large relic abundance. In order to satisfy the $\Omega_\chi h^2$ constraint one then needs to consider small m_χ and consequently large annihilation cross-section. In practice we find in this region $m_\chi \sim 70 \div 80\,\mathrm{GeV}$. The preferred region in the parameter space spans a wide range of m_0 and $m_{1/2}$, while we obtain $0.4 \lesssim \lambda \lesssim 0.6$ and $0.25 \lesssim \kappa \lesssim 0.4$. The parameter λ is bounded from below by requirement to enhance the Higgs signal rates, but it cannot be too large in order to obtain SM-like h_1. Small-to-intermediate values of κ are required to maximize the singlino component of χ. The smallness in κ has to be compensated by large values of A_κ for obtaining the correct value of the lighter pseudoscalar mass. A_0 almost always takes large negative values, which helps to maximize m_{h_1}. $\tan\beta$ is typically between 10 and 40.

In order to enhance the signal rates we need to keep μ noticeably smaller than 1 TeV. This has important consequences for the **pure higgsino region** in our analysis of the CNMSSM-NUHM in which one obtains too low DM relic density. However, as the primary aim of the analysis was to discuss the possible enhancement in $R_X^{bb}(a_1)$, we will assume in this case that thermally produced neutralinos contribute only partially to the total DM relic abundance, *i.e.*, $\Omega_\chi^{\rm th} h^2 \simeq \xi\, \Omega_{\rm DM,total} h^2$ with $\xi < 1$.[15] Another possibility would be that the entire relic abundance is due to an alternative DM candidate, *e.g.*, gravitino or axino. In the pure higgsino region we once again obtain wide range of allowed m_0 and $m_{1/2}$. It is also true for λ, κ and $\tan\beta$, although signal rates are enhanced significantly only for large λ. A_0 is again confined to be typically large and negative, while A_κ appears to be more close to zero.

When analyzing the **HB/FP region** we assumed negative $\mu_{\rm eff}$ which helps to satisfy the dark matter DD constraints as discussed above. The preferred values of most of the parameters follow the discussion for the CMSSM. However, $\tan\beta$ in this case is often limited to be not greater than about 15 since larger values would enhance too much Yukawa couplings of h_1 to $b\bar{b}$ and $\tau^+\tau^-$. This effective upper limit on $\tan\beta$, in turns, causes an increase of m_{a_1} above 126 GeV via the A_κ and A_λ running (see a discussion in [291]). The upper bound on $\tan\beta$ is relaxed for A_0 more close to zero, when the running is slower. The parameters λ and κ span wide ranges, while A_κ is typically close to zero.

In Fig. 7.12 we show the range of m_χ and the corresponding values of $\xi\sigma_p^{\rm SI}$ across all the regions for which an enhancement above one was obtained in a combined signal rate for h_1 and a_1 $R_{\gamma\gamma}^{bb}(h_1 + a_1)$. The corresponding value of $R_{\gamma\gamma}^{bb}(h_1 + a_1)$ are shown in the right panel. The HB/FP region is characterized by relatively smaller enhancement in the Higgs signal rates than the other two regions due to a heavier chargino $\chi_1^\pm$.

In Fig. 7.13 (left panel) we show the combined Higgs signal in the $b\bar{b}h$ production mode for $b\bar{b}$ and $\tau^+\tau^-$ decay channels for the pure higgsino region. As it is expected the rate increases for larger λ and smaller $\mu_{\rm eff}$. On the other hand, in the HB/FP region illustrated in Fig. 7.13 (right panel) $R_{b\bar{b}/\tau^+\tau^-}^{bb}(a_1)$ can have extremely large values, even about 100. However, this should not be interpreted as a characteristic feature specific to the HB/FP region, but as a result of negative $\mu_{\rm eff}$ assumed for this region. $R_{b\bar{b}/\tau^+\tau^-}^{bb}(a_1)$ increases as the denominator of $|P'_{11}|$, $A_\lambda^{\rm SUSY} + \kappa s$, approaches zero. For small negative $\mu_{\rm eff}$ and large positive λ, resulting in small negative $s = \mu_{\rm eff}/\lambda$, the size of the denominator reduces as κ grows. In Fig. 7.13 (right panel) we show how $R_{b\bar{b}/\tau^+\tau^-}^{bb}(a_1)$ enhances with increasing κ and decreasing value of the above denominator term. Evidently a similar effect of negative $\mu_{\rm eff}$

[15] In the following we assume $\xi = 1$ for the other two discussed regions in the parameter space of the CNMSSM-NUHM.

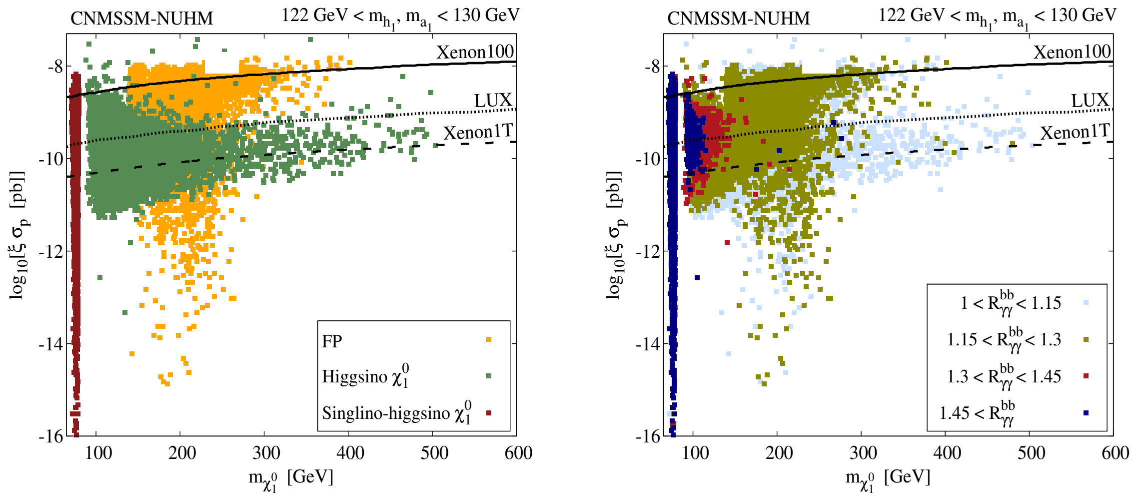

Figure 7.12: *Left panel*: The preferred regions of the parameter space of the CNMSSM-NUHM in the $(m_\chi, \xi\sigma_p^{\rm SI})$ plane giving an enhancement in $R^{bb}_{\gamma\gamma}(h_1 + a_1)$. Also shown are the 90% CL exclusion limits from XENON100 as well as the 90% CL limits expected (at the time of analysis) from the LUX and XENON1T experiments. Maroon squares denote the singlino-higgsino region, green squares the pure higgsino region and yellow squares the HB/FP region. *Right panel*: The $(m_\chi,\sigma_p^{\rm SI})$ plane showing the actual values of $R^{bb}_{\gamma\gamma}(h_1 + a_1)$ in the preferred regions. Taken from Ref. [291].

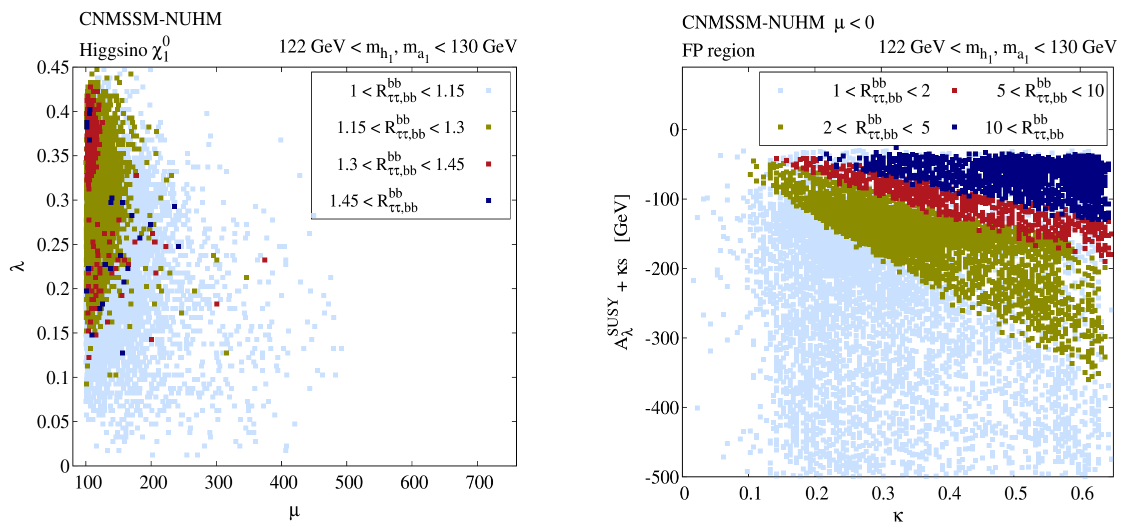

Figure 7.13: *Left panel*: Enhancement in $R^{bb}_{b\bar{b}/\tau^+\tau^-}(h_1 + a_1)$ obtained in the pure higgsino region as a function of the λ and $\mu_{\rm eff}$ parameters. *Right panel*: Enhancement in $R^{bb}_{b\bar{b}/\tau^+\tau^-}(h_1+a_1)$ obtained in the HB/FP region as a function of κ and $(A_\lambda^{\rm SUSY}+\kappa s)$ (see text for details). Taken from Ref. [291].

should manifest in the other two regions also, but it would cause a tension between m_{a_1} and m_{h_1} and would not allow both of these to be around 125 GeV.

7.4 Fine-tuning and 1 TeV higgsino dark matter

The results presented in this section are based on [292].

As discussed in Section 4.7 the little hierarchy problem arises since current lower limits on squark and gluino masses, as well as the measured value of the Higgs boson mass suggest that the characteristic mass scale for the SUSY particles $M_{\rm SUSY}$ lies above 1 TeV. In this section we will study the issue of fine-tuning for the GUT constrained models within the framework of the MSSM.[16] In particular we will focus on the phenomenologically interesting 1TH region for which $\mu \simeq 1\,\text{TeV}$ and therefore the problem is often the most severe.

CMSSM Let us begin with the simplest GUT constrained model discussed so far in this thesis, *i.e.*, the CMSSM. In the CMSSM the fundamental GUT-scale parameters to deal with when discussing the fine-tuning issue are m_0, $m_{1/2}$, A_0, the unified bilinear parameter, B_0, and the high-scale Higgs/higgsino mass parameter, μ_0 (at the EWSB scale the last two are typically traded for $\tan\beta$). Contributions to the total fine-tuning Δ that come from m_0 and $m_{1/2}$ are shown in Fig. 7.14. Another contributions are typically smaller, beside Δ_{μ_0} which will be discussed later. As can be seen Δ can easily reach large values (above 1000) in the 1TH region that appears in the upper right corner of the plots for large m_0 and $m_{1/2}$.

Another (large) contribution to the total fine-tuning can be calculated by differentiating M_Z^2 with respect to the top Yukawa y_t. In the following, for simplicity, we will fix y_t at the experimental value and focus on a possible reduction of contributions to Δ that come from the SUSY parameters.

Non-universal unification conditions The fine-tuning with respect to gaugino and scalar mass parameters can be reduced by employing some non-universality conditions at the GUT scale. This is illustrated in Fig. 7.15.

In particular, in the left panel we present the fine-tuning with respect to M_3 (here defined at the GUT scale) for various unification patterns with non-universal gaugino masses (NUGM). As can be seen, one can identify three well theoretically justified patterns of $M_1 : M_2 : M_3$, that is $19/10 : 5/2 : 1$, $10 : 2 : 1$, or $-5 : 3 : 1$, for which one obtains $\Delta_{M_3} \lesssim 100$ for a wide range of M_3.[17]

In the scalar sector, the amount of fine tuning strongly depends on the high-scale relation among $m_{H_u}^2$ and the soft stop masses at the GUT scale [311]. In $SU(5)$ (or in $SO(10)$) the fermions and the Higgs bosons belong to different representations, so that the corresponding soft-breaking masses are in general unrelated and the fine tuning can become very large (since there is no possibility of cancellation between

[16] For a discussion of the fine-tuning in the CNMSSM see Section 7.2.

[17] The last two patterns appear in the context of $SU(5)$ GUT unification (see [308, 309]), while the first one can be obtained for $SO(10)$ (see [310]).

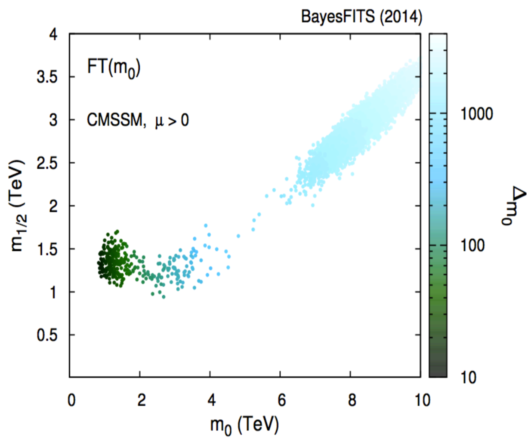

Figure 7.14: 95% CL regions in the CMSSM with contributions to the total fine-tuning that come from m_0 (left panel) and $m_{1/2}$ (right panel). Taken from Ref. [292].

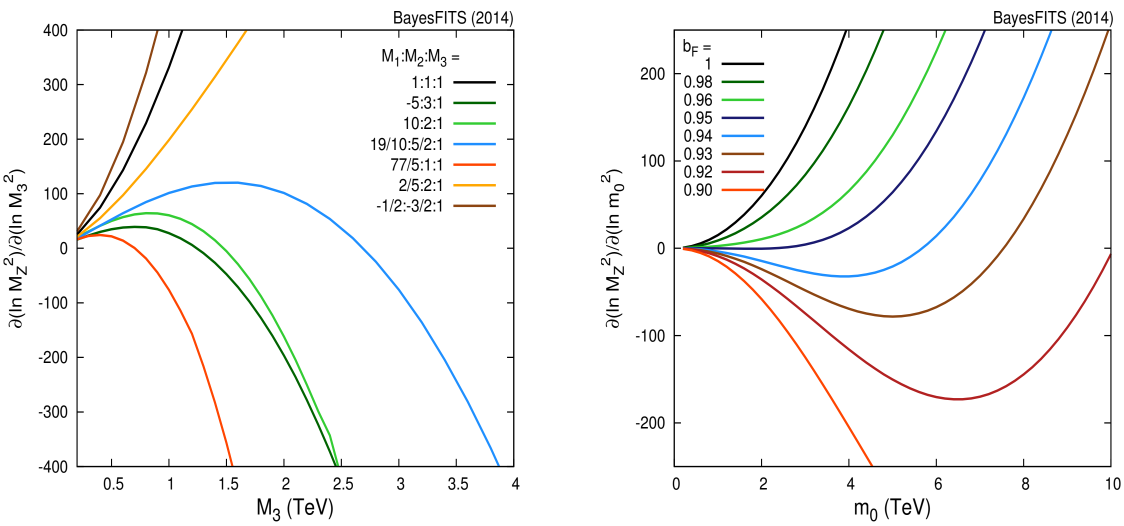

Figure 7.15: *Left panel*: The fine tuning due to M_3 for different GUT-scale gaugino mass patterns. *Right panel*: The fine tuning associated with GUT scale scalar masses for different choices of the parameter $b_F = m_{H_u}(M_{\text{GUT}})/m_0$. Taken from Ref. [292].

the corresponding fine-tuning contributions). However, if supergravity-inspired universality conditions are imposed at the high scale, the fine tuning can be reduced to the CMSSM levels.

By employing the RGEs evolution of m_{H_u} one can rewrite this parameter as a function of its value at the GUT scale and m_0 (assuming $m_{H_u} \neq m_0$ at high energy scale)

$$m_{H_u}^2(M_{\text{SUSY}}) \simeq -0.571 m_0^2 + 0.645 m_{H_u} + \text{gaugino and trilinear contributions}\,. \quad (7.9)$$

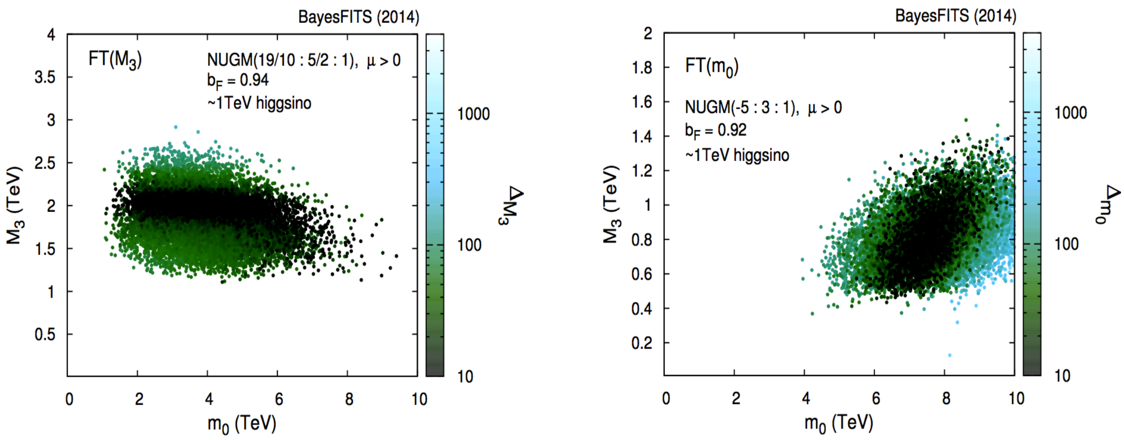

Figure 7.16: The 1TH 95% CL region obtained for two different non-universal GUT unification patterns. Scalar (left panel) and gaugino (righ panel) mass contributions to the total fine-tuning is shown with color. Taken from Ref. [292].

It is straightforward to see that one can obtain less fine tuning from the scalars than in the CMSSM when m_{H_u} and m_0^2 are related (but not simply unified) as

$$m_{H_u}^2 = b_F^2 m_0^2, \quad \text{with} \quad |b_F| \simeq \sqrt{0.57/0.64} = 0.94\,. \tag{7.10}$$

For simplicity we will consider b_F to be positive. Remarkably, b_F does not deviate substantially from one, *i.e.*, the value corresponding to universal scalar masses. In Fig. 7.15 (right panel), we show the scalar fine tuning as a function of m_0 for various values of b_F. The curves are drawn for fixed values $m_{1/2} = 1\,\text{TeV}$, $A_0 = -1\,\text{TeV}$ and $\tan\beta = 30$. As can be seen, one can obtain a significant reduction of the scalar Δ for $b_F \simeq 0.94$. Smaller (or slightly larger) b_F can also lead to very low fine-tuning, especially for specific values of m_0.

The impact of non-universality conditions on Δ_{m_0} and Δ_{M_3} in the 1TH region is illustrated in Fig. 7.16 for some selected unification patterns. The lowest values of both fine-tuning contribution separately can be lower than 10. Points shown in the scatter plots were *a priori* obtained without imposing condition that would minimize the fine-tuning. Interestingly, it appears that the 1TH region for a specific patterns shown in Fig. 7.16 coincides spectacularly with the region of the lowest contributions to Δ.[18]

The fine-tuning of μ Another substantial contribution to the total fine-tuning in the CMSSM, which remains sizable in the partially non-universal models discussed above, is associated with the μ_0 parameter. It is commonly defined at M_{SUSY}, and

[18]Black strips go along the middle of phenomenologically preferred regions in both plots.

is related to its GUT-scale value, μ_0, through RGE evolution. The running depends on the Yukawa couplings of the third generation, $y_{t,b,\tau}$ and the gauge couplings of the $SU(2)_L$ and $U(1)_Y$ groups, g_2 and g_1. In practice to some approximation

$$\mu = R\,\mu_0 \approx 0.9\mu_0\,. \tag{7.11}$$

Since the corresponding derivatives of $m_{H_u}(M_{\rm SUSY})$ and Σ_u^u with respect to μ_0 vanish (if μ_0 is unrelated to m_0) in the Barbieri-Giudice measure Eq. (4.47), one obtains approximately

$$\frac{\partial \ln M_Z^2}{\partial \ln \mu_0^2} \approx -2\frac{R^2\mu_0^2}{M_Z^2} = \frac{-2\mu^2}{M_Z^2}\,. \tag{7.12}$$

This shows the well-known fact that in the MSSM naturalness requires preferably small values of $\mu = R\mu_0$.

However, one can effectively cancel this contribution with the one from m_0 by imposing a unification condition between m_0 and μ_0. This can be realized, *e.g.*, within supergravity thanks to the Giudice-Masiero mechanism [312]. In its minimal implementation one introduces a set of visible-sector superfields and at least one additional set of hidden-sector superfields. If some symmetry forbids a SUSY-conserving bilinear term in the superpotential of the visible sector, a naturally small effective μ_0 proportional to the gravitino mass can be generated through interactions with hidden-sector fields. The same mechanism generates masses for the scalar fields. As a result, one expects to obtain a correlation between the μ_0 and m_0 parameters, $\mu_0 = C_h\,m_0$, where constant C_h is determined by the hidden sector. Combining this with Eq. (7.11) one derives

$$\mu = (R\,C_h)\,m_0 = c_H\,m_0. \tag{7.13}$$

The Barbieri-Giudice measure of the fine-tuning for m_0 related to μ_0 now reads

$$\begin{aligned}\frac{\partial \ln M_Z^2}{\partial \ln m_0^2} &\approx 2\frac{m_0^2}{M_Z^2}\left\{-\frac{\partial\mu^2}{\partial m_0^2} - \frac{\partial m_{H_u}^2(M_{\rm SUSY})}{\partial m_0^2}\left[1+\mathcal{O}(10^{-2})\right]\right\} \\ &\approx 2\frac{m_0^2}{M_Z^2}\left(-c_H^2 - 0.64\,b_F^2 + 0.57\right)\,. \end{aligned} \tag{7.14}$$

One can reduce this contribution to Δ by proper adjusting b_F and c_H parameters. We show examples of such adjustment for two choices of NUGM patterns in Fig. 7.17.

Note that it is necessary to have $b_F < 1$ to obtain low levels of m_0 fine-tuning, similarly to the cases where μ_0 is a fundamental parameter (discussed above). One way to control the amount of m_{H_u}/m_0 splitting, which is discussed in [292], is to employ RGE running above the GUT scale, if a larger GUT gauge group breaks down to the SM group at $M_{\rm GUT}$. Additionally, we assumed there that the μ term in the superpotential is forbidden by the anomalous $U(1)_A$ symmetry group introduced

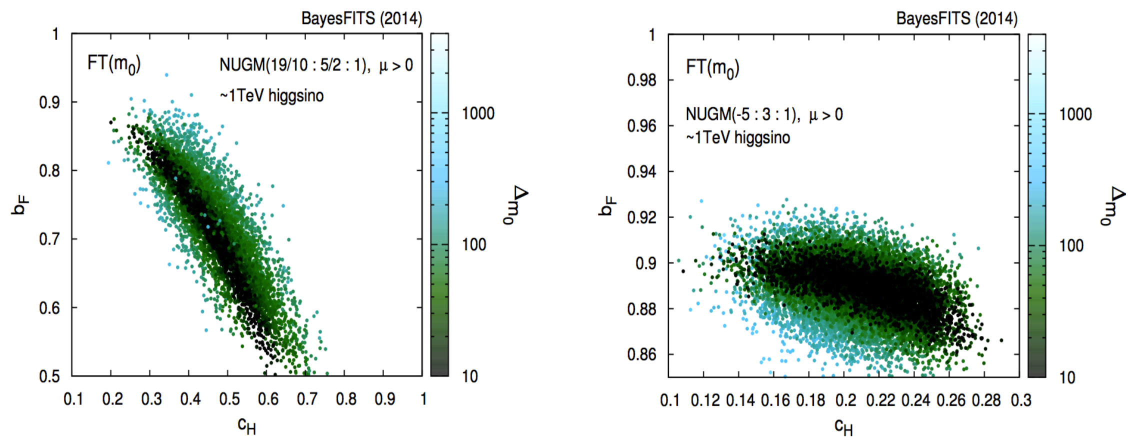

Figure 7.17: The 1TH 95% CL region in the (c_H, b_F) plane for two different gaugino unification patterns. Taken from Ref. [292].

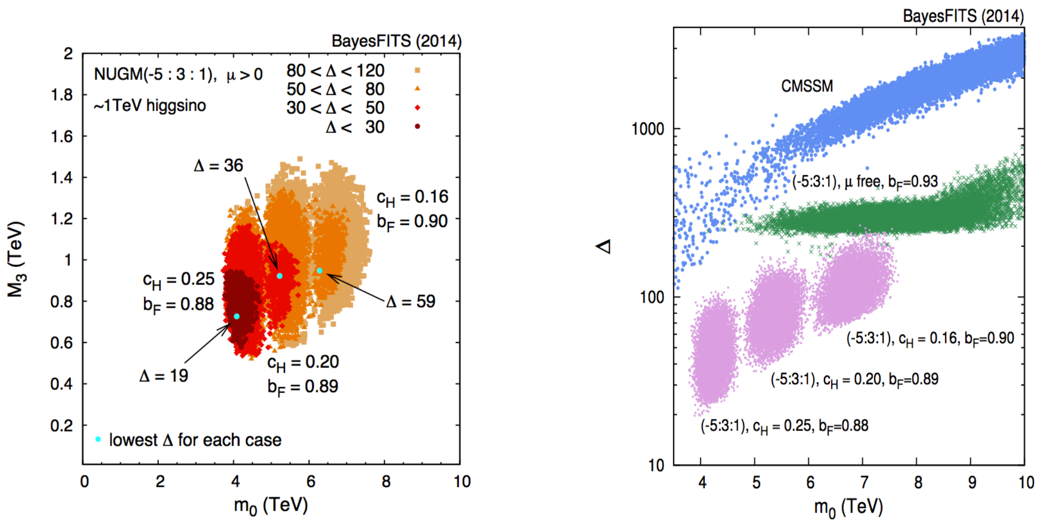

Figure 7.18: *Left panel*: The total fine-tuning in the 1TH region in the (m_0, M_3) plane for NUGM(-5:3:1) and three choices of b_F and c_H. Points with the lowest fine-tuning for each such choice are denoted by light blue dots. *Right panel*: Comparison of the total fine-tuning of three models shown in the left panel with the CMSSM and the model without μ_0 and m_0 relation at the GUT scale. Taken from Ref. [292].

in the Missing Partner mechanism [313, 314]. In particular, we referred to the model described in [315].

In Fig. 7.18 (left panel) we present the total fine-tuning in the (m_0, M_3) plane for NUGM condition $-5 : 3 : 1$ and several choices of b_F and c_H. As can be seen, Δ can be much reduced in comparison with the CMSSM (see also the right panel of Fig. 7.18).

Chapter 8

MSSM and NMSSM

Having discussed properties of some GUT constrained SUSY models we now move to an analysis of the MSSM (and the NMSSM) with some set of parameters defined at low energy scale. After short description of the standard case we will focus on the neutralino DM scenario with low reheating temperature of the Universe. This chapter is based on the results published in [293].

8.1 Dark matter relic density $\Omega_\chi h^2$ in the MSSM and the NMSSM

The p10MSSM model We begin with a short description of the neutralino DM scenario within the MSSM in the standard cosmological scenario where freeze-out of χ takes place in the RD epoch. In particular, we focus on the so-called p10MSSM with the parameters and their ranges given in Table 8.1. This set of parameters appears to be large enough to discuss all the important scenarios leading to the correct value of $\Omega_\chi h^2$ and simultaneously the set remains small enough to allow us to efficiently scan the parameter space. We perform a Bayesian scan of this model taking into account constraints listed in Table 6.1.

Although the choice of parameters and their ranges given in Table 8.1 is quite generous, one needs to mention its several limitations. For instance, it does not allow to consider coannihilations of χ with selectrons or smuons. However, from the point of view of our discussion it is enough to permit coannihilations with the lighter stau and not to distinguish between different sleptons being mass-degenerate with χ. Another important remark is such that in the following we will first put a special attention to the issue of heavy neutralino DM (up to 5 TeV). This is justified by the fact that a low mass regime has been already studied much more extensively in the literature and, beside that, by the current experimental limits on the masses of

Parameter	Range
bino mass	$0.1 < M_1 < 5$
wino mass	$0.1 < M_2 < 6$
gluino mass	$0.7 < M_3 < 10$
stop trilinear coupling	$-12 < A_t < 12$
stau trilinear coupling	$-12 < A_\tau < 12$
sbottom trilinear coupling	$A_b = -0.5$
pseudoscalar mass	$0.2 < m_A < 10$
μ parameter	$0.1 < \mu < 6$
3rd gen. soft squark mass	$0.1 < m_{\tilde{Q}_3} < 15$
3rd gen. soft slepton mass	$0.1 < m_{\tilde{L}_3} < 15$
1st/2nd gen. soft squark mass	$m_{\tilde{Q}_{1,2}} = M_1 + 100$ GeV
1st/2nd gen. soft slepton mass	$m_{\tilde{L}_{1,2}} = m_{\tilde{Q}_3} + 1$ TeV
ratio of Higgs doublet VEVs	$2 < \tan\beta < 62$

Table 8.1: The parameters of the p10MSSM and their ranges used in our scan. All masses and trilinear couplings are given in TeV, unless indicated otherwise. All the parameters of the model are given at the SUSY breaking scale.

SUSY particles.[1] Although such a heavy χ naturally leads to SUSY particles that avoid detection at the LHC, we will show that in this case the lightest neutralino can be often found in future dark matter DD (or ID) experiments. The issue of fine-tuning for this mass regime may be potentially resolved after embedding the p10MSSM into some GUT inspired theory similarly to the 1TH region case discussed in the previous chapter. We will not treat this in the thesis.

Since we focus on heavy DM, it is typically rather difficult for us to satisfy the a_μ constraint which requires relatively light smuons. Since the primary aim of our discussion is to present some properties of SUSY DM and the experimental error associated with a_μ is still substantial, we will neglect this constraint in the study.

Neutralino dark matter in the p10MSSM As it was discussed in Section 5.1.3, the correct DM relic density for the lightest neutralino can be obtained in the bulk region, or by employing several possible coannihilation mechanisms (*e.g.*, with the lighter stau, lighter stop or the lighter sbottom), or due to some resonant annihilations (in the AF region or in the h- or Z-resonance regions). The special case of 1 TeV higgsino dark matter is associated with efficient (co)annihilations between three lightest SUSY species, $\chi = \chi_1^0$, χ_2^0 and $\chi_1^\pm$.

These regions with bino-like or higgsino-like χ are shown in Fig. 8.1 on the $(m_\chi, \sigma_p^{\rm SI})$ plane. The basic features of the $m_\chi \lesssim 1\,\text{TeV}$ mass regime was already discussed for the CMSSM. The 1TH higgsino region in a more general framework of the p10MSSM remain to a large extend testable in the future Xenon1T experiment,

[1] These limits are not so stringent for the neutralino, but rather for the gluino or squarks. Nevertheless, we will focus on a possible scenario in which also the neutralino LSP is heavy.

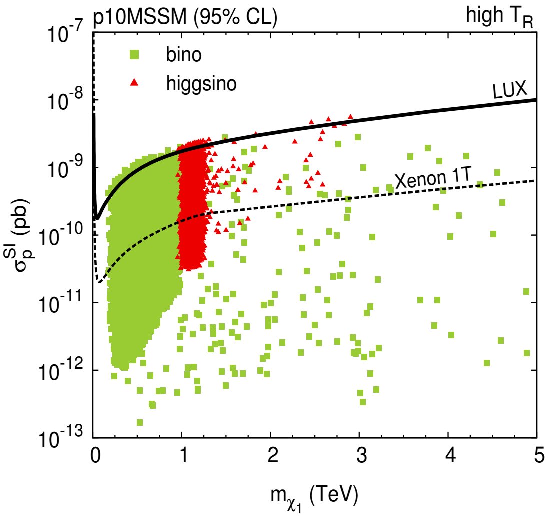

Figure 8.1: Direct detection $\sigma_p^{\rm SI}$ cross section as a function of m_χ in the p10MSSM 95% CL regions. The solid (dashed) black lines correspond to LUX (projected Xenon1T) limit on $sigma_p^{\rm SI}$. Green squares correspond to bino-like χ, while red triangles to higgsino-like χ. Taken from Ref. [293].

while in the case of bino-like neutralino $\sigma_p^{\rm SI}$ can vary by several order of magnitude depending on its higgsino (subdominant) composition. On the other hand, as can be clearly see, it is particularly difficult to obtain $\Omega_\chi h^2 \simeq 0.12$ for χ heavier than about 1 TeV. In particular, for the largest masses of our interest, this is possible in presence of coannihilations with the lighter stop or the gluino accompanied by the A-resonance condition. However, this requires a very specific mass pattern, *e.g.*, $m_\chi \simeq m_{\tilde{g}} \simeq 0.5 m_A$. Note that few higgsino-like points obtained for $m_\chi \sim 2 \div 3\,\text{TeV}$ are within a reach of the Xenon1T experiment.

Wino DM is not shown in Fig. 8.1. It is because this scenario in the MSSM has been recently claimed to be excluded by ID searches [316, 317, 318]. It is due to an accidental overlap of the mass range corresponding to the correct relic density and the region where the Sommerfeld enhancement of $\langle\sigma v\rangle$ plays an important role. In particular, the enhanced rates of present-day wino annihilations would give rise to diffuse gamma ray background in the H.E.S.S. data [319]. It could also lead to an excess in the antiproton signal from PAMELA [320]. Conclusions from such analyses [316, 317, 318] can be summarized in the exclusion of wino DM for the mass ranges below 800 GeV and between 1.8 TeV and 3.5 TeV when Einasto DM profile is assumed in the center of the Galaxy. The exclusion generally holds also for other DM profiles, except from the flat ones. On the other hand, wino DM with mass smaller than 1.8 TeV or larger than 3.5 TeV generically cannot satisfy the relic density constraint. Therefore a combination of the $\Omega_\chi h^2$ and ID constraints excludes wino-like χ as a DM candidate in a standard cosmological scenario where wino DM particles are produced thermally in the early Universe and freeze-out in the RD epoch. In the following, we will employ (as sharp cuts) mass bounds from [318] from which we also take the SE factors needed to calculate $\Omega_\chi h^2$ in presence of the SE.

One in principle obtains similar results in the case of the NMSSM. Important additions are the singlino-like lightest neutralino and some singlino mixed states. In the NMSSM, similarly to the MSSM, it is also very difficult to satisfy the relic density constraint for $m_\chi \gtrsim 3\,\mathrm{TeV}$. In particular, as it was mentioned in Section 5.1.3, obtaining the correct relic density for χ with significant singlino composition requires, *e.g.*, coannihilations with the lighter stau or gluino or non-negligible mixing between the singlino and the higgsino. Pure singlino DM is typically characterized by very low DD rates as it was shown in the case of the CNMSSM in Section 7.2. These rates can be enhanced to the level reachable by the Xenon1T experiment for a mixed singlino-higgsino neutralino.

8.2 Low reheating temperature T_R and heavy supersymmetric dark matter

As we will see it is particularly difficult to obtain $\Omega_\chi h^2 \simeq 0.12$ for heavy neutralino DM both in the framework of the MSSM and for the NMSSM. In this section we will show how this can be circumvented if one assumes that the reheating temperature of the Universe after a period of cosmological inflation was low enough so that DM freeze-out took place in the reheating period (*i.e.*, before the RD epoch).

8.2.1 Boltzmann equations and suppression of $\Omega_\chi h^2$

During the reheating period the total energy density of the Universe was dominated by the contribution from a decaying inflaton field. One should then take this into account when writing the set of Boltzmann equations needed to calculate the DM relic density. In particular, Eq. (2.16) for radiation needs to be modified. Moreover, it is necessary to add one more equation describing decays of the inflaton field to radiation. On the other hand, Eq. (2.15) associated with thermally produced DM remains unchanged for our discussion in this section. However, one needs to remember that some of the quantities in this equation are modified in the framework of SUSY as it was described in Section 5.1.1.

In principle we should also take into account a possibility that the inflaton field will produce DM particles via direct or cascade decays. However, this will serve as an additional source of DM different than a production in thermal equilibrium. On the other hand, when we focus on heavy DM, we typically face the problem of DM thermal overproduction. Thus we rather want to suppress $\Omega_\chi h^2$ and not to introduce an additional production mechanism. For this reason in this section we will assume that such inflaton decays to DM contribute negligibly to the DM relic density. We will treat these decays more accurately in the next section.

Thus the appropriate set of Boltzmann equations now reads:

$$
\begin{aligned}
\frac{d\rho_\phi}{dt} &= -3H\rho_\phi - \Gamma_\phi\rho_\phi, \\
\frac{d\rho_R}{dt} &= -4H\rho_R + \Gamma_\phi\rho_\phi + 2\langle\sigma v\rangle_{\text{eff}}\langle E\rangle_{\text{eff}}\big(n^2 - n_{\text{eq}}^2\big), \\
\frac{dn}{dt} &= -3Hn - \langle\sigma v\rangle_{\text{eff}}\big(n^2 - n_{\text{eq}}^2\big),
\end{aligned}
\tag{8.1}
$$

where ρ_ϕ is the energy density of the inflaton field and Γ_ϕ is the inflaton decay rate.

At the beginning of the reheating period the temperature of the Universe rapidly increases from $T \approx 0$ to some maximum value $T_{\max}$ due to inflaton decays to radiation.[2] At later times radiation is still effectively produced, but the additional entropy production, associated with decays of the inflaton field, leads to a decrease of T. The rate of this decrease with increasing scale factor is approximately given by $T \sim a^{-3/8}$. In other words, the same drop in the temperature corresponds to a faster expansion of the Universe during the reheating period than in the RD epoch where $T \sim a^{-1}$. This has a remarkable impact on the DM relic density assuming that the freeze-out of the DM particles took place during the reheating period. Between the freeze-out and the end of the reheating period the DM particles were effectively diluted away due to fast expansion. As a result one obtains a reduced value of $\Omega_\chi h^2$ in comparison with the standard result obtained for freeze-out in the RD epoch. This is summarized in Fig. 8.2.

The faster expansion of the Universe additionally result in a slightly earlier (in terms of higher T) freeze-out of the DM particles. This effect could potentially lead to an increased DM production, as can be deduced form Fig. 8.2. However, this increase is almost always by no means less important than the aforementioned dilution. Thus final $\Omega_\chi h^2$ for low T_R is reduced in comparison with the high T_R (standard) value [8]. In principle one might expect a slight increase of the DM relic density, if freeze-out occurred just at the end of reheating period, since then the dilution period would not be present. However, we found that the maximum increase is at best a few percent, *i.e.*, of the order of the error associated with this type of calculations.

An approximate analytical treating of Eqs (8.1) leads to relation between the standard value of the relic density $\Omega_\chi h^2$(high T_R) and the one calculated in the low

[2] The value of $T_{\max}$ does not play a role in the determination of the DM relic abundance, since $\Omega_{\text{DM}}h^2$ is set mainly by the the rate of (co)annihilation processes near freeze-out and typically $T_{\text{fo}} \ll T_{\max}$.

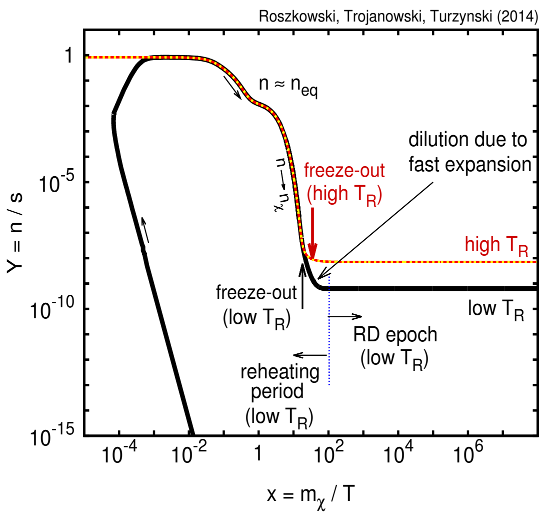

Figure 8.2: Total yield $Y = n/s$ as a function of $x = m_\chi/T$ in scenarios with low and high reheating temperature. A solid (dotted) curve corresponds to the low (high) T_R scenario. The beginning of the RD epoch for the low T_R scenario is denoted by vertical dotted blue line. Taken from Ref. [293].

T_R regime $\Omega_\chi h^2$

$$\Omega_{\rm DM} h^2(\text{high } T_R) \simeq \left(\frac{m_\chi}{T_R}\right)^3 \left(\frac{T_{\rm fo}}{m_\chi}\right)^3 \Omega_{\rm DM} h^2, \tag{8.2}$$

with $(T_{\rm fo}/m_\chi)^3$ factored out since its value changes only in a narrow range. From (8.2) it immediately follows that in scenarios with low reheating temperatures, $T_R < T_{\rm fo}$, the DM relic abundance is suppressed with respect to scenarios with high reheating temperatures. However, in a more accurate treatment Eq. (8.2) may be slightly misleading, as it does not show a certain degree of correlation between $T_{\rm fo}$ and $\Omega_{\rm DM} h^2(\text{high } T_R)$.

In the following we rather solve Eqs (8.1) numerically. We obtain both $\langle\sigma v\rangle_{\rm eff}$ and $\langle\sigma v\rangle_{\rm eff}\langle E\rangle_{\rm eff}$ as a function of temperature with appropriately modified `MicrOMEGAs`. We follow a general methodology from [8] described for a single particle DM. In order to treat SUSY DM we additionally apply the freeze-out approximation (see, *e.g.*, [321]) modified to our non-standard cosmological scenario. Some details of this are given in Appendix D. `MicrOMEGAs` v3.6.7 was used to obtain $\Omega_\chi h^2(\text{high } T_R)$, *i.e.*, the relic density in the standard cosmological scenario, and $\sigma_p^{\rm SI}$. We also checked that in the high T_R limit our numerical tool for solving the Boltzmann equations reproduces $\Omega_\chi h^2(\text{high } T_R)$ obtained with `MicrOMEGAs`.

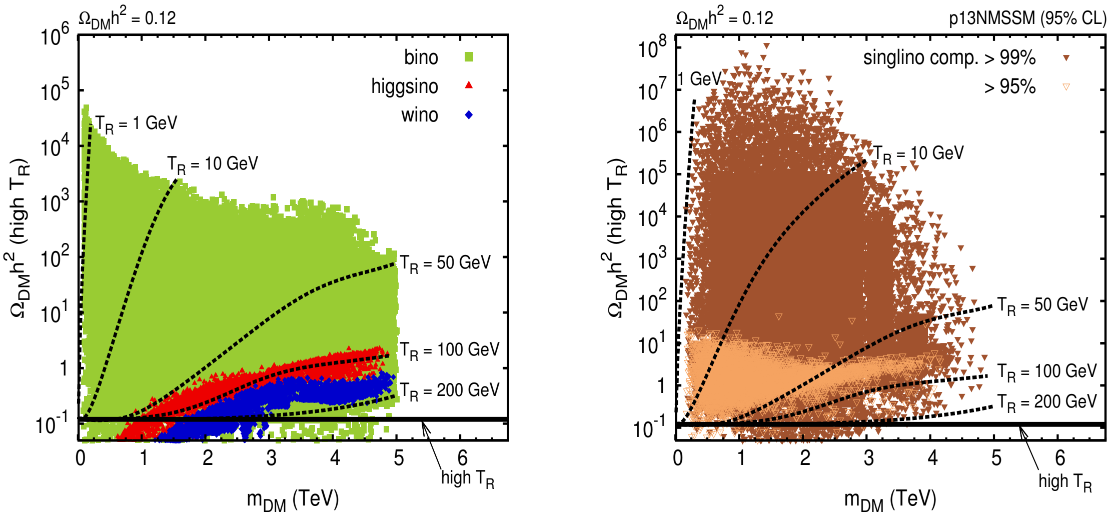

Figure 8.3: Contours (black dotted) of constant $\Omega_{\rm DM}h^2 = 0.12$ for different values of the reheating temperature T_R in the MSSM (left panel) and the NMSSM (right panel), for which only the (almost) pure singlino DM case is shown, in the $(m_{\rm DM}, \Omega_{\rm DM}h^2(\text{high } T_R))$ plane. The solid black horizontal line corresponds to the high T_R limit. Green squares correspond to the bino DM region, while red triangles (blue diamonds) to the higgsino (wino) DM case. In the left panel dark (light) brown triangles correspond singlino fraction > 99% (between 95% and 99%). Taken from Ref. [293].

8.2.2 MSSM and NMSSM at low T_R

In this section we apply the methodology of solving the Boltzmann equations for low T_R to the p10MSSM and the p13NMSSM (with three additional parameters[3], λ, κ and A_κ). We follow Table 8.1 for the choice of parameters and their ranges[4] and Table 6.1 for the constraints.

The main results of such study – but obtained without imposing the constraint on the DM relic abundance and direct detection rates – can be summarized in Fig. 8.3. We present there the lines of constant $\Omega_\chi h^2 \simeq 0.12$ as a function of m_χ obtained for several values of $T_R = 1, 10, 50, 100$ and $200\,$GeV. The horizontal line corresponding to the standard (high T_R) scenario is also shown. As can be seen, the standard result $\Omega_\chi h^2(\text{high } T_R)$ can be suppressed by several orders of magnitude in the low T_R regime.

The upper limit on $\Omega_\chi h^2(\text{high } T_R)$ in the left panel of Fig. 8.3 corresponds to **bino-like** χ annihilating via t-channel slepton exchange. The relic density is then given by Eq. (5.3) with maximum value of slepton masses in our scan that is about $10-15\,$TeV. In the low T_R regime one can easily obtain $\Omega_\chi h^2 \simeq 0.12$ for wide range

[3] A_λ is determined in terms of other parameters including $\mu_{\rm eff}$ and m_A.

[4] Additional parameters in the p13NMSSM have ranges: $0.001 < \lambda < 0.7$, $0.001 < \kappa < 0.7$, $-12\,\text{TeV} < \text{A}_\kappa < 12\,\text{TeV}$.

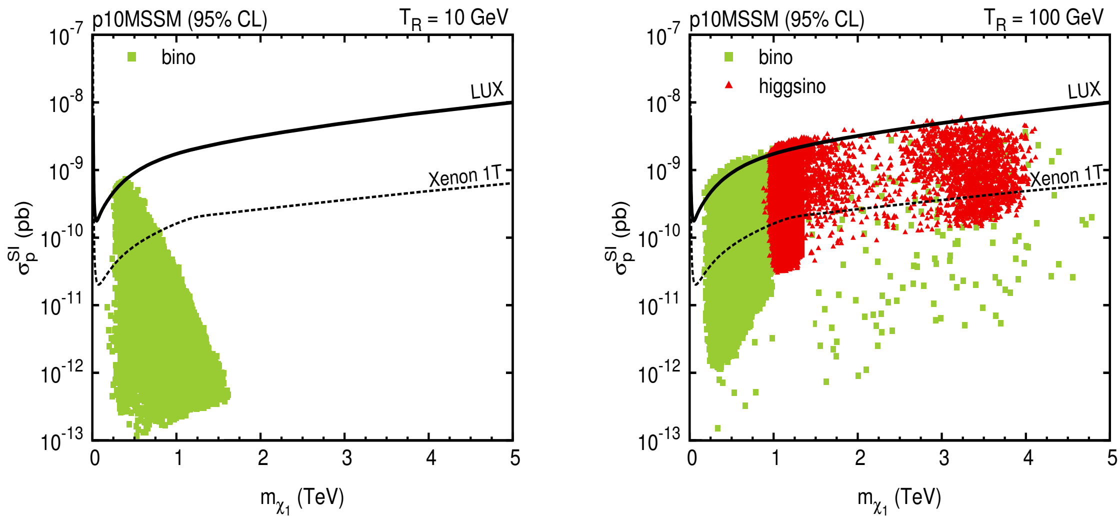

Figure 8.4: Direct detection $\sigma_p^{\rm SI}$ cross section as a function of m_χ in the p10MSSM 95% CL regions for $T_R = 10\,$GeV (left panel) and $T_R = 100\,$GeV (right panel). The solid (dashed) black lines correspond to LUX (projected Xenon1T) limit on $\sigma_p^{\rm SI}$. Color coding as in Fig. 8.3. Taken from Ref. [293].

of masses without imposing any other conditions on the SUSY mass spectrum. The similar is true for **singlino-like** χ as shown in the right panel of Fig. 8.3.

In the case of **higgsino** DM one can obtain the correct relic density for masses much heavier than 1 TeV. Remarkably, this happens only for $T_R \sim 100\,$GeV. One interesting consequence of this could be derived if in some combination of future DM experiments one would be able to find the DM particle recalling the higgsino but mass significantly exceeding 1 TeV. This could then be interpreted as a hint for the low T_R scenario with a value of the reheating temperature determined quite precisely.

The other important advantage is that **wino** DM in the low T_R scenario can become again viable provided that $T_R \sim 100 - 200\,$GeV. In this case the correct relic density can be obtained for $m_{\widetilde{W}} > 3.5\,$TeV. Thus it escapes from current ID exclusion limits, but may be potentially tested in some future ID experiments.

The dark matter DD rates $\sigma_p^{\rm SI}$ for several values of T_R are shown in Fig. 8.4 for bino and higgsino DM and Fig. 8.5 for wino DM. In particular, the heavy higgsino DM scenario can be almost entirely tested in Xenon1T experiment within a few years. Some part of the wino DM case is also testable. On the other hand, bino (and singlino) DM remains to a large extend beyond the reach of DD searches.

8.2.3 Constrained MSSM at low T_R

It is interesting to briefly discuss the impact of low T_R on the allowed parameter space in the CMSSM to compare this with the results shown in Section 7.1. In this

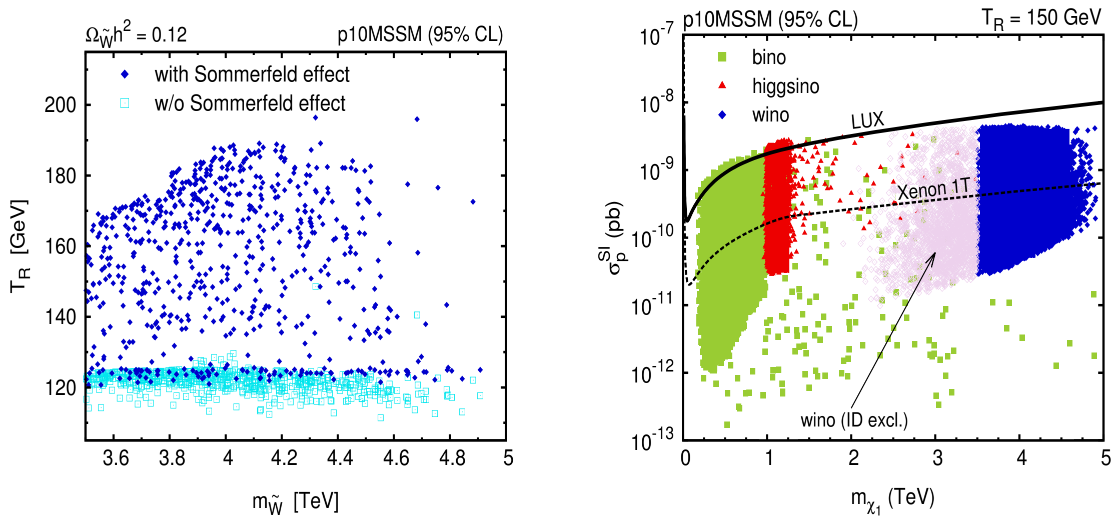

Figure 8.5: *Left panel*: the reheating temperature range in the wino DM scenario that gives the correct relic density for $m_{\widetilde{W}} > 3.5\,\text{TeV}$ where indirect detection limits are not violated. The results with (without) the Sommerfeld effect are shown as dark blue solid diamonds (light blue empty squares). *Right panel*: the 95% CL region of the p10MSSM for $T_R = 150$ GeV in the $(m_\chi, \sigma_p^{\rm SI})$ plane with the Sommerfeld effect included in calculating the relic density. In the case of wino DM, we use pink (blue) color to distinguish points which are excluded (not excluded) by the requirement $m_{\widetilde{W}} > 3.5\,\text{TeV}$ imposed by indirect detection searches. The solid (dashed) black line corresponds to the LUX (a projected Xenon1T) limit on $\sigma_p^{\rm SI}$. Remaining color coding as in Fig. 8.3. Taken from Ref. [293].

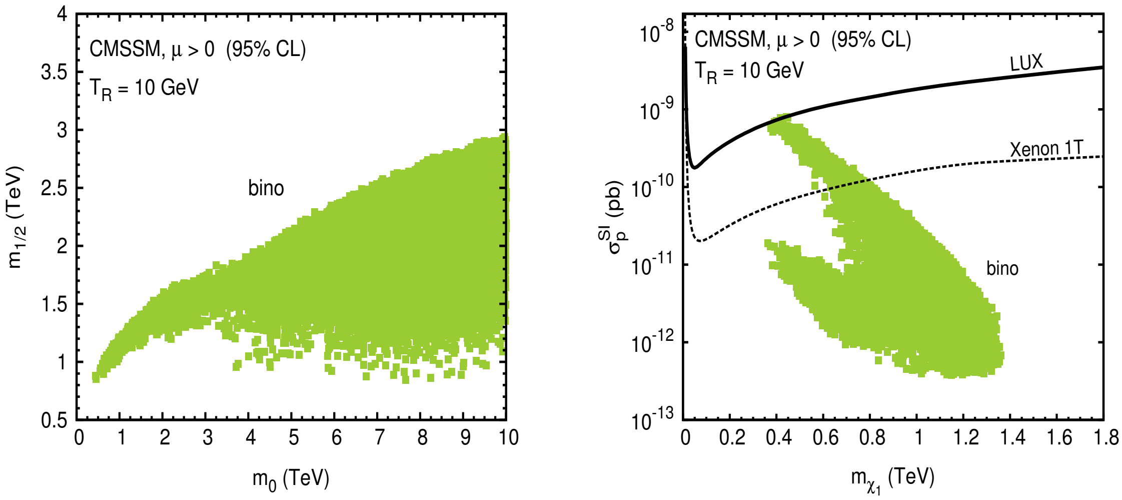

Figure 8.6: *Left panel*: The 95% CL regions in the $(m_0, m_{1/2})$ plane of the CMSSM for $T_R = 10\,\text{GeV}$. *Rigth panel*: The direct detection $\sigma_p^{\rm SI}$ cross section as a function of m_χ for the CMSSM 95% CL for $T_R = 10\,\text{GeV}$. Taken from Ref. [293]

analysis the ranges of parameters follow Table 7.2 (recent study), while experimental constraints are given in Table 6.1.

In particular in Fig. 8.6 (left panel) we present the 95% CL region in the (m_0,$m_{1/2}$) plane obtained for $T_R = 10\,\mathrm{GeV}$. As it is expected from Fig. 8.3 for such low reheating temperature only the bino can be a viable DM candidate. The lower left corner of the preferred region in (m_0,$m_{1/2}$) plane corresponds to stau coannihilation region, analogous to that obtained for high T_R.[5] For slightly higher values of the mass parameters, the suppression of the relic density by stau coannihilations is traded for low-T_R suppression and we find acceptable points there. In that region, the bino relic density for a fixed T_R and a fixed bino mass (or $m_{1/2}$) depends on many factors, in particular, on stau masses (which depend not only on m_0, but also on $\tan\beta$ and A_0), as well as on the small but non-negligible higgsino fraction of the lightest neutralino.

In Fig. 8.6 (right panel) the spin-independent direct detection cross section σ_p^{SI} is shown as a function of the neutralino mass for $T_R = 10\,\mathrm{GeV}$. As expected from results obtained for the p10MSSM, in the CMSSM for $T_R = 10\,\mathrm{GeV}$ prospects for DM discovery are much worse than in the high T_R case. Only a small fraction of the allowed region can be covered by Xenon1T. In this case the higgsino fraction of the bino-dominated DM goes up to even 5%.

8.3 Inflaton field decays to DM at low T_R

We have so far assumed that the direct and cascade decays of the inflaton field to DM species are negligible. In this section we will take into account this additional, *non-thermal* contribution to $\Omega_\chi h^2$. Our analysis follows here the model-independent approach used in [322, 323].

Direct and cascade decays of the inflaton field to superpartners of SM particles correspond to an additional term in the Boltzmann equation (8.1) for n, which is now given by,[6]

$$\frac{dn}{dt} = -3Hn - \langle\sigma v\rangle\big[n^2 - (n^{eq})^2\big] + \frac{b}{m_\phi}\Gamma_\phi\rho_\phi\,, \tag{8.3}$$

where b describes the average number of DM particles produced per one inflaton decay and m_ϕ is the inflaton mass.

We present our results in Fig. 8.7 in the (m_χ, T_R) plane in terms of the dimensionless quantity $\eta = b\cdot(100\,\mathrm{TeV}/m_\phi)$ for higgsino (left panel) and wino (right panel) DM where along the lines we fix a value of the total relic density, $\Omega_\chi h^2 \simeq 0.12$.[7] As

[5]For such low WIMP mass values the suppression due to low T_R is inefficient.

[6]The most important contribution from direct and cascade decays is associated with the period between the freeze-out of DM particles and the end of the reheating period when n becomes essentially equal to n_χ.

[7]The total DM relic density contains both thermal and non-thermal contributions. The thermal component corresponds to a production in thermal equilibrium (that lasts up to a time of freeze-out). The non-thermal production, instead, corresponds mainly to a production after the DM freeze-out, but before the inflaton field disappears completely. Decays of the inflaton field

can be seen, the non-thermal contribution to the DM relic abundance in the low T_R regime can help to increase otherwise too low $\Omega_\chi h^2$. Examples of such cases include the higgsino with mass below 1 TeV or wino with mass below 2 TeV.

The relic density of DM in this case is a sum of the thermal and the non-thermal components. The thermal component increases with the reheating temperature (up to a moment when the high T_R regime begins). On the other hand, the magnitude of the non-thermal component may depend, for fixed η and m_χ, on the reheating temperature in a non-monotonic way, as discussed in detail in [323]. When T_R is sufficiently low, non-thermal production leads to $\Omega_\chi \sim T_R$, while for larger reheating temperature DM relic density goes down with increasing T_R.

The latter behavior corresponds to a shortening (with increasing T_R) of a period between the DM freeze-out and the end of the reheating period. The DM particles produced from the inflaton decay before freeze-out can effectively thermalize. Hence their number density will be adjusted to the thermal one and one will not observe increase of the DM abundance from the inflaton decays. The situation changes after the DM freeze-out, but before the inflaton field disappears completely, since in this period newly produced DM particles will not thermalize and therefore indeed contribute additionally to $\Omega_\chi h^2$. The shorter this period is, the less amount of the additional DM produced. In other words the smaller fraction of the inflaton field number density, $F\, n_\phi = F\,(\rho_\phi/m_\phi)$, with $F < 1$, would decay effectively producing additional (non-thermalized) DM particles.[8] Hence $\Omega_\chi h^2$ increases with decreasing T_R for intermediate (but generally low) T_R.

However, for very low T_R the situation changes. In this regime one can safely assume that non-thermal production of DM dominates (thermal one is highly suppressed) and that a significant fraction of n_ϕ could decay producing the DM particles (as well as radiation in cascade decays), *i.e.*, F is more close to unity. Therefore by decreasing T_R one cannot increase F much. In this regime, to some approximation, one can describe the non-thermal DM production using the instantaneous reheating approximation. In particular, one can assume that the whole energy density of the inflaton field was transformed into radiation[9] $\rho_\phi = \rho_R \sim T_R^4$ in the (cascade) processes that also produced the DM particles, *i.e.*, $\rho_\chi \simeq m_\chi n_\chi \simeq b n_\phi \sim \eta\, \rho_\phi$. As a result, one obtains [323]

$$Y_0 = Y_\chi^{\rm RH} = \frac{\rho^{\rm RH}}{s^{\rm RH}} \sim \eta\, T_R, \qquad \text{for sufficiently low } T_R, \tag{8.4}$$

to DM particles being still in thermal equilibrium are also taken into account when numerically solving the Boltzmann equations. Their impact on the total relic density is limited, since produced DM particles quickly thermalize, but in principle these decays can slightly change the moment of freeze-out.

[8] In this regime F increases as T_R decreases.

[9] For the purpose of a qualitative discussion in this section we neglect the difference between T_R and $T_{\rm RD}$ mentioned in Section 2.2.

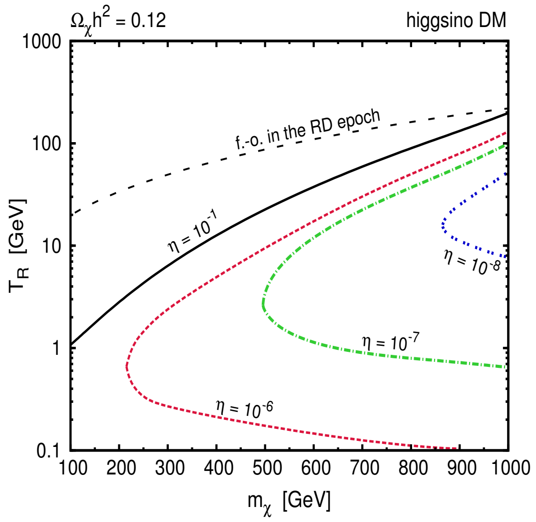

Figure 8.7: Contours of constant $\Omega_\chi h^2 = 0.12$ in the (m_χ, T_R) plane for different values of the dimensionless quantity $\eta = b\Big(100\,\text{TeV}/m_\phi\Big)$ for higgsino (left panel) and wino (right panel) DM. Solid black (dashed red, dot-dashed green, dotted blue) lines correspond respectively to $\eta = 10^{-1}$ (10^{-6}, 10^{-7}, 10^{-8}). In the wino DM case we take indirect detection limits following [318]. For the reheating temperatures above thin dashed black lines the freeze-out of the DM particles occurs after the reheating period (*i.e.*, in the RD epoch). The limit at $\sim$ 800 GeV comes from antiprotons and the one around 1.8 TeV from the absence of a γ-ray line feature towards the Galactic Center. taken from Ref. [293]

where we used $s^{\text{RH}} \sim T_R^3$ (index RH denotes the value at the end of the reheating period). Thus $\Omega_\chi h^2$ starts to decrease with decreasing T_R for sufficiently low reheating temperature.

This is summarized in Fig. 8.8 where we show $\Omega_\chi h^2$ (both from thermal and non-thermal production) as a function of T_R for several values of η and two masses of higgsino-like neutralino. Consequently, each curve corresponding to a fixed value of the relic density $\Omega_\chi h^2 = 0.12$ and fixed η in Fig. 8.7 is C-shaped. As m_χ increases required values of the T_R become larger (for the upper branches of C-shaped curves). Finally they reach the level at which freeze-out occurs after the reheating period, *i.e.*, in the RD epoch, and therefore direct and cascade decays of the inflaton field play no role in determining $\Omega_\chi h^2$.

For sufficiently large values of η, one can even generate too much DM from inflaton decays. The corresponding upper bound on $\eta \propto 1/m_\phi$ can be translated into a lower bound on the inflaton mass above which the direct production is negligible even for a branching ratio $\text{BR}(\phi \to \text{superpartners}) \sim \mathcal{O}(1)$. In particular, for $\eta < 10^{-9}$ we obtain no significant non-thermal production of DM particles. This value corresponds to the inflaton mass $m_\phi > b \cdot 10^{13}\,\text{GeV}$, as it is illustrated in Fig. 8.9.

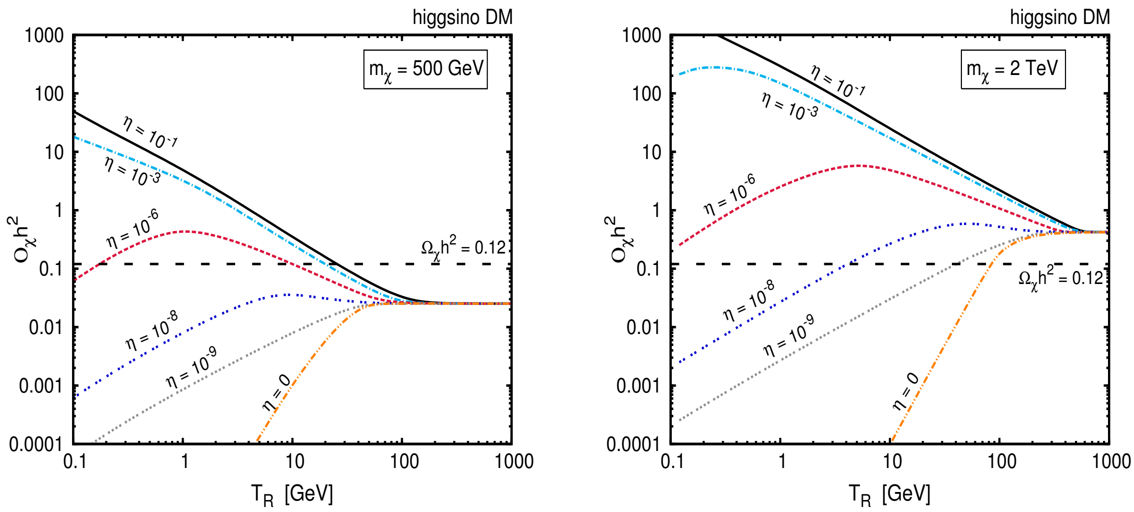

Figure 8.8: The DM relic density as a function of T_R for higgsino-like χ with $m_\chi = 500\,\text{GeV}$ (left panel) and $m_\chi = 2\,\text{TeV}$ (right panel) and various values of the η parameter.

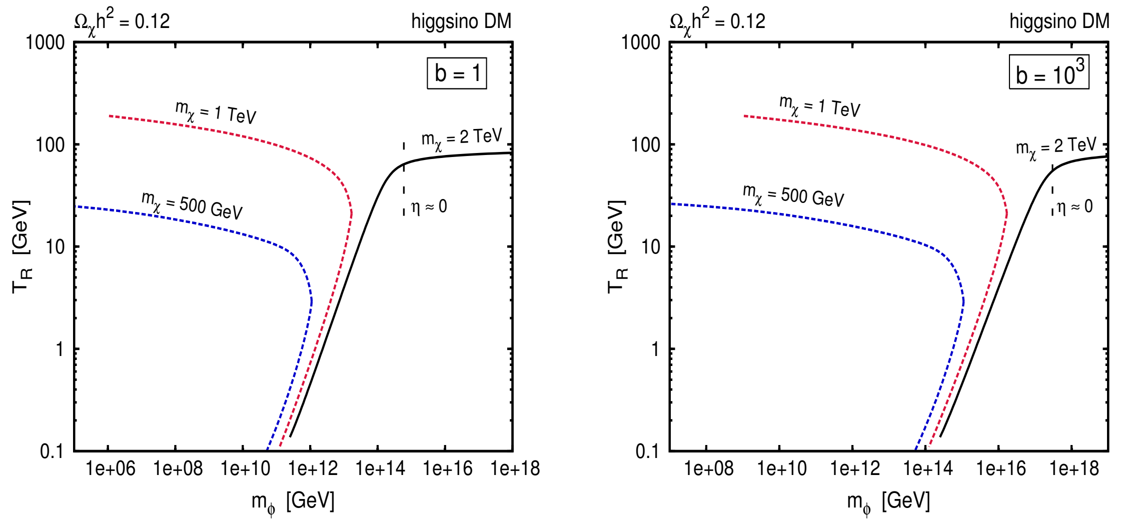

Figure 8.9: The reheating temperature required to obtain $\Omega_\chi h^2 = 0.12$ as a function of the inflaton mass for three fixed higgsino masses and two values of the b parameter (an average number of the DM particles produced per one inflaton decay). The vertical dashed black line corresponds to the minimum m_ϕ above which one obtains effectively the $\eta \approx 0$ regime (only thermal production).

Chapter 9

Gravitino and axino dark matter

In this chapter we will discuss in more details some specific scenarios with SUSY EWIMP DM that were so far rarely studied in the literature. We begin with a discussion of the case with gravitino DM and sneutrino being lightest ordinary supersymmetric particle[1] (LOSP) in the framework of constrained SUSY models (at the GUT or other high energy scale). We then study the impact of low reheating temperature on gravitino and axino DM scenarios within the p10MSSM. The results presented in this chapter are partly based on [287, 293] and partly on currently ongoing project.

9.1 Gravitino dark matter from sneutrino decays in supersymmetric models constrained at high energy scale

The results presented in this section are based on [287].

Gravitinos as the DM particles can be produced either thermally or non-thermally as discussed in Sections 3.2.3 and 5.2.2. In particular, if the reheating temperature of the Universe after a period of cosmological inflation T_R is large, the TP mechanism dominates and can easily lead to DM overabundance. This can be translated into an upper limit on T_R that depends mainly on the gravitino mass $m_{\tilde{G}}$ and the gluino mass $m_{\tilde{g}}$ as shown in Eq. 5.13. In this section we will examine this limit in a scenario with the sneutrino LOSP taking into account the BBN and the LSS constraints, as well as the recently measured value of the Higgs boson mass m_h for two selected, though as we will see in some sense representative, constrained SUSY models.

[1]It is the lightest of all supersymmetric particles beside possibly lighter SUSY EWIMPs. In the scenarios that we consider in this chapter, in which either the gravitino or the axino (but not both at the same time) are lighter than all the other SUSY particles, the LOSP is the NLSP.

Sneutrino LOSP in constrained SUSY To begin with we need to discuss the conditions imposed on soft SUSY breaking parameters that lead to the sneutrino LOSP scenario. From Eqs (4.39) and (4.40) one can easily derive a necessary condition for the sneutrino to be lighter than stau $\tilde{\tau}_1$ written in terms of the parameters evaluated at the SUSY scale

$$\begin{aligned} m^2_{\tilde{t}_L}(\mathrm{SUSY}) - m^2_{\tilde{t}_R}(\mathrm{SUSY}) &> \frac{m_\tau^2(\mu\tan\beta - A_\tau)^2}{m_\tau^2 - M_W^2\cos 2\beta} + \frac{3}{2}M_Z^2\cos 2\beta - M_W^2\cos 2\beta - m_\tau^2 \\ &\gtrsim \frac{m_\tau^2(\mu\tan\beta - A_\tau)^2}{M_W^2} + M_W^2 - \frac{3}{2}M_Z^2, \end{aligned} \tag{9.1}$$

where in the second line we assumed that $\tan\beta$ is noticeably larger than one. However, typically $\tan\beta$ cannot be too large, since then the term proportional to $\mu^2\tan^2\beta$ on the RHS could grow too much and it would be particularly difficult to satisfy Eq. (9.1).

One can rephrase Eq. (9.1) in terms of the parameters defined at high energy scale by solving the corresponding RGEs. Approximate, though accurate enough for our discussion, solutions that one can obtain (for more details see Appendices A and B) read[2]

$$m^2_{\tilde{\tau}_R} = m^2_{\tilde{\tau}_R,0} + c_{R1}M_1^2 + \tilde{c}_{RU}m^2_{U,0} - \frac{1}{11}D^2\left(1 - \frac{g_1^2}{g_{1,0}^2}\right) + \delta^2_{R,y_\tau} \tag{9.2}$$

$$m^2_{\tilde{\tau}_L} = m^2_{\tilde{\tau}_L,0} + c_{L1}M_1^2 + c_{L2}M_2^2 + \tilde{c}_{LQ}m^2_{Q,0} + \frac{1}{22}D^2\left(1 - \frac{g_1^2}{g_{1,0}^2}\right) + \delta^2_{L,y_\tau} \tag{9.3}$$

where by $m^2_{S,0}$ (with an additional index 0) for $S = Q, U, D$ we denote third generation soft squark masses at the high scale, while $M_{1,2}$ are low-scale $U(1)$ and $SU(2)$ gaugino soft mass parameters. The coefficients c_{R1} and c_{Li} can be found by solving the one-loop RGEs, whereas $\tilde{c}_{RU}$, $\tilde{c}_{LQ}$ by solving the two-loop RGEs and identifying the leading effects. They are given in Table 9.1 for some representative choices for the high scale Q and the SUSY scale.[3] D^2 (denoted in literature also as $\mathcal{S}_0$) is defined as

$$D^2 = \mathcal{S}_0 = \mathrm{tr}\left[Y\mathbf{M}^2_{\mathrm{scalars},0}\right] = m^2_{H_u} - m^2_{H_d} + \mathrm{tr}\left[\mathbf{m}^2_{Q,0} - 2\mathbf{m}^2_{U,0} + \mathbf{m}^2_{D,0} - \mathbf{m}^2_{\tilde{\tau}_L,0} + \mathbf{m}^2_{\tilde{\tau}_R,0}\right], \tag{9.4}$$

[2]The approximate method of solving one-loop RGEs follows [100] and is valid for not too large $\tan\beta$. This is however consistent with the requirement of having the sneutrino LOSP, as mentioned above.

[3]We assume that at the high scales the soft supersymmetry breaking parameters are the same for all three generations. Beyond that framework, *e.g.*, in models with inverted hierarchy of soft supersymmetry breaking masses, two-loop contributions proportional to squark masses can drive $m^2_{\tilde{\tau}_L}$ to values smaller than $m^2_{\tilde{\tau}_R}$, opening up a possibility for yet another example of sneutrino LOSP [324] which we do not treat here.

$M_{\rm SUSY}$	c_{R1}	c_{L1}	c_{L2}	$\tilde{c}_{RU}$	$\tilde{c}_{LQ}$
			$Q = 10^{14}$ GeV		
500 GeV	0.47	0.12	0.52	−0.0027	−0.0049
1000 GeV	0.45	0.11	0.51	−0.0026	−0.0048
$M_{\rm SUSY}$	c_{R1}	c_{L1}	c_{L2}	$\tilde{c}_{RU}$	$\tilde{c}_{LQ}$
			$Q = 10^{16}$ GeV		
500 GeV	0.62	0.15	0.64	−0.0038	−0.0060
1000 GeV	0.59	0.15	0.62	−0.0037	−0.0059

Table 9.1: Numerical values of the coefficients c_{R1}, c_{L1}, c_{L2}, $\tilde{c}_{RU}$, $\tilde{c}_{LQ}$ in Eq. (9.2) for two representative choices of the high scale Q and of the EWSB mass scale $M_{\rm SUSY} = \sqrt{m_{\tilde{t}_1} m_{\tilde{t}_2}}$.

where $\mathbf{m}_{i,0}^2$ are the 3×3 sfermion mass matrices at the high scale, $m_{H_u}^2$ and $m_{H_u}^2$ are the soft supersymmetry breaking masses of the Higgs doublets at the high scale, and g_1 ($g_{1,0}$) is the $U(1)_Y$ gauge coupling at the low (high) scale. Leading corrections arising due to the τ Yukawa couplings are denoted by δ^2_{E,y_τ} and δ^2_{L,y_τ}. For small and moderate values of $\tan\beta$ they are small and their only role is to make the third generation of sleptons slightly lighter than the first two, but they can become important, *e.g.*, if the mass parameter $\sqrt{m_{H_d}^2}$ at the high scale is much larger than $\sqrt{m_L^2}$ and $\sqrt{m_E^2}$. Adding the leading two-loop contributions to the RGEs allows to obtain $\mathcal{O}(10\,\text{GeV})$ accuracy in a mass determination.

Substituting (9.2) and (9.3) into (9.1), we see that the sneutrino can be the LOSP in two (mutually not exclusive) cases.[4] One possibility is to assume $D^2 < 0$, which drives left slepton mass to $m^2_{\tilde{\tau}_L} < M_1^2$. Moreover, in this case the sign difference in the coefficients multiplying D^2 in (9.2) and (9.3) can lead to $m^2_{\tilde{\tau}_L} < m^2_{\tilde{\tau}_R}$. We will discuss this scenario for the non-universal Higgs mass (NUHM) model, in which $m_{H_u} \neq m_{H_d}$ and both of them are not unified to m_0, while the remaining parameters follow the CMSSM. The second option is to relax the gaugino mass universality. This possibility is naturally realized in, *e.g.*, generalized gauge mediation (GGM) models.[5]

Allowed parameter space of the models We performed a grid scan over the parameter spaces of the NUHM and the GGM (see Appendix C) models. The values of the fixed parameters in each case were chosen so as to maximize the allowed region with the sneutrino LOSP and simultaneously make it possible to

[4]Note that in models with $D^2 = 0$ and universal gaugino masses, such as the CMSSM for which $M_2 \approx 2M_1$, and a high scale is greater than 10^{14} GeV, the sneutrino cannot be the LOSP, since it is always heavier than the bino. The stau LOSP case in the CMSSM corresponds to the "right" stau $\tilde{\tau}_R$.

[5]Another way would be to assume large $m_{Q,0}$, since it would give a negative contribution to $m^2_{\tilde{\tau}_L}$. However, this would lead to large μ, hence would increase the left-right mixing in the stau sector and would thus make the lighter stau lighter than the sneutrino.

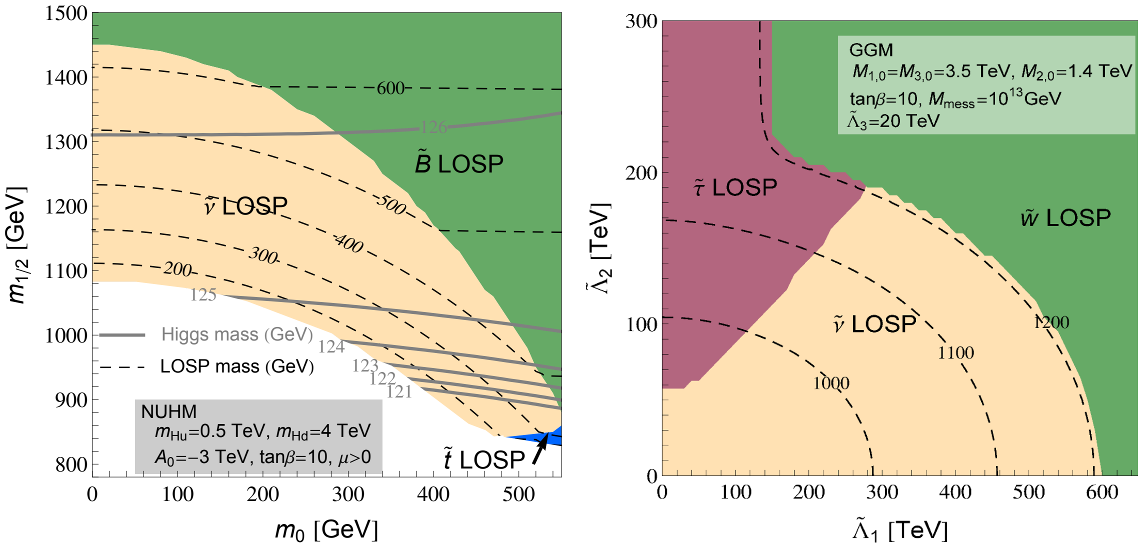

Figure 9.1: *Left panel*: Slice of the NUHM model parameter space in the $(m_0, m_{1/2})$ plane with the values of $m_{H_u} = 500\,\text{GeV}$, $m_{H_d} = 4000\,\text{GeV}$, $A_0 = -3\,\text{TeV}$ fixed at the unification scale and $\tan\beta = 10$, $\mu > 0$. Contours of constant LOSP (Higgs boson) masses are shown as dashed (solid) lines. Unphysical regions are marked in white. *Right panel*: Sections of the GGM model parameter space in the $(\tilde{\Lambda}_1, \tilde{\Lambda}_2)$ plane and with fixed ratio $M_{1,0} : M_{2,0} : M_{3,0} = 5 : 2 : 5$ and fixed values of $\tan\beta = 10$, the messenger scale $M_{\text{mess}} = 10^{13}\,\text{GeV}$ and $\tilde{\Lambda}_3 = 20\,\text{TeV}$ with $\mu > 0$. Taken from Ref. [287].

obtain $m_{h_1} \simeq 126\,\text{GeV}$. In particular for the NUHM model we keep $m_{H_u} < m_{H_d}$ and therefore $D^2 < 0$, while for the GGM model it follows from (9.2) that sneutrino LOSP is viable for $M_2/M_1 \lesssim 2$ at the electroweak scale.

Slice of the allowed parameter space in the $(m_0, m_{1/2})$ plane for the NUHM model is shown in Fig. 9.1 (left panel). We present the LOSP identity and its mass, as well as the mass of the Higgs boson. In the left panel the sneutrino LOSP region is bounded from above at large values of $m_{1/2}$. This can be easily understood since, according to Eq. (9.3) and assuming gaugino mass unification at the GUT scale, $m^2_{\tilde{\tau}_L}$ grows faster with $m_{1/2}$ than the bino mass squared M_1^2. As a result, for sufficiently large $m_{1/2}$, the bino becomes lighter than the sneutrino.[6] On the other hand, for too low $m_{1/2}$ and m_0 one obtains $m_{\tilde{\tau}_L} < 0$ (unphysical region) because large negative contribution from $D^2 < 0$ is not compensated by other terms in Eq. (9.3). Beside the large negative contribution to $m^2_{\tilde{U}}$ (proportional to D^2) can drive, for sufficiently small values of $m_{1/2}$, the lighter stop mass below the sneutrino mass. Thus we observe a lower bound on $m_{1/2} \gtrsim 800\,\text{GeV}$. This also limits from below acceptable gluino masses which has an important impact on the maximum T_R as discussed above. The lower limit on $m_{\tilde{g}}$ even increases when one takes into account the condition for the Higgs boson mass $m_{h_1} \simeq 126\,\text{GeV}$. It is because M_3 has a large

[6] The sneutrino mass also grows with m_0. That is the reason why the bino LOSP region (green area in the plot) increases for larger m_0.

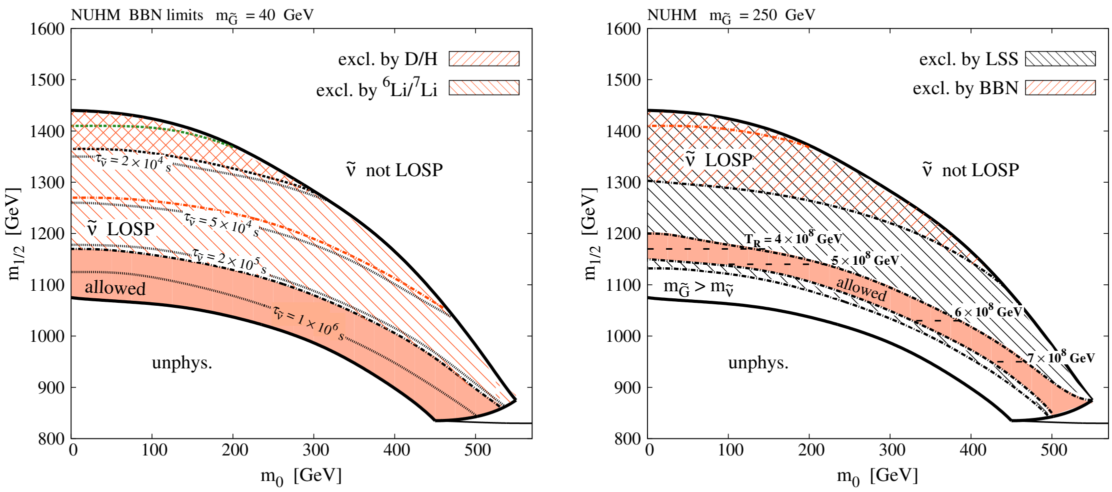

Figure 9.2: BBN and LSS bounds for the sneutrino LOSP region in the NUHM shown in the left panel of Fig. 9.1 for the values of gravitino mass of $m_{\tilde{G}}$ = 40 and 250 GeV. For ^{6}Li/^{7}Li the stringent limit was used Eq. (6.56). The conservative limit is denoted by red dash-dotted line.

impact on the RGE evolution of the soft squark masses which, in turn, determines M_{SUSY} and therefore a size of loop corrections to m_{h_1}.

In the case of the GGM model described in terms of the parameters given in Appendix C we can utilize the possibility of non-universal gaugino masses. We adopt $M_{1,0} = M_{3,0}$ (at high energy scale), while $M_{2,0}$ is kept lower. More specifically, we assume $M_{1,0} : M_{2,0} : M_{3,0} = 5 : 2 : 5$, which predicts that the lightest gaugino-like neutralino is a wino. A slice of the allowed parameter space in this case is shown in Fig. 9.1 (right panel).

BBN and LSS constraints For the region with sneutrino LOSP shown in the left panel of Fig. 9.1 for the NUHM model we calculate the abundances of light elements and apply both the BBN and the LSS constraints. In Fig. 9.2 we show a sample of such results for two masses of gravitino $m_{\tilde{G}} = 40, 250$ GeV. We find no constraints for the gravitino masses smaller than 7.5 GeV. At $m_{\tilde{G}} = 40$ GeV a part of the parameter space corresponding to $m_{\tilde{\nu}} \gtrsim 500$ GeV is excluded because of too large D/H abundance, but typically the bounds from ^{6}Li/^{7}Li are more stringent.

For large gravitino masses non-thermal gravitinos produced in sneutrino LOSP decays will have present-day (after redshift) velocities much larger than those characteristic for thermal distribution.Such fast moving dark matter particles tend to erase small scales of Large Scale Structures (LSS), especially when they constitute a sizable fraction of the dark matter density as discussed in Section 6.6.2. The impact of this bound on the parameter space of the NUHM model is shown in Fig. 9.2 (right panel) for $m_{\tilde{G}} = 250$ GeV. At such large $m_{\tilde{G}}$, the LSS bounds become more stringent than the BBN ones. For $m_{\tilde{G}} > 270$ GeV, we find that the LSS bounds exclude

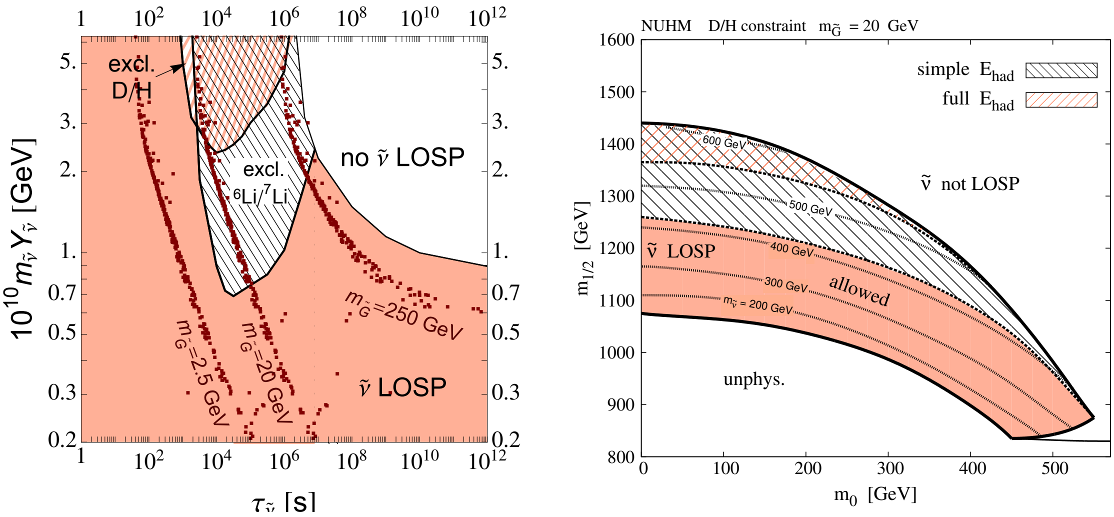

Figure 9.3: *Left panel*: BBN constraints shown in the $\tau_{\tilde{\nu}}$ vs $m_{\tilde{\nu}}Y_{\tilde{\nu}}$ plane for the sneutrino LOSP region shown in the left panel of Fig. 9.1. Dots show the results of our scan with fixed $m_{\tilde{G}} = 2.5$, 20 and 250 GeV. *Right panel*: The impact of different estimates of hadronic energy release on the D/H bounds for $m_{\tilde{G}} = 20\,\mathrm{GeV}$. For the excluded region marked "simple Ehad" an approximation $E_{\mathrm{had}} = (m_{\tilde{\nu}} - m_{\tilde{G}})/3$ was used, while the excluded region marked "full Ehad" corresponds to a computation of E_{had} involving integration over the full 4-body phase space.

the entire section of the parameter space in the NUHM model that we analyze here. This has important consequences for the maximum reheating temperature, since limits on T_R become weaker with increasing gravitino mass according to Eq. (5.13).

In order to understand better the origin of the BBN constraints, we first project all the analyzed points onto the $\tau_{\tilde{\nu}}$ vs $m_{\tilde{\nu}}Y_{\tilde{\nu}}$ plane for several gravitino masses, $m_{\tilde{G}} = 2.5$, 20, 250 GeV. This is shown in the left panel of Fig. 9.3 where we also present the D/H and ^{6}Li/^{7}Li bounds. As can be seen with increasing $m_{\tilde{G}}$, the BBN constraints first appear, next tighten up and then eventually become weaker.[7]

The D/H bound is quite sensitive to the hadronic energy release. In Fig. 9.3 (right panel) we compare the approximate estimate Eq. (6.61) and more exact treatment Eq. (6.62). It turns out that the lower boundary of the respective excluded region could shift downwards by as much as 100 GeV in the approximate treatment. In other words, one would significantly overestimate the sneutrino LOSP region excluded by the constraint.

In Fig. 9.4 we show regions in the $(m_{\tilde{G}}, m_{\tilde{\nu}})$ plane excluded in the case of the NUHM model. Taking into account only the BBN constraints one finds two separate allowed regions in the plot. The first one, for small $m_{\tilde{G}} < 10\,\mathrm{GeV}$, corresponds to relatively low values of the maximum reheating temperature, $T_R^{\mathrm{max}} \sim 10^7\,\mathrm{GeV}$.

[7] This can be understood taking into account that the sneutrino lifetime $\tau_{\tilde{\nu}} \propto m_{\tilde{G}}^2 m_{\tilde{\nu}}^{-5}$ for $m_{\tilde{G}} \ll m_{\tilde{\nu}}$ and $\Omega_{\tilde{\nu}}h^2 \propto m_{\tilde{\nu}}^2$. Interestingly, for $m_{\tilde{\nu}}$ close to the bino mass we obtain an increase of the sneutrino relic density; this is an example of scenario in which the LSP-NLSP mass degeneracy causes an increase of $\Omega_{\mathrm{LSP}}h^2$ that is discussed in Section 5.1.2.

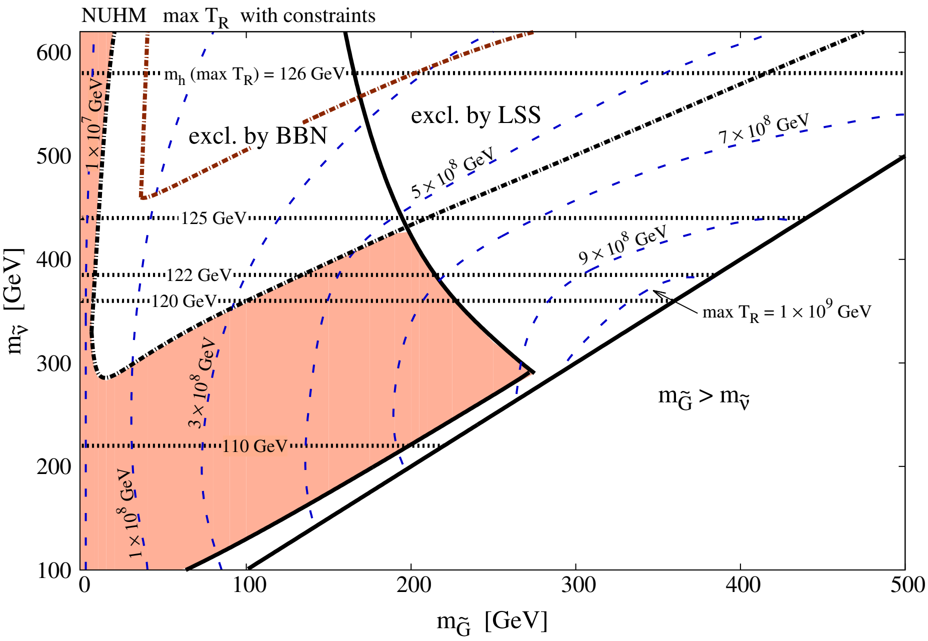

Figure 9.4: A summary of the bounds in the NUHM in the $(m_{\tilde{G}}, m_{\tilde{\nu}})$ plane. The thick dashed line bounds the region excluded by BBN, the solid red line marks the boundary of the region excluded by LSS. Thinner dashed lines show the maximum reheating temperature, $T_R^{\max}$, and thinner dotted lines show the Higgs boson mass corresponding to $T_R^{\max}$. For ^{6}Li/^{7}Li the stringent limit was used; the boundary of the excluded region with the more conservative constraint for ^{6}Li/^{7}Li is represented by a red dash-dotted line.

On the other hand, for larger $m_{\tilde{G}}$, the region allowed by the BBN bounds is characterized by the maximum reheating temperature of the order of 10^9 GeV when $m_{\tilde{\nu}} \sim m_{\tilde{G}}$. However, imposing the LSS bounds closes this second region, thus slightly reducing the maximum reheating temperature. It is further reduced when one add a constraint from the Higgs boson mass. As can be seen, the requirement that the Higgs boson mass is at least 125 GeV, brings $T_R^{\max}$ down to below 10^8 GeV.

These bounds on maximum T_R as a function of $m_{\tilde{G}}$ are shown in the left panel of Fig. 9.5 for the same sets of constraints. We impose there the BBN bounds and we show the results with and without the LSS bounds and with and without the requirement that the Higgs boson mass is at least 122 GeV (at the time of the analysis we took into account theoretical error of m_h in a quite conservative way). We see that in each case the maximum T_R lies close to 10^9 GeV. In the right panel of Fig. 9.5 we show the maximum T_R versus the Higgs boson mass with and without BBN and LSS constraints.

In the GGM model we find a similar value of the maximum reheating temperature when the Higgs boson mass and the BBN constraints are taken into account. The

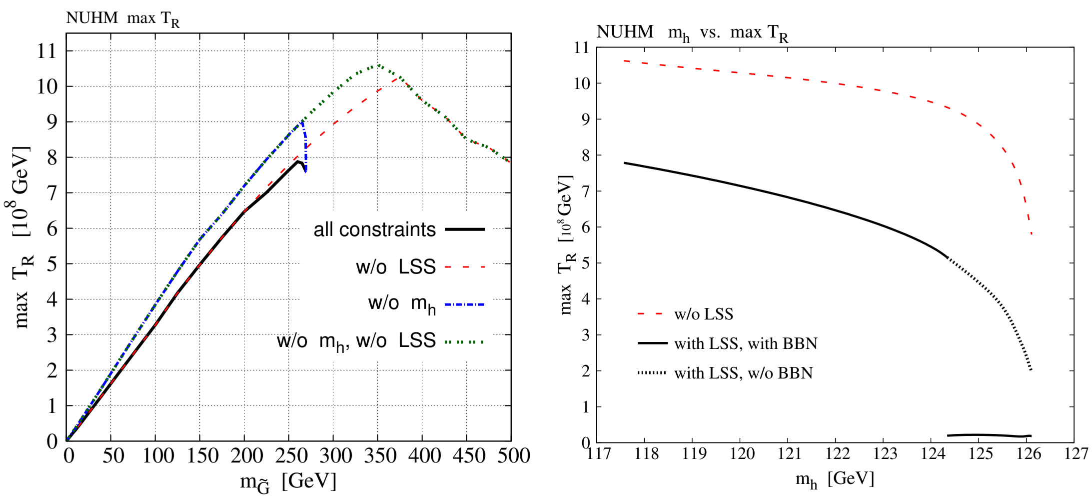

Figure 9.5: *Left panel*: The maximum reheating temperature as a function of $m_{\widetilde{G}}$ with the BBN, the LSS and the Higgs boson mass constraints ($m_h > 122\,\mathrm{GeV}$) applied, as well as without one or both of the LSS and the Higgs boson mass constraints. *Right panel*: The maximum reheating temperature versus the Higgs boson mass without the LSS constraint (upper red dashed line) and with the LSS constraint (lower line). The solid (dotted) segments correspond to the cases where the BBN bound is (is not) applied.

LSS constraints are not important since in these models typically $m_{\widetilde{G}} \ll m_{\tilde{\nu}}$ which is assumed to allow a natural suppression of the FCNC processes.[8]

9.2 Gravitino dark matter with low reheating temperature

The results presented in this section were published in [293].

In this section we will analyze the impact of taking low values of the reheating temperature on the scenario with gravitino DM. As we will show, in this scenario a combination of the relic density and the BBN constraints allows one to derive a lower limit on T_R. This complements the study of the upper limit on T_R discussed above.

As it was shown in Eq. (5.12) gravitino relic density from thermal production is suppressed for low T_R and not too low $m_{\widetilde{G}}$. In particular, for $T_R \ll 10^6\,\mathrm{GeV}$ and $m_{\widetilde{G}} \gtrsim 1\,\mathrm{GeV}$, that we are interested in here, this component is much smaller than the measured value of the DM relic density.[9] In the following, we want to focus

[8]In gauge-mediated models the leading contributions to the soft masses are flavor-diagonal, while the subdominant gravity-mediated contributions, of the order of $m_{\widetilde{G}}$, do not have to exhibit any such structure.

[9]In fact, for such low values of T_R that we employ there may appear additional reduction of $\Omega_{\widetilde{G}}h^2$ going beyond Eq. 5.11. It is due to a Boltzmann suppression of number densities of heavier

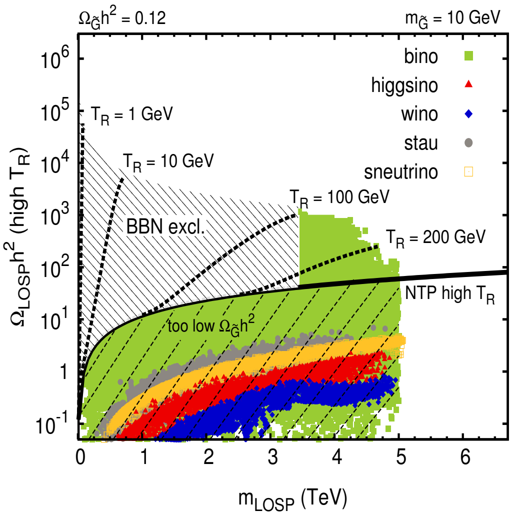

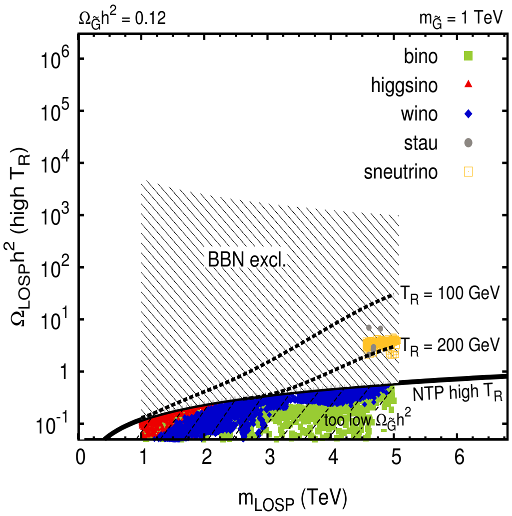

Figure 9.6: Contours of constant $\Omega_{\tilde{G}}h^2 = 0.12$ for different values of the reheating temperature T_R and for $m_{\tilde{G}} = 10$ GeV and 1 TeV in the p10MSSM with BBN constraints imposed. Color coding as in Fig. 8.3.

on scenarios in which the gravitino constitutes the whole DM relic abundance. Its relic density for low T_R has to be then dominated by the non-thermal component. In this case the gravitino abundance is related to the abundance of the LOSP by Eq. (3.13) with $\Omega_{\rm NLSP}h^2$ replaced by $\Omega_{\rm LOSP}h^2$. The LOSP relic abundance has to be calculated taking into account low values of T_R following the methodology described in Sections 8.2 and 8.3.

Long after they have frozen out, during or after BBN, the LOSPs can decay into gravitinos and SM particles. Hadronic and electromagnetic cascades initiated in this processes can change abundances of light elements and therefore possibly ruin an agreement between the BBN predictions and current observational limits. We implement the BBN constraints following the methodology described in Section 6.6.1.

Typical results for $m_{\tilde{G}} = 10\,\text{GeV}$ and $1\,\text{TeV}$ obtained in the p10MSSM are given in Fig. 9.6. In both figures we fix the gravitino abundance $\Omega_{\tilde{G}} \simeq 0.12$. This is achieved by a proper adjustment of the reheating temperature so that $\Omega_{\rm LOSP}(\text{low } T_R) \simeq (m_{\rm LOSP}/m_{\tilde{G}}) \times 0.12$. The corresponding lines of constant reheating temperature for different points in the $(m_\chi, \Omega_{\rm LOSP}h^2)$ plane are shown by dashed black lines. The line corresponding to the correct NTP gravitino abundance in high-T_R case is naturally not horizontal in this plane, since it is described by $\Omega_{\rm LOSP}(\text{high } T_R) \simeq (m_{\rm LOSP}/m_{\tilde{G}}) \times 0.12$.[10] We assume that the LOSP can be either the lightest neutralino or slepton (in particular, the lighter stau or the tau sneutrino).

SUSY particles that produce gravitinos in their scatterings in thermal plasma (similarly to axino DM case discussed in Section 5.3.2).

[10]An addition of TP for high T_R would allow one to obtain the correct value of the gravitino relic density also for points lying in the hatched regions labeled by "too low $\Omega_{\tilde{G}}h^2$". We show only the pure NTP case for a comparison with the low T_R scenario in which TP is negligible.

We note that the sneutrino LOSP is always mass degenerate with the lighter (left) stau. Thus coannihilations do play an important role in determining $\Omega_{\tilde{\nu}}h^2$. This may result in $\Omega_{\rm LOSP}h^2$(high T_R) smaller for the sneutrino LOSP than for the (right) stau LOSP.

As long as $m_{\widetilde{G}} \lesssim 100$ GeV, **the bino LOSP** is the only possibility for gravitino DM with $\Omega_{\widetilde{G}}h^2 \simeq 0.12$ in the low T_R regime. In this case typically hadronic branching ratio $B_{\rm h} \sim 1$. Additionally, $\Omega_{\rm LOSP}h^2$(low T_R) has to exceed 0.12 in order to keep the correct value of the relic density for gravitino. Thus the BBN constraints are quite severe. In order not to violate them one then simply requires that the LOSP lifetime is less than about 0.1 s. According to Eq. (6.57) this leads to

$$m_{\rm LOSP} \gtrsim 1400 \left(\frac{m_{\widetilde{G}}}{\rm GeV}\right)^{2/5} \rm GeV\,, \tag{9.5}$$

which is consistent with the results shown in the left panel of Fig. 9.6.[11]

On the other hand, it follows from Fig. 9.6 that a lower bound on $m_{\rm LOSP}$ can be translated into a lower bound on T_R. We show such bounds for the bino LOSP in Fig. 9.7 (left panel) as a function of the gravitino mass assuming that the inflaton field is heavy enough so that its direct and cascade decays to DM are negligible (see a discussion in Section 8.3). As we argued in Section 8.2, the upper boundary of the points in Fig. 9.6 corresponds to the maximum value of the stau mass. Therefore the lower limits on T_R with the bino LOSP are presented for three maximum values of the stau mass: 5, 10 and 15 TeV.

On the other hand, when $m_{\widetilde{G}} \gtrsim 100$ GeV, the LOSP lifetime is typically so large that the BBN bounds can only be evaded when $B_{\rm h}$ is small. Moreover, in the low T_R regime where the LOSP yield at freeze-out is suppressed one requires $m_{\rm LOSP} \gtrsim 1$ TeV to satisfy the relic density constraint for NTP gravitino. This naturally points towards a scenario with **the slepton LOSP** which can be either the sneutrino or, very rarely, for the lighter stau [276, 277]. We present typical result for $m_{\widetilde{G}} = 1$ TeV in the right panel of Fig. 9.6.[12] Similarly to the bino LOSP case, for $m_{\widetilde{G}} \gtrsim 100$ GeV we also find a lower bound $T_R \gtrsim 150$ GeV, as can be seen in Fig. 9.7 (right panel).

The lower limits on the reheating temperature that we derive for gravitino DM and both the bino or slepton LSP lie typically around $T_R \sim 100$ GeV if the gravitino is not too light. Remarkably, it is much larger value than $T \sim 1$ MeV characteristic for the beginning of the BBN, which is often mentioned in the literature as the theoretical lower bound on T_R.

[11] One needs to notice that, for fixed $m_{\widetilde{G}}$, $\Omega_{\rm LOSP}h^2$(low T_R) is constant along the vertical lines in Fig. 9.6 that correspond to $m_\chi = const$. Along these lines we also obtain fixed values of the LOSP lifetime and to a good approximation hadronic branching ratios B_h (for each of the possible LOSPs separately). Thus the BBN bounds appear in Fig. 9.6 as sharp vertical exclusion lines.

[12] In our case the stau LOSP scenario is only slightly constrained by the possibility of forming bound states with nuclei discussed in Section 6.6.1 due to a relatively low stau lifetime. For the same reason the CMB constraint plays no role here.

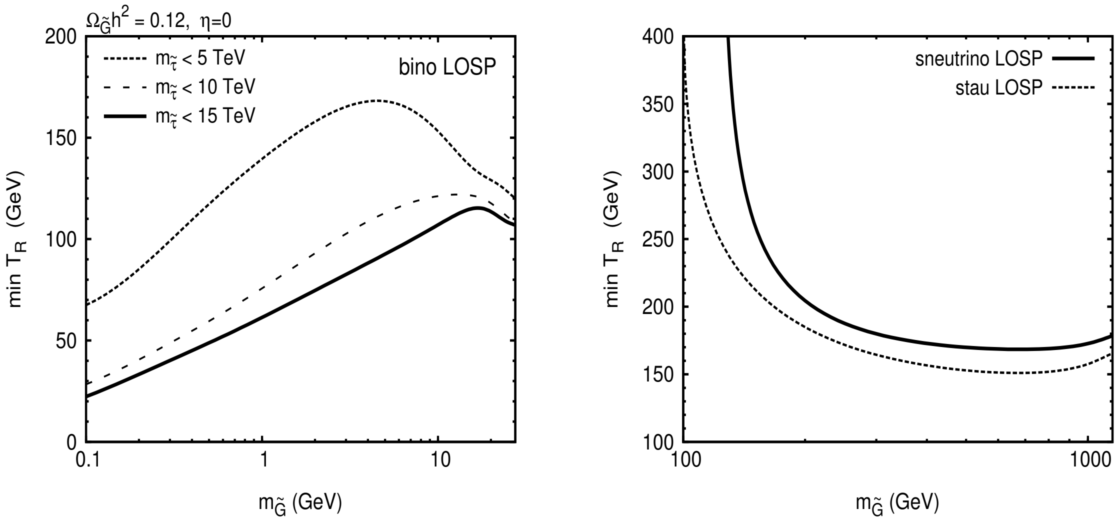

Figure 9.7: Lower bounds on T_R as a function of $m_{\tilde{G}}$ for gravitino DM with a bino LOSP (left panel) and a slepton LOSP (right panel). Direct and cascade decays of the inflaton field to the LOSP are neglected. For the bino LOSP three choices of the maximal stau mass $m_{\tilde{\tau}} = 5$, 10 and 15 TeV are shown. Taken from Ref. [293].

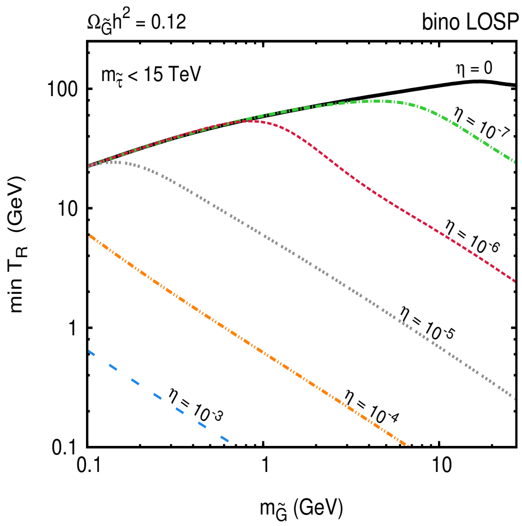

Figure 9.8: Lower bounds on T_R as a function of $m_{\tilde{G}}$ for gravitino DM with a bino LOSP. The effects of the inclusion of the direct and cascade decays of the inflaton is shown for different values of η and fixed $m_{\tilde{\tau}} = 15$ TeV. Taken from Ref. [293].

The aforementioned lower limits on T_R become weaker if direct and cascade decays of the inflaton field to the LOSP cannot be neglected, as can be seen in Fig. 9.8 for the bino LOSP. It is because thermal production of LOSPs (later decaying to gravitinos) can be suppressed more by allowing low T_R, while the condition $\Omega_{\rm LOSP}h^2 = (m_{\rm LOSP}/m_{\tilde{G}}) \times 0.12$ will be maintained thanks to additional non-thermal production of LOSPs. However, the weakened lower limits on T_R typically remain significantly larger than 1 MeV.

9.3 Axino dark matter with low reheating temperature

According to our discussion in Section 5.3.2 (see the right panel of Fig. 5.2) in the axino DM scenario with $m_{\tilde{a}} \gtrsim 0.01\,\text{GeV}$ we are naturally confined to assuming low values of the reheating temperature $T_R \lesssim 10^3\,\text{GeV}$. However, this regime was so far treated in the literature (see [26] and references therein) without taking into account the details of the expansion of the Universe in the reheating period. The non-thermal production of axinos can be described similarly to the gravitino DM case discussed in the previous Section. In addition, axino interaction rates are much less suppressed than the ones for the gravitino, since typically $f_a \ll M_P$. As a result, in contrast to the gravitino DM scenario, axino thermal production can play a non-negligible (though still often subdominant) role in determining $\Omega_{\tilde{a}}h^2$ even for low values of the reheating temperature.

In this section we will study the impact of taking low T_R on the allowed values of the axino mass. We will assume that the axino can be produced both thermally and non-thermally from late-time LOSP decays.[13] Both TP and NTP in general depend on the SUSY spectrum. In order to take this into account we perform our analysis within the framework of the p10MSSM (see Section 8.1).

Axino TP with non-instantaneous reheating Before we present the results of our study we first briefly describe the impact of the reheating period on the axino TP (for a more detailed discussion about a methodology see Appendix E). We will focus on the KSVZ axino, but will give some remarks about the DFSZ one, too.

Although the impact of the non-instantaneous reheating on $\Omega_{\tilde{a}}h^2$ is generally larger for low values of the reheating temperature, it is also non-negligible in the **high-$\boldsymbol{T_R}$ regime** (see [196]). In this limit scatterings associated with the $SU(3)$ group dominate $Y_{\tilde{a}}^{\text{TP}}$. In the standard cosmological scenario with an instantaneous reheating the axino relic yield from TP is given by Eq. (5.17) with $T_R = T_{\text{RD}}$ (the temperature at which the RD epoch begins). This contribution to $Y_{\tilde{a}}^{\text{TP}}$ remains intact when the non-instantaneous reheating is taken into account. However, in this scenario there appears an additional contribution associated with scatterings taking place during the reheating period, when the temperature of the Universe is higher than T_{RD}

$$Y_{\tilde{a}}^{\text{TP,non-inst. reh.}}(T_R) = Y_{\tilde{a}}^{\text{TP,stand.}}(T_{\text{RD}}) + Y_{\tilde{a}}^{\text{TP,reh.}}(T_R). \tag{9.6}$$

In the limit of high T_R, to a good approximation the TP axino yield does not depend on the SUSY spectrum, as discussed in Section 5.3.2. As a result, when one estimates the excess of $Y_{\tilde{a}}^{\text{TP, non-inst. reh.}}$ over the standard result, it depends only on

[13] We neglect possible other sources of relic axinos that can be associated, *e.g.*, with saxion decays [325].

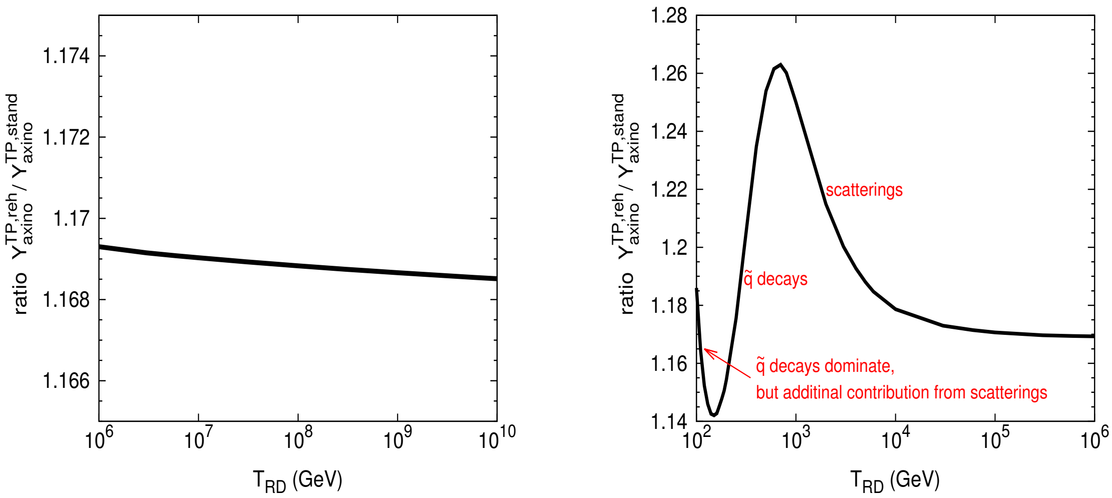

Figure 9.9: The ratio between $Y_{\tilde{a}}^{\mathrm{TP}}$ for the KSVZ axino obtained assuming instantaneous and non-instantaneous reheating in high-T_R (left panel) and intermediate-T_R (right panel) regimes. For the intermediate values of T_R we assume the gluino mass and squark masses to be equal 1 TeV.

details of the evolution of the Universe. The excess turns out to be always about 1/6 of the standard result as can be seen in Fig. 9.9 (left panel) (see a discussion in Appendix E). In other words, in the high T_R limit axinos are produced with a "constant rate" and therefore to a good approximation the longer the production lasts, the larger is the final abundance. The presence of non-instantaneous reheating before the RD epoch effectively extends the period of production and therefore increases the axino yield.[14]

For **intermediate values of the reheating temperature** $\mathbf{10^2\,GeV \lesssim \boldsymbol{T_R} \lesssim 10^4\,GeV}$ a phase space suppression of the scattering terms associated with the heavy superparticles starts to play a non-negligible role. For a given T_{RD} such suppression is smaller for $Y_{\tilde{a}}^{\mathrm{TP,non\text{-}inst.\ reh.}}$ than for $Y_{\tilde{a}}^{\mathrm{TP,stand.}}$ because of the additional contribution to the axino yield, *i.e.*, $Y_{\tilde{a}}^{\mathrm{TP,reh.}}$, which is associated with the production at larger temperatures. As a result, the ratio between yields calculated for both non-instantaneous and instantaneous reheating becomes larger than $1 + 1/6$ obtained in the high-T_R regime. This can be seen in Fig. 9.9 (right panel).

[14]In [196] a constant reduction (instead of the increase) of $Y_{\tilde{a}}^{\mathrm{TP}}$ of the level of about 0.75 was obtained. However, this is not in contradiction with our result. In [196] results obtained for instantaneous and non-instantaneous reheating are compared for the same value of T_R which is a conventional parameter used in this kind of studies. However, we believe that it is more proper to compare both yields assuming the same value of T_{RD} which has an exact physical meaning for non-instantaneous reheating in contrast to T_R (see a discussion in Section 2.2). If we, instead, used the same methodology as the one used in [196] we would obtain a similar level of reduction in the yield.

If the reheating temperature is smaller than about 1 TeV (for a reference point with the gluino and squark masses $m_{\tilde{g}} = m_{\tilde{q}} = 1\,\mathrm{TeV}$), the contribution to the TP axino yield from squark decays also becomes important. However, in the case of decays the impact of the reheating period is generally smaller than for scatterings. In principle, larger temperature during the reheating period leads to a larger equilibrium number density of decaying squarks or gluinos and therefore an increase of Y^{TP} but this effect appears to be much less important than the one associated with the phase space suppression for scatterings. Hence, as long as the role of decays in determining $Y_{\tilde{a}}^{\mathrm{TP}}$ increases, the ratio in Fig. 9.9 (right panel) drops down even below $1 + 1/6$.

The difference between the instantaneous and non-instantaneous reheating scenarios can become significantly larger for the **low-T_R regime** with $T_R \lesssim 100\,\mathrm{GeV}$. This is in particular true if $C_{aYY} = 0$ or if C_{aYY} is non-zero, but the lightest neutralino is heavy enough (see the left panel of Fig. 9.10).[15] The phase space suppression of the SU(3) scatterings, which is responsible for a reduction of the standard result $Y_{\tilde{a}}^{\mathrm{TP,stand.}}$ in the low T_R regime, can then be partially avoided for higher temperatures in the reheating period. On the other hand, if C_{aYY} is non-zero and the lightest neutralino is relatively light, $Y_{\tilde{a}}^{\mathrm{TP}}$ is dominated by the U(1) contributions (mainly decays,[16] and only partially by scatterings) and the impact of non-instantaneous reheating is much smaller (see the right panel of Fig. 9.10). In practice, we observe in our p10MSSM analysis that the TP yield, if non-negligible, is increased by of most about 50% in comparison with the standard cosmological scenario.

Last, but not least, as it was mentioned above, the non-instantaneous reheating modifies the scattering contribution to $Y_{\tilde{a}}^{\mathrm{TP}}$ rather than the decay one. Thus it plays less important role in the framework of the DFSZ models, where TP is for wide range of T_R dominated by the higgsino decays (see a discussion in Section 5.3.2).

Results for the p10MSSM In the axino DM scenario possible lower limits on T_R, that could be derived in a way similar to the one described in the previous section, are much weaker than for gravitino DM.[17] In practice we find in our p10MSSM analysis that even for the lowest values of $T_R \simeq 1\,\mathrm{GeV}$ that we take into account, we can obtain $\Omega_{\tilde{a}} h^2 \simeq 0.12$ for some specific SUSY spectra by adding TP and NTP contributions unless the axino is too light.

[15]In the case of the bino LOSP with mass $m_{\tilde{B}} \gtrsim 500\,\mathrm{GeV}$ its decays to the axino in thermal equilibrium contribute negligibly to axino TP. For the higgsino or the wino with a small bino composition the $U(1)$ decays become negligible for even lower masses of χ.

[16]This corresponds to the decays of neutralino being in thermal equilibrium and should be distinguished from NTP in late-time decays of out-of-equilibrium neutralinos.

[17]This is because one can further suppress non-thermal production by reducing T_R, since the total relic abundance can be supplemented with the contribution from TP.

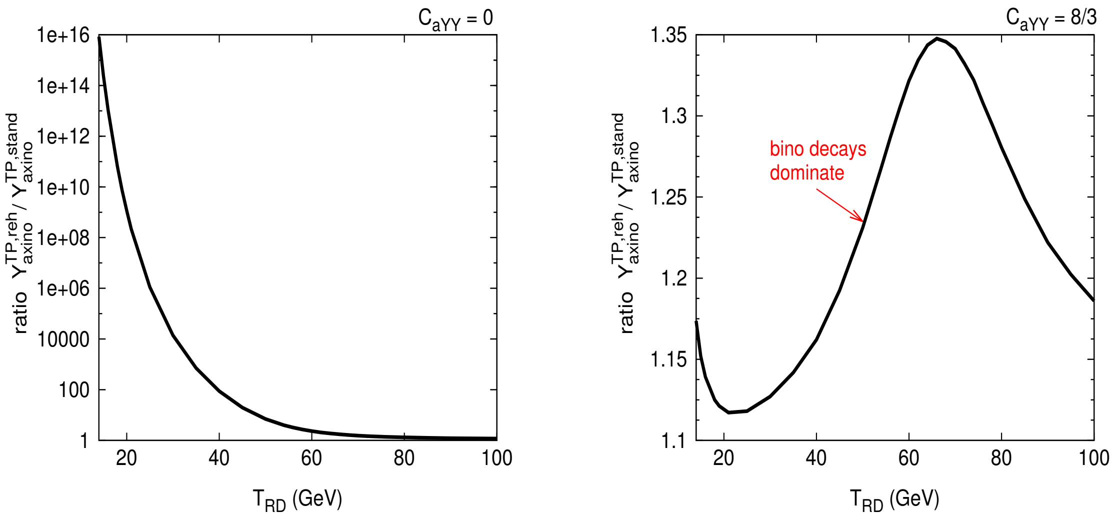

Figure 9.10: The ratio between $Y_{\tilde{a}}^{\mathrm{TP}}$ for the KSVZ axino obtained assuming instantaneous and non-instantaneous reheating in the low-T_R regime for negligible (left panel) and non-negligible (right panel) contributions from the lightest neutralino decays (in thermal equilibrium). We assume the gluino mass and squark masses to be equal 1 TeV. The lightest neutralino is bino-dominated with mass $m_\chi \sim 140\,\mathrm{GeV}$.

As discussed in Section 6.6.1, the BBN constraints for the axino are typically mild. The lifetime of the neutralino LOSP decaying to the axino can hardly exceed 0.1 sec., unless one considers very light neutralinos or assumes a mass degeneracy $m_{\tilde{a}} \simeq m_\chi$ (see Eq. (6.58)). However, for light neutralinos one often obtains too low $\Omega_\chi h^2$ that is further suppressed for low T_R. This additionally weakens the impact of the BBN bounds.[18] The only exception is a scenario with a sufficiently light axino and, simultaneously, light bino LOSP that is characterized by very large $\Omega_\chi h^2$ close to the upper boundary in Fig. 8.3 which is associated with annihilations via t-channel slepton exchange. In this case axino TP is suppressed, but the correct relic density can be achieved due to NTP given large $\Omega_\chi h^2$.[19] Simultaneously, one can obtain a large lifetime of the bino and it can be abundant enough to violate the BBN constraints. That is the reason why we see in Fig. 9.11 a region excluded by the BBN constraints for light (instead of heavy) axinos.

On the other hand, for too heavy axinos and $T_R \gtrsim 50\,\mathrm{GeV}$ the considered scenario suffers from DM overabundance. It is because both TP and NTP contributions to the relic density increase with increasing $m_{\tilde{a}}$. In this regime TP plays a dominant role when determining $\Omega_{\tilde{a}} h^2$. For values of the reheating temperature $T_R \sim 50\,\mathrm{GeV}$ NTP starts to play a major role and sets an upper limit on the axino mass. If

[18] It is because at late time there is not enough LOSPs decaying to axinos to effectively violate the BBN bounds. The correct axino relic density in this case can be achieved thanks to TP if $m_{\tilde{a}}$ is not too small.

[19] The smallness of the axino mass is required for these points to satisfy the relic density constraint since $\Omega_{\tilde{a}} h^2 \propto (m_{\tilde{a}}/m_\chi) \times \Omega_\chi h^2$ and $\Omega_\chi h^2$ is large even for low (but not too low) T_R.

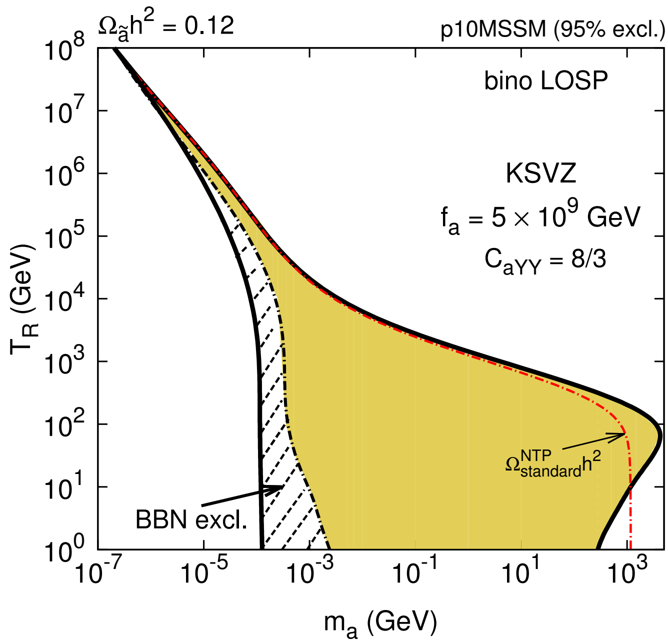

Figure 9.11: The upper bound on the axino mass $m_{\tilde{a}}$ as a function of the reheating temperature T_R for axino DM with a bino LOSP. KSVZ model is assumed with $f_a = 5 \times 10^9\,\text{GeV}$ and $C_{aYY} = 8/3$. Dash-dotted red line corresponds to the upper limit on $m_{\tilde{a}}$ in the instantaneous reheating scenario.

non-instantaneous reheating is assumed this limit is weakened in comparison with the standard cosmological scenario, as can be seen in Fig. 9.11. This is so due to a suppression of NTP that appears if the LOSP freeze-out had taken place before the RD epoch began.

For even lower values of the reheating temperature, $T_R \lesssim 50\,\text{GeV}$, NTP is suppressed so much that in order to satisfy the relic density constraint one needs to assume that the LOSP is characterized by very low $\langle\sigma v\rangle_{\text{eff}}$ (equivalently large $\Omega_\chi h^2(\text{high } T_R)$). These can, however, be only obtained for the bino LOSP with not too large mass m_χ, as can be seen in Fig. 8.3. As a result, one obtains an effective upper limit on the axino LSP mass from a condition $m_{\tilde{a}} \lesssim m_{\tilde{B}}$.

Chapter 10

Conclusions

Over the past eighty years after the first speculation about the existence of dark matter many astronomical observations have confirmed this hypothesis. We have learned a lot about the distribution of DM in galaxies and clusters of galaxies, as well as about its relic abundance. However, the nature of dark matter particles remains a puzzle.

Given current data and exclusion limits from both direct and indirect DM searches, undoubtedly the lightest supersymmetric particle remains one of the most popular DM candidates. In this thesis we discussed this scenario in more detail. We showed preferred cases and prospects for their discovery.

In particular, we considered selected GUT constrained supersymmetric models that are most commonly considered in the literature, *i.e.*, the CMSSM and the CNMSSM. We also discussed some non-universality conditions at the GUT scale that could either open up interesting possibility associated with the measured signal of the recently discovered Higgs boson or drastically reduce the overall amount of fine-tuning. We conclude that such GUT constrained supersymmetric models with neutralino DM often remain valid after applying many experimental constraints within the framework of Bayesian statistics. In particular, it is also true for the 1TH region with 1 TeV almost pure higgsino DM, which was in the past treated as not so appealing. However, in order to simultaneously find phenomenologically interesting regions in the parameter space and satisfy the naturalness requirement, one may be prompted to consider some special non-universality conditions at the high energy scale that can be justified within the framework of a more fundamental theory valid for the physics above the GUT scale.

In a more general framework of the MSSM with ten free parameters defined at the low energy scale we find similar preferred regions in the parameter space, including the 1TH region, which are accompanied by several other specific scenarios that can lead to the correct value of the relic density. We showed that this can be much improved by assuming low values of the reheating temperature T_R of the Universe after a period of cosmological inflation. In this scenario one can obtain

$\Omega_\chi h^2 \simeq 0.12$ for a wide range of masses and annihilation rates for the lightest neutralino depending on its composition, as well as effectiveness of direct and cascade decays of the inflaton field to DM. Remarkably, often the DM particles remain detectable in future DD and ID experiments. In particular, it is true for the wino DM scenario. This case is claimed to be excluded in the standard cosmological scenario by dark matter ID due to Sommerfeld enhancement of the present-day annihilation rate, but can become again viable for low T_R and both larger and lower masses than the ones typically considered.

Last, but not least, we discussed the other two supersymmetric DM candidates: the gravitino and the axino. For gravitino DM originating from sneutrino LOSP decays and thermal production we presented upper limits on T_R in some representative GUT constrained models. We found that in the non-universal Higgs mass model they can be close to the lower limit desired by thermal leptogenesis when one takes into account theoretical uncertainties in the determination of the Higgs boson mass.

Considering gravitino and axino DM scenarios in a regime of low reheating temperature also allowed us to derive interesting results. In the case of gravitino DM we obtained the lower bound on T_R that is much larger than typically mentioned value associated with the beginning of the Big Bang Nucleosynthesis. On the other hand in the axino DM case we improved the existing simplified upper bounds on the axino mass and found them to be either weaker or stronger depending on the actual value of the reheating temperature.

Appendix A

Approximate solutions to the 1-loop RGEs of the MSSM

Approximate solutions to the one-loop RGE for soft mass parameters of the MSSM can be obtained following the method from [100]. This leads to[1]

$$m^2_{H_d}(t) = m^2_{H_d}(0) + \sum_{i=1}^{3} \eta_{H_d,i}\, M_i(0)^2 - D_{H_d}, \tag{A.1}$$

$$m^2_{L,3}(t) = m^2_{L,3}(0) + \sum_{i=1}^{3} \eta_{L,i}\, M_i(0)^2 - D_L, \tag{A.2}$$

$$m^2_{\bar{e},3}(t) = m^2_{\bar{e},3}(0) + \sum_{i=1}^{3} \eta_{e,i}\, M_i(0)^2 - D_E, \tag{A.3}$$

$$m^2_{\bar{d},3}(t) = m^2_{\bar{d},3}(0) + \sum_{i=1}^{3} \eta_{d,i}\, M_i(0)^2 - D_d, \tag{A.4}$$

$$\begin{aligned} m^2_{H_u}(t) &= \Big(1 - \frac{1}{2}y\Big) m^2_{H_u}(0) - \frac{1}{2}\, y \left(m^2_{Q,3}(0) + m^2_{\bar{u},3}(0)\right) \\ &\quad -\frac{1}{2}y(1-y)\Big(A_0^2 - 2A_0 \sum_{i=1}^{3} \hat{\xi}_i M_i\Big) \\ &\quad + \sum_{i=1}^{3}\sum_{j\geqslant i}^{3} \Big\{\delta_{i,j}\, \eta_{H_u,i} + \frac{1}{2}y\big[-(\hat{\eta}_{i,j} + \delta_{i,j}\,\hat{\eta}_{j,i}) + (2-\delta_{i,j}) y\, \hat{\xi}_i\, \hat{\xi}_j\big]\Big\} M_i(0) M_j(0) - D_{H_u}, \end{aligned} \tag{A.5}$$

[1] We assume that $\tan\beta$ is not too large and therefore neglect the tau and the bottom Yukawa couplings.

$$\begin{aligned}
m^2_{Q,3}(t) &= \Big(1-\frac{1}{6}y\Big)m^2_{Q,3}(0)-\frac{1}{6}\,y\,\Big(m^2_{H_u}(0)+m^2_{\bar u,3}(0)\Big)\\
&\quad -\frac{1}{6}y(1-y)\Big(A_0^2-2A_0\sum_{i=1}^{3}\hat\xi_i M_i\Big) \qquad\qquad (A.6)\\
&\quad +\sum_{i=1}^{3}\sum_{j\geqslant i}^{3}\Big\{\delta_{i,j}\,\eta_{Q,i}+\frac{1}{6}y\big[-(\hat\eta_{i,j}+\delta_{i,j}\,\hat\eta_{j,i})+(2-\delta_{i,j})y\,\hat\xi_i\,\hat\xi_j\big]\Big\}M_i(0)M_j(0)-D_Q,
\end{aligned}$$

$$\begin{aligned}
m^2_{\bar u,3}(t) &= \Big(1-\frac{1}{3}y\Big)m^2_{\bar u,3}(0)-\frac{1}{3}\,y\,\Big(m^2_{H_u}(0)+m^2_{Q,3}(0)\Big)\\
&\quad -\frac{1}{3}y(1-y)\Big(A_0^2-2A_0\sum_{i=1}^{3}\hat\xi_i M_i\Big) \qquad\qquad (A.7)\\
&\quad +\sum_{i=1}^{3}\sum_{j\geqslant i}^{3}\Big\{\delta_{i,j}\,\eta_{u,i}+\frac{1}{3}y\big[-(\hat\eta_{i,j}+\delta_{i,j}\,\hat\eta_{j,i})+(2-\delta_{i,j})y\,\hat\xi_i\,\hat\xi_j\big]\Big\}M_i(0)M_j(0)-D_u,
\end{aligned}$$

where

$$D_K = a'_K S(0)\Big(\frac{1}{1+\frac{33}{5}\alpha_1(0)\,t}-1\Big), \qquad (A.8)$$

with $a'_Q=-\frac{1}{66}$, $a'_{\bar u}=\frac{2}{33}$, $a'_{\bar d}=-\frac{1}{33}$, $a'_L=\frac{1}{22}$, $a'_{\bar e}=-\frac{1}{11}$, $a'_{H_d}=\frac{1}{22}$, $a'_{H_u}=-\frac{1}{22}$ and $t=(1/2\pi)\log M/Q$. The auxiliary functions are given by

$$\eta_{K,i}(t)=I\left[\frac{d^i_K\alpha_i^3(t)}{\alpha_i^2(0)}\right], \qquad \hat\xi_i(t)=H\left[\frac{a^i_u\alpha_i^2(t)}{\alpha_i(0)}\right], \qquad (A.9)$$

$$\hat\eta_{i,j}(t)=\delta_{i,j}\,H\left[\frac{\bar d^i\alpha_i^3(t)}{\alpha_i^2(0)}\right]+H\left[\frac{\bar d^i\,\alpha_i^2(t)}{\alpha_i(0)}\xi_{u,j}(t)\right], \qquad (A.10)$$

where

$$\xi_{u,j}(t)=I\left[\frac{a^j_u\,\alpha_j^2(t)}{\alpha_j(0)}\right], \qquad \text{with}\quad I[f(t)]=\int_0^t f(t')\,dt', \qquad (A.11)$$

and

$$H[f(t)]=\int_0^t f(t')\,dt'-\frac{1}{F(t)}\int_0^t F(t')\,f(t')\,dt', \qquad (A.12)$$

$$F(t)=\int_0^t E(t')\,dt' \quad \text{where} \quad E(t')=\Pi_{i=1,2,3}\Big(\frac{\alpha_i(0)}{\alpha_i(t')}\Big)^{\frac{a_i}{b_i}}, \qquad (A.13)$$

with $a^i_{\bar u}=(\frac{13}{15},3,\frac{16}{3})$ and $d^i_Q=(\frac{1}{15},3,\frac{16}{3})$, $d^i_{\bar u}=(\frac{16}{15},0,\frac{16}{3})$, $d^i_{H_d}=d^i_{H_u}=(\frac{3}{5},3,0)$, $\bar d^i=d^i_Q+d^i_{\bar u}+d^i_{H_u}=(\frac{26}{15},6,\frac{32}{3})$. The one-loop RGE solutions for the gauge couplings read

$$\alpha_a^2(t)=\frac{\alpha_a^2(0)}{1-b_a\,\alpha_a^2(0)\,t}, \qquad (A.14)$$

where $a=1,2,3$ for $U(1)$, $SU(2)$ and $SU(3)$, respectively.

Appendix B

Approximate 2-loop solutions to the RGEs for slepton masses

In order to treat the RGE running of the supersymmetric parameters more precisely than in Appendix A it is necessary to include at least the leading two-loop corrections. As an example we will now discuss this issue for the third generation slepton mass parameters $m_{L,3} = m_L = m_{\tilde{\tau}_L}$ and $m_{\bar{e},3} = m_E = m_{\tilde{\tau}_R}$. The full two-loop RGEs can be found in [99]. In this Appendix we will limit ourselves only to the terms that play the most important role from a point of view of the analytical estimation of the sneutrino and the stau masses in Section 9.1.

In the case of m_L one can find that among various possible 2-loop contributions the most important correction is typically connected with high m_Q ("left" squark mass). Simplified, though exact enough, treatment of this dependence is to take into account term proportional to σ_2 in the 2-loop RGE for m_L from [99]. Moreover, it is enough to consider only the part of this term that is proportional to m_Q. In order not to deal with the full second order equation, we use perturbative approach. This means that we calculate m_Q using the one-loop equation, and then integrate it in order to obtain two-loop correction for the m_L

$$m_L^2(t) \simeq m_{L,\text{1-loop}}^2(t) - \frac{9}{8\pi}\int_0^t \alpha_2^2(s)\,\bar{m}_{Q,\text{1-loop}}^2(s)\,ds, \tag{B.1}$$

where the one-loop solution is given by Eq. (A.2), while is given by Eq. (A.7) with D_Q and $(1 - y/6)\,m_{Q,3}^2(0)$ replaced with $3\,D_Q$ and $(3 - y/6)\,m_Q^2(0)$, respectively.[1] Collecting all the terms together one obtains

$$\begin{aligned} m_L^2(t) \;&\simeq\; m_L^2(0) + \sum_{i=1}^{3}\eta_{L,i}\,M_i(0)^2 - D_L - \frac{9}{8\pi}\Big(3\,\alpha_2(0)\,\alpha_2(t)\,t - \frac{1}{6}c_2(t)\Big)m_Q^2(0) \\ &\quad -\frac{1}{6}c_2(t)\,\Big(m_{H_u}^2(0) + m_u^2(0)\Big), \end{aligned} \tag{B.2}$$

[1] Additional factors of 3 are connected with the first and the second generation masses.

where the function c_2 is given below.

The other mass parameter important in our considerations, which has a non-negligible two-loop corrections, is $m_E = m_{\tilde{\tau}_L}$. In this case one can identify three important 2-loop contributions in the corresponding β function [99]

$$\beta^{(2)}_{m_E^2} \sim \frac{12}{5}\, g_1^2\, S' + \frac{2808}{25}\, g_1^4\, M_1^2 + \frac{12}{5}\, g_1^2\, \sigma_1, \tag{B.3}$$

where[2] $S' \sim Y_t^2(m^2_{Q,3} + 4m^2_{\bar{u},3})$ and $\sigma_1 \sim \frac{1}{5}\, g_1^2\, \mathrm{Tr}[\mathbf{m}^2_Q + 8\mathbf{m}^2_{\bar{u}} + 2\mathbf{m}^2_{\bar{d}}]$. Integrating all the terms one obtains

$$\begin{aligned} m_E^2(t) \;\simeq\;& m_E^2(0) + \left\{ \eta_{E,1} - \frac{1}{8\pi}\frac{312}{55}\,\alpha_1(0)\Big[1 - (1 + \frac{33}{5}\alpha_1(0)\,t)^{-3}\Big]\right\} M_1(0)^2 \\ &+ \sum_{i=2}^{3} \eta_{E,i}\, M_i(0)^2 - D_E \qquad\qquad (\mathrm{B.4}) \\ &- \frac{1}{8\pi}\left\{ \frac{36}{25}\Big[3\,\alpha_2(0)\,\alpha_1(t)\,t - \frac{17}{6}c_1(t)\Big] + \frac{12}{5}\Big[d_1(t) - \frac{13}{6}f_1(t)\Big]\right\} m_Q^2(0) \\ &- \frac{1}{8\pi}\left\{ \frac{36}{25}\Big[24\,\alpha_2(0)\,\alpha_1(t)\,t - \frac{17}{6}c_1(t)\Big] + \frac{12}{5}\Big[4\,d_1(t) - \frac{13}{6}f_1(t)\Big]\right\} m_u^2(0) \\ &+ \frac{1}{8\pi}\left\{ \frac{102}{25}c_1(t) + \frac{26}{5}f_1(t)\right\} m^2_{H_u}(0) - \frac{1}{8\pi}\frac{216}{25}\,\alpha_1(0)\,\alpha_1(t)\,t\,m_d^2(0), \end{aligned}$$

where:

$$c_i(t) = \int_0^t y(s)\,\alpha_i^2(s)\,ds \qquad d_i(t) = \int_0^t Y_t(s)\,\alpha_i^2(s)\,ds \qquad f_i(t) = \int_0^t y(s)\,Y_t(s)\,\alpha_i^2(s)\,ds, \tag{B.5}$$

where $Y_t = y_t^2/4\pi$. Both Y_t and function y can be read from, *e.g.*, from [100]. We assumed $m_d^2(t) = m_d^2(0)$ in the appropriate 2-loop correction to $m_E^2(t)$.

[2] Once again we focus only on terms proportional to squark masses and neglect Yukawa couplings other than the top one. In S' we also neglect flavor mixing.

Appendix C

Mass parameters for generalized gauge-mediation models

In GGM models, the soft supersymmetry breaking masses at the high scale in the notation of [97] read

$$M_a = (\alpha_a/4\pi)\Lambda_a \qquad \text{for } a = 1,2,3 \tag{C.1}$$
$$m_Q^2 = (8/3)(\alpha_3^2/16\pi^2)\tilde{\Lambda}_3^2 + (3/2)(\alpha_2^2/16\pi^2)\tilde{\Lambda}_2^2 + (1/30)(\alpha_1^2/16\pi^2)\tilde{\Lambda}_1^2 \tag{C.2}$$
$$m_{\bar{u}}^2 = (8/3)(\alpha_3^2/16\pi^2)\tilde{\Lambda}_3^2 + (8/15)(\alpha_1^2/16\pi^2)\tilde{\Lambda}_1^2 \tag{C.3}$$
$$m_{\bar{d}}^2 = (8/3)(\alpha_3^2/16\pi^2)\tilde{\Lambda}_3^2 + (2/15)(\alpha_1^2/16\pi^2)\tilde{\Lambda}_1^2 \tag{C.4}$$
$$m_L^2 = m_{H_u}^2 = m_{H_d}^2 = (3/2)(\alpha_2^2/16\pi^2)\tilde{\Lambda}_2^2 + (3/10)(\alpha_1^2/16\pi^2)\tilde{\Lambda}_1^2 \tag{C.5}$$
$$m_{\bar{e}}^2 = (6/5)(\alpha_1^2/16\pi^2)\tilde{\Lambda}_1^2\,. \tag{C.6}$$

The trilinear scalar couplings are all equal to zero and $\tan\beta$, $\mathrm{sgn}(\mu)$ are free parameters. The free parameters are related to $\langle S\rangle$ and $\langle F_S\rangle$ as described in [97].

Appendix D

Solving Boltzmann equations for low T_R

We rewrite set of Boltzmann equations (8.1) in terms of dimensionless quantities $\Phi = \frac{\rho_\phi}{T_R}a^3$, $R = \rho_R a^4$, $X = n_X a^3$ and $A = \frac{a}{a_I}$

$$\begin{aligned}
\frac{d\Phi}{dA} &= -\sqrt{\frac{\pi^2 g_*(T_R)}{30}}\,\frac{A^{1/2}\Phi}{\sqrt{\Phi + \frac{R}{A} + \frac{X\langle E_X\rangle}{T_R}}},\\
\frac{dR}{dA} &= \sqrt{\frac{\pi^2 g_*(T_R)}{30}}\,\frac{A^{3/2}\Phi}{\sqrt{\Phi + \frac{R}{A} + \frac{X\langle E_X\rangle}{T_R}}} + \sqrt{\frac{3}{8\pi}}\,\frac{A^{-3/2}M_{Pl}\langle\sigma v\rangle 2\langle E_X\rangle}{\sqrt{\Phi + \frac{R}{A} + \frac{X\langle E_X\rangle}{T_R}}}\big[X^2 - X_{eq}^2\big],\\
\frac{dX}{dA} &= -\sqrt{\frac{3}{8\pi}}\,\frac{A^{-5/2}M_{Pl}\langle\sigma v\rangle T_R}{\sqrt{\Phi + \frac{R}{A} + \frac{X\langle E_X\rangle}{T_R}}}\big[X^2 - X_{eq}^2\big]. \qquad \text{(D.1)}
\end{aligned}$$

where, since none of the physical results will depend on the initial value of the scale factor (at the end of a period of cosmological inflation), we fixed $a_I = T_R^{-1}$.

D.1 Freeze-out approximation

The method which we use to deal with numerical integration of Eqs (D.1) is a generalization of the freeze-out approximation used in the context of standard cosmological scenario to the case with non-instantaneous reheating.

We can rewrite the Boltzmann equation for X in terms of

$$y = 1 + \Delta = \frac{X}{X_{eq}}, \qquad \text{(D.2)}$$

and notice that $y \approx 1$, when X is in thermal equilibrium. Hence we do not have to solve Boltzmann equation for y for intermediate values of $A_{\rm eq} < A < A_*$, where A_{eq} describes the moment, in which thermal equilibrium is established, while A_*

describes the moment, when X starts to decouple (it corresponds to $T_{f,\mathrm{beg}}$ introduced in Section 3.2.2). For these intermediate values of A we simply assume $y \equiv 1$. Therefore the Boltzmann equation for radiation decouples from equation for X and can be solved independently (with the equation for the inflaton field). For $A > A_*$ we integrate the full set of equations (D.1) taking $R(A_*)$ and $\Phi(A_*)$ as the initial values.

To find proper A_* we notice that in thermal equilibrium, since $y \approx 1$, to some approximation

$$0 \approx \frac{d\ln y}{dA} = f(y, A), \tag{D.3}$$

where function f is derived below. From Eq. (D.3) we find A_* that corresponds to y_*, which, in turns, is some arbitrary chosen value adjusted in numerical tests (in practice we choose $y \simeq 1.01$).

D.2 Equations and procedure of calculations

Equations In order to find $f(y, A)$ we rewrite the Boltzmann equation for X in terms of y

$$\frac{d\ln(1+\Delta)}{dA} = \frac{d\ln y}{dA} = \frac{1}{y}\frac{dy}{dA} = \frac{1}{y\,X_{eq}}\frac{dX}{dA} - \frac{1}{X_{eq}}\frac{dX_{eq}}{dA}. \tag{D.4}$$

According to (D.3) we get

$$y \approx \frac{dX}{dA}\left(\frac{dX_{eq}}{dA}\right)^{-1}, \tag{D.5}$$

where

$$\frac{dX}{dA} = C\,X_{eq}^2\left[y^2-1\right], \qquad \text{with } \; C = -\sqrt{\frac{3}{8\pi}}\,\frac{A^{-5/2}M_{Pl}\langle\sigma v\rangle T_R}{\sqrt{\Phi + \frac{R}{A} + \frac{X_{eq}\langle E_X\rangle}{T_R}}}. \tag{D.6}$$

The total equilibrium number density $n = \Sigma_i n_i$ used in the framework of SUSY can be rewritten in terms of X and used to derive

$$\frac{dX_{eq}}{dA} = 3\,\frac{X_{eq}}{A} + 3X_{eq}\frac{d\ln T}{dA} + \frac{d\ln T}{dA}\frac{A^3}{T_R^3}\sum_i \frac{g_i m_i^3}{2\pi^2}\,K_1\!\left(\frac{m_i}{T}\right) \tag{D.7}$$

Note that it does not depend explicitly on y.

The temperature dependence on the radiation energy density Eq. (2.4) can be used to derive

$$\frac{d\ln T}{dA} = \frac{\frac{1}{4}\frac{1}{R}\frac{dR}{dA} - \frac{1}{A}}{1 + \frac{1}{4}\frac{d\ln g_*(T)}{d\ln T}} \tag{D.8}$$

where the Boltzmann equation for radiation can be approximately simplified to

$$\frac{dR}{dA} \approx \sqrt{\frac{\pi^2 g_*(T_R)}{30}} \frac{A^{3/2}\Phi}{\sqrt{\Phi + \frac{R}{A} + \frac{X_{eq}\langle E_X\rangle}{T_R}}} \tag{D.9}$$

Using (D.5) and (D.6) one can obtain

$$y \approx C\, X_{eq}^2 \left[y^2 - 1\right] \left(\frac{dX_{eq}}{dA}\right)^{-1} \tag{D.10}$$

Thus

$$y \approx \frac{1}{2\,C\,X_{eq}^2} \left\{ \frac{dX_{eq}}{dA} - \sqrt{\left(\frac{dX_{eq}}{dA}\right)^2 + 4\left(C\,X_{eq}^2\right)^2} \right\} \tag{D.11}$$

It is the only positive root of the quadratic equation (D.10), since $C < 0$.

Procedure of calculation The procedure of calculation is the following:

1. We solve full set of Boltzmann equations (D.1) for $1 < A < A_{eq}$ (till the moment, when thermal equilibrium of the X particles is established). For very early times $X/X_{eq} \ll 1$ and then this ratio grows. We choose A_{eq} by assuming, that it corresponds to $X/X_{eq} = 0.99$.

2. For $A_{eq} < A < A_*$ we assume $X = X_{eq}$. We solve only two Boltzmann equations for the inflaton field and radiation (with no impact of X). We calculate y using (D.11). The end of the thermal equilibrium period corresponds to

$$A_* = \frac{1}{\mathrm{COR}} \cdot A_{y=1.01} \tag{D.12}$$

   The need of multiplication by correction factor 1/COR is described in the next section.

3. For $A > A_*$ we once again solve the full set (D.1) with the initial conditions $\Phi(A_*)$, $R(A_*)$ and $X = 1.01\, X_{eq}(A_*)$.

Correction factor COR In the Fig. D.1 (left panel) X/X_{eq} and y dependence on A and T is shown for some sample point from the p10MSSM parameter space. In this figure X/X_{eq} is obtained by solving the full set of Boltzmann equations (D.1) for the whole range of A, while y is calculated via approximate eq. (D.11). As can be seen y given by the approximate formula starts to grow later than true X/X_{eq}. Therefore $A_{y=1.01}$ overestimates the true value of A_*. In order to take this into account we introduce the additional correction in Eq. (D.12). It can be estimated semi-analytically to be typically of the order of COR$\simeq$ $(6 \div 40)$. In practice we begin with COR$= 1$ and than increase it gradually until the final result for the relic density stabilizes. This is illustrated in Fig. D.1 (right panel).

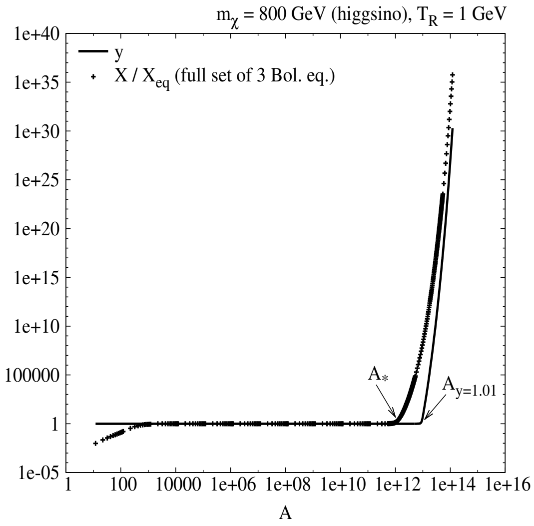

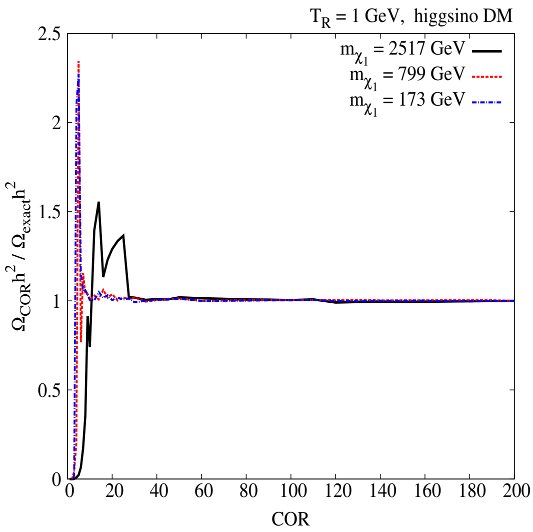

Figure D.1: *Left panel*: Difference between A_* and $A_{y=1.01}$. *Rigth panel*: Stabilization of the value of the relic density calculated for an increasing correction factor COR.

Appendix E

Axino thermal production (TP) with low reheating temperature

In scenarios with a non-instantaneous reheating one has to take into account a modified expansion rate of the Universe when calculating $Y_{\tilde{a}}^{\mathrm{TP}}$. We briefly describe below the methodology that can be used to calculate the axino TP yield.

E.1 Axino TP yield with non-instantaneous reheating

It results in a modification of temperature dependence on the scale factor $T(a)$. The Boltzmann equation (3.11) can then be rewritten as

$$\frac{dX_{\tilde{a}}}{dT}\frac{dT}{da} = \frac{a^2}{H}\Big(\Sigma_{scat} + \Sigma_{dec}\Big), \tag{E.1}$$

where $X_{\tilde{a}} = a^3\, n_{\tilde{a}.}$. Thus Eq. (3.12) is now modified to

$$Y_{\tilde{a},0} = \frac{1}{s_0 A_0^3}\int_{T_0}^{T_{\mathrm{up}}}\Big(-T\frac{d\ln T}{dA}\Big)^{-1}\frac{A^2}{H}\Big(\Sigma_{scat} + \Sigma_{dec}\Big), \tag{E.2}$$

where T_{up} corresponds to an effective upper limit in the integration,[1], we used $A = a/a_I = aT_R$ (we put $a_I = T_R$ as in Appendix D) and $d\ln T/dA$ is given by Eq. (D.8). One can verify that Eq. (E.2) is equivalent to (3.12) in the RD epoch when $T \propto a^{-1}$ and $s \propto T^3$.

[1] In practice it is enough to perform integration to $T_{\mathrm{up}} \simeq (5 \div 10)T_{\mathrm{RD}}$ or even lower. For larger temperatures TP of axinos is more efficient, but the fast expansion of the Universe in the reheating period dilutes away all the axinos produced at that early times.

E.2 The scattering term

In order to deal with the scattering contribution to $Y_{\tilde{a}}^{\rm TP}$ we substitute $\langle\sigma(i+j\to\tilde{a}+\ldots)v\rangle\, n_{i,\rm eq}\, n_{j,\rm eq}$ (from $\Sigma_{\rm scat}$; see, *e.g.*, [171]) into (E.2) and obtain

$$Y_{\tilde{a},0}^{{\rm scat},i,j} = \frac{1}{s_0 A_0^3}\frac{g_i g_j}{16\pi^4}\int_{T_0}^{T_{\rm up}}\int_{(m_1+m_2)/T}^{\infty} dx\left[\left(-T\frac{d\ln T}{dA}\right)^{-1}\frac{A^2}{H}\right]\times$$
$$T^2\,K_1(x)\,\sigma(x^2T^2)\Big[\left(x^2T^2-m_1^2-m_2^2\right)^2-4m_1^2m_2^2\Big]. \tag{E.3}$$

We then change the order of integration and decompose the above integral into

$$Y_{\tilde{a},0}^{{\rm scat},i,j} = \frac{1}{s_0 A_0^3}\frac{g_i g_j}{16\pi^4}\left(\mathbb{I}-\mathbb{III}\right), \tag{E.4}$$

where

$$\mathbb{III} = \int_{(m_1+m_2)/T_0}^{\infty} dx\int_{(m_1+m_2)/x}^{T_0} dT\,\ldots\approx 0, \tag{E.5}$$

since $T_0\approx 0$. From the remaining integral $\mathbb{I}$ one obtains

$$Y_{\tilde{a},0}^{{\rm scat},i,j} \simeq \frac{\bar{g}\,g_i\,g_j\,M_{Pl}}{16\pi^4}\int_{(m_1+m_2)/T_{\rm up}}^{\infty} dt\,t^3K_1(t)\int_{m_1+m_2}^{tT_{\rm up}} d(\sqrt{s})$$
$$f(\sqrt{s})\,\sigma(s)\,\frac{\left(s-m_1^2-m_2^2\right)^2-4m_1^2m_2^2}{s^2}, \tag{E.6}$$

where $\bar{g}=\frac{135\sqrt{10}}{2\pi^3\,g_*^{3/2}}$ and

$$f(\sqrt{s}) = \frac{\pi}{T_0^3A_0^3}\sqrt{\frac{g_*}{30}}\left(-T\frac{d\ln T}{dA}\right)^{-1}\frac{A^2T^6}{\sqrt{\frac{\Phi\,T_R^4}{A^3}+\frac{RT_R^4}{A^4}}},\qquad \text{with } T=\frac{\sqrt{s}}{t}. \tag{E.7}$$

The whole correspondence of Eq. (E.6) to the non-standard cosmological scenario is hidden in function f. In the RD epoch Eq. (E.6) reduces to the standard formula from [171] (*i.e.*, $f(\sqrt{s})$ becomes constant and equal to unity) obtained for the instantaneous reheating approximation where we take $T_{\rm up}=T_{\rm RD}=T_R$. A careful analysis of Eq. (E.7) in the reheating period shows that to some approximation $f\propto T^7$.[2] Thus Eq. (E.7) can be approximately rewritten as

$$f = \begin{cases} \left(T_{\rm RD}/T\right)^{-a} & (\leqslant 1)\ \text{in the reheating period,}\\ 1 & \text{in the RD epoch,}\end{cases} \tag{E.8}$$

[2] One could argue that this is in principle written explicitly in Eq. (E.7). However, one has to remember about the "hidden" temperature dependence of other terms, $d\ln T/dA$, A, Φ, R and g_*. A careful verification shows that these dependences approximately cancel each other.

where $a \simeq -7$ and $T_{\rm RD} \sim 0.5\,T_R$. In practice we find more exact values of a and $T_{\rm RD}$ numerically, but they depend only slightly on details of a SUSY spectrum.

High $\mathbf{T_R}$ limit of the scattering term The integral (E.6) can be rewritten as a sum of three integrals such that

$$Y^{scat,i,j}_{\tilde{a},0} \sim \int_{(m_1+m_2)/T_{up}}^{(m_1+m_2)/T_{\rm RD}} \int_{m_1+m_2}^{tT_{up}} + \int_{(m_1+m_2)/T_{\rm RD}}^{\infty} \int_{m_1+m_2}^{tT_{\rm RD}} + \int_{(m_1+m_2)/T_{\rm RD}}^{\infty} \int_{tT_{\rm RD}}^{tT_{up}} = \mathcal{A}+\mathcal{B}+\mathcal{C}. \tag{E.9}$$

One can verify that $\mathcal{A} \xrightarrow{T_{\rm RD}\to\infty} 0$, since external range of integration shrinks to zero ($T_{\rm up} > T_{\rm RD} \to \infty$), while the integrand does not diverge as $T_{\rm RD} \to \infty$. The second integral $\mathcal{B}$ corresponds to the the standard result obtained for the instantaneous reheating approximation. In the limit of high reheating temperature the inner integral can be simplified to[3]

$$\begin{aligned} \int_{m_1+m_2}^{tT_{\rm RD}} d(\sqrt{s})\, f(s)\, \sigma(s,t)\, \frac{(s-m_1^2-m_2^2)^2 - 4m_1^2m_2^2}{s^2} &\simeq \int_{m_1+m_2}^{tT_{\rm RD}} d(\sqrt{s})\, 1 \times \sigma(t) \times 1 \\ &\simeq t\,\sigma(t)\,T_{\rm RD}, \end{aligned} \tag{E.10}$$

where we noticed that the integral is mainly determined by the values of the integrand in high s limit in which, to a good approximation, $\sigma(s,t) = \sigma(t)$.

For the third integral $\mathcal{C}$ we similarly note that inner integration leads to

$$\int_{tT_{\rm RD}}^{tT_{up}} d(\sqrt{s})\, f(s)\, \sigma(s,t)\, \frac{(s-m_1^2-m_2^2)^2 - 4m_1^2m_2^2}{s^2} \simeq \sigma(t) \int_{tT_{\rm RD}}^{tT_{up}} d(\sqrt{s})\, f(s) = (*). \tag{E.11}$$

In the integration range $T = \sqrt{s}/t > T_{\rm RD}$ and therefore

$$(*) = t\,\sigma(t) \int_{T_{\rm RD}}^{T_{up}} dT \left(\frac{T_{\rm RD}}{T}\right)^7 \simeq \frac{1}{6}\, t\,\sigma(t)\, T_{\rm RD},$$

where we assumed $T_{\rm up} = cT_{\rm RD}$ with c high enough so that effectively $T_{\rm up}$ can be replaced by ∞ in the integration. The remaining (external) integrals for both $\mathcal{B}$ and $\mathcal{C}$ are the same. Hence

$$\frac{\mathcal{C}}{\mathcal{B}} \simeq \frac{1}{6} \simeq 0.17, \qquad \text{for high } T_{\rm RD}. \tag{E.12}$$

Eq. (E.12) remains valid for each contribution to the scattering term.

[3] σ depends on t via m_{eff} (see, *e.g.*, [181]).

E.3 The decay term

In the case of the decay term we substitute $\langle\Gamma\rangle n_i^{eq}$ (see, *e.g.*, [171]) into (E.2) and obtain

$$Y_{\tilde{a},0}^{\mathrm{dec},i} = \frac{1}{s_0 A_0^3}\,\frac{\Gamma\, g_i\, m_i}{2\pi^2}\int_{T_0}^{T_{\mathrm{up}}} dT \int_{m_i/T}^{\infty} dx \left[\left(-T\frac{d\ln T}{dA}\right)^{-1}\frac{A^2}{H}\right] T^2\,\frac{\sqrt{x^2-\frac{m_i^2}{T^2}}}{e^x \mp 1}. \tag{E.13}$$

Once again we change the order of integration and find that one term is negligible, while the other leads to

$$Y_{\tilde{a},0}^{dec,i} \simeq \frac{\bar{g}\, g_i\, \Gamma\, m_i\, M_{Pl}}{2\pi^2}\int_{m/T_{up}}^{\infty} dt\,\frac{t^4}{e^t \mp 1}\int_{m_i}^{tT_{up}} dE\, f(E)\,\frac{1}{E^4}\sqrt{1-\frac{m_i^2}{E^2}}, \tag{E.14}$$

where f is given by Eq. (E.8) with $\sqrt{s}$ replaced by E.

The inner integral

$$g_{m_i,T_R}(t) = \int_{m_i}^{tT_{up}} dE\, f(T=E/t)\,\frac{1}{E^4}\sqrt{1-\frac{m_i^2}{E^2}}, \tag{E.15}$$

where $m_i/T_{up} \leqslant t \leqslant \infty$ can be calculated analytically. Depending on the value of t one obtains:

1. for $m_i/T_{up} \leqslant t \leqslant m_i/T_{\mathrm{RD}}$

$$g_{m_i,T_R}(t) = g_{m_i,T_R}^{reh}(t) = \frac{T_{\mathrm{RD}}^7\, t^7}{m_i^{10}}\left(\frac{1}{3}w^3 - \frac{4}{5}w^5 + \frac{6}{7}w^7 - \frac{4}{9}w^9 + \frac{1}{11}w^{11}\right)\Bigg|_0^{\sqrt{1-\left[m_i/(tT_{up})\right]^2}}. \tag{E.16}$$

2. for $t \geqslant m_i/T_{\mathrm{RD}}$ temperature can be either larger or smaller than T_{RD} and we can write

$$g_{m_i,T_R}(t) = g_{m_i,T_R}^{\mathrm{RD}}(t) + g_{m_i,T_R}^{reh}(t), \tag{E.17}$$

where ($t_R = m_i/T_{\mathrm{RD}}$)

$$g_{m_i,T_R}^{\mathrm{RD}}(t) = \frac{1}{8m_i^3}\left(\frac{\pi}{2} - \arctan\frac{t_R}{\sqrt{t^2-t_R^2}} + \frac{t_R}{t^4}(t^2-2t_R^2)\sqrt{t^2-t_R^2}\right), \tag{E.18}$$

$$g_{m_i,T_R}^{reh}(t) = \frac{T_{\mathrm{RD}}^7\, t^7}{m_i^{10}}\left(\frac{1}{3}w^3 - \frac{4}{5}w^5 + \frac{6}{7}w^7 - \frac{4}{9}w^9 + \frac{1}{11}w^{11}\right)\Bigg|_{\sqrt{1-\left[m_i/(tT_{\mathrm{RD}})\right]^2}}^{\sqrt{1-\left[m_i/(tT_{up})\right]^2}}, \tag{E.19}$$

One can verify that in the case of instantaneous reheating the standard result [171] is rederived.

Bibliography

[1] S. Chatrchyan *et al.* [CMS Collaboration], Phys. Lett. B **716** (2012) 30

[2] G. Aad *et al.* [ATLAS Collaboration], Phys. Lett. B **716** (2012) 1

[3] P. A. R. Ade *et al.* [Planck Collaboration], Astron. Astrophys. **571** (2014) A16

[4] E. W. Kolb, M. S. Turner, *The Early Universe*, Addison-Wesley (1990).

[5] S. Dodelson, "Modern cosmology", Amsterdam, Netherlands: Academic Pr. (2003) 440 p

[6] E. Hubble, Proc. Nat. Acad. Sci. **15** (1929) 168.

[7] K. A. Olive *et al.* [Particle Data Group Collaboration], Chin. Phys. C **38** (2014) 090001.

[8] G. F. Giudice, E. W. Kolb and A. Riotto, Phys. Rev. D **64** (2001) 023508

[9] J. Edsjo, P. Gondolo, *Neutralino Relic Density including Coannihilations*, *Phys. Rev. D* **56** (1997) 1879

[10] V. N. Lukash, E. V. Mikheeva and A. M. Malinovsky, Phys. Usp. **54** (2011) 983

[11] M. Goetz and J. Sommer-Larsen, Astrophys. Space Sci. **284** (2003) 341

[12] A. Del Popolo, Int. J. Mod. Phys. D **23** (2014) 1430005

[13] F. Zwicky, Helv. Phys. Acta **6** (1933) 110.

[14] H. W. Babcock, Lick Obs. Bull. **19**, (1939) 1.

[15] V. C. Rubin and W. K. Ford, Jr., Astrophys. J. **159** (1970) 379.

[16] M. S. Roberts, R. N. Whitehurst, Astrophys. J. **201**, (1975) 327.

[17] V. C. Rubin, N. Thonnard and W. K. Ford, Jr., Astrophys. J. **238** (1980) 471.

[18] R. Massey, T. Kitching and J. Richard, Rept. Prog. Phys. **73** (2010) 086901

[19] M. Petrou, PhD Thesis, Univ. Cambridge (1981)

[20] B. Paczynski, Astrophys. J. **304** (1986) 1.

[21] P. Tisserand *et al.* [EROS-2 Collaboration], Astron. Astrophys. **469** (2007) 387

[22] H. Baer, K. Y. Choi, J. E. Kim and L. Roszkowski, Phys. Rept. **555** (2015) 1

[23] B. Audren, J. Lesgourgues, G. Mangano, P. D. Serpico and T. Tram, JCAP **1412** (2014) 12, 028

[24] B. W. Lee and S. Weinberg, Phys. Rev. Lett. **39** (1977) 165.

[25] J. L. Feng and J. Kumar, Phys. Rev. Lett. **101** (2008) 231301

[26] K. Y. Choi, J. E. Kim and L. Roszkowski, J. Korean Phys. Soc. **63** (2013) 1685

[27] J. L. Feng, A. Rajaraman and F. Takayama, Phys. Rev. D **68** (2003) 063504 [hep-ph/0306024].

[28] L. J. Hall, K. Jedamzik, J. March-Russell and S. M. West, JHEP **1003** (2010) 080

[29] K. Y. Choi, L. Roszkowski and R. Ruiz de Austri, JHEP **0804** (2008) 016

[30] J. R. Ellis, D. V. Nanopoulos and S. Sarkar, Nucl. Phys. B **259** (1985) 175.

[31] J. R. Ellis, G. B. Gelmini, J. L. Lopez, D. V. Nanopoulos and S. Sarkar, Nucl. Phys. B **373** (1992) 399.

[32] J. E. Kim, Phys. Rept. **150** (1987) 1.

[33] R. D. Peccei, Lect. Notes Phys. **741** (2008) 3

[34] J. E. Kim and G. Carosi, Rev. Mod. Phys. **82** (2010) 557

[35] R. D. Peccei and H. R. Quinn, Phys. Rev. Lett. **38** (1977) 1440.

[36] R. D. Peccei and H. R. Quinn, Phys. Rev. D **16** (1977) 1791.

[37] W. A. Bardeen, R. D. Peccei and T. Yanagida, Nucl. Phys. B **279** (1987) 401.

[38] J. E. Kim, Phys. Rev. Lett. **43** (1979) 103.

[39] M. A. Shifman, A. I. Vainshtein and V. I. Zakharov, Nucl. Phys. B **166** (1980) 493.

[40] M. Dine, W. Fischler and M. Srednicki, Phys. Lett. B **104** (1981) 199.

[41] A. P. Zhitnitskii, Sov. J. Nucl. Phys **31** (1980) 260.

[42] W. A. Bardeen and S.-H. H. Tye, Phys. Lett. B **74** (1978) 229.

[43] K. J. Bae, J. H. Huh and J. E. Kim, JCAP **0809** (2008) 005

[44] P. Sikivie and Q. Yang, Phys. Rev. Lett. **103** (2009) 111301

[45] L. F. Abbott and P. Sikivie, Phys. Lett. B **120** (1983) 133.

[46] M. Dine and W. Fischler, Phys. Lett. B **120** (1983) 137.

[47] J. Preskill, M. B. Wise and F. Wilczek, Phys. Lett. B **120** (1983) 127.

[48] Y. Nambu, Phys. Rev. Lett. **4** (1960) 380.

[49] Y. Nambu and G. Jona-Lasinio, Phys. Rev. **122** (1961) 345.

[50] J. Goldstone, Nuovo Cim. **19** (1961) 154.

[51] J. Goldstone, A. Salam and S. Weinberg, Phys. Rev. **127** (1962) 965.

[52] F. Englert and R. Brout, Phys. Rev. Lett. **13** (1964) 321.

[53] P. W. Higgs, Phys. Rev. Lett. **13** (1964) 508.

[54] G. S. Guralnik, C. R. Hagen and T. W. B. Kibble, Phys. Rev. Lett. **13** (1964) 585.

[55] P. W. Higgs, Phys. Rev. **145** (1966) 1156.

[56] T. W. B. Kibble, Phys. Rev. **155** (1967) 1554.

[57] A. Djouadi, Phys. Rept. **457** (2008) 1

[58] M. J. G. Veltman, Acta Phys. Polon. B **8** (1977) 475.

[59] A. Djouadi, Phys. Rept. **459** (2008) 1

[60] E. Witten, Nucl. Phys. B **188** (1981) 513.

[61] N. Sakai, Z. Phys. C **11** (1981) 153.

[62] S. Dimopoulos and H. Georgi, Nucl. Phys. B **193** (1981) 150.

[63] E. Witten, Nucl. Phys. B **202** (1982) 253.

[64] R. K. Kaul and P. Majumdar, Nucl. Phys. B **199** (1982) 36.

[65] H. Georgi and S. L. Glashow, Phys. Rev. Lett. **32** (1974) 438.

[66] T. Fukuyama, Int. J. Mod. Phys. A **28** (2013) 1330008

[67] S. P. Martin, Adv. Ser. Direct. High Energy Phys. **21** (2010) 1

[68] D. Buttazzo, G. Degrassi, P. P. Giardino, G. F. Giudice, F. Sala, A. Salvio and A. Strumia, JHEP **1312** (2013) 089

[69] [ATLAS and CDF and CMS and D0 Collaborations],

[70] M. Bobrowski, G. Chalons, W. G. Hollik and U. Nierste, Phys. Rev. D **90** (2014) 3, 035025

[71] M. F. Sohnius, Phys. Rept. **128** (1985) 39.

[72] S. Weinberg, "The quantum theory of fields. Vol. 3: Supersymmetry," Cambridge, UK: Univ. Pr. (2000) 419 p

[73] H. Baer and X. Tata, "Weak scale supersymmetry: From superfields to scattering events," Cambridge, UK: Univ. Pr. (2006) 537 p

[74] S. R. Coleman and J. Mandula, Phys. Rev. **159** (1967) 1251.

[75] E. Witten, "Introduction to supersymmetry," Proc. Intern. School of Subnuclear Physics, Erice 1981, ed. A Zichichi (Plenum Press, 1983) p. 305

[76] R. Haag, J. T. Lopuszanski and M. Sohnius, Nucl. Phys. B **88** (1975) 257.

[77] J. Wess and B. Zumino, Nucl. Phys. B **70** (1974) 39.

[78] F. Takayama and M. Yamaguchi, Phys. Lett. B **485** (2000) 388

[79] H. B. Kim and J. E. Kim, Phys. Lett. B **527** (2002) 18

[80] L. Girardello and M. T. Grisaru, Nucl. Phys. B **194** (1982) 65.

[81] L. O'Raifeartaigh, Nucl. Phys. B **96** (1975) 331.

[82] P. Fayet and J. Iliopoulos, Phys. Lett. B **51** (1974) 461.

[83] P. Fayet, Nucl. Phys. B **90** (1975) 104.

[84] A. H. Chamseddine, R. L. Arnowitt and P. Nath, Phys. Rev. Lett. **49** (1982) 970.

[85] R. Barbieri, S. Ferrara and C. A. Savoy, Phys. Lett. B **119** (1982) 343.

[86] L. J. Hall, J. D. Lykken and S. Weinberg, Phys. Rev. D **27** (1983) 2359.

[87] L. Alvarez-Gaume, J. Polchinski and M. B. Wise, Nucl. Phys. B **221** (1983) 495.

[88] M. Dine and W. Fischler, Phys. Lett. B **110** (1982) 227.

[89] C. R. Nappi and B. A. Ovrut, Phys. Lett. B **113** (1982) 175.

[90] L. Alvarez-Gaume, M. Claudson and M. B. Wise, Nucl. Phys. B **207** (1982) 96.

[91] M. Dine and A. E. Nelson, Phys. Rev. D **48** (1993) 1277

[92] M. Dine, A. E. Nelson and Y. Shirman, Phys. Rev. D **51** (1995) 1362

[93] M. Dine, A. E. Nelson, Y. Nir and Y. Shirman, Phys. Rev. D **53** (1996) 2658

[94] D. Shih, JHEP **0802** (2008) 091

[95] C. Cheung, A. L. Fitzpatrick and D. Shih, JHEP **0807** (2008) 054

[96] P. Meade, N. Seiberg and D. Shih, Prog. Theor. Phys. Suppl. **177** (2009) 143

[97] L. M. Carpenter, M. Dine, G. Festuccia and J. D. Mason, Phys. Rev. D **79** (2009) 035002

[98] J. Rosiek, Phys. Rev. D **41** (1990) 3464. Erratum [hep-ph/9511250].

[99] S. P. Martin and M. T. Vaughn, Phys. Rev. D **50** (1994) 2282 [Erratum-ibid. D **78** (2008) 039903]

[100] M. S. Carena, P. H. Chankowski, M. Olechowski, S. Pokorski and C. E. M. Wagner, Nucl. Phys. B **491** (1997) 103

[101] S. P. Martin, Phys. Rev. D **65** (2002) 116003

[102] S. P. Martin, Phys. Rev. D **66** (2002) 096001

[103] H. Baer, V. Barger, P. Huang, D. Mickelson, A. Mustafayev and X. Tata, Phys. Rev. D **87** (2013) 11, 115028

[104] H. E. Haber and R. Hempfling, Phys. Rev. Lett. **66** (1991) 1815.

[105] J. R. Ellis, G. Ridolfi and F. Zwirner, Phys. Lett. B **257** (1991) 83.

[106] Y. Okada, M. Yamaguchi and T. Yanagida, Prog. Theor. Phys. **85** (1991) 1.

[107] P. H. Chankowski, S. Pokorski and J. Rosiek, Phys. Lett. B **274** (1992) 191.

[108] H. E. Haber, R. Hempfling and A. H. Hoang, Z. Phys. C **75** (1997) 539

[109] S. P. Martin and M. T. Vaughn, Phys. Lett. B **318** (1993) 331

[110] U. Ellwanger, C. Hugonie and A. M. Teixeira, Phys. Rept. **496** (2010) 1

[111] J. R. Ellis, K. Enqvist, D. V. Nanopoulos and F. Zwirner, Mod. Phys. Lett. A **1** (1986) 57.

[112] R. Barbieri and G. F. Giudice, Nucl. Phys. B **306** (1988) 63.

[113] S. Akula, P. Nath and G. Peim, Phys. Lett. B **717** (2012) 188

[114] M. E. Cabrera, J. A. Casas and R. R. de Austri, JHEP **1307** (2013) 182

[115] K. Kowalska, L. Roszkowski and E. M. Sessolo, JHEP **1306** (2013) 078

[116] G. Jungman, M. Kamionkowski and K. Griest, Phys. Rept. **267** (1996) 195

[117] J. Ellis and K. A. Olive, In *Bertone, G. (ed.): Particle dark matter* 142-163

[118] R. Catena and L. Covi, Eur. Phys. J. C **74** (2014) 2703

[119] K. Griest and D. Seckel, *Three exceptions in the calculation of relic abundances*, *Phys. Rev. D* **43** (1991) 3191.

[120] P. Gondolo and G. Gelmini, *Cosmic abundances of stable particles: Improved analysis*, *Nucl. Phys. B* **360** (1991) 145.

[121] S. Profumo, K. Sigurdson and M. Kamionkowski, Phys. Rev. Lett. **97** (2006) 031301

[122] T. Bringmann, New J. Phys. **11** (2009) 105027

[123] T. Falk, K. A. Olive and M. Srednicki, Phys. Lett. B **339** (1994) 248

[124] D. S. Akerib *et al.* [LUX Collaboration], Phys. Rev. Lett. **112** (2014) 9, 091303

[125] M. Drees and M. M. Nojiri, Phys. Rev. D **47** (1993) 376

[126] G. Aad *et al.* [ATLAS Collaboration], JHEP **1405** (2014) 071

[127] V. Khachatryan *et al.* [CMS Collaboration], Eur. Phys. J. C **74** (2014) 9, 3036

[128] J. R. Ellis, T. Falk and K. A. Olive, Phys. Lett. B **444** (1998) 367

[129] R. L. Arnowitt, B. Dutta and Y. Santoso, Nucl. Phys. B **606** (2001) 59

[130] S. Profumo and C. E. Yaguna, Phys. Rev. D **69** (2004) 115009

[131] J. R. Ellis, L. Roszkowski and Z. Lalak, Phys. Lett. B **245** (1990) 545.

[132] K. A. Olive and M. Srednicki, Phys. Lett. B **230** (1989) 78.

[133] K. Griest, M. Kamionkowski and M. S. Turner, Phys. Rev. D **41**, 3565 (1990).

[134] K. A. Olive and M. Srednicki, Nucl. Phys. B **355** (1991) 208.

[135] S. Mizuta and M. Yamaguchi, Phys. Lett. B **298** (1993) 120

[136] N. Arkani-Hamed, A. Delgado and G. F. Giudice, Nucl. Phys. B **741** (2006) 108

[137] L. Roszkowski, Phys. Lett. B **262** (1991) 59.

[138] L. Roszkowski, E. M. Sessolo and A. J. Williams, JHEP **1502** (2015) 014

[139] S. Profumo and A. Provenza, JCAP **0612** (2006) 019

[140] S. Mizuta, D. Ng and M. Yamaguchi, Phys. Lett. B **300** (1993) 96

[141] J. Hisano, S. Matsumoto, M. Nagai, O. Saito and M. Senami, Phys. Lett. B **646** (2007) 34

[142] A. Hryczuk, R. Iengo and P. Ullio, JHEP **1103** (2011) 069

[143] M. Beneke, C. Hellmann and P. Ruiz-Femenia, arXiv:1411.6930 [hep-ph].

[144] G. Belanger, F. Boudjema, C. Hugonie, A. Pukhov and A. Semenov, JCAP **0509** (2005) 001

[145] K. L. Chan, U. Chattopadhyay and P. Nath, Phys. Rev. D **58** (1998) 096004

[146] J. L. Feng, K. T. Matchev and T. Moroi, Phys. Rev. D **61** (2000) 075005

[147] A. Birkedal-Hansen *et al.* [Michigan Center for Theoretical Physics, U. of Michigan Collaboration], Phys. Rev. D **67** (2003) 095006

[148] H. Baer, T. Krupovnickas, A. Mustafayev, E. K. Park, S. Profumo and X. Tata, JHEP **0512** (2005) 011

[149] K. J. Bae, R. Dermisek, H. D. Kim and I. W. Kim, JCAP **0708** (2007) 014

[150] D. Feldman, Z. Liu, P. Nath and B. D. Nelson, Phys. Rev. D **80** (2009) 075001

[151] P. Nath and R. L. Arnowitt, Phys. Lett. B **56** (1975) 177.

[152] R. L. Arnowitt, P. Nath and B. Zumino, Phys. Lett. B **56** (1975) 81.

[153] D. Z. Freedman, P. van Nieuwenhuizen and S. Ferrara, Phys. Rev. D **13** (1976) 3214.

[154] S. Deser and B. Zumino, Phys. Lett. B **62** (1976) 335.

[155] S. Deser and B. Zumino, Phys. Rev. Lett. **38** (1977) 1433.

[156] E. Cremmer, B. Julia, J. Scherk, P. van Nieuwenhuizen, S. Ferrara and L. Girardello, Phys. Lett. B **79** (1978) 231.

[157] E. Cremmer, B. Julia, J. Scherk, S. Ferrara, L. Girardello and P. van Nieuwenhuizen, Nucl. Phys. B **147** (1979) 105.

[158] E. Cremmer, S. Ferrara, L. Girardello and A. Van Proeyen, Nucl. Phys. B **212** (1983) 413.

[159] J. L. Feng, S. f. Su and F. Takayama, Phys. Rev. D **70** (2004) 063514

[160] J. Pradler and F. D. Steffen, Phys. Lett. B **648** (2007) 224

[161] J. R. Ellis, A. D. Linde and D. V. Nanopoulos, Phys. Lett. B **118** (1982) 59.

[162] H. Pagels and J. R. Primack, Phys. Rev. Lett. **48** (1982) 223.

[163] M. Bolz, A. Brandenburg and W. Buchmuller, Nucl. Phys. B **606** (2001) 518 [Erratum-ibid. B **790** (2008) 336]

[164] J. Pradler and F. D. Steffen, Phys. Rev. D **75** (2007) 023509

[165] V. S. Rychkov and A. Strumia, Phys. Rev. D **75** (2007) 075011

[166] G. F. Giudice, A. Notari, M. Raidal, A. Riotto and A. Strumia, Nucl. Phys. B **685** (2004) 89

[167] S. Antusch and A. M. Teixeira, JCAP **0702** (2007) 024

[168] S. Davidson, M. Losada and A. Riotto, Phys. Rev. Lett. **84** (2000) 4284

[169] J. Racker,

[170] N.-E. Bomark and L. Roszkowski, Phys. Rev. D **90** (2014) 1, 011701

[171] K. Choi, K. Hwang, H. B. Kim and T. Lee, Phys. Lett. B **467** (1999) 211

[172] H. Fukushima and R. Kitano, JHEP **1401** (2014) 081

[173] G. F. Giudice, I. Tkachev and A. Riotto, JHEP **9908** (1999) 009

[174] R. Kallosh, L. Kofman, A. D. Linde and A. Van Proeyen, Phys. Rev. D **61** (2000) 103503

[175] H. P. Nilles, M. Peloso and L. Sorbo, Phys. Rev. Lett. **87** (2001) 051302

[176] L. Covi, J. E. Kim and L. Roszkowski, Phys. Rev. Lett. **82** (1999) 4180

[177] L. Covi, H. B. Kim, J. E. Kim and L. Roszkowski, JHEP **0105** (2001) 033

[178] H. P. Nilles and S. Raby, Nucl. Phys. B **198** (1982) 102.

[179] K. Tamvakis and D. Wyler, Phys. Lett. B **112** (1982) 451.

[180] J. M. Frere and J. M. Gerard, Lett. Nuovo Cim. **37** (1983) 135.

[181] K. Y. Choi, L. Covi, J. E. Kim and L. Roszkowski, JHEP **1204** (2012) 106

[182] K. J. Bae, K. Choi and S. H. Im, JHEP **1108** (2011) 065

[183] J. E. Kim and H. P. Nilles, Phys. Lett. B **138** (1984) 150.

[184] E. J. Chun, Phys. Rev. D **84** (2011) 043509

[185] J. E. Kim and M. S. Seo, PoS DSU **2012** (2012) 009

[186] J. E. Kim, A. Masiero and D. V. Nanopoulos, Phys. Lett. B **139** (1984) 346.

[187] P. Moxhay and K. Yamamoto, Phys. Lett. B **151** (1985) 363.

[188] T. Goto and M. Yamaguchi, Phys. Lett. B **276** (1992) 103.

[189] E. J. Chun, J. E. Kim and H. P. Nilles, Phys. Lett. B **287** (1992) 123

[190] E. J. Chun and A. Lukas, Phys. Lett. B **357** (1995) 43

[191] K. Rajagopal, M. S. Turner and F. Wilczek, Nucl. Phys. B **358** (1991) 447.

[192] A. Brandenburg and F. D. Steffen, JCAP **0408** (2004) 008

[193] K. J. Bae, E. J. Chun and S. H. Im, JCAP **1203** (2012) 013

[194] L. Covi, L. Roszkowski and M. Small, JHEP **0207** (2002) 023

[195] E. Braaten and R. D. Pisarski, Nucl. Phys. B **337** (1990) 569.

[196] A. Strumia, JHEP **1006** (2010) 036

[197] F. James, Hackensack, USA: World Scientific (2006) 345 p

[198] B. de Finetti, Annales de l'institut Henri Poincaré **7** (1937) 001

[199] R. R. de Austri, R. Trotta and L. Roszkowski, JHEP **0605** (2006) 002

[200] R. Trotta, Contemp. Phys. **49** (2008) 71

[201] N. Metropolis, A. W. Rosenbluth, M. N. Rosenbluth, A. H. Teller and E. Teller, J. Chem. Phys. **21**, 1087 (1953).

[202] J. Skilling, Bayesian Anal. **1** (2006) 883.

[203] F. Feroz and M. P. Hobson, Mon. Not. Roy. Astron. Soc. **384** (2008) 449

[204] F. Feroz, M. P. Hobson and M. Bridges, Mon. Not. Roy. Astron. Soc. **398** (2009) 1601

[205] R. Trotta, F. Feroz, M. P. Hobson, L. Roszkowski and R. Ruiz de Austri, JHEP **0812** (2008) 024

[206] A. Fowlie, M. Kazana, K. Kowalska, S. Munir, L. Roszkowski, E. M. Sessolo, S. Trojanowski and Y. L. S. Tsai, Phys. Rev. D **86** (2012) 075010

[207] K. Kowalska, S. Munir, L. Roszkowski, E. M. Sessolo, S. Trojanowski and Y. L. S. Tsai, Phys. Rev. D **87** (2013) 115010

[208] B. C. Allanach, Comput. Phys. Commun. **143** (2002) 305

[209] U. Ellwanger, J. F. Gunion and C. Hugonie, JHEP **0502** (2005) 066

[210] U. Ellwanger and C. Hugonie, Comput. Phys. Commun. **175** (2006) 290

[211] U. Ellwanger and C. Hugonie, Comput. Phys. Commun. **177** (2007) 399

[212] A. Arbey and F. Mahmoudi, Comput. Phys. Commun. **181** (2010) 1277

[213] G. Belanger, F. Boudjema, A. Pukhov and A. Semenov, Comput. Phys. Commun. **149** (2002) 103

[214] G. Belanger, F. Boudjema, A. Pukhov and A. Semenov, Comput. Phys. Commun. **174** (2006) 577

[215] G. Belanger, F. Boudjema, A. Pukhov and A. Semenov, Comput. Phys. Commun. **185** (2014) 960

[216] S. Heinemeyer, W. Hollik and G. Weiglein, Comput. Phys. Commun. **124** (2000) 76

[217] A. Fowlie, K. Kowalska, L. Roszkowski, E. M. Sessolo and Y. L. S. Tsai, Phys. Rev. D **88** (2013) 055012

[218] E. Aprile *et al.* [XENON100 Collaboration], Phys. Rev. Lett. **107** (2011) 131302

[219] E. Aprile *et al.* [XENON100 Collaboration], Phys. Rev. Lett. **109** (2012) 181301

[220] J. C. Park, S. C. Park and K. Kong, Phys. Lett. B **733** (2014) 217

[221] K. Y. Choi and O. Seto, Phys. Lett. B **735** (2014) 92

[222] [CMS Collaboration], CMS-PAS-HIG-12-041.

[223] [ATLAS Collaboration], ATLAS-CONF-2012-162,
ATLAS-COM-CONF-2012-198.

[224] S. Dittmaier *et al.* [LHC Higgs Cross Section Working Group Collaboration], arXiv:1101.0593 [hep-ph].

[225] S. Dittmaier, S. Dittmaier, C. Mariotti, G. Passarino, R. Tanaka, S. Alekhin, J. Alwall and E. A. Bagnaschi *et al.*, arXiv:1201.3084 [hep-ph].

[226] http://cms.web.cern.ch/org/cms-papers-and-results.

[227] J. Baglio and A. Djouadi, JHEP **1103** (2011) 055

[228] S. Chatrchyan *et al.* [CMS Collaboration], Phys. Rev. D **85** (2012) 012004

[229] CMS Collaboration [CMS Collaboration], CMS-PAS-SUS-12-005.

[230] B. C. Allanach, Phys. Rev. D **83** (2011) 095019

[231] P. Bechtle, B. Sarrazin, K. Desch, H. K. Dreiner, P. Wienemann, M. Kramer, C. Robens and B. O'Leary, Phys. Rev. D **84** (2011) 011701

[232] M. Artuso, D. M. Asner, P. Ball, E. Baracchini, G. Bell, M. Beneke, J. Berryhill and A. Bevan *et al.*, Eur. Phys. J. C **57** (2008) 309

[233] M. Misiak, arXiv:1112.5978 [hep-ph].

[234] M. Misiak, AIP Conf. Proc. **1317** (2011) 276

[235] U. Nierste, arXiv:1212.5805 [hep-ph].

[236] G. Buchalla and A. J. Buras, Nucl. Phys. B **400** (1993) 225.

[237] M. Misiak and J. Urban, Phys. Lett. B **451** (1999) 161

[238] C. Bobeth, T. Ewerth, F. Kruger and J. Urban, Phys. Rev. D **64** (2001) 074014

[239] C. Bobeth, A. J. Buras, F. Kruger and J. Urban, Nucl. Phys. B **630** (2002) 87

[240] K. De Bruyn, R. Fleischer, R. Knegjens, P. Koppenburg, M. Merk, A. Pellegrino and N. Tuning, Phys. Rev. Lett. **109** (2012) 041801

[241] C. Bobeth, M. Gorbahn, T. Hermann, M. Misiak, E. Stamou and M. Steinhauser, Phys. Rev. Lett. **112** (2014) 101801

[242] A. J. Buras, P. H. Chankowski, J. Rosiek and L. Slawianowska, Nucl. Phys. B **659** (2003) 3

[243] A. Arbey, M. Battaglia, F. Mahmoudi and D. MartĂnez Santos, Phys. Rev. D **87** (2013) 3, 035026

[244] F. Mahmoudi, S. Neshatpour and J. Orloff, JHEP **1208** (2012) 092

[245] G. Isidori and P. Paradisi, Phys. Lett. B **639** (2006) 499

[246] K. Hara *et al.* [Belle Collaboration], Phys. Rev. D **82** (2010) 071101

[247] I. Adachi *et al.* [Belle Collaboration], Phys. Rev. Lett. **110** (2013) 13, 131801

[248] B. Aubert *et al.* [BaBar Collaboration], Phys. Rev. D **81** (2010) 051101

[249] J. P. Lees *et al.* [BaBar Collaboration], Phys. Rev. D **88** (2013) 3, 031102

[250] M. Kaminski, M. Misiak and M. Poradzinski, Phys. Rev. D **86** (2012) 094004

[251] M. Misiak, H. M. Asatrian, K. Bieri, M. Czakon, A. Czarnecki, T. Ewerth, A. Ferroglia and P. Gambino *et al.*, Phys. Rev. Lett. **98** (2007) 022002

[252] M. Misiak and M. Steinhauser, Nucl. Phys. B **764** (2007) 62

[253] G. Degrassi, P. Gambino and G. F. Giudice, JHEP **0012** (2000) 009

[254] J. Foster, K. i. Okumura and L. Roszkowski, JHEP **0508** (2005) 094

[255] J. Foster, K. i. Okumura and L. Roszkowski, Phys. Lett. B **609** (2005) 102

[256] G. W. Bennett *et al.* [Muon G-2 Collaboration], Phys. Rev. D **73** (2006) 072003

[257] D. Stockinger, J. Phys. G **34** (2007) R45

[258] J. P. Miller, E. de Rafael and B. L. Roberts, Rept. Prog. Phys. **70** (2007) 795

[259] P. H. Chankowski, A. Dabelstein, W. Hollik, W. M. Mosle, S. Pokorski and J. Rosiek, Nucl. Phys. B **417** (1994) 101.

[260] D. Garcia and J. Sola, Mod. Phys. Lett. A **9** (1994) 211.

[261] S. Heinemeyer, W. Hollik and G. Weiglein, Phys. Rept. **425** (2006) 265

[262] S. Heinemeyer, W. Hollik, F. Merz and S. Penaranda, Eur. Phys. J. C **37** (2004) 481

[263] T. Aaltonen *et al.* [CDF and D0 Collaborations], Phys. Rev. D **86** (2012) 092003

[264] S. Chatrchyan *et al.* [CMS Collaboration], JHEP **1107** (2011) 049

[265] A. H. Mahmood *et al.* [CLEO Collaboration], Phys. Rev. D **67** (2003) 072001

[266] C. Schwanda *et al.* [Belle Collaboration], Phys. Rev. D **78** (2008) 032016

[267] J. Abdallah *et al.* [DELPHI Collaboration], Eur. Phys. J. C **55** (2008) 525

[268] B. Aubert *et al.* [BaBar Collaboration], Phys. Rev. D **81** (2010) 032003

[269] S. Bethke, Eur. Phys. J. C **64** (2009) 689

[270] [CMS Collaboration], CMS-PAS-HIG-13-005.

[271] Y. Amhis *et al.* [Heavy Flavor Averaging Group Collaboration], arXiv:1207.1158 [hep-ex].

[272] R. Aaij *et al.* [LHCb Collaboration], Phys. Rev. Lett. **111** (2013) 101805

[273] S. Chatrchyan *et al.* [CMS Collaboration], Phys. Rev. Lett. **111** (2013) 101804

[274] F. Iocco, G. Mangano, G. Miele, O. Pisanti and P. D. Serpico, Phys. Rept. **472** (2009) 1

[275] L. Covi, L. Roszkowski, R. Ruiz de Austri and M. Small, JHEP **0406** (2004) 003

[276] L. Roszkowski, R. Ruiz de Austri and K. Y. Choi, JHEP **0508** (2005) 080

[277] D. G. Cerdeno, K. Y. Choi, K. Jedamzik, L. Roszkowski and R. Ruiz de Austri, JCAP **0606** (2006) 005

[278] K. Jedamzik, K. Y. Choi, L. Roszkowski and R. Ruiz de Austri, JCAP **0607** (2006) 007

[279] S. Bailly, K. Y. Choi, K. Jedamzik and L. Roszkowski, JHEP **0905** (2009) 103

[280] K. Jedamzik, Phys. Rev. D **74** (2006) 103509

[281] M. Pospelov, Phys. Rev. Lett. **98** (2007) 231301

[282] K. Jedamzik, JCAP **0803** (2008) 008

[283] L. Covi, J. Hasenkamp, S. Pokorski and J. Roberts, JHEP **0911** (2009) 003

[284] T. Kanzaki, M. Kawasaki, K. Kohri and T. Moroi, Phys. Rev. D **75** (2007) 025011

[285] F. D. Steffen, JCAP **0609** (2006) 001

[286] K. Jedamzik, M. Lemoine and G. Moultaka, JCAP **0607** (2006) 010

[287] L. Roszkowski, S. Trojanowski, K. Turzynski and K. Jedamzik, JHEP **1303** (2013) 013

[288] W. Hu and J. Silk, Phys. Rev. D **48** (1993) 485.

[289] W. Hu and J. Silk, Phys. Rev. Lett. **70** (1993) 2661.

[290] D. J. Fixsen, E. S. Cheng, J. M. Gales, J. C. Mather, R. A. Shafer and E. L. Wright, Astrophys. J. **473** (1996) 576

[291] S. Munir, L. Roszkowski and S. Trojanowski, Phys. Rev. D **88** (2013) 5, 055017

[292] K. Kowalska, L. Roszkowski, E. M. Sessolo and S. Trojanowski, JHEP **1404** (2014) 166

[293] L. Roszkowski, S. Trojanowski and K. Turzyński, JHEP **1411** (2014) 146

[294] E. Komatsu *et al.* [WMAP Collaboration], Astrophys. J. Suppl. **192** (2011) 18

[295] K. Nakamura et al. (Particle Data Group), JP G 37, 075021 (2010) and 2011 partial update for the 2012 edition

[296] D. Asner *et al.* [Heavy Flavor Averaging Group Collaboration],

[297] R. Aaij *et al.* [LHCb Collaboration], Phys. Rev. Lett. **108** (2012) 231801

[298] D. Hooper, arXiv:0901.4090 [hep-ph].

[299] L. Roszkowski, E. M. Sessolo and A. J. Williams, JHEP **1408** (2014) 067

[300] C. Hugonie, G. Belanger and A. Pukhov, JCAP **0711** (2007) 009

[301] [CMS Collaboration], CMS-PAS-HIG-12-045.

[302] R. Aaij *et al.* [LHCb Collaboration], Phys. Rev. Lett. **110** (2013) 2, 021801

[303] CMS Collaboration [CMS Collaboration], CMS-PAS-HIG-14-009.

[304] ATLAS Collaboration [ATLAS Collaboration], Summary plots from the ATLAS Higgs physics groups,

[305] N. E. Bomark, S. Moretti, S. Munir and L. Roszkowski, JHEP **1502** (2015) 044

[306] N. D. Christensen, T. Han and S. Su, Phys. Rev. D **85** (2012) 115018

[307] M. Carena, S. Heinemeyer, O. Stal, C. E. M. Wagner and G. Weiglein, Eur. Phys. J. C **73** (2013) 9, 2552

[308] J. R. Ellis, K. Enqvist, D. V. Nanopoulos and K. Tamvakis, Phys. Lett. B **155** (1985) 381.

[309] G. Anderson, C. H. Chen, J. F. Gunion, J. D. Lykken, T. Moroi and Y. Yamada, eConf C **960625** (1996) SUP107

[310] S. P. Martin, Phys. Rev. D **79** (2009) 095019

[311] S. Antusch, L. Calibbi, V. Maurer, M. Monaco and M. Spinrath, JHEP **1301** (2013) 187

[312] G. F. Giudice and A. Masiero, Phys. Lett. B **206** (1988) 480.

[313] A. Masiero, D. V. Nanopoulos, K. Tamvakis and T. Yanagida, Phys. Lett. B **115** (1982) 380.

[314] B. Grinstein, Nucl. Phys. B **206** (1982) 387.

[315] Z. Berezhiani and Z. Tavartkiladze, Phys. Lett. B **396** (1997) 150

[316] T. Cohen, M. Lisanti, A. Pierce and T. R. Slatyer, JCAP **1310** (2013) 061

[317] J. Fan and M. Reece, JHEP **1310** (2013) 124

[318] A. Hryczuk, I. Cholis, R. Iengo, M. Tavakoli and P. Ullio, JCAP **1407** (2014) 031

[319] A. Abramowski *et al.* [H.E.S.S. Collaboration], Phys. Rev. Lett. **110** (2013) 041301

[320] O. Adriani *et al.* [PAMELA Collaboration], Phys. Rev. Lett. **105** (2010) 121101

[321] G. Belanger *et al.* [Collaboration],

[322] G. Gelmini, P. Gondolo, *Neutralino with the Right Cold Dark Matter Abundance in (Almost) Any Supersymmetric Model*, *Phys. Rev. D* **74** (2006) 023510

[323] G. Gelmini, G. Gondolo, A. Soldatenko, C. E. Yaguna, *The effect of a late decaying scalar on the neutralino relic density*, *Phys. Rev. D* **74** (2006) 083514

[324] M. Badziak, private communication.

[325] K. Choi, K. Y. Choi and C. S. Shin, Phys. Rev. D **86** (2012) 083529